MECHANICAL PROPERTIES OF AEROSPACE STRUCTURAL ALLOYS UNDER BIAXIAL-STRESS CONDITIONS

Charles W. Bert
Earl J. Mills
Walter S. Hyler

Battelle Memorial Institute
Columbus Laboratories

Technical Report AFML TR-66-229

August 1966

Project No. 7381
Task No. 738103

Air Force Materials Laboratory
Research and Technology Division
Air Force Systems Command
Wright-Patterson Air Force Base, Ohio

NOTICES

When Government drawings, specifications, or other data are used for any purpose other than in connection with a definitely related Government procurement operation, the United States Government thereby incurs no responsibility nor any obligation whatsoever; and the fact that the Government may have formulated, furnished, or in any way supplied the said drawings, specifications, or other data, is not to be regarded by implication or otherwise as in any manner licensing the holder or any other person or corporation, or conveying any rights or permission to manufacture, use, or sell any patented invention that may in any way be related thereto.

Copies of this report should not be returned to the Research and Technology Division unless return is required by security considerations, contractual obligations, or notice on a specific document.

AFLC–WPAFB–MAR 66 1500

AFML-TR-66-229

MECHANICAL PROPERTIES OF AEROSPACE STRUCTURAL ALLOYS UNDER BIAXIAL-STRESS CONDITIONS

Charles W. Bert, Earl J. Mills, and Walter S. Hyler

FOREWORD

This report was prepared by Battelle Memorial Institute, 505 King Avenue, Columbus, Ohio, under USAF Contract No. AF 33(657)-10076. Dr. Charles W. Bert, Associate Professor, School of Aerospace and Mechanical Engineering, University of Oklahoma, Norman, Oklahoma, was retained in a consultant capacity. This contract was initiated under Project No. 7381, Materials Applications, Task No. 738103, "Development of Property Design Criteria for Metals". The work was administered under the direction of the Air Force Materials Laboratory, Research and Technology Division, Air For Systems Command, Wright-Patterson Air Force Base, Ohio, with Mr. D. A. Shinn, Project Engineer.

This report covers work performed during the period January 1965 to January 1966. The manuscript was released by the authors in April 1966, for publication as a technical report.

This technical report has been reviewed and is approved.

D. A. SHINN
Chief, Materials Information Branch
Materials Applications Division
Air Force Materials Laboratory

ABSTRACT

This report is concerned with the mechanical properties of metals under biaxial-stress conditions. First, there is presented a discussion of the fundamentals of biaxial-stress systems; this is followed by descriptions and critical evaluations of various types of biaxial-stress tests, the associated test specimens, biaxial-stress property criteria, and data presentation for Military Handbook 5. The major portion of the report is devoted to the graphical presentation of biaxial-stress property data from various published and unpublished sources. The properties covered include biaxial stress-strain curves, biaxial yield stress, biaxial ultimate stress, strain at biaxial ultimate stress, and strain at biaxial-stress fracture. The alloys considered include twenty steels (standard and specialized engineering steels heat treated to high ultimate-tensile-stress levels, stainless steels, tool steels, and high-nickel maraging steels), five aluminum alloys, three magnesium alloys, and one titanium alloy.

Supplementary theoretical considerations are covered in the three appendices. The report concludes with a discussion of the biaxial-stress properties, the factors affecting them, and suggestions for additional tests needed to provide more complete material-property data for designers.

TABLE OF CONTENTS

LIST OF FIGURES

LIST OF FIGURES
(Continued)

LIST OF FIGURES
(Continued)

LIST OF FIGURES
(Continued)

LIST OF FIGURES
(Continued)

LIST OF FIGURES
(Continued)

LIST OF FIGURES
(Continued)

LIST OF FIGURES
(Continued)

LIST OF TABLES

SYMBOLS AND NOMENCLATURE

a	Constant in the generalized-conic biaxial-stress envelope equation, Equation (26)
B	Biaxial-stress ratio
b	Constant in the generalized-conic biaxial-stress envelope equation, Equation (26)
C	Location of center of Mohr stress circle
c, d, e	Constants in the generalized-conic biaxial-stress envelope equation, Equation (26)
D	Nominal diameter
E	Young's modulus of elasticity (uniaxial)
E_B	Biaxial modulus of elasticity
e_1, e_2, e_3	Principal nominal strains
e_{p1}, e_{p2}, e_{p3}	Principal nominal plastic strains
$\bar{e}_p$	Effective nominal plastic strain, defined by Equation (24)
e_{po}	Equivalent uniaxial plastic strain (nominal)
e_x, e_y	Normal nominal strains in the x and y directions
e_{xy}	Shear strain (nominal) on the edges of an element with edges oriented in the x and y directions
F_{Ay}	Nominal axial yield stress under biaxial-stress conditions
F_{Au}	Nominal axial ultimate stress under biaxial-stress conditions
F_{Hy}	Nominal hoop yield stress under biaxial-stress conditions
F_{Hu}	Nominal hoop ultimate stress under biaxial-stress conditions
F_{tu}	Ultimate tensile stress (nominal uniaxial normal)
F_{ty}	Tensile yield stress (nominal, normal uniaxial in the reference direction)
f_1, f_2	Principal in-plane nominal stresses

SYMBOLS AND NOMENCLATURE
(Continued)

f_A	Total axial normal stress (nominal)
f_{AE}, f_{AP}	Axial normal stresses (nominal) caused by P and by p
f_H	Hoop (circumferential) nominal normal stress
f_{HP}	Hoop nominal normal stress due to p
f_s	Shear stress, including torsional (nominal)
f_x, f_y	Normal nominal stresses in the x and y directions
f_{xy}	Shear stress (nominal) on the edges of an element with edges oriented in the x and y directions
$\bar{f}$	von Mises effective nominal stress, defined by Equation (22)
f_m	Normal nominal stress at maximum pressure or maximum load
f_o	Uniaxial nominal stress, see discussion following Equation (24)
G	Shear modulus
L	Length of cylindrical portion; length of side of square plate (in Appendix III)
P	External axial force on a cylinder; force per edge of square plate (in Appendix III)
p	Internal pressure
r	Radius of Mohr stress circle
T	Applied torque
t	Wall thickness
t_m	Wall thickness at maximum pressure (see Appendix III)
UTS	Ultimate tensile stress (nominal, uniaxial normal)
V	Volume of material
x	f_C/F_{ty}, see Appendix II
y	f_A/F_{ty}, see Appendix II
ϵ^*	True strain, see Appendix III

I

INTRODUCTION

Most mechanical-property data for metallic materials are obtained from simple tensile tests. However, in many aerospace applications the material is often highly stressed in two mutually perpendicular directions, rather than in only one direction as in a simple tensile test. Such applications include pressure-storage bottles, pressurized aircraft fuselages, liquid-propellant tankage, and solid-propellant motor cases. Curiously, metallic materials behave quite differently under these biaxial-stress conditions than they do in a simple tensile test. Biaxial loading changes the stress-strain curve of a material in both the elastic and plastic ranges. Reported values of the nominal stress at burst in a pressure vessel have been as high as 121 percent of the ultimate tensile strength (UTS) obtained in a tensile test. In other instances nominal stress values at burst have been as low as 60 percent of the UTS.

Obviously it is very important to those having responsibility for design and material selection for advanced aerospace vehicles to know as accurately as possible the biaxial strength of the various materials under consideration in these applications. If there is going to be considerable increase in strength under biaxial conditions, this can result in a significant saving in structural weight or an increase in the structural reliability. On the other hand, if failures occur at stress values appreciably below the UTS, this can limit vehicle performance rather severely.

Some investigators have attempted to predict the biaxial strength from uniaxial tensile properties by the application of the theories of elasticity and plasticity. Today it is possible to predict reliably the slope of the biaxial stress-strain curve in the elastic range for all isotropic (or nearly isotropic) metallic materials and the shape of the biaxial stress-strain curve in the plastic range for some isotropic metallic materials. However, it is not possible to predict whether failure will occur at a low nominal-stress level in a brittle fashion, or whether the stress-strain curve will proceed a short distance into the plastic range or continue far into the plastic range and permit failure to finally occur by a ductile necking-down action.

Since failure under biaxial-stress conditions could not be predicted reliably on the basis of tensile-test data only, many investigators have attempted to devise relatively inexpensive laboratory specimens to simulate the biaxial-stress conditions presented in the full-scale structure. As will be seen in the next section, most of these simplified specimens have not correlated well with failure data from full-scale tests. Thus, considerable caution must be used in applying failure-stress data obtained from laboratory specimens to the design of full-scale structures. In fact, the only reliable small-scale specimen which yields failure data which correlates at all with data obtained from full-scale tests is a relatively expensive pressurized specimen which has certain geometrical relationships to the full-scale structure.

Even a small-scale pressure-vessel test is considerably more expensive than a simple tensile test. Thus, it is expensive to run tests on the dozens of alloys of current interest. This has been recognized for some time by the Military Handbook 5 Coordination Group, who as early as 1960 began to consider criteria for biaxial-stress properties. Some of the considerations involved in selection of criteria are discussed in Reference 1, while Reference 2 describes the criteria finally adopted.

The present study is limited entirely to information already generated by various governmental and industrial laboratories. Over 300 references, including articles, papers, books, and formal and informal reports, have been scanned for pertinent data. The purposes of this study are as follows:

(1) To discuss the validity of various test specimens in order to provide guidance for future tests and possible standardization of tests in this area

(2) To discuss the biaxial-property criteria adopted by the Military Handbook 5 Coordination Group in order to promote more standardization in this area

(3) To reduce quantitative data from reliable tests to the standard property format adopted by the Military Handbook 5 Coordination Group

(4) To make suggestions relating to the type and extent of information which is needed in order to "pin down" the effects of the many variables involved.

II

FUNDAMENTALS OF BIAXIAL STRESS SYSTEMS

General

The stress-strain system acting at any given point in a loaded body is most conveniently handled in terms of principal stresses and principal strains. In this section, these concepts and other fundamental definitions are explained by way of review.

Normal, Shear, and Principal Stresses

The stresses acting at any point in a stressed member can be resolved into components acting on various planes passing through the point.

The stress component acting normal (perpendicular) to the plane is called normal stress (such as f_x in Figure 1). Normal stresses are of two kinds: tension stresses, which tend to pull apart adjacent particles, and compression stresses, which tend to press together adjacent particles. In multiaxial stress systems, it is customary to use a sign convention in which tension stresses are denoted as positive (+) and compression stresses are considered to be negative (-).

Any stress component which acts in the plane under consideration is called shear stress (such as f_{xy} and f_{xz} in Figure 1). Shear stresses tend to cause adjacent particles to slide past each other.

In order to define the sign convention used for shear stresses, it is necessary to consider an infinitesimal square element cut from the plane of a thin-sheet type structure (see Figure 2a). Suppose there exists a shear stress acting downward on the right-hand face of the element (face a in Figure 2b). Then equilibrium of vertical forces acting on the element requires that there be a shear force acting upward on the left-hand face (face b in Figure 2b). Furthermore, equilibrium of moments acting about any point on the plane shown requires that the pure couple in the clockwise direction produced by shear stresses f_{sa} and f_{sb} be balanced by a counterclockwise couple of the same magnitude. This couple can be produced only by shear stresses acting on the upper and lower faces (faces c and d). Thus, there must be shear stresses f_{sc} acting to the left on the upper face and f_{sd} acting toward the right on the bottom face, as shown in Figure 2b. Thus, it is shown that, if a shear stress exists on one face of an infinitesimal plane element within a body, it must exist on all four faces in the form of two pairs of stresses. The shear stresses which produce a clockwise couple are denoted as positive (+), while the shear stresses which produce a counterclockwise couple are considered to be negative (-). Equilibrium of normal stresses is shown in Figure 2c.

If one selects three orthogonal (mutually perpendicular) planes through a point, there always exists some orientation of this system such that only normal stresses exist, the shear stresses all being zero. These normal stresses are called principal stresses, and the numerically largest of these is denoted the maximum principal stress. The directions perpendicular to the three orthogonal planes are known as principal-stress directions.

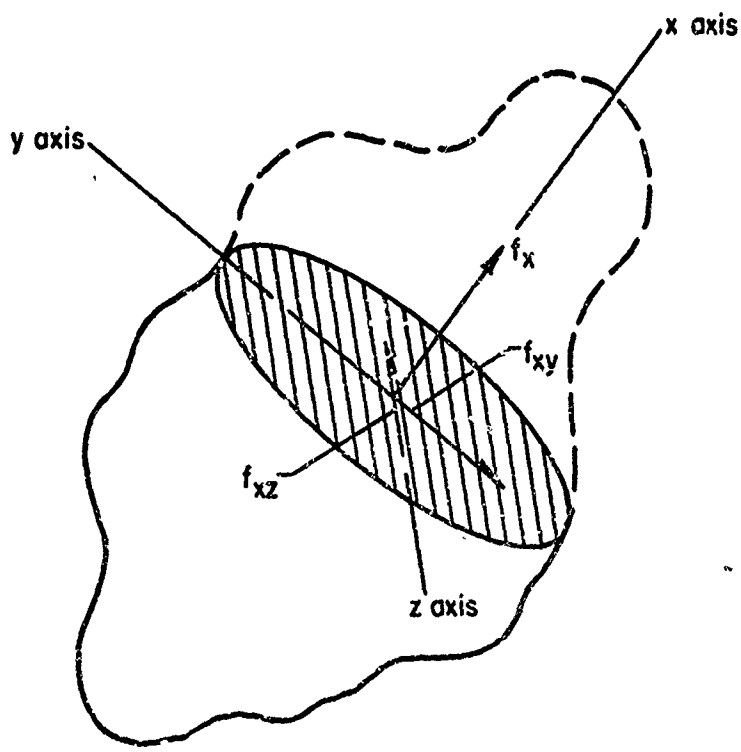

FIGURE 1. STRESS COMPONENTS ACTING ON A PLANE
(Shown cross-hatched)

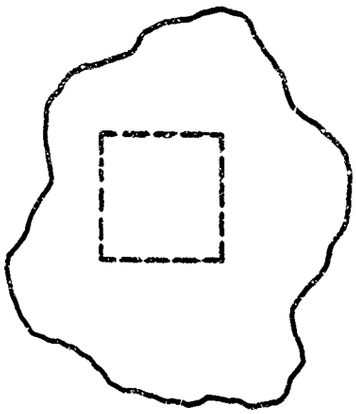

a. Typical infinitesimal element

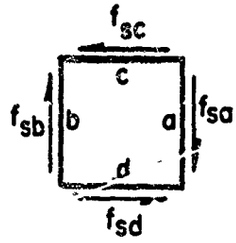

b. Equilibrium of shear stresses ($f_{sa} = f_{sb} = f_{sc} = f_{sd}$)

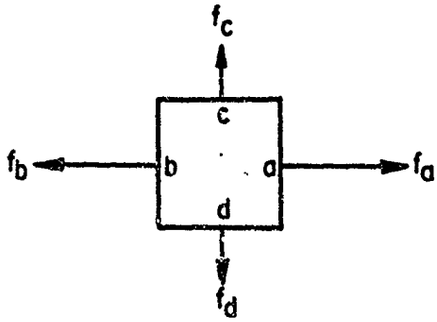

c. Equilibrium of normal stresses ($f_a = f_b$; $f_c = f_d$)

FIGURE 2. EQUILIBRIUM OF STRESSES ACTING ON AN INFINITESIMAL ELEMENT

The easiest way to visualize the relationships involved in a multi-axial stress system is to use a Mohr stress-circle diagram. This serves as an aid in calculating the principal stresses and principal-stress directions. In this report the chief concern is with determination of principal stresses. For information on calculation of principal-stress directions, refer to any modern text on elementary stress analysis or strength of materials.

To construct a Mohr stress-circle diagram, the abscissa of the diagram is denoted as the normal-stress axis and the ordinate as the shear-stress axis. That is, taking due account of the sign conventions mentioned, all normal stresses are plotted as the abscissa and all shear stresses as the ordinate. Figure 3a is a typical biaxially loaded two-dimensional element. On face a of this element there are acting a normal tension stress, f_x, and a positive shear stress, f_{xy}. Thus, on the Mohr stress-circle diagram (Figure 3b), point a is plotted with coordinates (f_x, f_{xy}). Note that point a on the Mohr diagram corresponds to the stress situation at faces a and b of the element. Similarly, corresponding to faces c and d on the element, point c is plotted on the Mohr diagram with coordinates (f_y, $-f_{xy}$).

The geometry of the Mohr diagram is such that all Mohr circles have centers located on the normal-stress axis. Since points a and c are two points lying on the circle, and since they are equidistant from the normal-stress axis, points a and c must be ends of a diameter of the circle. Thus, the center of the Mohr circle is located at the point where line ac intercepts the normal stress axis and the radius of the circle is equal to one-half of distance ac (see Figure 3c). In terms of the stress components, f_x, f_y, and f_{xy}, the center is located at an abscissa C of

$$C = 1/2(f_x + f_y),$$

and the radius is

$$r = 1/2\ (\overline{ac}) = \sqrt{\left(\frac{f_x - f_y}{2}\right)^2 + f_{xy}^2}\ .$$

Each point on the Mohr circle is associated with a particular orientation of the infinitesimal square element. Thus, the principal stresses (denoted by f_1, f_2 in Figure 3c) occurs at the two points on the Mohr circle where the shear stresses are zero. From the geometry of the diagram, the principal stresses are calculated as follows:

$$f_1 = C + r = \frac{f_x + f_y}{2} + \sqrt{\left(\frac{f_x - f_y}{2}\right)^2 + f_{xy}^2}\ , \qquad (1)$$

$$f_2 = C - r = \frac{f_x + f_y}{2} - \sqrt{\left(\frac{f_x - f_y}{2}\right)^2 + f_{xy}^2}\ . \qquad (2)$$

Equations (1) and (2) can be used to calculate the principal stresses f_1, f_2 from the component stresses f_x, f_y, f_{xy} for any biaxial-stress sytem.

It should be noted here that the most general stress system which can exist at a point in a body is one in which none of the three principal stresses are zero; this is called a triaxial-stress state. Thus, a biaxial-stress state can be considered as a special case in which one principal stress is essentially zero. In thin-walled members,

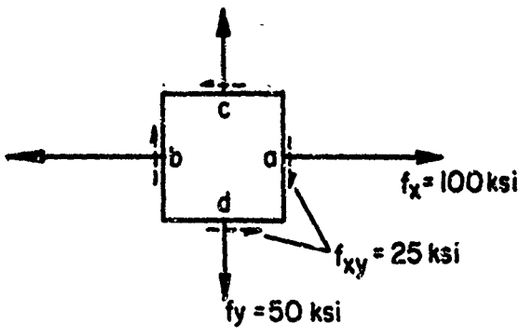

a. Element considered

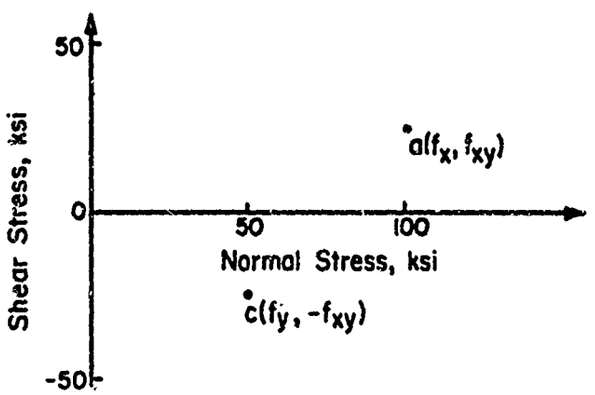

b. Location of Points a and c on Mohr diagram

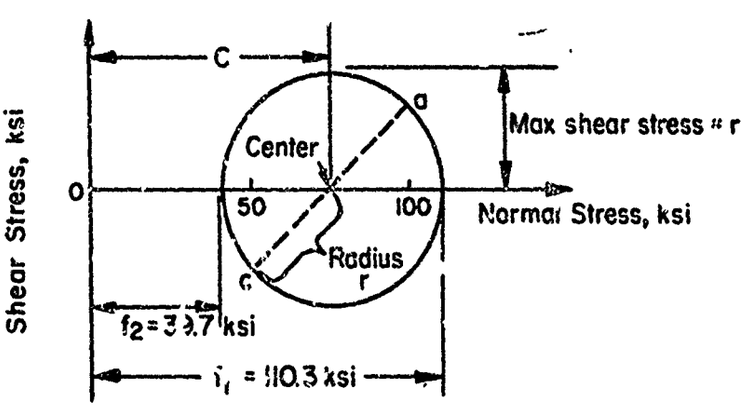

c. Mohr stress circle

FIGURE 3. A TYPICAL BIAXIALLY STRESSED ELEMENT AND THE REPRESENTATION OF ITS STRESS STATE BY A MOHR STRESS-CIRCLE DIAGRAM

the principal stress which is zero is the one in the thickness direction. Finally, the simplest stress state is the uniaxial one, such as that which exists in a long, slender pin-jointed tensile member with no eccentricity.

In biaxial stress systems, it is often convenient to refer to the state of stress in terms of a dimensionless ratio, the biaxial-stress ratio B, which is defined as the ratio of one in-place principal stress to the other, the latter acting in a principal-stress direction arbitrarily selected as the reference principal-stress direction.

Normal, Shear, and Principal Strains

Nominal strain is defined as the change in length per unit of original length in a member or a portion (gage length) of a member.

Normal strain is the change in dimensions of a member in the direction in which the original dimension was measured. Shear strain is the angular distortions (in radians) of a member under loading. For example, consider a square element shown by dashed lines in Figure 4. If the unit square deforms to the diamond shape shown by solid lines in Figure 4, the normal strains e_x and e_y and shear strain e_{xy} are as defined in the figure.

If one selects three orthogonal planes passing through any given point in a loaded member, there always exists some orientation of this system of orthogonal planes such that only normal strains are present, all shear stresses being zero. The orthogonal directions associated with this orientation are known as principal-strain directions and the associated normal strains are called principal strains. The analogy to the concept of principal stresses is readily apparent. However, it must be noted that in general the principal-strain directions coincide with the principal-stress directions only for isotropic materials (defined subsequently).

Using a Mohr strain-circle diagram[3] which is somewhat analogous to the Mohr stress-circle diagram discussed previously, the following expressions for the principal strains e_1 and e_2 can be obtained:

$$e_1 = \left(\frac{1}{2}\right)\left[\left(e_x + e_y\right) + \sqrt{\left(e_x - e_y\right)^2 + e_{xy}^2}\right] \quad , \tag{3}$$

$$e_2 = \left(\frac{1}{2}\right)\left[\left(e_x + e_y\right) - \sqrt{\left(e_x - e_y\right)^2 + e_{xy}^2}\right] \quad , \tag{4}$$

where e_x, e_y, and e_{xy} are the component strains as defined previously.

Elastic Deformation Under Biaxial Stresses

A material is said to be elastically isotropic that has elastic properties (modulus of elasticity, Poisson's ratio, and shear modulus) that are independent of the directional orientation with which the test specimen is taken from the material. An anisotropic material is one having different elastic properties in different directions. There are many different forms of anisotropic elastic behavior (see Reference 4), some of which

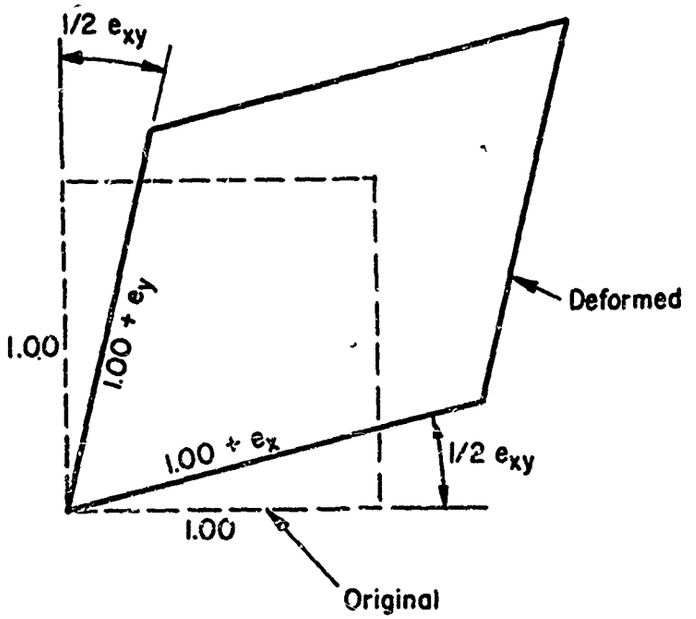

FIGURE 4. NORMAL STRAINS e_x AND e_y AND SHEAR STRAIN e_{xy}

are quite complicated. Fortunately, however, nearly all alloys of structural importance are elastically isotropic or nearly so (within 10 percent maximum variation in modulus of elasticity with directional orientation). Thus, in engineering, it is satisfactory to use the classic stress-strain relations of classical isotropic linear elasticity theory[5]. For the case of biaxial stresses, these are

$$e_1 = (f_1 - \mu f_2)/E \tag{5}$$

$$e_2 = (f_2 - \mu f_1)/E \tag{6}$$

$$e_3 = -\mu(f_1 + f_2)/E, \tag{7}$$

where e_1 and e_2 are the in-plane principal strains, e_3 is the principal strain in the thickness direction; f_1, f_2, and f_3 are the corresponding principal stresses; E is the modulus of elasticity; and μ is Poisson's ratio.

Solving Equations (5) and (6) simultaneously for the principal stresses f_1 and f_2 gives the following more convenient expressions:

$$f_1 = \frac{E}{1-\mu^2}(e_1 + \mu e_2) \tag{8}$$

$$f_2 = \frac{E}{1-\mu^2}(e_2 + \mu e_1) \ . \tag{9}$$

It is noted that Equations (5) through (9) contain only two independent elastic constants, E and μ. This is a considerable simplification compared to a general anisotropic material, which has 21 independent elastic constants. In an isotropic elastic material there are some other simplifications. As previously mentioned, the principal-strain directions coincide with the principal-stress directions. Furthermore, the following relationship among E, μ, and the shear modulus, G, must hold:

$$G = \frac{E}{2(1+\mu)} \ . \tag{10}$$

For design purposes, it is often more convenient to use a biaxial modulus rather than Equations (8) and (9). The biaxial modulus E_B is defined as the slope of the elastic portion of the maximum principal stress vs maximum principal-strain curve. Thus,

$$f_1 = E_B e_1 \tag{11}$$

where f_1 is assumed to be the maximum principal stress.

From the previously given definition of the biaxial-stress ratio B and Equations (8) and (11), the following equation for calculating E_B is obtained:

$$E_B = \frac{E}{(1-\mu B)} \ , \tag{12}$$

where here B is defined as f_2/f_1 and $f_1 > f_2$. Thus, the biaxial modulus depends only upon the tensile elastic properties E and μ and the biaxial-stress ratio B.

Plastic Deformation Under Biaxial Stresses

Although the theory of elastic deformation is well established and widely used in engineering, this is not the situation for the case of plastic deformation. There are many more factors which affect plastic deformation. The most rigorous plasticity theories, which nevertheless do not adequately account for all of the observed effects, are too unwieldy for widespread use in engineering. However, before discussing these aspects it is well to state some definitions.

Figure 5 shows a typical stress-strain curve taken from a test to failure. Whether the loading is biaxial or only uniaxial is immaterial at this juncture. The plot is of nominal stress versus total nominal strain. The portion of the curve beyond the point where the stress-strain relation is no longer linear and the entire deformation is no longer recoverable is known as the plastic range of the curve; the linear portion is the elastic range discussed in "Elastic Deformation Under Biaxial Stresses".

At any point P within the plastic range, the total strain may be considered to consist of two components: an elastic component and a plastic component (see Figure 5). There are several reasons why these two strain components are distinguished. The primary reason is that the elastic strain is recoverable upon removal of the load, while the plastic strain is not. Thus, the plastic strain is sometimes called permanent strain. Another reason is that the elastic component may be considered as having a lateral-contraction ratio equal to the conventional elastic Poisson's ratio, while the plastic component may be considered as having a lateral-contraction ratio of one-half (this is synonymous with stating that the plastic deformation results in no change in material volume). The total lateral-contraction effect in the plastic range then is the sum of these two mechanisms; thus, the total lateral-contraction ratio changes from the elastic (Poisson's) value to the higher plastic value, the change being a fairly gradual one.

The total behavior of a metal at any point in the plastic range is determined by the different mechanisms: (1) that of elastic deformation which is governed by the equations presented in "Elastic Deformation Under Biaxial Stress", and (2) that of plastic deformation which is governed by much more complicated relationships. An "elastic-perfectly plastic" metal (not to be confused with polymers) is one having a flat stress-strain curve (i.e., constant stress) throughout the plastic range. A "rigid-plastic"[1] material is one having no elastic deformation at all, only ideally plastic deformation; this of course is not a very realistic assumption to make for most structural-design analyses. Most real materials, especially the metals of importance in aerospace structures, exhibit an increasing stress with increasing strain, although the increase is much less than it is in the elastic range for the same change in strain (see Figure 5). Such materials are said to be "strain-hardening". Note that the term "hardening" here means increasing in stress and does not refer to ordinary hardness such as measured with an indentation hardness tester.

1. The term "rigid" is used here in the sense of volumetric rigidity, since there is a volume change in purely elastic deformation, while there is not volume change associated with the plastic component. Thus, a material having no elastic deformation does not change volume and is said to be rigid.

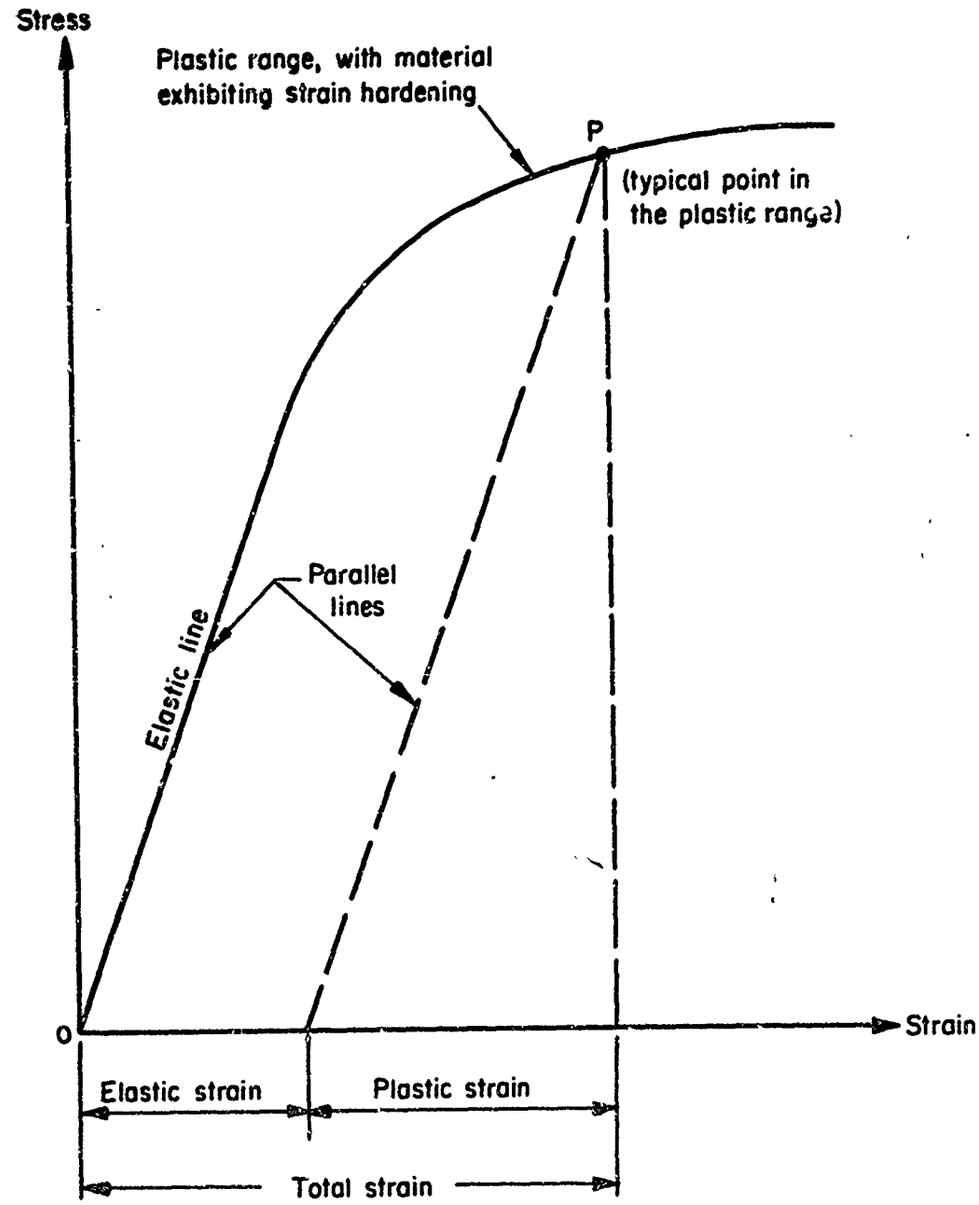

FIGURE 5. TYPICAL STRESS-STRAIN CURVE SHOWING ELASTIC AND PLASTIC STRAIN COMPONENTS

There are two main types of plasticity theory[6]:

(1) Deformation theory, in which the stress is considered to be a function of the total strain (deformation).

(2) Flow (or incremental) theory, in which the stress is considered to be a function of the strain increment.

The flow theory is generally conceded to be more correct; however, it is much more difficult to apply to engineering-design situations. Fortunately, for the common situation of continuous loading at a constant biaxial-stress ratio (called "proportional" loading), the two theories coincide exactly. Furthermore, even for the situations in which this condition is not met, for the small strains associated with yielding of current high-strength aerospace alloys, the difference between the total deformation and the incremental deformation is usually not very large. Therefore, the simpler deformation theory of plasticity is most widely used in engineering design. This theory presents expressions for the effective stress and effective strain which are given by Equations (22) and (24), respectively, in Appendix I.

III

TYPES OF BIAXIAL-STRESS TESTS AND SPECIMENS

Among the earliest tests conducted to determine the behavior of metallic materials under biaxial-stress conditions were those by Lode[7]. In these tests thin-walled cylinders (Figure 6a) were subjected to various combinations of internal pressure, p, and externally applied axial load, P, (either tension or compression). The internal pressure produced the following stresses: (a) a hoop stress f_{HP} in the circumferential direction given by

$$f_{HP} = \frac{pD}{2t} \quad , \tag{13}$$

where p is the internal pressure, D is the nominal diameter, and t is the wall thickness and (b) provided the ends of the cylinder are closed so that the axial force due to pressure is carried to the cylinder walls, an axial stress f_{AP} given by

$$f_{AP} = \frac{pD}{4t} \quad . \tag{14}$$

The axial stress f_{AE} produced by an external force P is computed by

$$f_{AE} = \frac{P}{\pi Dt} \quad , \tag{15}$$

where P is taken as positive if the external force is tension and negative if the external force is compression.

Then the principal stresses f_H and f_A acting on a typical element (Figure 6b) in the hoop and axial directions, respectively, are given by

$$f_H = f_{HP} \tag{16}$$

$$f_A = f_{AP} + f_{AE} \quad . \tag{17}$$

Stress-strain relations can be obtained at various constant biaxial-stress ratios as follows: a series of tests is run on a number of tubular specimens, each specimen is tested at a constant ratio of external load P to internal pressure p, then by varying the value of the constant ratio for each specimen, the desired data are obtained.

Numerous practical difficulties have limited the use of the tube-type specimen just described. Improved testing apparatus of this type have been described by Osgood[8], Marin[9], and Fitzgibbon[10].

A relatively simple test for obtaining a biaxial-stress field with a biaxial-stress ratio of 1/2 is to use an internally pressurized tube with closed ends. Thus, this is a special case of the combined-loading test just described. This type of test has been particularly popular in the pressure-vessel and missile-motor-case industries, in qualification work as well as in material and process evaluations and in applied research. In some of these tests very small laboratory-type specimens have been

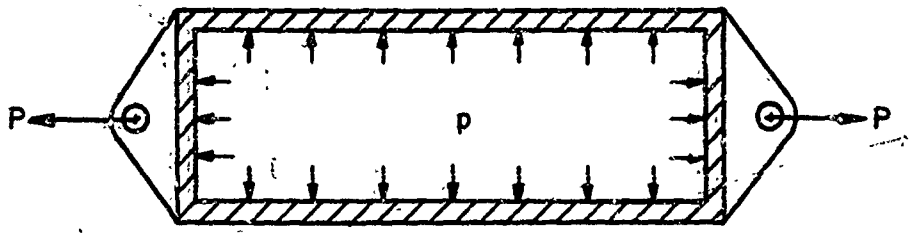

a. Thin-walled cylinder loaded by internal pressure p and external axial load P (shown as tension load)

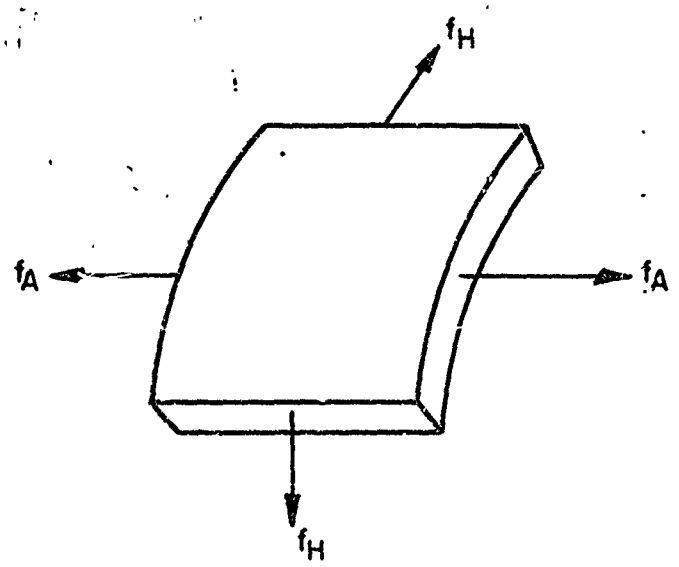

b. Stresses acting on a typical element of the cylinder wall

FIGURE 6. CYLINDRICAL-SHELL BIAXIAL-STRESS TEST SPECIMEN

used, while in others fraction-scale models and full-scale vessels have been used. Although these tests were undoubtedly of considerable value in connection with the particular development program of which they were a part, there are many pitfalls to be avoided in applying data obtained in this fashion to other applications. Some of these pitfalls are discussed in Section VI.

The pressurized tube subject to external load is relatively satisfactory for obtaining biaxial-stress fields in which both of the principal stresses in the plane of the tube wall are tension-type stresses. However, the possibility of buckling when the resultant axial stress f_A is compressive limits the use of this type of loading in obtaining data for cases when it is desired to have one principal stress be tension and another compression. For such a situation, Taylor and Quinney[11] and Marin[12] have used a thin-walled tubular specimen subjected to external axial tension and torsion. The torsional shear stress f_s is computed by the following approximate equation:

$$f_s = 2T/\pi D^3 t \quad , \tag{18}$$

where T is the applied torque. Then by applying Equations (1) and (2), the principal stresses are found to be

$$f_1 = (f_{AE}/2) + \sqrt{(f_{AE}/2)^2 + f_s^2} \tag{19}$$

$$f_2 = (f_{AE}/2) - \sqrt{f_{AE}/2)^2 + f_s^2} \tag{20}$$

where f_{AE} is given by Equation (15). Inspection of Equations (19) and (20) shows that the biaxial-stress ratio f_{min}/f_{max} can range from -1 to 0, assuming f_{AE} ranges from 0 (pure torsion test) to tension values only (in the latter case, $f_s = 0$).

Recently Pugh, et al, have described a machine capable of applying simultaneous internal pressure and axial load[13].

Another pressure-vessel type of specimen, an internally pressurized thin-walled sphere (Figure 7), has been used by Marin and his associates (Reference 14). Such a specimen has a uniform biaxial stress state, so that the hoop and axial stresses are equal to

$$f_H = f_A = pD/4t, \tag{21}$$

where D is the nominal diameter of the sphere. Then, since there is no practical means of applying any external loads (other than external pressure which would merely counteract the effect of the internal pressure) uniformly, this type of specimen is limited to tests at only one biaxial-stress ratio, a ratio of unity. Thus, this type of specimen is not nearly as flexible as the dual-loaded cylindrical pressure vessel.

To avoid the high costs of fabricating pressure-vessel specimens, a number of other specimens have been devised to stress sheet material biaxially. One of these is the flat-diaphragm specimen subject to pressure on one side (Figure 8). This test is known as the bulge test, since the specimen bulges excessively before fracture if the

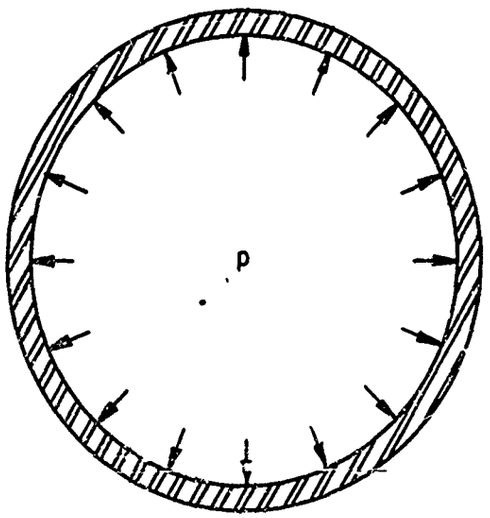

FIGURE 7. INTERNALLY PRESSURIZED, THIN-WALLED SPHERICAL BIAXIAL-STRESS TEST SPECIMEN

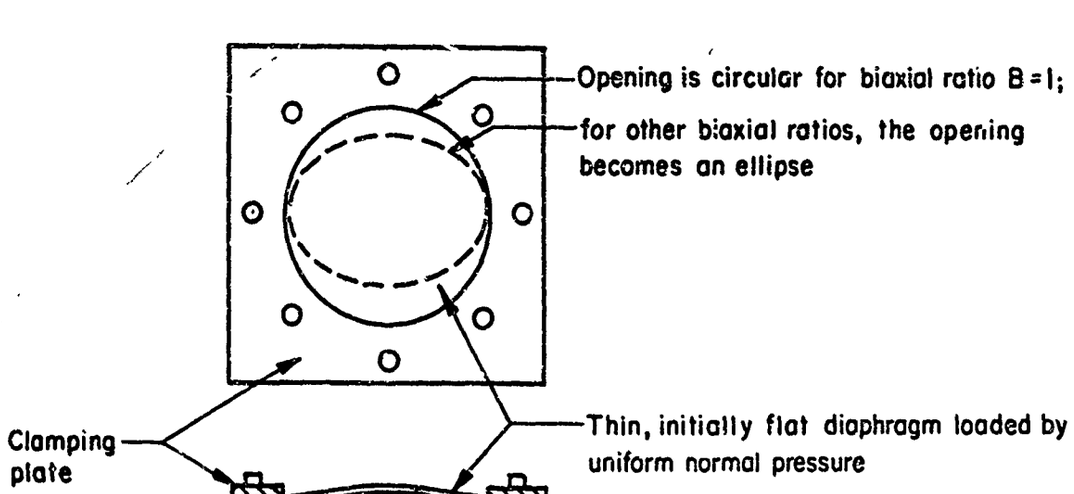

FIGURE 8. PRESSURIZED FLAT DIAPHRAGM (BULGE TEST) BIAXIAL-STRESS TEST SPECIMEN

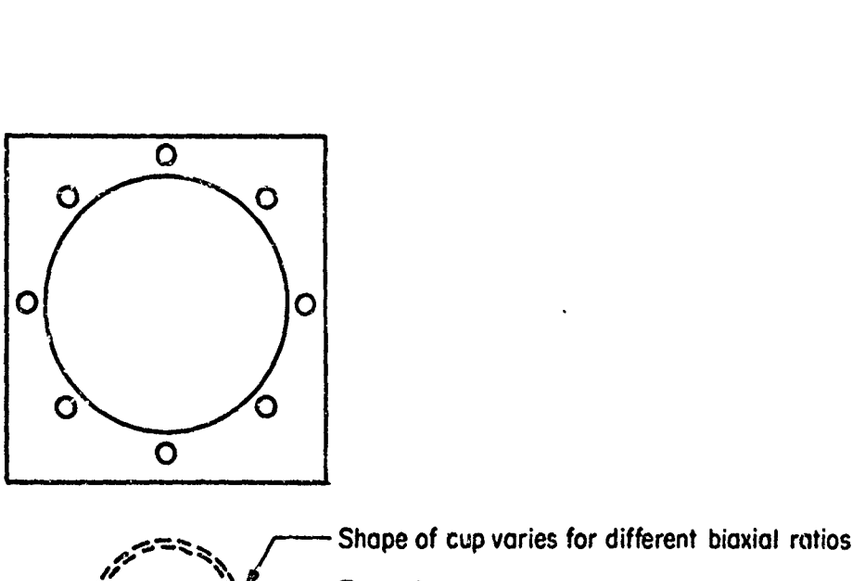

FIGURE 9. PRESSURIZED FORMED-CUP BIAXIAL-STRESS TEST SPECIMEN

material has sufficient ductility. If the planform of the diaphragm is circular, the stress field at the center has a biaxial-stress ratio of unity; by using elliptical planforms of various eccentricities, various biaxial-stress ratios can be achieved at the center of the diaphragm. The primary disadvantage of this specimen is that it has a nonuniform biaxial-stress distribution. Consequently, the unyielded material adjacent to the yielded portion constrains the yielded material and allows the specimen to reach much higher maximum stress and strain values than would be attained by a specimen of the same material with a uniform biaxial-stress field. Nevertheless because of its simplicity, the bulge test has been widely used to qualitatively rate or compare various materials[15-19].

A specimen somewhat similar to both pressure-vessel-type and diaphragm-type specimens is the formed cup specimen (Figure 9). This has been used to evaluate missile-motor-case materials under biaxial-stress ratios of unity (hemispherical cup[20, 21] and 1/2 (ellipsoidal cup[22]. This specimen suffers from the same disadvantage, nonuniform stress distribution, as the diaphragm specimen, although to a lesser degree. Therefore, stress values obtained from tests on such a specimen cannot be used directly in design, but only for qualitative comparison purposes.

Another type of biaxial-stress specimen which has been used recently is the direct in-plane loading type. This includes the cruciform (four-arm) specimen (Figure 10b) developed by Chance Vought Corporation[23] and the eight-arm specimen (Figure 10a) developed by Douglas[24]. Several questions have been raised as to the validity of data obtained from tests on these specimens. One of these is concerned with the degree of uniformity of the stress field in such specimens in view of the possibilities of eccentricity of loading and stress concentration at the intersections of the arms. A perhaps more serious point is that such specimens are not valid for obtaining ultimate strength for applications to pressure-vessel-type structures even though the data are valid for biaxially loaded flat-sheet structure. This point will be explained and elaborated on in Section VI.

According to classical plasticity theory, a flat tension or bending specimen with a groove across a face develops a biaxial-stress ratio of 1/2 when loaded well into the plastic range. This principal was recently applied to static biaxial-stress testing of motor-case weldments by Corrigan, Travis, et al, who used a face-grooved tensile specimen[25] (Figure 11). However, later tests by Travis, et al, in which this type specimen was used[26] did not correlate very satisfactorily with cylindrical-pressure-vessel burst tests conducted by the same investigators. In fact, the hoop-stress values at burst were much closer to the uniaxial ultimate tensile strength than to the strength of the face-grooved specimens. Two possible explanations for this discrepancy are nonuniformity of stress field and its effect on restraint (as previously discussed in connection with the bulge test) or the fact that the ultra-high-strength steels tested did not exhibit enough ductility to permit the material to go far enough into the plastic range to test the conditions of the theoretical solution.

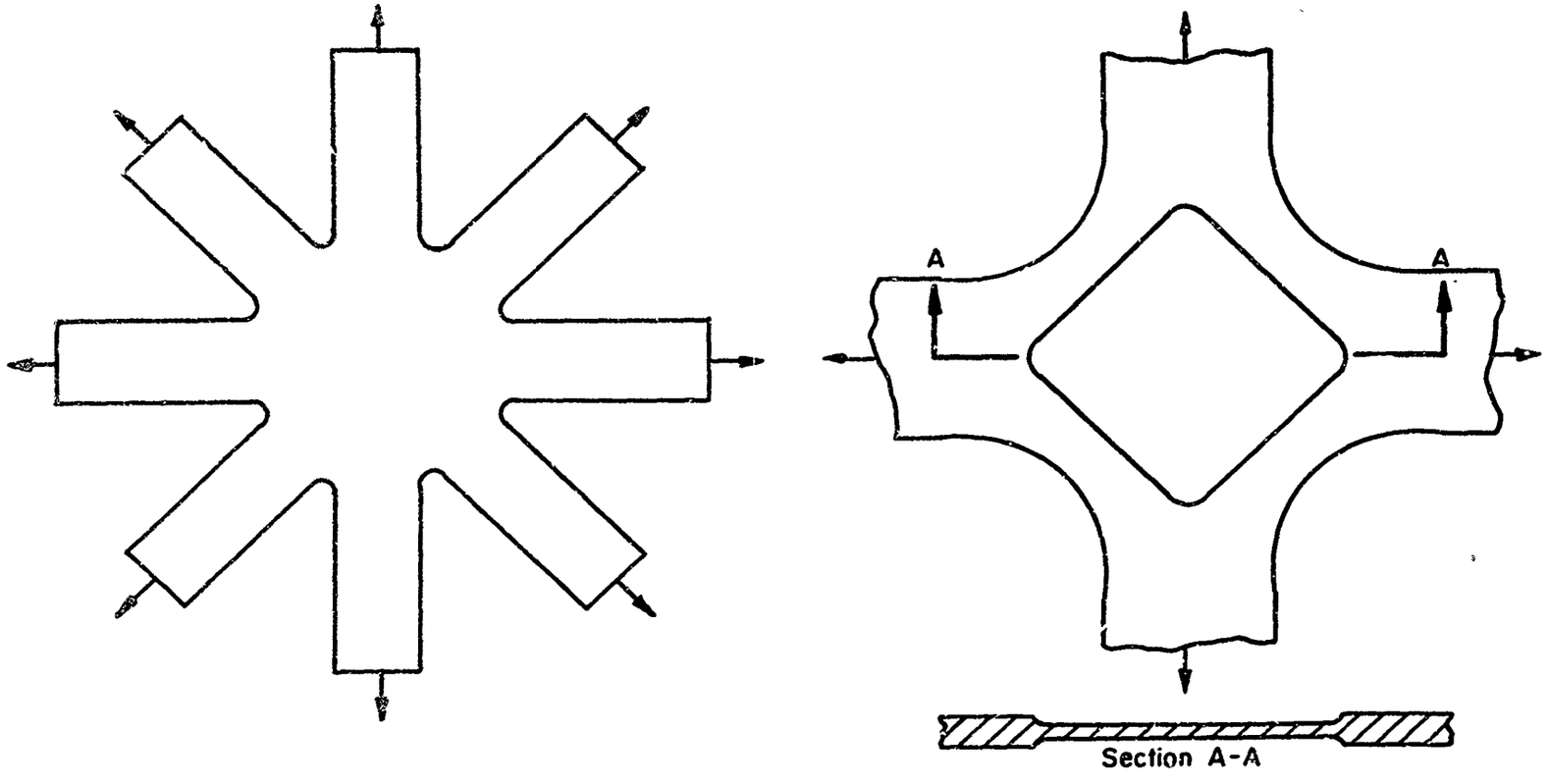

a. Douglas Eight-Arm Specimen

b. Vought Cruciform Specimen

FIGURE 10. DIRECT IN-PLANE LOADING TYPES OF BIAXIAL-STRESS TEST SPECIMENS

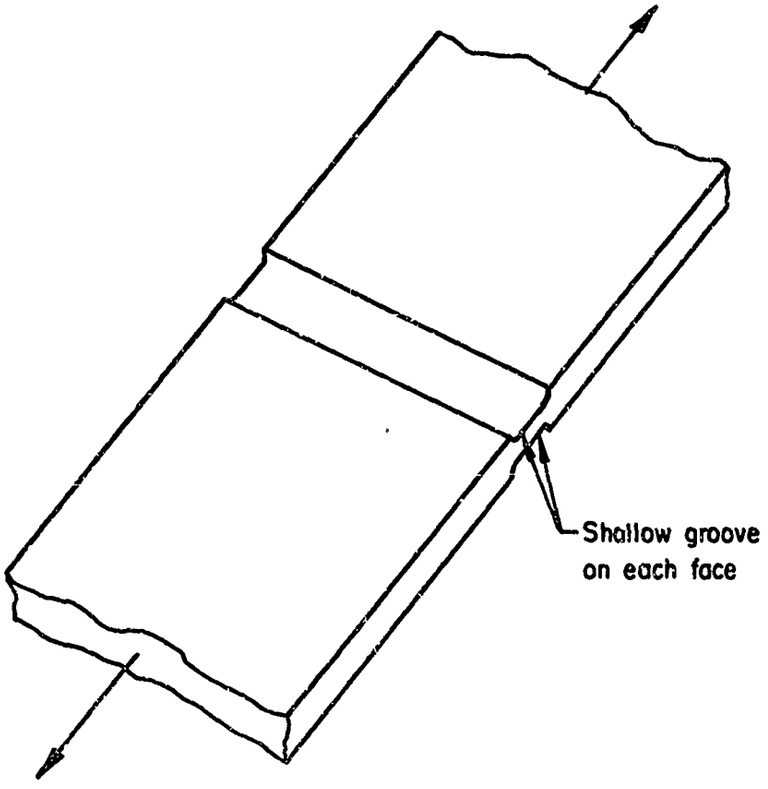

FIGURE 11. FACE-GROOVED TENSILE SPECIMEN

IV

BIAXIAL-STRESS PROPERTY CRITERIA AND DATA PRESENTATION

General

Since the fundamentals of biaxial-stress systems and the type of biaxial tests have been discussed, it is now possible to direct attention to the biaxial properties, the criteria for determining them, and ways of presenting the data.

Biaxial Stress-Strain Curves

Undoubtedly the most complete information on the behavior of a metal under biaxial-stress conditions is conveyed to the designer by a series of stress-strain curves to failure, with two curves for each biaxial-stress ratio of interest. One curve would represent maximum principal stress versus the corresponding strain and the other would depict a similar stress-strain relationship corresponding to the minimum principle stress.

Unfortunately, due to brevity in reporting data, very few investigators have reported stress-strain curves for the minimum principal stresses; thus, the question as to the behavior in this direction must remain largely unavailable today. The bright aspect of this situation is that in the large majority of design situations, the designer is primarily interested in the maximum-principal-stress behavior.

Typical biaxial stress-strain curves obtained by Goodman are presented in Figure 12 in format proposed for MIL-HDBK-5. The data are presented as plots of maximum principal stress versus the corresponding strain for various values of biaxial-stress ratio. These particular plots happen to cover tension-tension/loading only (i.e., both in-plane principal stresses are tension); these are primarily of interest in internally pressurized structures with limited externally applied compressive loadings. As will be seen in Section V some investigators have conducted tests in tension-compression loading; these are primarily of interest in internally pressurized structures subject to very high externally applied loadings in the axial direction. Apparently to date very few investigators have conducted tests under loadings of both types (tension-tension and tension-compression) on the same material; in fact, probably, none on metals of aerospace importance.

Biaxial Yield-Stress Criterion

For design purposes, certain characteristics of the uniaxial stress-strain curve have become standardized design criteria. These include the yield stress (0.002 in./in. offset), ultimate stress, total elongation, etc.

In design for biaxial-stress loadings, it is also desirable to have standardized design criteria. However, in the case of yield stress, a number of different approaches have been either used or proposed, each resulting in slightly different numerical values

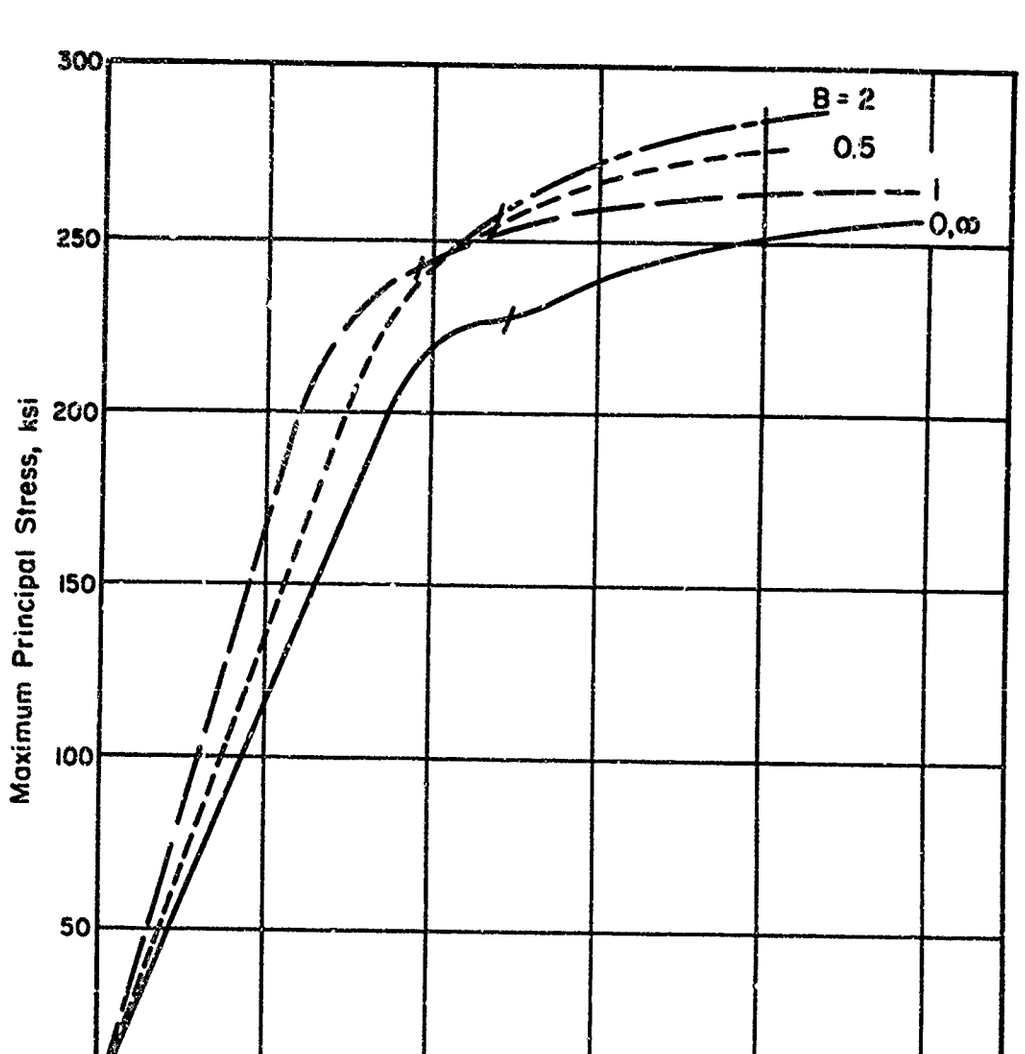

FIGURE 12. TYPICAL BIAXIAL STRESS-STRAIN CURVES AT ROOM TEMPERATURE FOR AISI 4340 ALLOY STEEL (MACHINED THIN-WALL CYLINDERS, F_{tu} = 260 KSI). A BIAXIAL RATIO B OF ZERO CORRESPONDS TO THE HOOP DIRECTION

for the biaxial yield stress even though they all reduce to the 0.002 in./in. offset strain for the case of uniaxial loading. Three different approaches or ways to determine the biaxial yield stress are described and discussed in detail in Appendix I.

The Military Handbook 5 Working Group has approved the uniform-plastic-strain criterion as the standardized criterion to be used in MIL-HDBK-5. In using this criterion, the biaxial yield stress is determined from a biaxial stress-strain curve in exactly the same way as the uniaxial yield stress is found from a uniaxial stress-strain curve. As shown in Figure 13, a straight line (called the offset line) is drawn from the 0.002 in./in. point on the abscissa, parallel to the straight-line (elastic) portion of the stress-strain curve, to the point p where it intercepts the stress-strain curve. The stress value at which the offset line intersects the stress-strain curve is the yield stress. It is noted that although the offset lines for various biaxial-stress ratios (including uniaxial) all emanate from the same point, they do not all have the same slope since the elastic portions of the curves do not all have the same slope (biaxial modulus - see "Elastic Deformation Under Biaxial Stress").

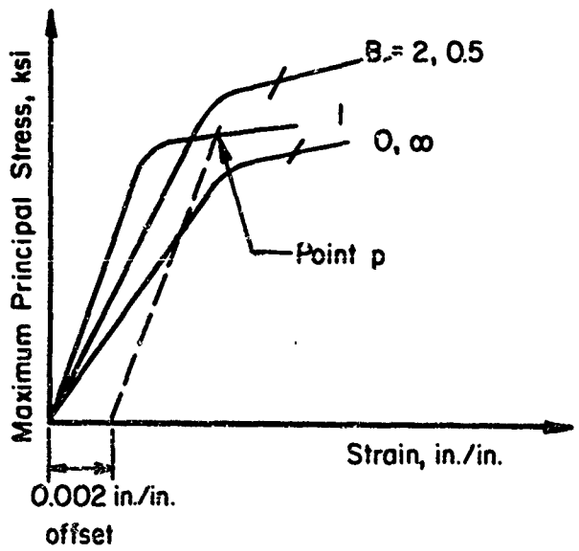

FIGURE 13. UNIFORM-PLASTIC-STRAIN YIELD CRITERION FOR UNIAXIAL AND BIAXIAL LOADINGS

Biaxial Ultimate-Stress and Other Criteria

As in uniaxial loading, the ultimate stress for biaxial-stress conditions is defined simply as the highest nominal stress value reached. One of the minor problems in connection with this criterion is the old one as to how to distinguish between the ultimate stress and the rupture (or fracture) stress if the highest stress level reached occurred at fracture. However, in such a case the material must be quite "brittle", and there is no reason why the same numerical value cannot be reported for both quantities.

Another perculiarity which has arisen recently in connection with certain specially heat treated high-strength steels is that the highest point on the stress-strain curve is

reached before the 0.002 in./in. offset strain is attained. When the 0.002 in./in. offset strain is reached the nominal stress has dropped somewhat.

Other biaxial-stress criteria of design interest but which are seldom reported include:

(1) Fracture (rupture) stress - nominal stress at final fracture

(2) Strain at fracture (total elongation) - self-explanatory

(3) Strain at ultimate stress - also self-explanatory, but believed to be more significant than strain at fracture.

Presentation of Biaxial-Stress Property Data

As stated previously in "Biaxial Stress-Strain Curves", the best way to convey biaxial-property information to the designer is in the form of a series of biaxial stress-strain curves, each for a given biaxial-stress ratio. However, often data are required at values of biaxial-stress ratio falling between those for which stress-strain curves are presented. These can be obtained by selecting points (for example, yield-stress values) from the biaxial stress-strain curves and plotting the value of one in-plane principal stress versus the other one, both values being the respective stress levels at which yielding (as defined by 0.002 in./in. offset - see "Biaxial Yield-Stress Criterion") occurs. A smooth curve drawn through a series of such points is called a biaxial-stress envelope. This envelope greatly increases the accuracy of determining the stress values corresponding to intermediate biaxial-stress ratios as compated to linear interpolation.

A technique for establishing the biaxial-stress envelope by curve fitting to a generalized second-degree ("conic") equation was presented to the MIL-HDBK-5 Working Group in April, 1963,[27] and was subsequently described in a paper[1]. Since neither of these publications have received widespread publication, this technique is presented in Appendix II for completeness. Figure 14 shows a biaxial envelope for D6AC Steel. It should be mentioned here that, although the generalized conic equation is more general than any of those associated with the four most widely used theories of strength and reduces to all of them in special cases, it is limited to curves which are never concave (looking from outside the curve, as in Figure 14 toward the origin). However, as will be seen in Figure 65, for example, biaxial-stress envelopes for certain materials occassionally do have concave regions. For such cases, the easiest way to fit a curve to the data appears to be judicious manual curve fitting. In spite of this limitation on the generalized conic approach, it does give a more quantitative way of specifying the biaxial envelope than the traditional one of saying, for example, that the biaxial-stress material behavior of the material "appears to be closer to that of the von Mises yield criterion than it is to the maximum-shear-stress theory".

Some years ago, the ANC-5 Panel (predecessor of the MIL-MDBK-5 Working Group) agreed that elevated-temperature yield stresses should be plotted in dimensionless form as percentages of the room-temperature yeild stress. Likewise, to facilitate interpolation to intermediate strength levels, it was suggested that biaxial yield-stress envelopes be plotted as percentages of the room-temperature uniaxial yield stress in a specified reference direction. This has been done in preparing envelopes for biaxial yield stress and biaxial ultimate stress in Section V and in Figure 14.

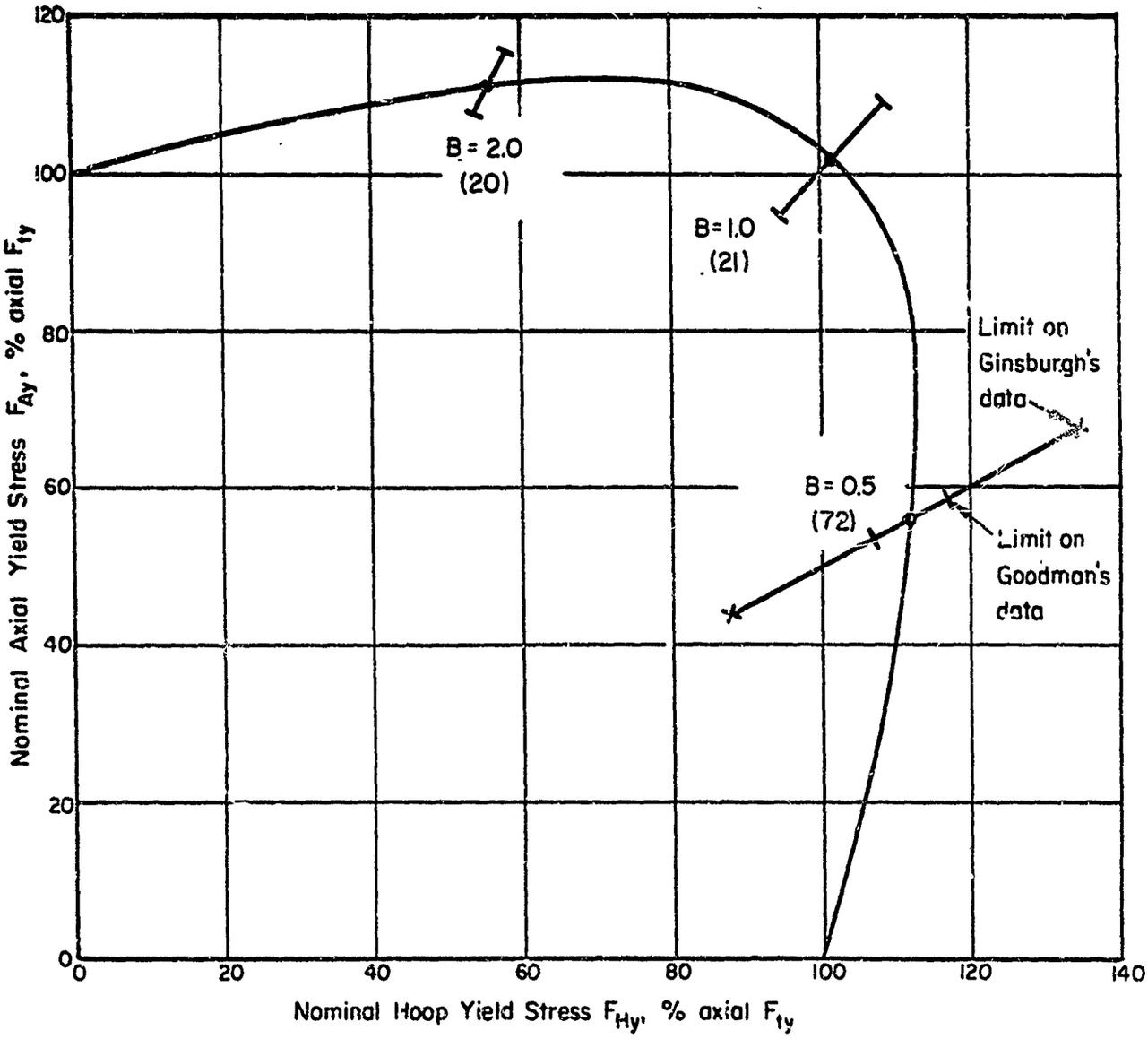

FIGURE 14. BIAXIAL YIELD-STRESS FNVELOPE AT ROOM TEMPERATURE FOR D6AC STEEL (SOLID CURVE DENOTES MEAN VALUE; NUMBERS IN PARENTHESES ARE THE NUMBERS OF DATA POINTS USED FOR EACH BIAXIAL-STRESS RATIO B). DATA FROM FIGURES 40, 41, AND 42

Most of the alloys currently in use in aircraft and space-structures applications are nearly isotropic (see "Elastic Deformation Under Biaxial Stresses"). For anisotropic materials, it is important to relate the biaxial yield stresses to the uniaxial yield stress in a reference direction. Traditionally the reference direction is defined as the longitudinal (rolling) direction for all flat products, and the hoop (circumferential) direction for shells of revolution (tubes, cones, etc.). However, to prevent any possible confusion from arising, the reference direction used for the uniaxial yield stress should always be indicated clearly.

Since the biaxial yield stress and the biaxial ultimate stress are so strongly affected by the corresponding uniaxial properties (F_{ty} and F_{tu}), it is advantageous to plot biaxial yield stress (for a specified biaxial-stress ratio B) versus uniaxial tensile yield stress and similarly biaxial ultimate stress (for a given B) versus F_{tu}. This method of data presentation is used extensively in Section V.

V

BIAXIAL PROPERTIES BY ALLOY

Biaxial data were obtained for a number of steels and light metals and are presented in this section of the report. The metals were selected to be of interest because of their structural importance in aerospace-vehicle structures. The metals chosen are not limited to those in MIL-HDBK-5.

Tables I, II, and III contain a detailed summary of pertinent data reported in the publications reviewed.

Table I is a summary of all of the available biaxial data examined and shows how much data are available as stress-strain curves, biaxial yield and ultimate stress, strain at ultimate stress, and at fracture. Individual references are identified by principal author. Only a cursory examination of Table I is needed to conclude that few materials have been evaluated sufficiently to determine biaxial stress-strain curves and biaxial yield and ultimate stress envelopes.

Table II identifies the chemical composition and heat treatment and other processing used for materials in Table I.

Table III contains a geometric description of all specimens used in obtaining the biaxial-stress information described in Table I.

Following the tables are Figures 15 through 89 that contain the detailed data described in Table I. These figures include the following types of presentations:

(1) Biaxial stress-strain curves

(2) Yield-stress envelopes

(3) Ultimate-stress envelopes

(4) For steels, effect of tensile yield stress versus nominal hoop yield stress

(5) For steels, effect of ultimate tensile stress versus nominal hoop burst stress.

As seen on these figures, relatively few biaxial-yield and ultimate-stress envelopes were found for the steels as compared with the light metals. For this reason, the curves showing the effects of tensile yield and ultimate stress on the nominal biaxial yield and burst stress were included as discussed in Section IV of this report.

The alloys for which data were found include many low-alloy steels, tool steels, precipitation-hardening stainless steels, aluminum alloys, magnesium alloys, and one titanium alloy.

The specific alloy list broken down into the two categories of Steel and Light Metals is as follows:

Steels

4130	300M
4135	X-200
4137	MBMC-1
MX-2	R-270
4140	H-11
4330M	17-7 PH
4335V	AM-350
AMS 6434	PH 15-7 Mo
4340	18 Ni
D6AC	25 Ni

Light Metals

2014-T4	7178-T6
2014-T6	AZ 31 B
2024-T	AZ 61 A
2024-T3	AZ 80 A
7075-T6	6 AL-4V

TABLE I. SUMMARY OF BIAXIAL DATA[a]

Material	Reference	Stress-Strain Curve			Yield Stress			Ultimate Stress			Strain at Ultimate			Fracture Strain			Test Temp
		B = 0.5	B = 1.0	B = 2.0	B = 0.5	B = 1.0	B = 2.0	B = 0.5	B = 1.0	B = 2.0	B = 0.5	B = 1.0	B = 2.0	B = 0.5	B = 1.0	B = 2.0	
Part A Steels																	
4130	28	--	--	--	--	--	--	--	--	--	--	--	--	--	--	--	--
	29	--	--	--	5	--	--	5	--	--	--	--	--	--	--	--	R.T.
	30	--	--	--	5	--	--	5	--	--	--	--	--	--	--	--	--
	31	√	--	--	--	--	--	1	--	--	1	--	--	--	--	--	R.T.
4135	21	√	--	--	5	--	--	5	--	--	--	--	--	--	--	--	R.T.
4137	22	--	--	--	--	--	--	2	--	--	--	--	--	--	--	--	R.T.
MX-2 or	22	--	--	--	--	--	--	4	--	--	--	--	--	--	--	--	R.T.
4137 Co	21	--	--	--	4	--	--	4	--	--	--	--	--	--	--	--	R.T.
Ditto	31	√	--	--	--	--	--	1	--	--	1	--	--	1	--	--	R.T.
4140	32	--	--	--	3	--	--	3	--	--	--	--	--	--	--	--	R.T.
4330 M	33	--	--	--	--	--	--	--	17	--	--	--	--	--	--	--	R.T.
4335-V4	21	√	--	--	4	--	--	4	--	--	--	--	--	--	--	--	R.T.
AMS-6434	31	√	--	--	--	--	--	1	--	--	--	--	--	--	--	--	R.T.
"	34	--	--	--	--	--	--	6	--	--	--	--	--	--	--	--	R.T.
AMS-6434 Mod.	32	--	--	--	2	--	--	2	--	--	--	--	--	--	--	--	R.T.
4340	35	--	--	--	3	--	--	--	--	--	--	--	--	--	--	--	R.T.
"	31	--	--	--	--	--	--	1	--	--	1	--	--	1	--	--	R.T.
"	28	√	√	√	11	10	10	14	13	13	14	13	13	14	13	13	R.T.
"	36	--	--	--	--	--	--	1	2	--	--	--	--	--	--	--	R.T.
"	26	--	--	--	--	--	--	2	--	--	--	--	--	--	--	--	R.T.
D6AC	35	--	--	--	1	--	--	--	--	--	--	--	--	--	--	--	R.T.
"	37	--	--	--	32	--	--	32	--	--	--	--	--	--	--	--	R.T.
"	28	√	√	√	21	17	20	21	17	20	21	17	20	21	17	20	R.T.
"	38	--	--	--	4	--	--	5	--	--	--	--	--	--	--	--	R.T.
"	39	--	--	--	2	--	--	2	--	--	--	--	--	--	--	--	R.T.
"	23	--	--	--	--	4	--	--	--	--	--	--	--	--	--	--	R.T.
"	40	--	--	--	12	--	--	12	--	--	4	--	--	4	--	--	R.T.
"	40	--	--	--	3	--	--	3	--	--	--	--	--	--	--	--	350 F
"	41	--	--	--	--	--	--	1	--	--	--	--	--	--	--	--	R.T.
"	41	--	--	--	--	--	--	1	--	--	--	--	--	--	--	--	340 F
300 M	21	--	--	--	1	--	--	1	--	--	--	--	--	--	--	--	R.T.
"	31	√	--	--	--	--	--	1	--	--	1	--	--	1	--	--	R.T.
"	29	--	--	--	3	--	--	5	--	--	--	--	--	--	--	--	R.T.
"	39	--	--	--	--	--	--	2	--	--	--	--	--	--	--	--	R.T.

TABLE I. (Continued)

Material	Reference	Stress-Strain Curve			Yield Stress			Ultimate Stress			Strain at Ultimate			Fracture Strain			Test Temp
		B = 0.5	B = 1.0	B = 2.0	B = 0.5	B = 1.0	B = 2.0	B = 0.5	B = 1.0	B = 2.0	B = 0.5	B = 1.0	B = 2.0	B = 0.5	B = 1.0	B = 2.0	
Part A Steels (Continued)																	
300 M	26	--	--	--	--	--	--	1	--	--	--	--	--	--	--	--	R.T.
X-200	29	--	--	--	3	--	--	5	--	--	--	--	--	--	--	--	R.T.
"	23	--	--	--	--	5	--	--	5	--	--	--	--	--	--	--	R.T.
"	26	--	--	--	--	--	--	3	--	--	--	--	--	--	--	--	R.T.
"	31	√	--	--	--	--	--	--	--	--	--	--	--	--	--	--	R.T.
MBMC-1	32	--	--	--	2	--	--	4	--	--	--	--	--	--	--	--	R.T.
"	29	--	--	--	3	--	--	5	--	--	--	--	--	--	--	--	R.T.
"	26	--	--	--	--	--	--	2	--	--	--	--	--	--	--	--	R.T.
R-270	21	√	--	--	3	--	--	3	--	--	--	--	--	--	--	--	R.T.
"	31	--	--	--	--	--	--	1	--	--	1	--	--	1	--	--	R.T.
H-11	22	--	--	--	--	--	--	3	--	--	--	--	--	--	--	--	R.T.
"	31	√	--	--	--	--	--	1	--	--	1	--	--	1	--	--	R.T.
"	31	--	--	--	--	--	--	2	--	--	--	--	--	--	--	--	350 F
"	34	--	--	--	14	--	--	17	--	--	--	--	--	--	--	--	R.T.
"	3[illegible]	--	--	--	4	--	--	4	--	--	--	--	--	--	--	--	R.T.
"	29	--	--	--	1	--	--	5	--	--	--	--	--	--	--	--	R.T.
"	39	--	--	--	--	--	--	2	--	--	--	--	--	--	--	--	R.T.
"	23	√	√	--	--	--	--	7	--	--	--	--	--	--	--	--	R.T.
"	42	--	--	--	--	--	--	8	--	--	--	--	--	--	--	--	R.T.
"	26	--	--	--	--	--	--	4	--	--	--	--	--	--	--	--	R.T.
17-7PH (TH)	33	--	--	--	--	--	--	22	11	--	--	--	--	--	--	--	R.T.
17-7PH (RH)	33	--	--	--	--	--	--	--	6	--	--	--	--	--	--	--	R.T.
AM-350	33	--	--	--	--	--	--	--	8	--	--	--	--	--	--	--	R.T.
PH15-7 Mo	34	--	--	--	--	--	--	5	--	--	--	--	--	--	--	--	R.T.
18Ni	31	--	--	--	--	--	--	2	--	--	2	--	--	2	--	--	R.T.
"	40	√	--	--	3	--	--	3	--	--	3	--	--	3	--	--	R.T.
25Ni	43	--	--	--	1	--	--	1	--	--	--	--	--	--	--	--	R.T.
Part B Light Metals																	
2014-T4	44	√	B = -0.2,	-0.46,	-0.73,	-1.0	Compression and Press										
2014-T6	45	1	1	--	--	--	--	--	--	--	--	--	--	1	1	1	R.T.
2024-T	8	--	1	--	1	1	1	1	1	1	--	-	--	--	--	--	R.T.
"	12	√	B = ∞,	-5,	-2.5,	-1.5,	-1.25	Tension and Torsion									

TABLE I. (Continued)

Material	Reference	Stress-Strain Curve			Yield Stress			Ultimate Stress			Strain at Ultimate			Fracture Strain			Test Temp
		B = 0.5	B = 1.0	B = 2.0	B = 0.5	B = 1.0	B = 2.0	B = 0.5	B = 1.0	B = 2.0	B = 0.5	B = 1.0	B = 2.0	B = 0.5	B = 1.0	B = 2.0	
Part B Light Metals (Continued)																	
2024-T3	46	--	--	--	--	--	--	--	--	--	--	--	--	--	--	--	R.T.
7075-T6	47	1	1	--	--	--	--	2	3	3	--	--	--	--	--	--	R.T.
7075-T6	46	--	--	--	--	--	--	--	--	--	--	--	--	--	--	--	R.T.
7178-T6	28	1	1	1	2	2	2	2	2	2	--	--	--	--	--	--	R.T.
AZ31B	48	--	--	--	--	--	--	--	--	--	--	--	--	--	--	--	R.T.
AZ61A	48	--	--	--	--	--	--	--	--	--	--	--	--	--	--	--	R.T.
AZ80A	48	--	--	--	--	--	--	--	--	--	--	--	--	--	--	--	R.T.
6AL4V	28	3	3	3	3	1	3	3	1	4	--	--	--	--	--	--	R.T.

(a) Numbers indicate number of individual biaxial-stress tests represemed. Check marks indicate sources used for typical stress-strain curves.

TABLE II. CHEMICAL ANALYSES AND PROCESSING

Material	Reference	Melting Method	Chemical Composition, percent by weight								
			C	Mn	P	S	Si	Ni	Cr	Mo	V
											Part A.
4130	28	No data available									
"	29	Unknown	0.32	0.47	0.009	0.012	0.23	--	1.00	0.16	--
"	30	Unknown	0.32	0.47	0.009	0.012	0.23	--	1.0	0.16	--
"	31	Unknown	--	--	--	--	--	--	--	--	--
4135	21	Air	0.34	0.56	--	--	0.24	0.12	0.92	0.18	--
4137	22	Unknown	0.39	1.00	0.010	0.010	1.00	--	1.10	0.25	--
MX-2 or	22	Unknown	0.39	0.70	0.010	0.010	1.00	--	1.10	0.25	0.15
4137 Co	21	Air	0.41	0.72	--	--	0.88	0.04	1.01	0.28	0.14
	31	Unknown	0.40	0.63	0.008	0.004	0.90	0.09	0.93	0.27	0.15
4140	32	Air	0.40	0.81	0.014	0.013	0.22	0.35	0.66	0.22	--
4330M	33	No data available									
4335-VA	21	Air	0.40	0.79	--	--	0.33	1.76	0.82	0.35	0.19
AMS-	31	Unknown	0.38	0.76	0.006	0.007	0.43	1.81	0.79	0.35	0.19
6434	34	Unknown	0.35	0.50	0.02	0.02	0.30	1.80	0.75	0.35	0.20
AMS-	32	Air	0.35	0.68	0.013	0.010	0.24	1.64	0.77	0.42	0.29
6434 Mod.											
4340	35	Unknown	0.39	0.69	0.008	0.012	0.24	1.85	0.38	0.25	--
"	31	Unknown	0.42	0.66	0.010	0.013	0.31	1.87	0.88	0.26	--
"	28	Air	0.39	0.71	--	--	0.30	0.78	0.71	0.20	--
"	36	No data available									
"	26	Air	0.42	0.73	0.008	0.007	0.31	1.72	0.76	0.24	--
D6AC	35	Unknown	0.43	0.84	0.008	0.007	0.24	0.51	1.20	1.05	--
"	37	CEVA	0.44	0.70	0.007	0.008	0.24	0.51	0.97	1.04	0.07
"	28	CEVA	0.46	0.74	--	--	0.28	0.44	1.10	0.86	0.05
"	38	No data available									
"	39	CEVA	0.47	0.65	0.004	0.007	0.24	0.60	0.94	0.98	0.34
"	23	Unknown	0.49	0.78	0.007	0.006	0.25	0.53	1.01	1.05	0.06
"	40	No data available									
"	41	No data available									
300 M	21	Air	0.42	0.88	--	--	1.48	1.85	0.91	0.30	0.11
"	31	Unknown	0.43	0.90	0.006	0.008	1.70	1.92	0.90	0.31	0.11
"	29	Air	0.40	0.80	0.009	0.009	1.48	1.72	0.83	0.37	0.11
"	39	CEVA	0.42-0.44	0.62-0.67	0.010	0.005	1.52-1.63	1.85	0.70-0.93	0.28-0.41	0.10-0.19
"	26	Air	0.40-0.43	0.80-0.82	0.009-0.018	0.013	1.66-1.90	1.72-1.94	0.83	0.34-0.44	0.04-0.10
X-200	29	Unknown	0.40	0.99	0.010	0.010	1.41	--	1.98	0.40	0.07
"	23	Unknown	0.43	0.87	0.010	0.008	1.59	--	2.15	0.58	0.07
"	26	CEVA	0.45	0.82	0.008	0.008	1.55	0.077	2.00	0.40	0.06
"	26	Air	0.42	0.80	0.011	0.009	1.57	--	2.06	0.51	0.07
MBMC-1	32	Air	0.44	0.84	0.010	0.015	1.72	0.39	0.72	0.20	0.02
"	29	Air	0.39	0.79	0.016	0.016	1.68	--	0.80	--	0.05
"	26	Air	0.44	0.82	0.020	0.018	1.68	--	1.58	--	0.05

DATA FOR MATERIALS IN TABLE I

Others	Heat Treatment: Austenitising Temp, F	Austenitising Time, min	Quench Medium	Quench Temp, F	Tempering Temp, F	Tempering Time, hr	Fabrication Method
Steels							
--	1625	60	Salt	400	400 800	2 2	Roll and Weld
--	1625	60	Salt	400	400	2	Roll and Weld
--	1625	20	Oil	--	450	2	--
--	No further data available			--	--	--	Deep drawn
--	1700-1725	--	Oil Salt	400	500 600		Deep drawn
1.00 Co	1700	30-45	Oil	--	550	Twice	Deep drawn
1.09 Co	1700	--	--	--	550	Twice	Deep drawn
1.03 Co 0.06 Al	1700	25	Oil	--	550	2+1-1/2	Deep drawn
--	1550	120	Oil	--	450	2+2	Deep drawn
--	No further data available			--	--	--	Deep drawn
0.038 Al	1625	20	Oil	--	450	2+1	Deep drawn
--	1575	Unknown	Oil	--	Various	Unknown	Roll and Weld
--	1600	120	Oil	--	450	2+2	Deep drawn
--	1525	Unknown	Oil	--	425-900	Twice	Roll and Weld
--	1625	20	Oil	--	450	2+1	Deep drawn
--	1525	10	Oil	--	Various	4	Machined forging
--	1550	30	Oil	--	400	2.5	Roll and Weld
--	1550	Unknown	Air	--	800	Twice	Roll and Weld
--	1550	30	Salt	400	300-1150	--	Machined forging
--	1550	45	Air	--	--	4	Machined forging
--	--	--	--	--	--	--	--
--	1550	60	Air	--	600	2+2	Sheet material
--	No further data available			--	--	--	Deep drawn
0.05 Al	1750	20	Oil	--	600	2+1	Deep drawn
--	1600-1700	60	Salt Air	400 --	600	2+2	Roll and Weld
0.06-0.10 Al	1650	60	Salt Air	400 --	605-600	2+2	Roll formed
0.86 Cu	1600	30	Oil	--	600	2.5	Roll and Weld
--	1750	30	Air	--	700	0.5	Roll and Weld
	1750	60	Argon	--	700	1	
--	1750	30	Air	--	1000 800 600	1 1 1	Flat Specimens
--	1750	15	Air	--	600	2.5	Roll and Weld
--	1750	15	Air	--	700		
--	1600	120	Oil	--	600	2+2	Deep drawn
--	1600	60	Oil Salt	-- 400	600	1.0	Roll and Weld
--	1600	30	Salt	400	600	2.5	Roll and Weld

TABLE II.

Material	Reference	Melting Method	Chemical Composition, percent by weight C	Mn	P	S	Si	Ni	Cr	Mo	V
											Part A.
R-270	21	Air	0.46	0.62	--	--	1.13	1.06	1.68	0.52	0.21
"	31	Unknown	0.45	0.55	0.007	0.003	1.22	1.28	1.70	0.47	0.20
H-11	22	No data available									
"	31	Unknown	0.42	0.29	0.013	0.009	0.87	--	4.81	1.33	0.51
"	34	Unknown	0.40	0.30	0.010	0.010	0.90	--	5.00	1.30	0.50
"	32	Unknown	0.38	0.43	0.012	0.012	1.08	0.08	5.02	1.35	0.45
"	29	Unknown	0.41	0.44	0.009	0.006	0.91	--	5.29	1.36	0.51
"	39	Unknown	0.40-0.45	0.20-0.40	0.02	0.02	0.80-1.00	--	4.75-5.25	1.20-1.40	0.40-0.60
"	23	Unknown	0.43	0.37	0.001	0.003	0.89	--	4.84	1.29	0.54
"	42	No data available									
"	26	Air	0.39-0.41	0.32-0.40	0.008-0.019	0.006-0.011	0.84-0.92	--	5.03-5.16	1.20-1.34	0.47-0.50
17-7Ph (TH)	33	No data available									
17-7Ph (RH)	33	No data available									
AM-350	33	No data available									
PH15-7 Mo	34	Unknown	0.07	0.50	0.02	0.02	0.30	7.10	15.10	2.25	--
18 Ni	31	Unknown	0.02	0.02-0.07	0.004-0.007	0.008-0.009	0.04-0.08	18.43-19.00	--	4.9	--
25 Ni	43	Unknown	0.03	0.011	--	--	<0.01	24.4	--	--	--

Material	Reference	Si	Fe	Cu	Mn	Cr	Zn	Mg
								Part B.
2014-T4	44	0.8	--	4.4	0.8	--	--	0.4
2014-T6	23	0.5-1.2	1.0	3.9-5.0	0.40-1.20	0.10	0.25	0.20-0.80
2014-T6	45	0.8	--	4.4	0.8	--	--	0.4
2024-T	12	--	--	4.4	0.6	--	--	1.5
7075-T6	47	--	--	1.6	Trace	Trace	--	2.5
7178-T6	28	0.28	--	0.46	0.74	1.10	--	--
AZ31B	48	0.01	0.009	0.01	0.27	--	0.90	Bal.
AZ61A	48	0.01	0.001	0.01	0.22	--	0.74	Bal.
AZ80A	48	0.01	0.001	0.01	0.27	--	0.43	Bal.
6AL-4V	28	--	0.18	0.025	--	--	--	--
6Al-4V	28	--	0.15	0.022	--	--	--	--
6Al-4V	28	--	0.15	0.025	--	--	--	--

(Continued)

Others	Heat Treatment: Austenitizing Temp, F	Austenitizing Time, min	Quench Medium	Quench Temp, F	Tempering Temp, F	Tempering Time, hr	Fabrication Method
Steels (Continued)							
0.32 W; 1.70 Co	No further data available		--	--	--	--	Deep drawn
0.035 Al; 0.31 W	1750	20	Oil	--	600	2+2	Deep drawn
--	1850	15	Oil	--	975	2+2+2	Deep drawn
--	1850	--	Air	--	--	--	Roll and Weld
--	1850	120	Air	--	1000	2+2+2	Deep Drawn
					1100	2+2+2	Deep Drawn
--	1850	60	Air	--	1000	2+2	Roll and Weld
					1025	2	Roll and Weld
--	1850	60	Air	--	1000	2+2	Nearly flat sheet
--	1850	30	Air	--	1000	2+2	Hydrospin and weld
--	1900	15	Air	--	1000	2.5	Roll and Weld
	1850	20			900	2.5	Roll and Weld
1.17 Al	Standard "TH" Treatment			--	--	--	Roll and Weld
7.6-9.4 Cr, 0.39-0.55 Ti	1500 (Solut. anneal)	60	Air	--	915 (Maraged)	4	Roll and Weld
1.7 Ti	1500 (Solut. anneal)	60	Air	--	1300	4	Machined forging
					900 (Maraged)	1	

Ti	Al	Ni	Mo	Cd	Pb	Sn	O	V	H
Light Metals									
--	Bal.	--	--	--	--	--	--	--	--
0.15	Bal.	--	--	--	--	--	--	--	--
--	Bal.	--	--	--	--	--	--	--	--
--	Bal.	--	--	--	--	--	--	--	--
--	Bal.	--	--	--	--	--	--	--	--
--	Bal.	0.44	0.96	--	--	--	--	0.05	--
--	2.4	0.001	--	0.01	0.006	0.004	--	--	--
--	5.8	0.001	-	0.01	0.032	0.004	--	--	--
--	7.8	0.001	--	0.01	0.018	0.004	--	--	--
Bal.	5.2	0.023	--	--	--	--	0.018	4.1	0.009
Bal.	6.65	0.015	--	--	--	--	0.019	4.2	0.0026
Bal.	5.98	0.025	--	--	--	--	0.07	4.28	0.0049

TABLE III. GEOMETRICAL CHARACTERISTICS OF SPECIMENS IN TABLE I

Material	Reference	Type Vessel	Dimensions, inches: Wall Thickness	Length	Diameter	L/D	Type End Closures	Remarks
			Part A. Steels					
4130	28	Cyl.	0.050	5.5	2.0	2.75	Threaded	--
"	29	Cyl.	0.094	22	12	1.83	Spherical	Subscale test vessel
"	30	Cyl.	0.094	--	11.85	--	--	--
"	22	Cyl.	0.075	13.125	3.375	3.89	--	--
4135	21	Cyl.	0.050	24.0	5.75	4.17	Ellipsoidal	M-58 Falcon
4137	22	Cyl.	0.050	27.0	5.75	4.70	Ellipsoidal	Subscale test vessel
MX-2 or	22	Cyl.	0.050	27.0	5.75	4.70	Ellipsoidal	Falcon motor case design
4137 Co	21	Cyl.	0.070	12.0	3.43	3.50	Spherical	Subscale test vessel
	31	Cyl.	0.073	13.0	3.45	3.77	Spherical	Subscale test vessel
4140	32	Cyl.	0.100	53.5	11.55	4.63	Nearly flat	Subscale test vessel
4330M	33	Sph.	Unknown	0	6.50	0	--	Subscale test vessel
4335-VA	21	Cyl.	0.070	12.0	3.43	3.50	Spherical	Subscale test vessel
AMS	31	Cyl.	0.073	13.0	3.45	3.77	Spherical	Subscale test vessel
6434	34	Cyl.	Unknown	12.0	6.00	2.00	Ellipsoidal	Subscale test vessel
AMS6434	32	Cyl.	0.100	53.5	11.55	4.63	Nearly flat	Subscale test vessel
Mod.								
4340	35	Cyl.	Unknown	4.00	4.00	1.00	Flat	Subscale test vessel
"	31	Cyl	0.073	13.0	3.45	3.77	Spherical	Subscale test vessel
"	22	Cyl.	Unknown	2.00	2.00	1.00	Threaded	Subscale test vessel
"	36	Dome	Unknown	--	Unknown	--	--	RC-10 motor case
"	36	Sph.	Unknown	0	Unknown	0	--	Storage vessel
"	26	Cyl.	Unknown	8.0-14.0	8.0	1.00-1.75	Spherical	Subscale test vessel
D6AC	35	Cyl.	Unknown	4.00	4.00	1.00	Flat	Subscale test vessel
"	37	Cyl.	0.070	Unknown	10.00	Unknown	Flat bolted	Subscale test vessel
"	28	Cyl.	Unknown	2.00	2.00	1.00	Threaded	Subscale test vessel
"	38	Cyl.	Unknown	20.0	24.0	0.833	Unknown	Subscale test vessel
"	39	Cyl.	0.040	Unknown	24.0	Unknown	Unknown	Subscale test vessel
"	23	Flat cruc.	0.026	--	--	--	--	Special specimen
"	40	Cyl.	Unknown	208.0	65.0	3.20	Ellips. + skirt	Fullscale motor case
"	40	Cyl.	Unknown	21.75	14.5	1.50	Flat bolted	Subscale test vessel
"	41	Cyl.	0.080	37	37.35	0.99	Ellips. + skirt	Fullscale MM/1st stage
300M	21	Cyl.	0.070	12.0	3.43	3.50	Spherical	Subscale test vessel
"	31	Cyl.	0.073	13.0	3.45	3.77	Spherical	Subscale test vessel
"	29	Cyl.	0.082	22.0	12.0	1.83	Spherical	Subscale test vessel
"	39	Cyl.	0.123	Unknown	55.0	Unknown	Ellipsoidal	Polaris A2a 2d stage
"	26	Cyl.	0.067	8.0-14.0	8.00	1.00-1.75	Spherical	Subscale test vessel
X-200	29	Cyl.	0.072	22.0	12.0	1.83	Spherical	Subscale test vessel
"	23	Flat cruc.	0.026	--	--	--	--	Special specimen
"	26	Cyl.	0.063-0.082	8.0-14.0	8.0	1.0-1.75	Spherical	Subscale test vessel
MBMC-1	32	Cyl.	0.100	53.5	11.55	4.63	Nearly flat	Subscale test vessel
"	22	Cyl.	0.085	22.0	12.0	1.83	Spherical	Subscale test vessel
"	26	Cyl	0.082	8.0-14.0	8.00	1.0-1.75	Spherical	Subscale test vessel
R-270	21	Cyl.	0.070	12.0	3.43	3.50	Spherical	Subscale test vessel
"	31	Cyl.	0.073	13.0	3.45	3.77	Spherical	Subscale test vessel
R-32	22	Cyl.	0.050	27.00	5.70	4.73	One spherical one flat	Subscale test vessel
"	31	Cyl.	0.090	13.0	3.45	3.77	Spherical	Subscale test vessel

TABLE III. (Continued)

Material	Reference	Type Vessel	Dimensions, inches: Wall Thickness	Length	Diameter	L/D	Type End Closures	Remarks
			Part A. (Continued)					
H-11	34	Cyl.	Unknown	12.00	3.00	2.00	Ellipsoidal	Subscale test vessel
"	32	Cyl.	0.109	53.5	11.55	4.63	Nearly flat	Subscale test vessel
"	29	Cyl.	0.085	22	12	1.83	Spherical	Subscale test vessel
"	39	Cyl.	0.063	Unknown	54	Unknown	Unknown	Subscale test vessel
"	23	Cyl.	0.040	9.0	9.0	1.0	Spherical	Subscale test vessel
"	42	Cyl.	Unknown	Unknown	8.4	Unknown	Spherical	Subscale test vessel
"	26	Cyl.	0.047-0.083	8.0-14.0	8.0	1.0-1.75	Spherical	Subscale test vessel
17-7PH (TH)	33	Cyl.	Unknown	Unknown	6.50	Unknown	Unknown	Subscale test vessel
	33	Sph.	Unknown	0	6.50	0	--	Subscale test vessel
17-7PH (RH)	33	Sph.	Unknown	0	6.50	0	--	Subscale test vessel
AM-350	33	Sph.	Unknown	0	6.50	0	--	Subscale test vessel
PH 15-7 Mo	3/	Cyl.	Unknown	12.00	6.00	2.00	Ellipsoidal	Subscale test vessel
18 Ni	31	Cyl.	0.073	13.0	3.45	3.77	Ellipsoidal	Subscale test vessel
"	40	Cyl.	Unknown	28.0	40.0	0.70	Ellips. + skirt	Subscale motor case
"	40	Cyl.	Unknown	210.0	65.5	3.21	Ellips. + skirt	Fullscale motor case
"	40	Cyl.	Unknown	9.3	6.19	1.50	Flat bolted	Subscale test vessel
25 Ni	43	Cyl.	0.070	Unknown	6.00	Unknown	Unknown	Subscale test vessel
			Part B. Light Metals					
2014-T4	44	Cyl.	0.05 0.075	7.0	1.0	7.0	Threaded	Subscale test vessel
2014-T6	45	Cyl.	0.05 0.07	7.0	1.0	7.0	Threaded	Subscale test vessel
2024-T	9	Cyl.	0.10	16.0	2.0	8.0	Threaded	Subscale test vessel
	12	Cyl.	0.10	7.0	1.0	7.0	Threaded	Subscale test vessel
2024-T3	46	Cyl.	0.027-0.096	Unknown	0.375-1.5	Unknown	Unknown	Subscale test vessel
7075-T6	47	Cyl.	0.10	16.0	2.0	8.0	Threaded	--
	46	Cyl.	0.025-0.057	Unknown	0.375-0.750	Unknown	Unknown	Subscale test vessel
7178-T6	28	Cyl.	Unknown	2.00	2.00	1.0	Threaded	--
AZ31B	48	Cyl.	0.03	2.00	0.4375	4.57	Threaded	Subscale test vessel
AZ61A	48	Cyl.	0.03	2.00	0.4375	4.57	Threaded	Subscale test vessel
AZ80A	48	Cyl.	0.03	2.00	0.4375	4.57	Threaded	Subscale test vessel
6AL4V	28	Cyl.	Unknown	2.00	2.00	1.00	Threaded	Subscale test vessel

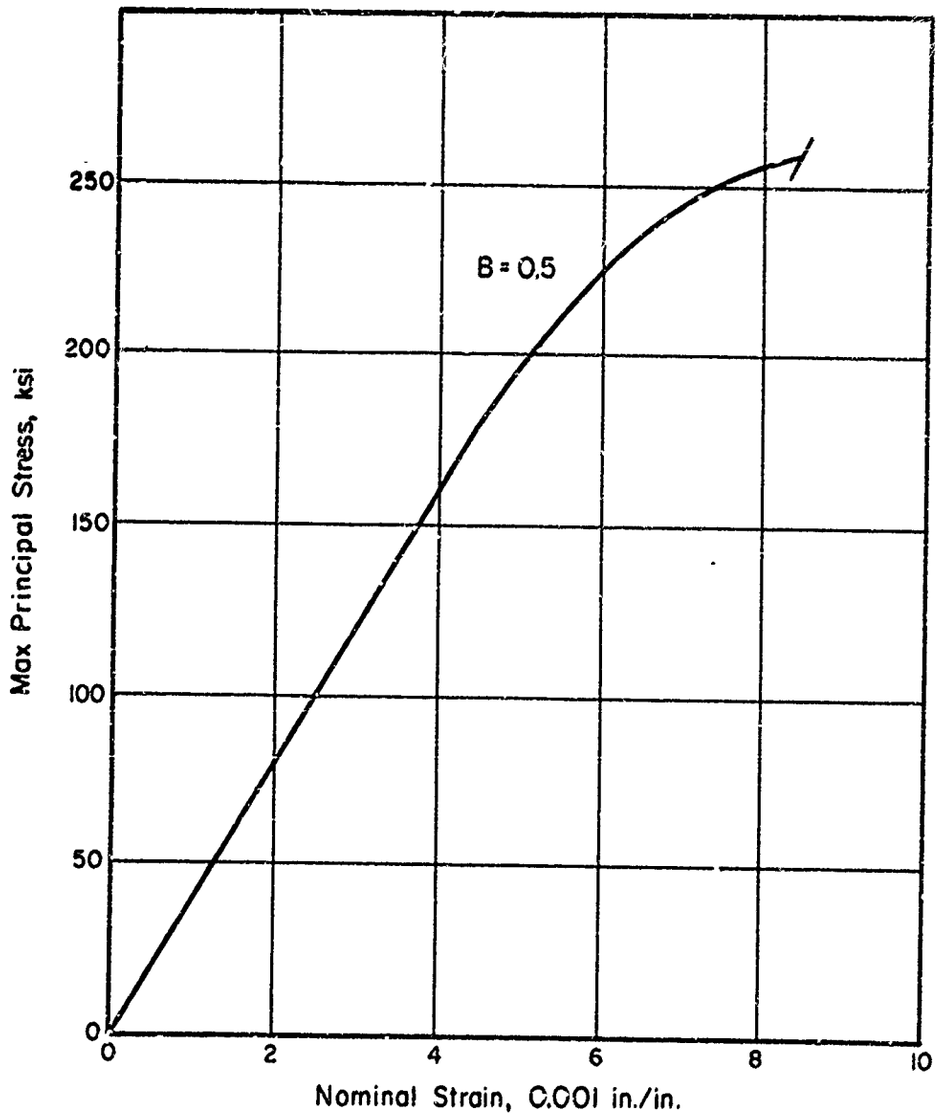

FIGURE 15. TYPICAL BIAXIAL STRESS-STRAIN CURVE AT ROOM TEMPERATURE FOR AISI 4130 STEEL. CYLINDRICAL SHELL WITH LENGTH/DIAM RATIO OF 3.89
Data Source: BHAT (31)

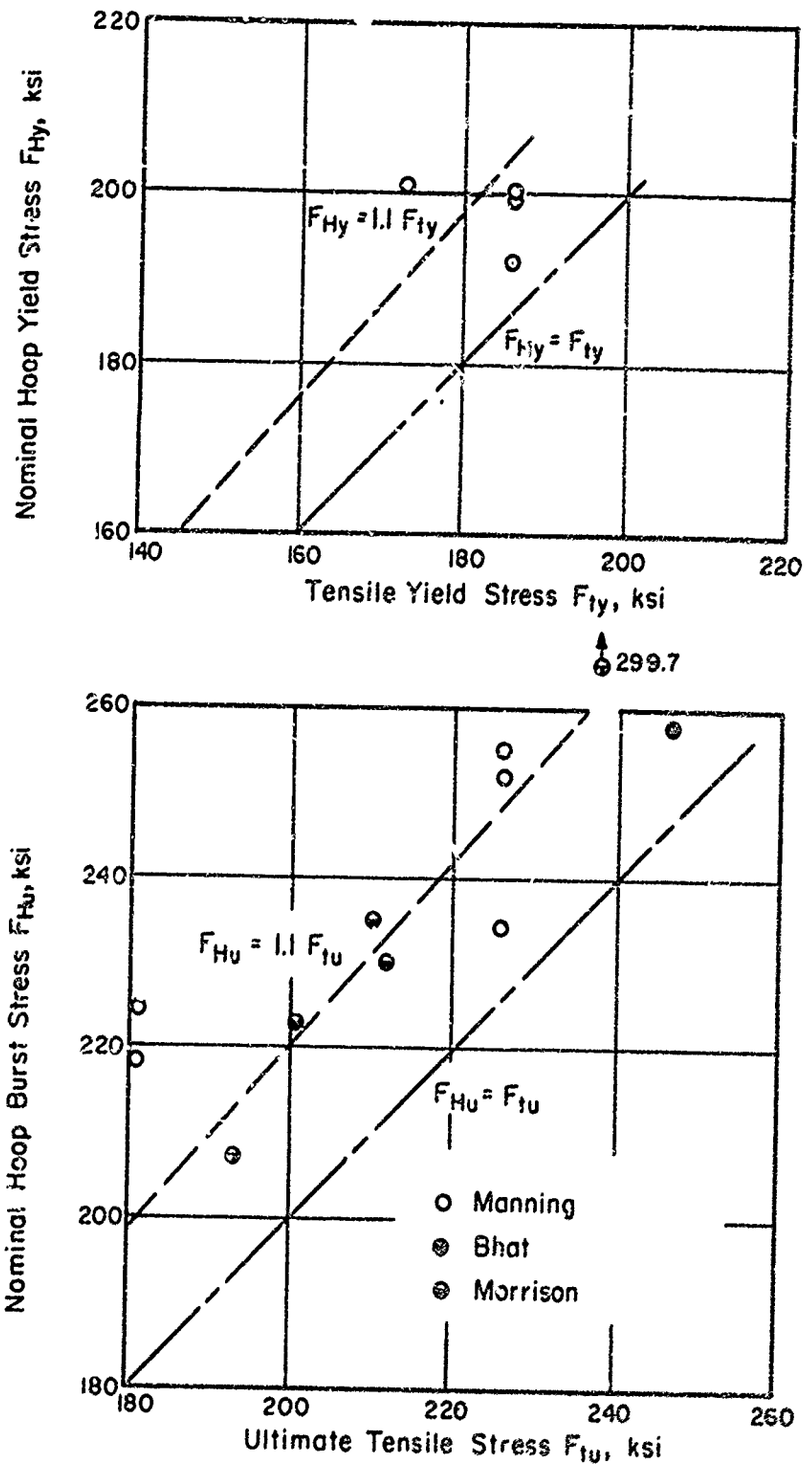

FIGURE 16. EFFECT OF TENSILE YIELD STRESS ON NOMINAL HOOP YIELD STRESS AND OF ULTIMATE TENSILE STRESS ON NOMINAL HOOP BURST STRESS AT A BIAXIAL-STRESS RATIO OF 0.5 AND ROOM TEMPERATURE FOR AISI 4130 STEEL. CYLINDRICAL SHELLS WITH LENGTH/DIAM RATIO OF 1.83 (MANNING), 3.89 (BHAT)
Data Source: Manning, Murphy, Nichols, Caine[29], BHAT[31], Morrison & Kattus[30]

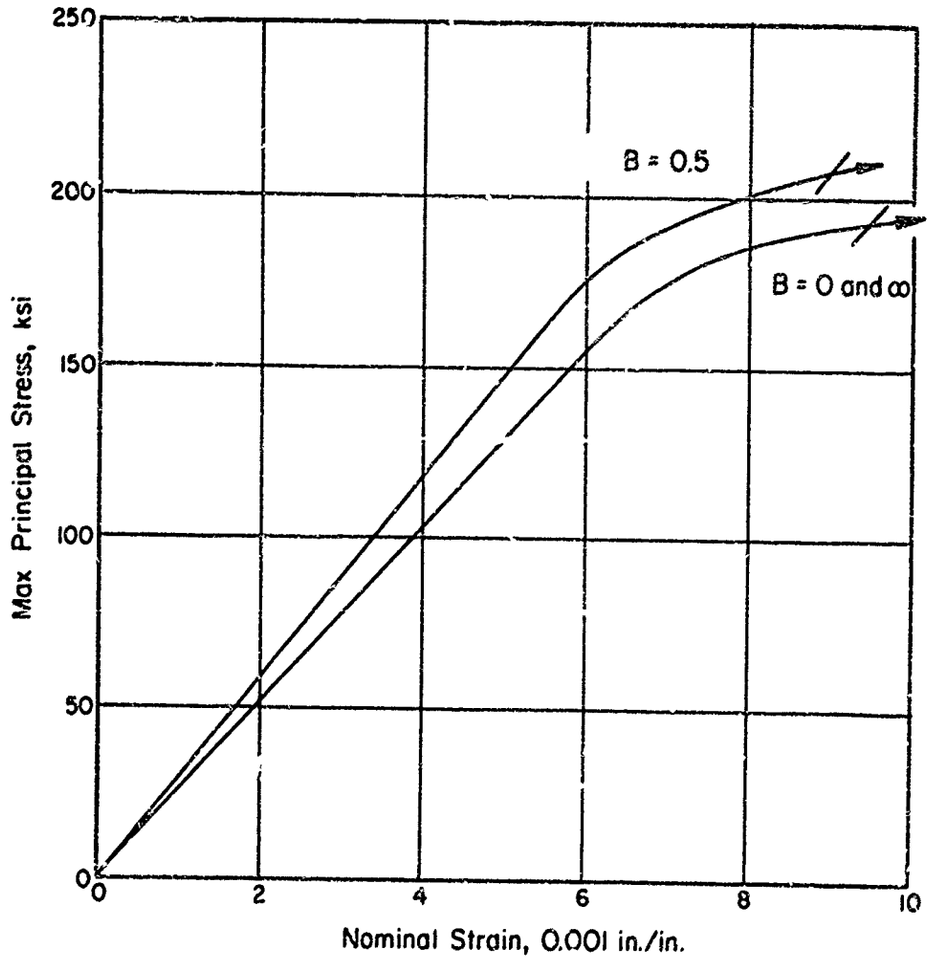

FIGURE 17. TYPICAL BIAXIAL STRESS-STRAIN CURVES AT ROOM TEMPERATURE FOR AISI 4135 STEEL. CYLINDRICAL SHELL WITH LENGTH/DIAM RATIO OF 4.17
Data Source: Bhat & Lindh (21)

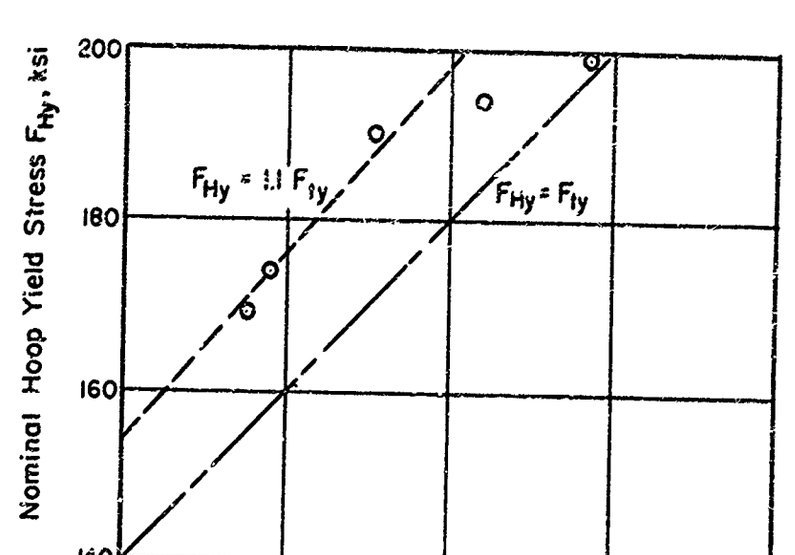

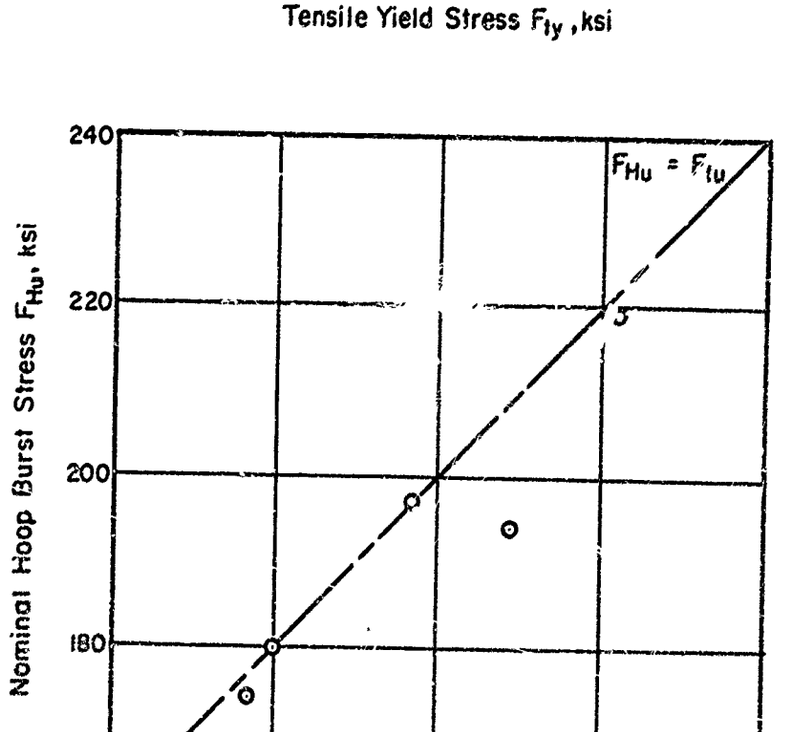

FIGURE 18. EFFECT OF TENSILE YIELD STRESS ON NOMINAL HOOP YIELD STRESS AND OF ULTIMATE TENSILE STRESS ON NOMINAL HOOP BURST STRESS AT A BIAXIAL-STRESS RATIO OF 0.5 AND ROOM TEMPERATURE FOR AISI 4135 STEEL. CYLINDRICAL SHELLS WITH LENGTH/DIAM RATIO OF 4.17
Data Source: Bhat & Lindh (21)

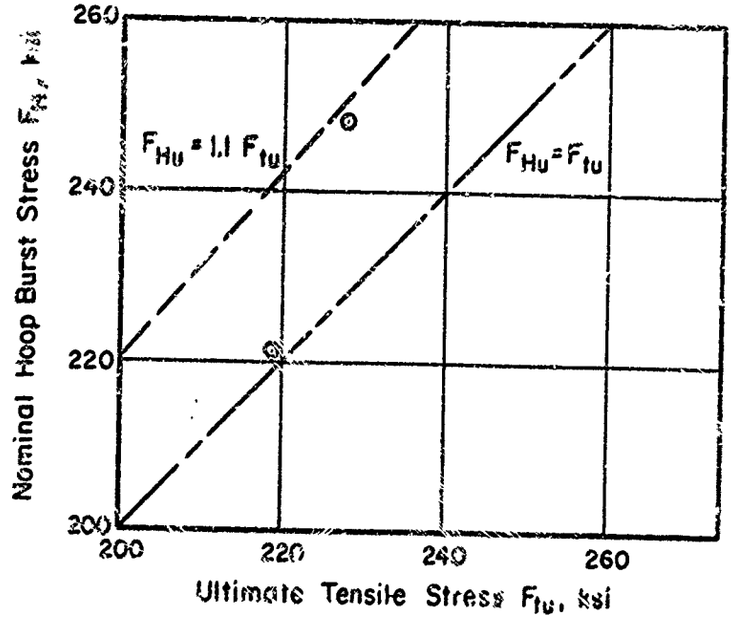

FIGURE 19. EFFECT OF ULTIMATE TENSILE STRESS ON NOMINAL HOOP BURST STRESS AT A BIAXIAL-STRESS RATIO OF 0.5 AND ROOM TEMPERATURE FOR AISI 4137 STEEL CYLINDRICAL SHELLS WITH LENGTH/DIAM RATIO OF 4.70

Data Source: Bhat (22)

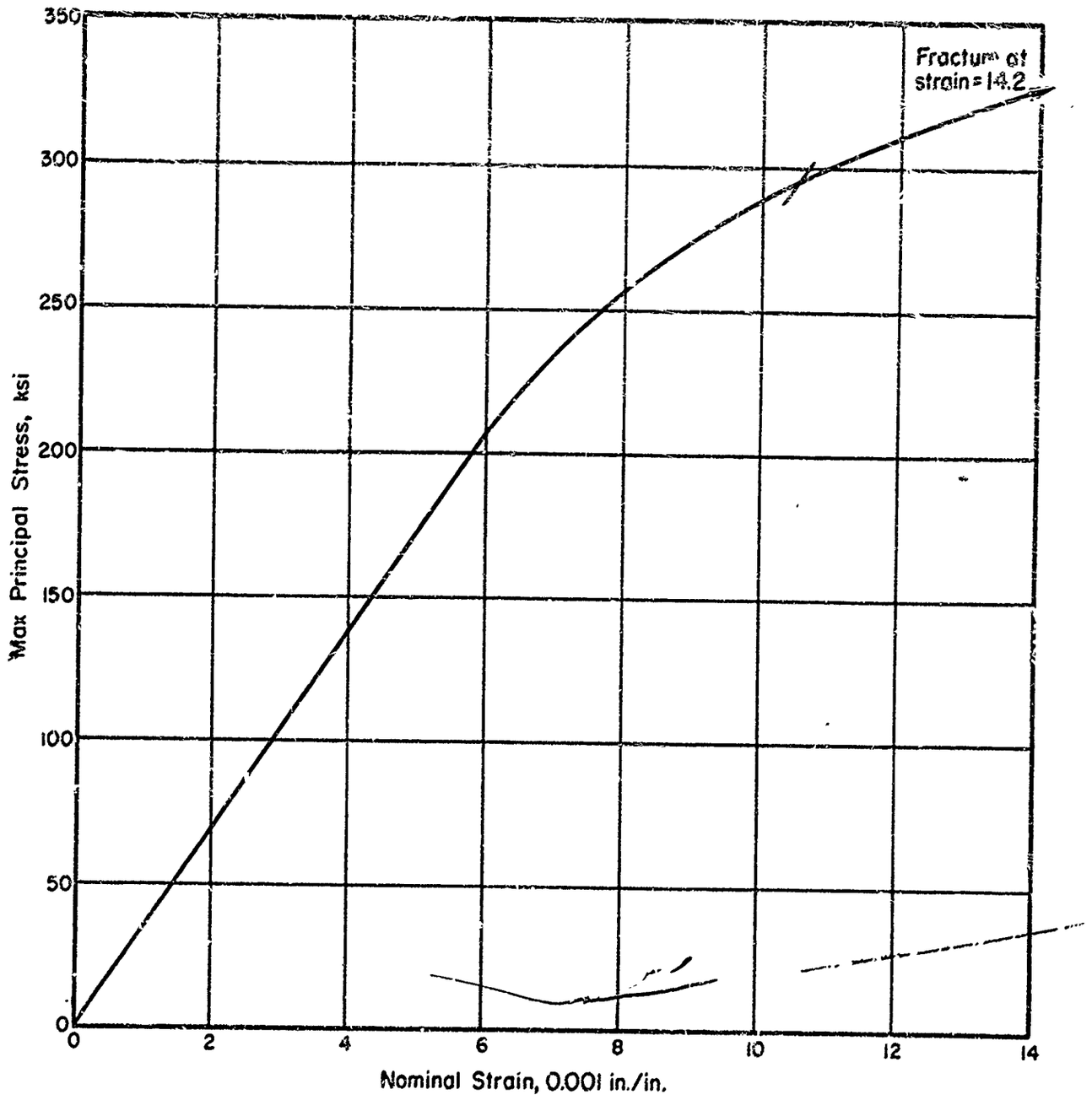

FIGURE 20. TYPICAL BIAXIAL STRESS-STRAIN CURVE AT ROOM TEMPERATURE FOR MX-2 STEEL (4137 Co) AT A BIAXIAL-STRESS RATIO OF 0.5. CYLINDRICAL SHELL WITH LENGTH/DIAM RATIO OF 3.77

Data Source: Bhat (22)

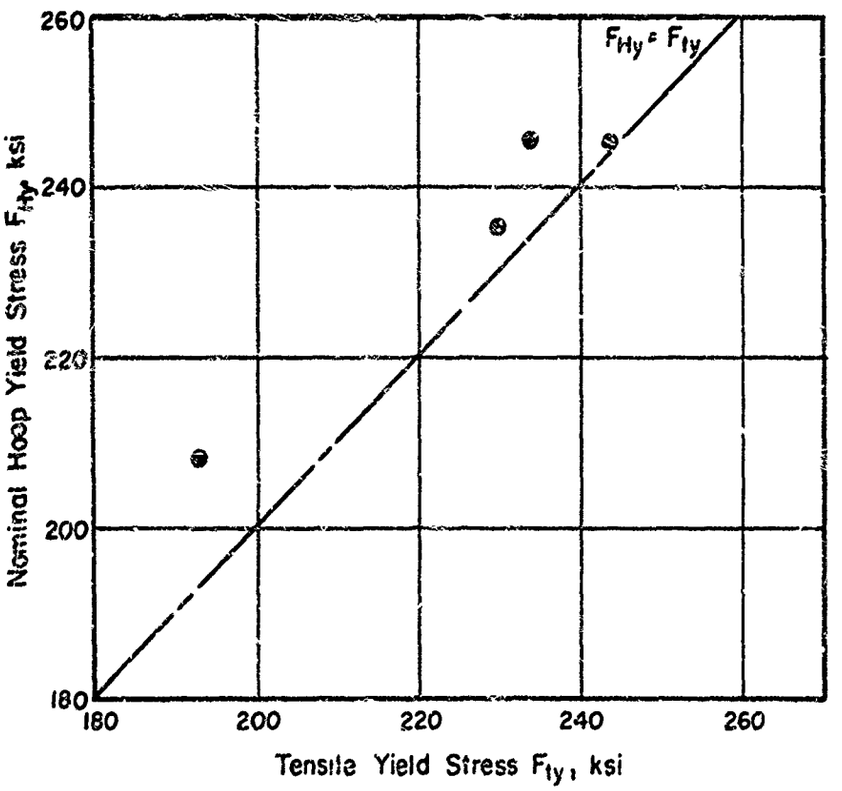

FIGURE 21. EFFECT OF TENSILE YIELD STRESS ON NOMINAL HOOP YIELD STRESS AT A BIAXIAL-STRESS RATIO OF 0.5 AND ROOM TEMPERATURE FOR MX-2 STEEL (4137 Co). CYLINDRICAL SHELLS

Data Source: Bhat & Lindh (21)

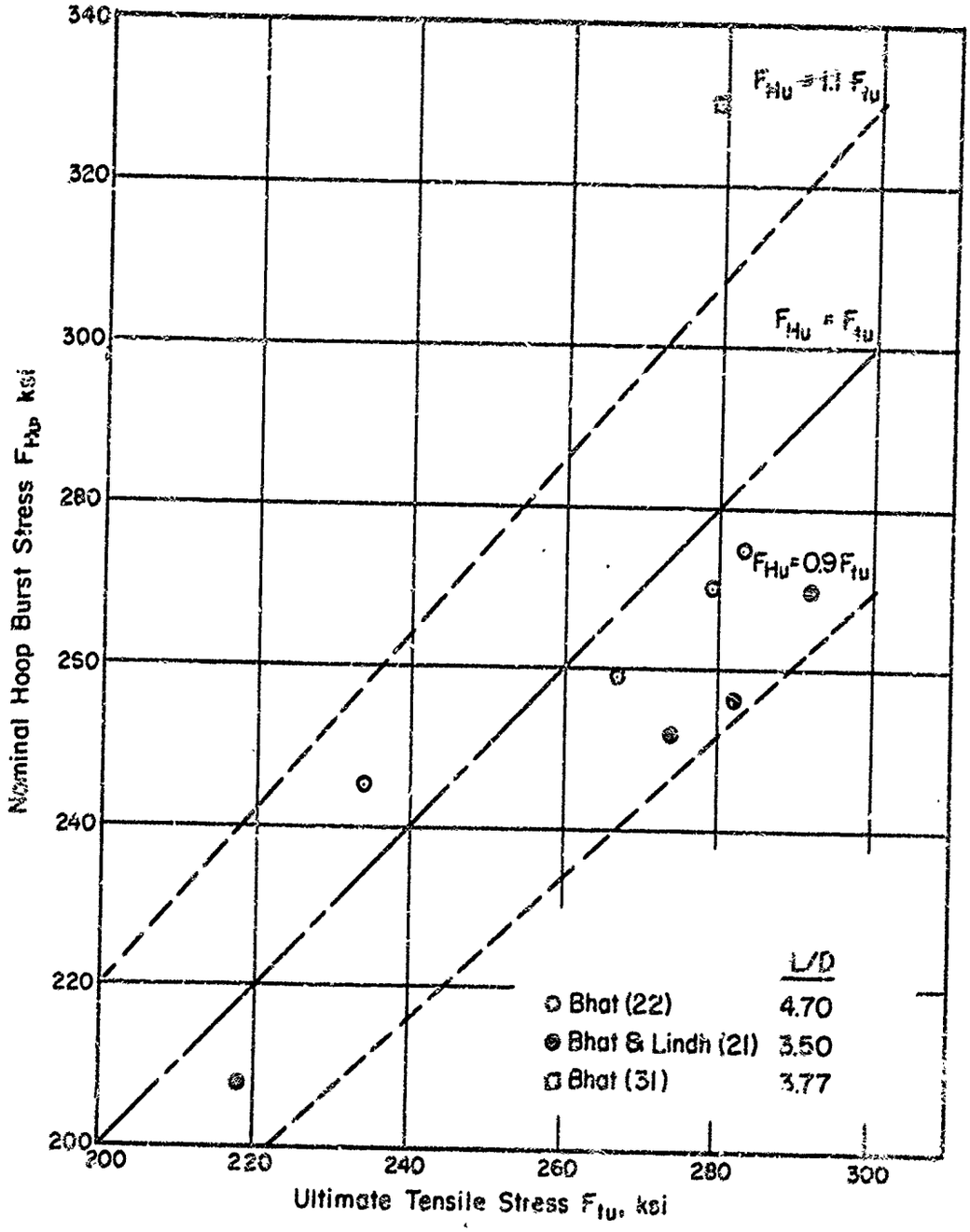

FIGURE 22. EFFECT OF ULTIMATE TENSILE STRESS ON NOMINAL HOOP BURST STRESS AT A BIAXIAL-STRESS RATIO OF 0.5 AND ROOM TEMPERATURE FOR MX-2 STEEL (4137 Co). CYLINDRICAL SHELLS WITH LENGTH/DIAM RATIOS AND DATA SOURCES INDICATED IN LEGEND

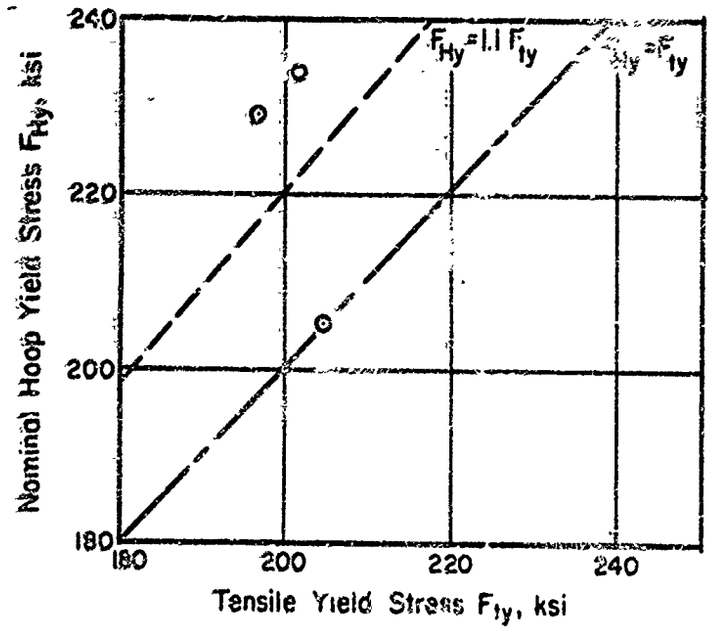

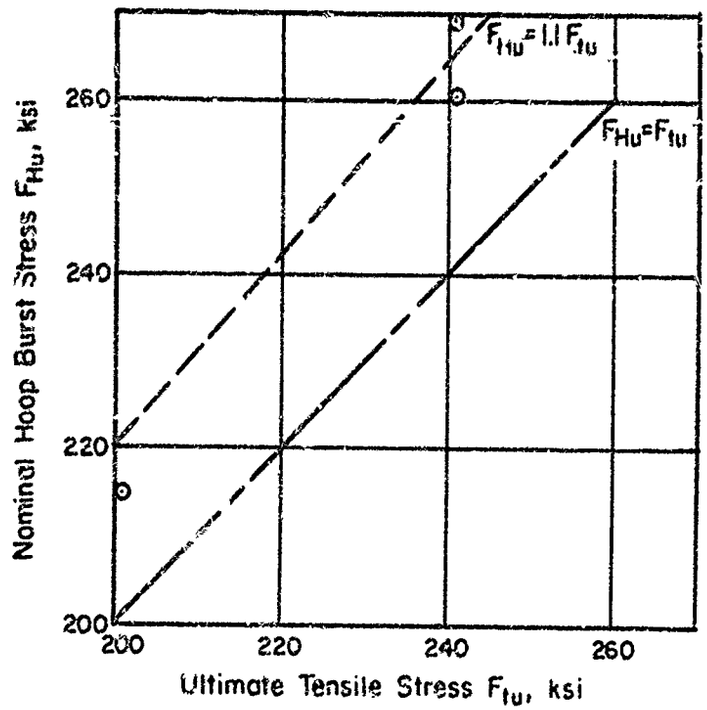

FIGURE 23 EFFECT OF TENSILE YIELD STRESS ON NOMINAL HOOP YIELD STRESS AND OF ULTIMATE TENSILE STRESS ON NOMINAL HOOP BURST STRESS AT A BIAXIAL STRESS RATIO OF 0.5 AND ROOM TEMPERATURE FOR AISI 4140 STEEL CYLINDRICAL SHELLS WITH LENGTH/DIAM RATIO OF 4.63

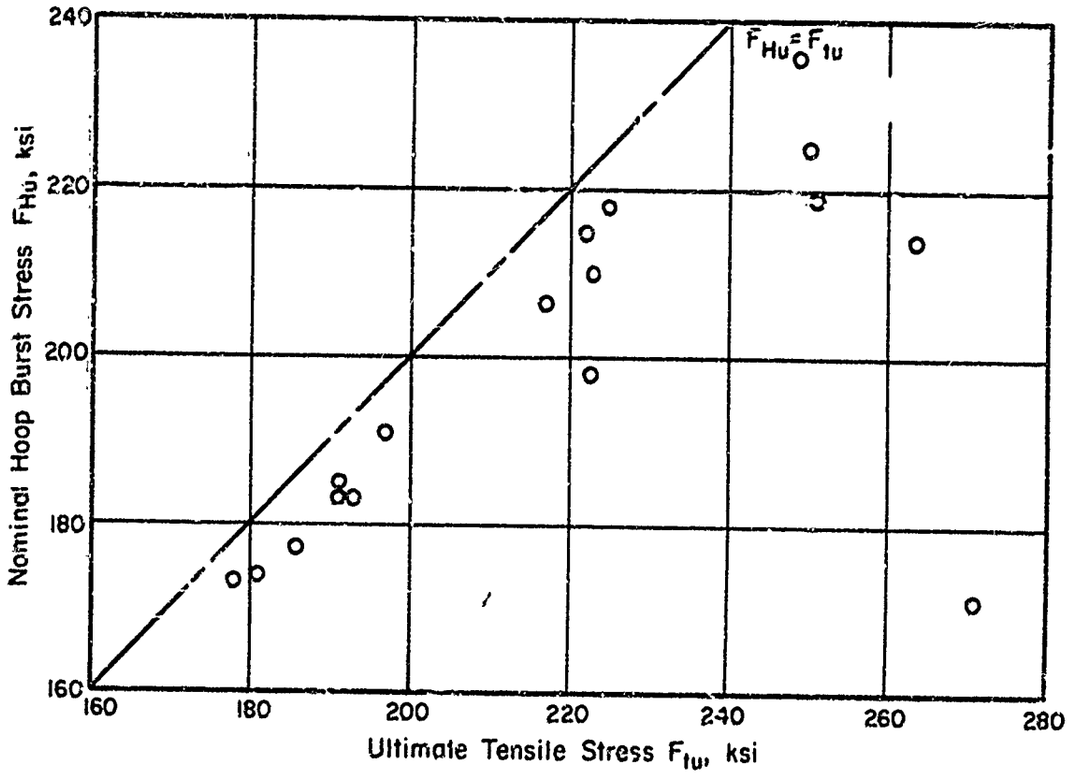

FIGURE 24. EFFECT OF ULTIMATE TENSILE STRESS ON NOMINAL HOOP BURST STRESS AT A BIAXIAL-STRESS RATIO OF 1.0 AND ROOM TEMPERATURE FOR 4330 M STEEL. SPHERICAL SHELLS

Data Source: Kinnaman et al (33)

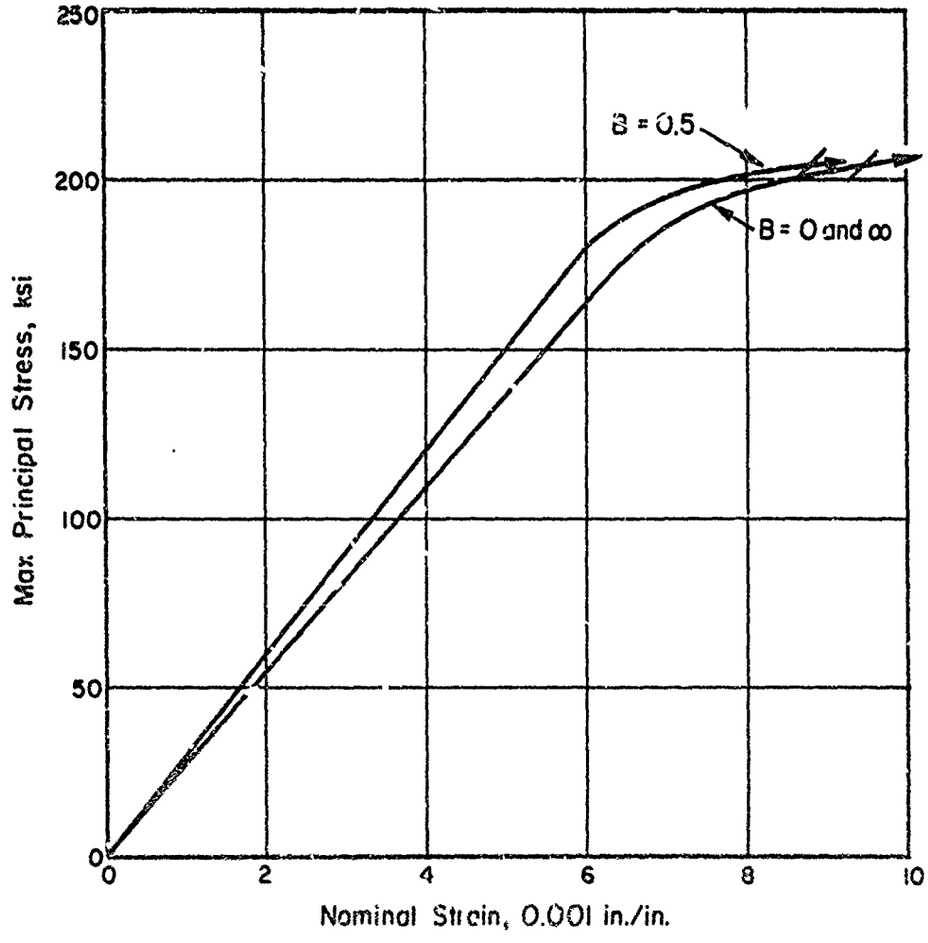

FIGURE 25. TYPICAL BIAXIAL STRESS-STRAIN CURVES AT ROOM TEMPERATURE FOR 4335-VA STEEL. CYLINDRICAL SHELL WITH LENGTH/DIAM RATIO OF 3.50
Data Source: Bhat & Lindh (21)

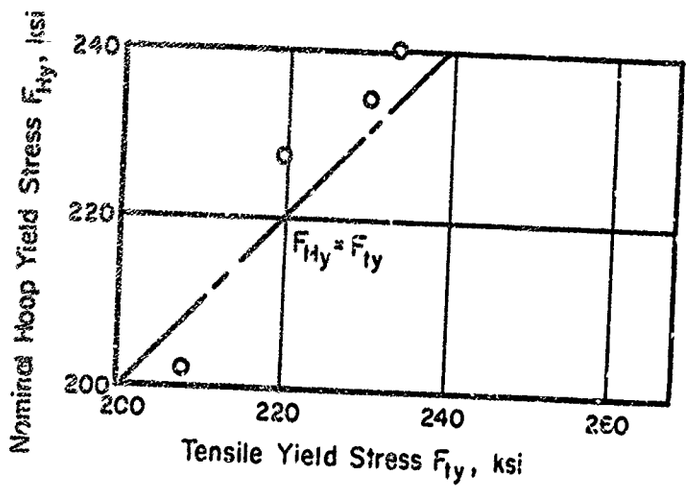

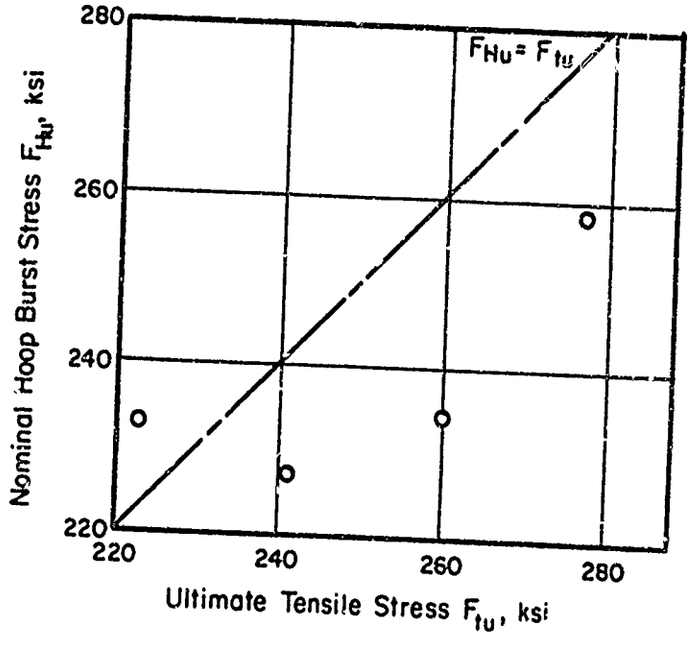

FIGURE 26. EFFECT OF TENSILE YIELD STRESS ON NOMINAL HOOP YIELD STRESS AND OF ULTIMATE TENSILE STRESS ON NOMINAL HOOP BURST STRESS AT A BIAXIAL STRESS RATIO OF 0.5 AND ROOM TEMPERATURE FOR 4335-VA STEEL. CYLINDRICAL SHELLS WITH LENGTH/DIAM RATIO OF 3.50
Data Source: Bhat & Lindh (21)

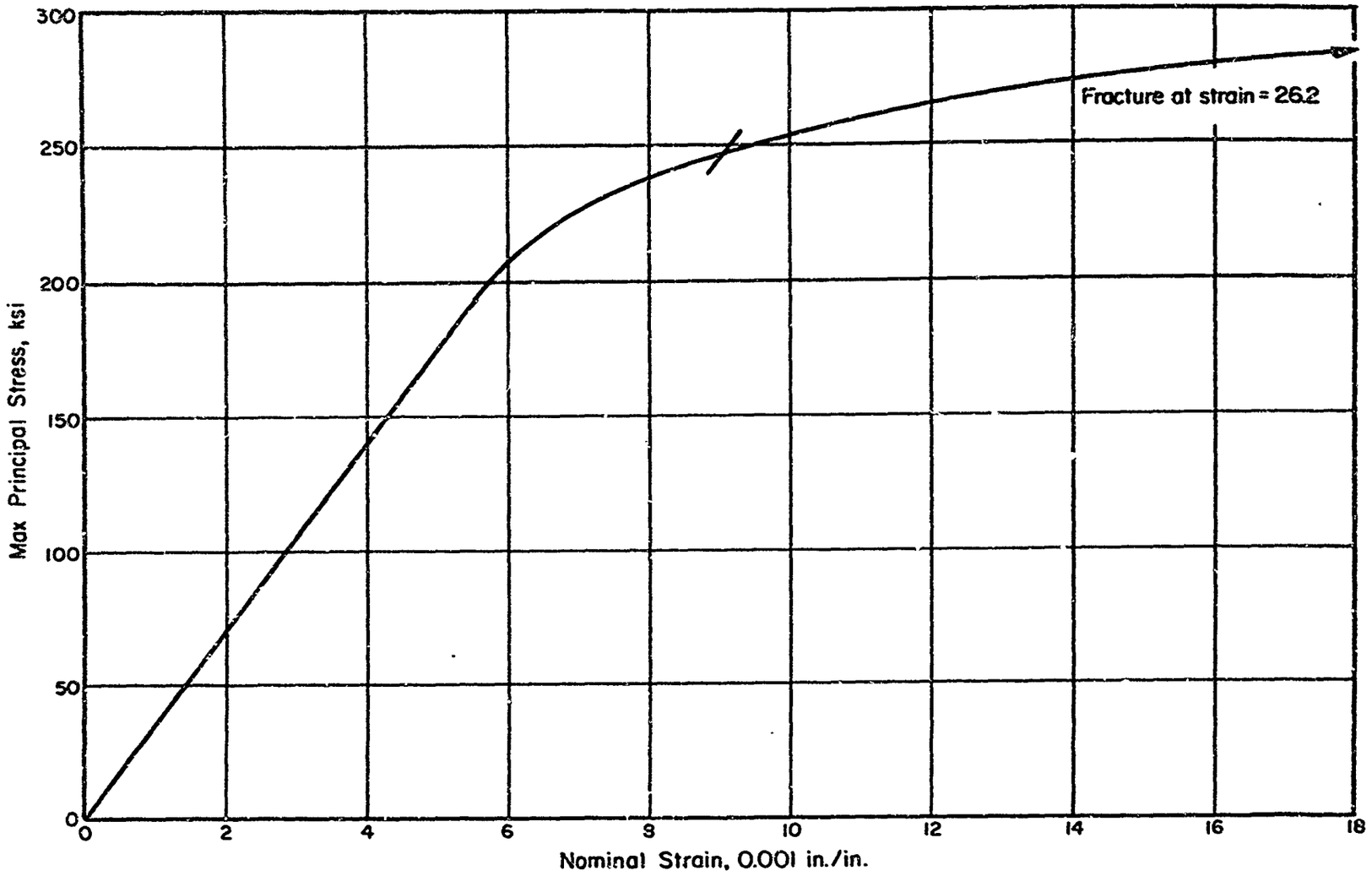

FIGURE 27. TYPICAL BIAXIAL STRESS-STRAIN CURVE AT ROOM TEMPERATURE FOR AMS 6434 STEEL AT A BIAXIAL-STRESS RATIO OF 0.5. CYLINDRICAL SHELL WITH LENGTH/DIAM RATIO OF 3.77
Data Source: Bhat (31)

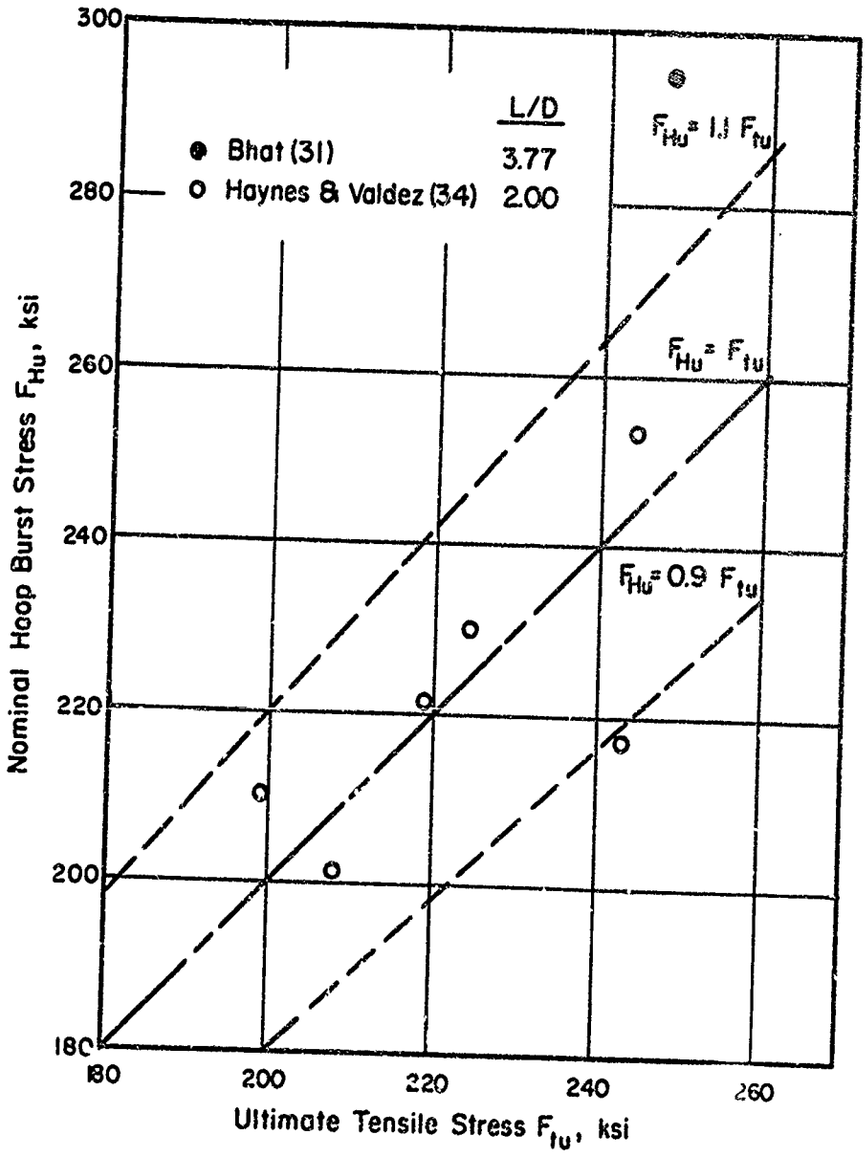

FIGURE 28. EFFECT OF ULTIMATE TENSILE STRESS ON NOMINAL HOOP BURST STRESS AT A BIAXIAL-STRESS RATIO OF 0.5 AND ROOM TEMPERATURE FOR AMS 6434 STEEL CYLINDRICAL SHELLS WITH LENGTH/DIAM RATIOS AND DATA SOURCES INDICATED IN LEGEND

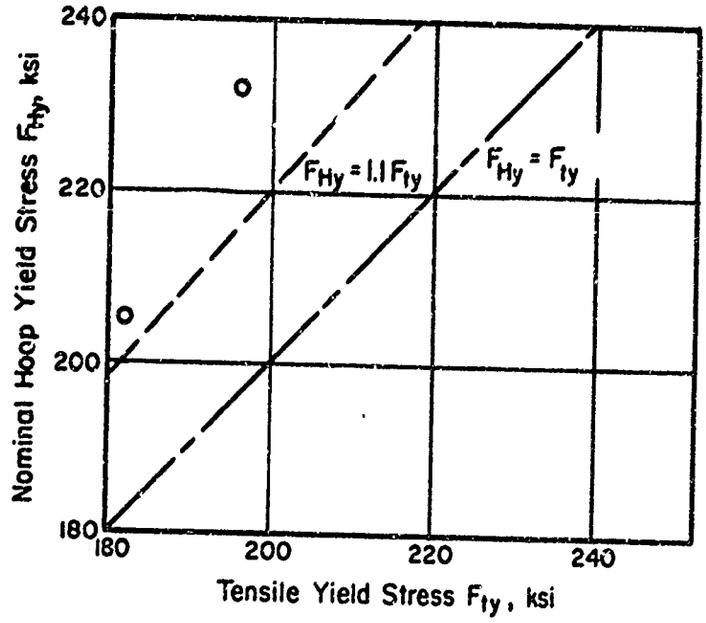

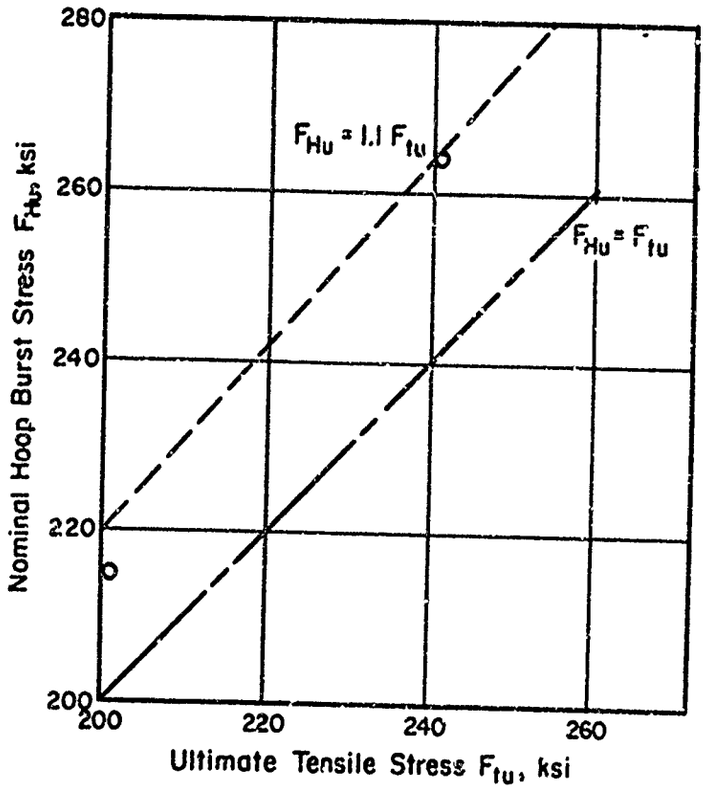

FIGURE 29. EFFECT OF TENSILE YIELD STRESS ON NOMINAL HOOP YIELD STRESS AND OF ULTIMATE TENSILE STRESS ON NOMINAL HOOP BURST STRESS AT A BIAXIAL STRESS RATIO OF 0.5 AND ROOM TEMPERATURE FOR AMS 6434 MOD STEEL. CYLINDRICAL SHELLS WITH LENGTH/DIAM RATIO OF 4.63
Data Source: Kajola & Cantor (32)

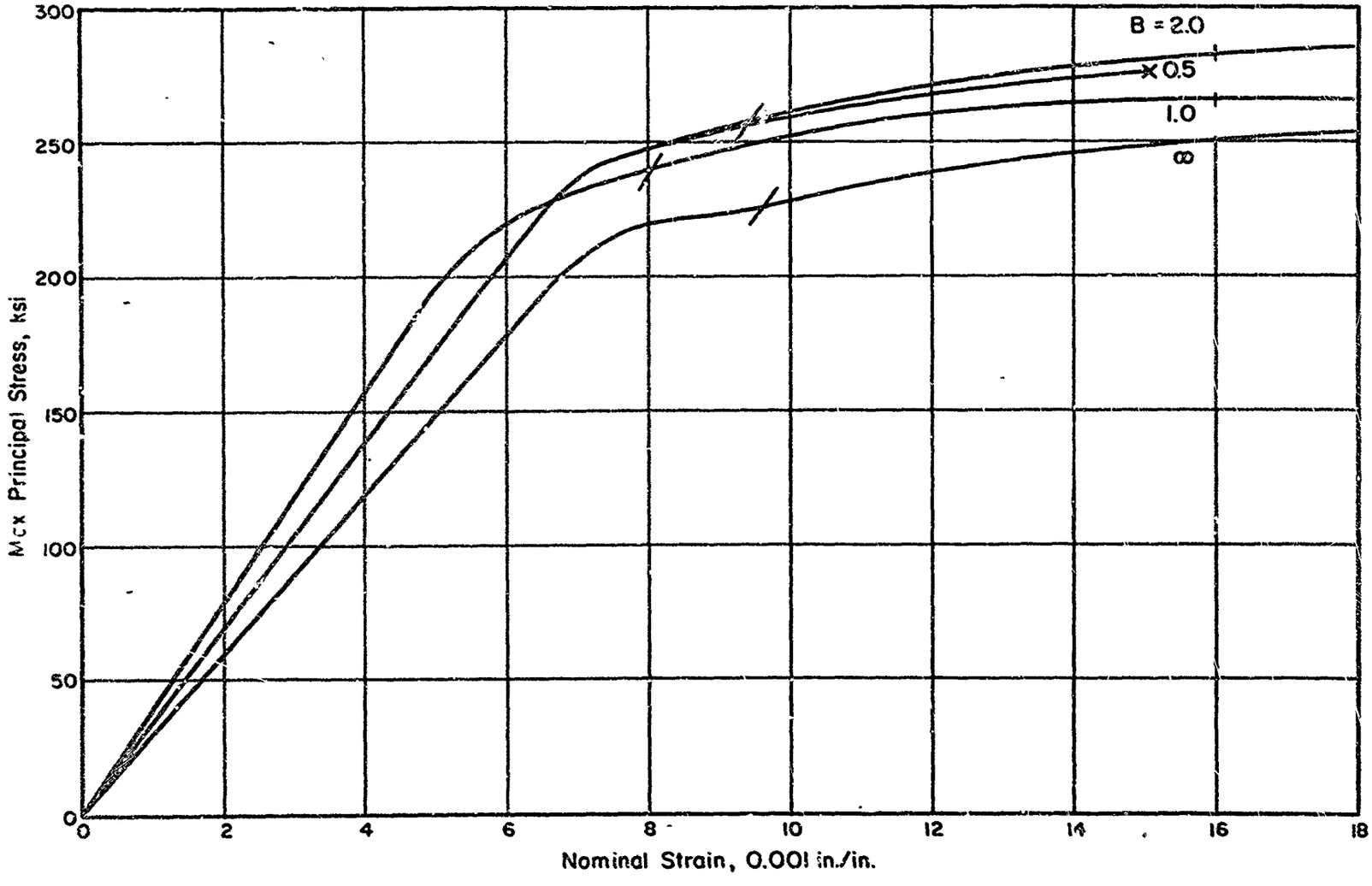

FIGURE 30. TYPICAL BIAXIAL STRESS-STRAIN CURVES AT ROOM TEMPERATURE FOR AISI 4340 STEEL. CYLINDRICAL SHELL WITH LENGTH/DIAM RATIO OF 1.0. BIAXIAL-STRESS RATIO B=0 CORRESPONDS TO THE HOOP DIRECTION
Data Source: Goodman (28)

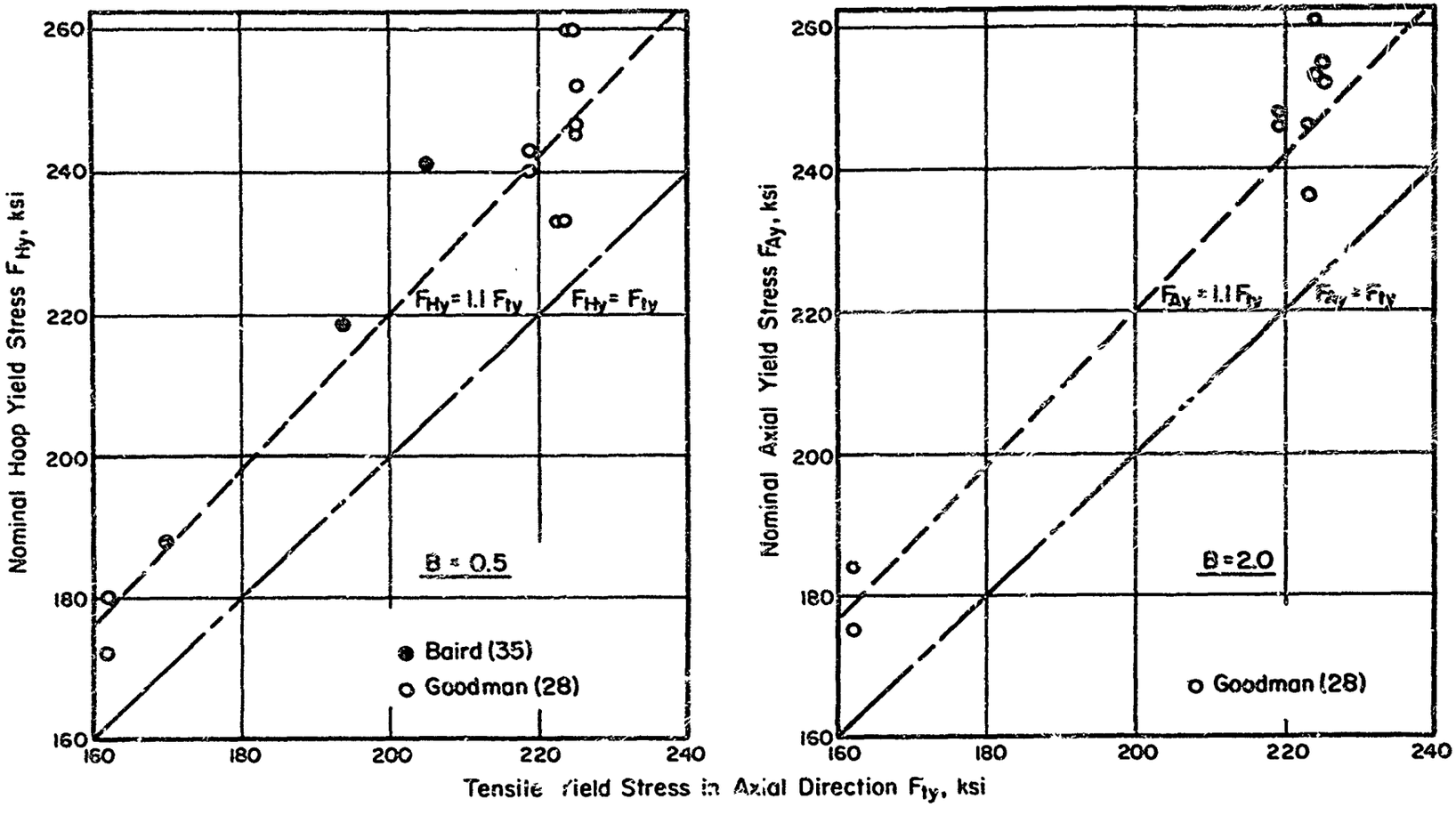

FIGURE 31. EFFECT OF TENSILE YIELD STRESS IN AXIAL DIRECTION ON NOMINAL BIAXIAL YIELD STRESS AT BIAXIAL-STRESS RATIOS OF 0.5 AND 2.0 AND AT ROOM TEMPERATURE FOR AISI 4340 STEEL. CYLINDRICAL SHELLS WITH A LENGTH/DIAM RATIO OF 1.0, DATA SOURCES INDICATED

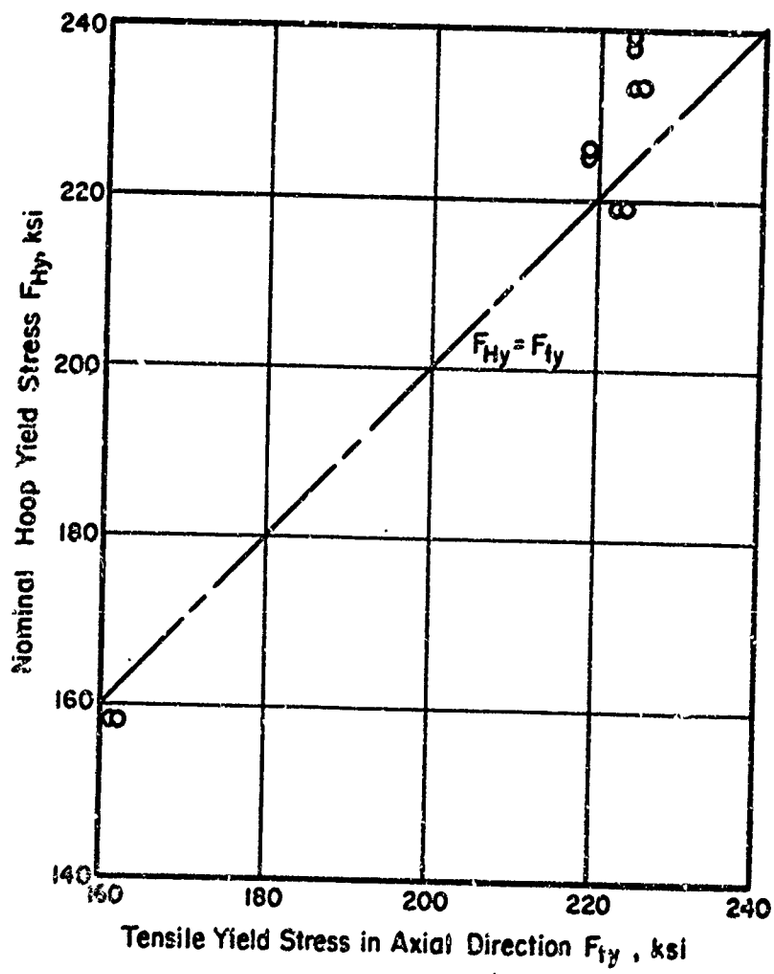

FIGURE 32. EFFECT OF TENSILE YIELD STRESS IN AXIAL DIRECTION ON NOMINAL HOOP YIELD STRESS AT A BIAXIAL-STRESS RATIO OF 1.0 AND ROOM TEMPERATURE FOR AISI 4340 STEEL. CYLINDRICAL SHELLS WITH LENGTH/DIAM RATIO OF 1.0.
Data Source: Goodman (28)

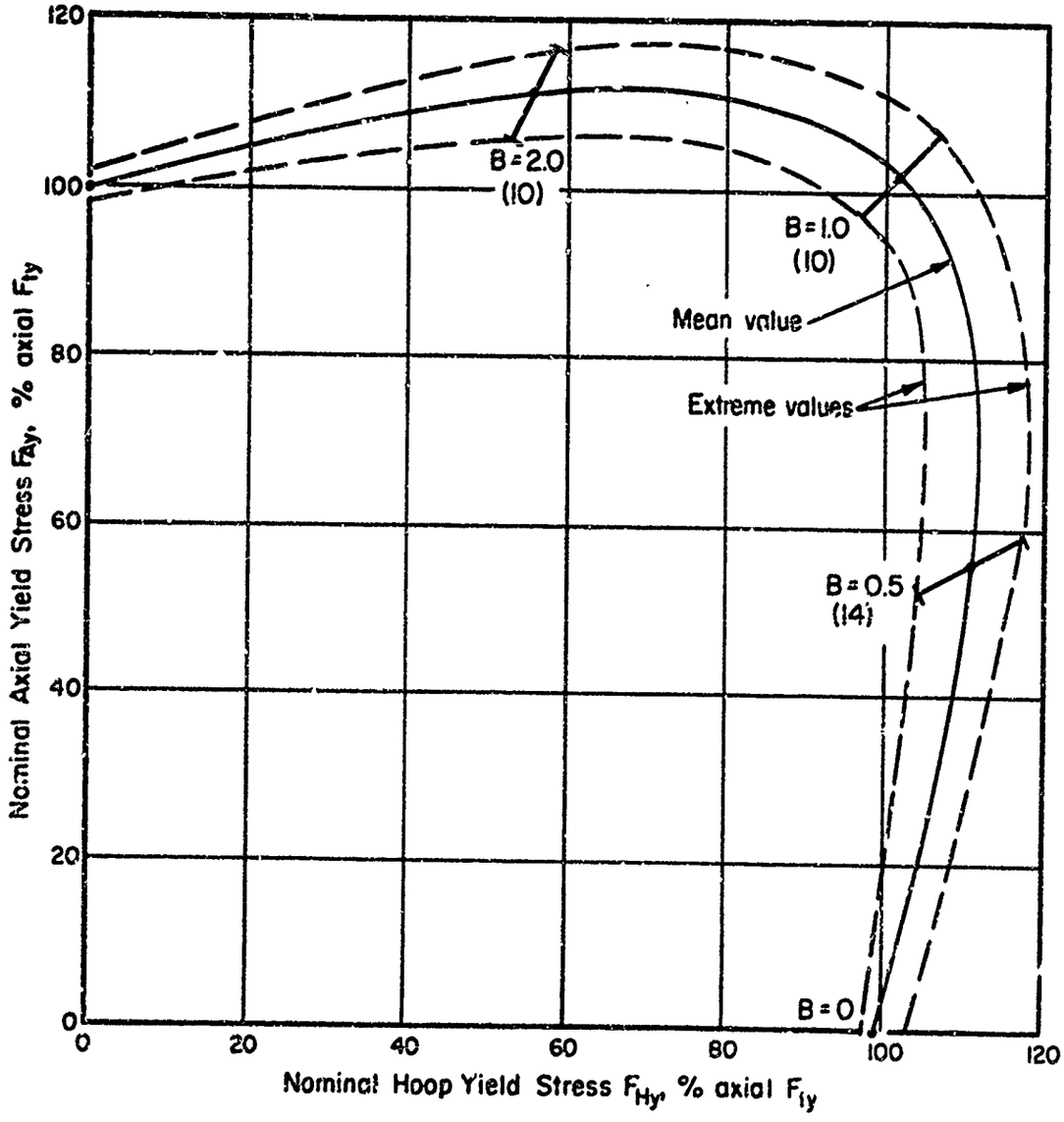

FIGURE 33. BIAXIAL YIELD-STRESS ENVELOPE AT ROOM TEMPERATURE FOR AISI 4340 STEEL. NUMBERS IN PARENTHESES ARE THE NUMBERS OF DATA POINTS USED FOR EACH BIAXIAL-STRESS RATIO B
Data from Figures 31 & 32

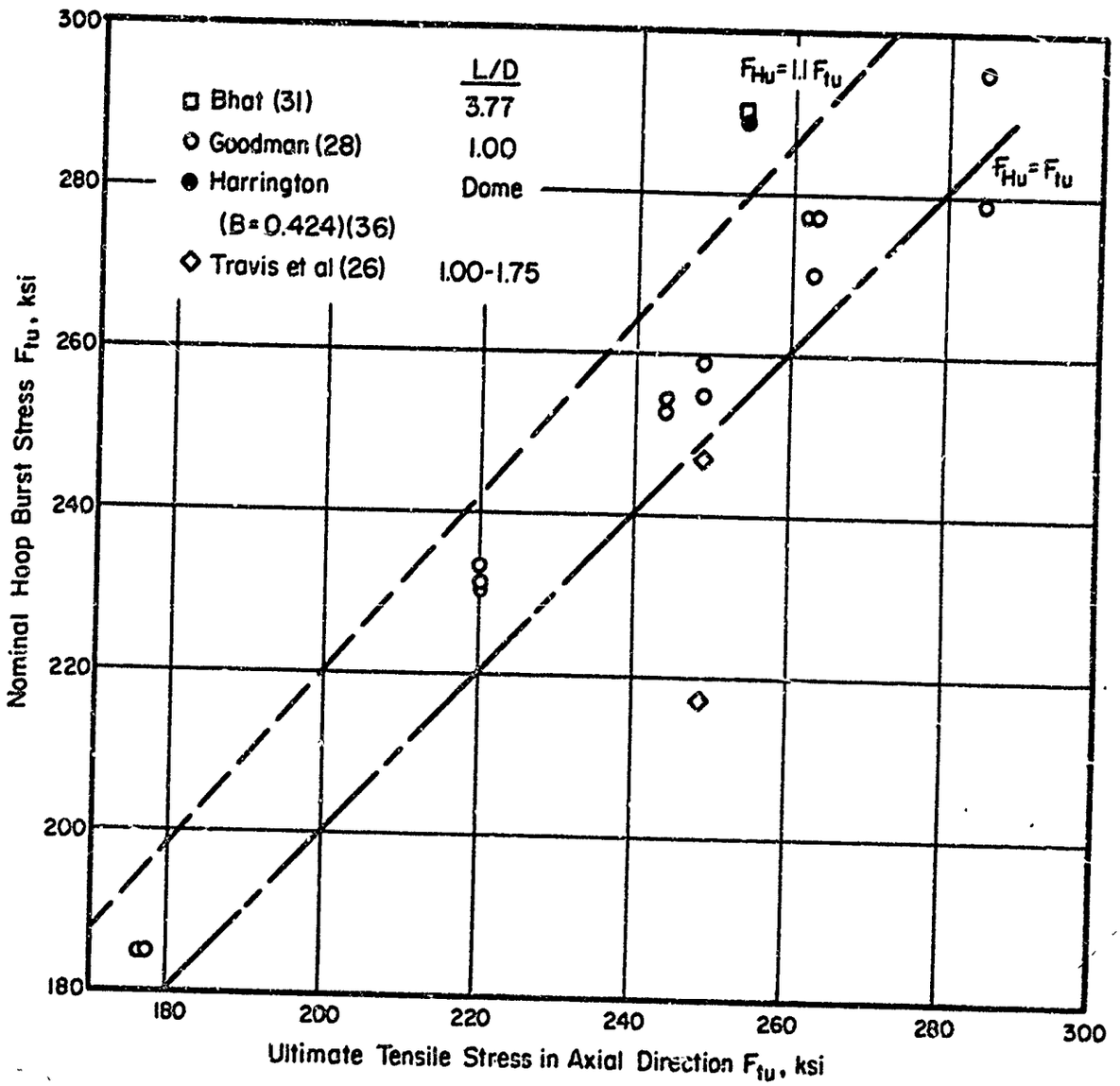

FIGURE 34. EFFECT OF ULTIMATE TENSILE STRENGTH IN AXIAL DIRECTION ON NOMINAL HOOP BURST STRESS AT A BIAXIAL-STRESS RATIO OF APPROXIMATELY 0.5 AND ROOM TEMPERATURE FOR AISI 4340 STEEL. CYLINDRICAL SHELLS WITH LENGTH/DIAM RATIOS AND DATA SOURCES INDICATED IN LEGEND

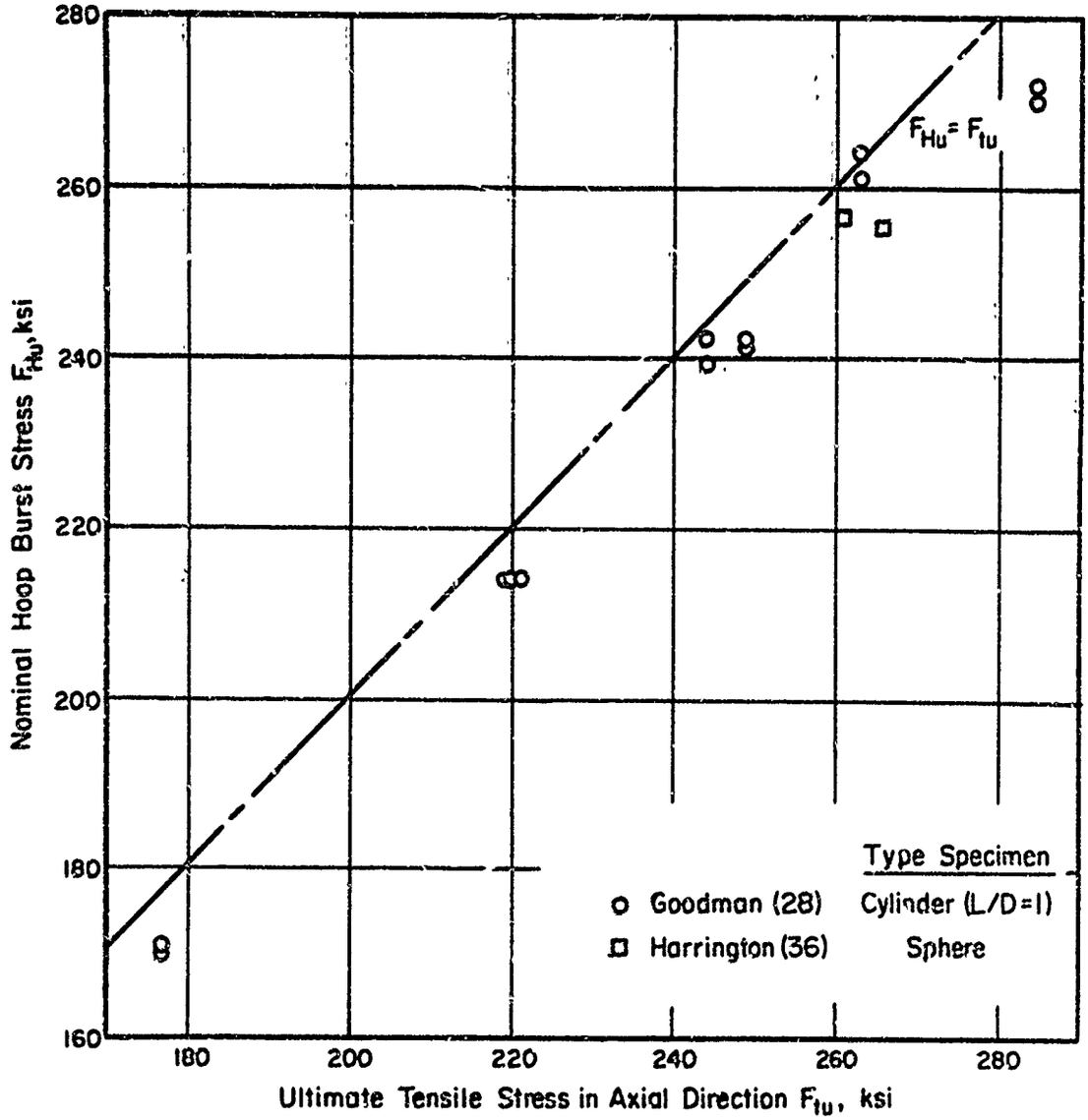

FIGURE 35. EFFECT OF ULTIMATE TENSILE STRESS IN AXIAL DIRECTION ON NOMINAL HOOP BURST STRESS AT A BIAXIAL-STRESS RATIO OF 1.0 AND ROOM TEMPERATURE FOR AISI 4340 STEEL.
Data Sources: Shown in legend

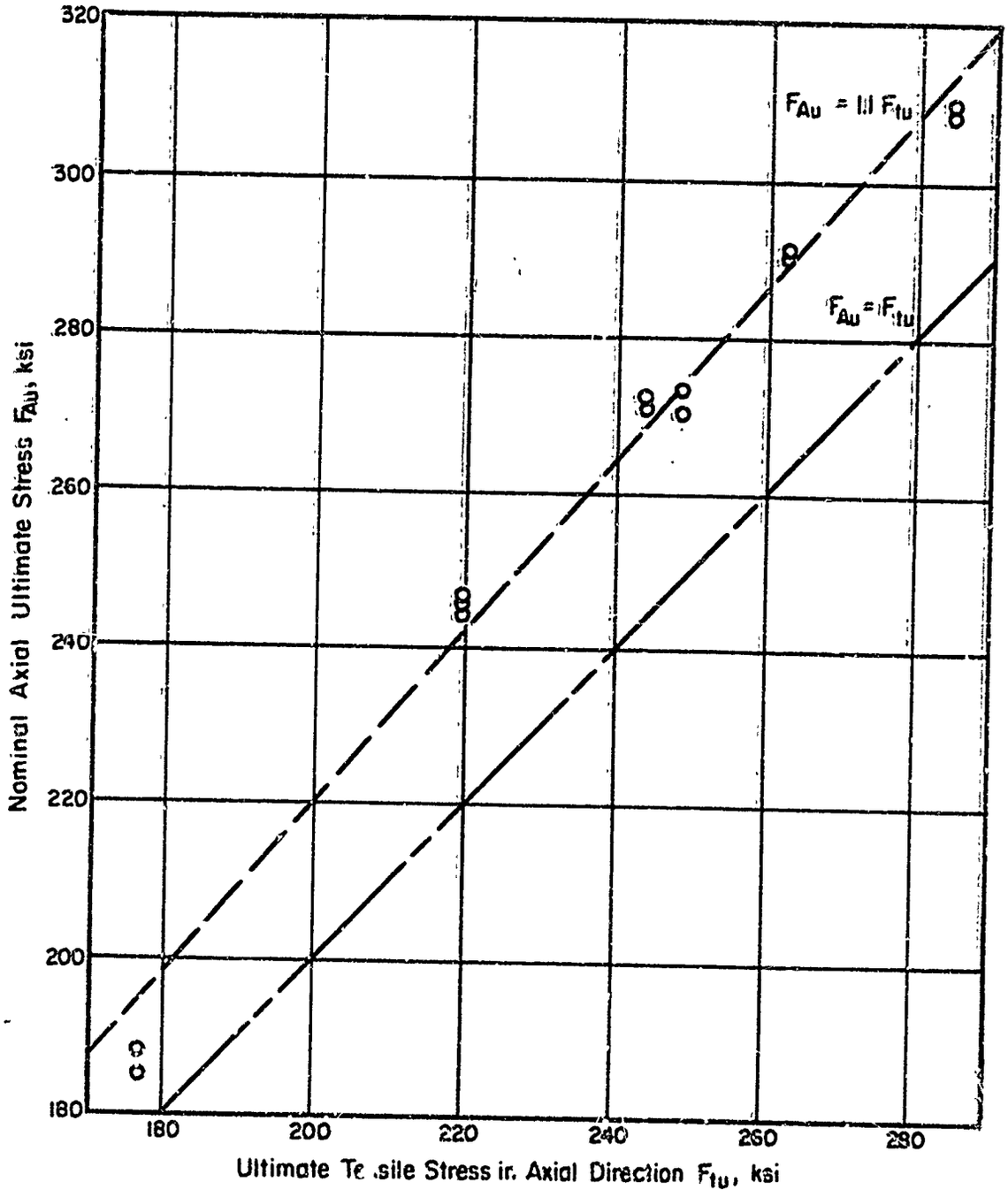

FIGURE 36. EFFECT OF ULTIMATE TENSILE STRESS IN AXIAL DIRECTION ON NOMINAL AXIAL ULTIMATE STRESS AT A BIAXIAL-STRESS RATIO OF 2.0 AND ROOM TEMPERATURE FOR AISI 4340 STEEL. CYLINDRICAL SHELLS WITH LENGTH/DIAM RATIO OF 1.0
Data Source: Goodman (28)

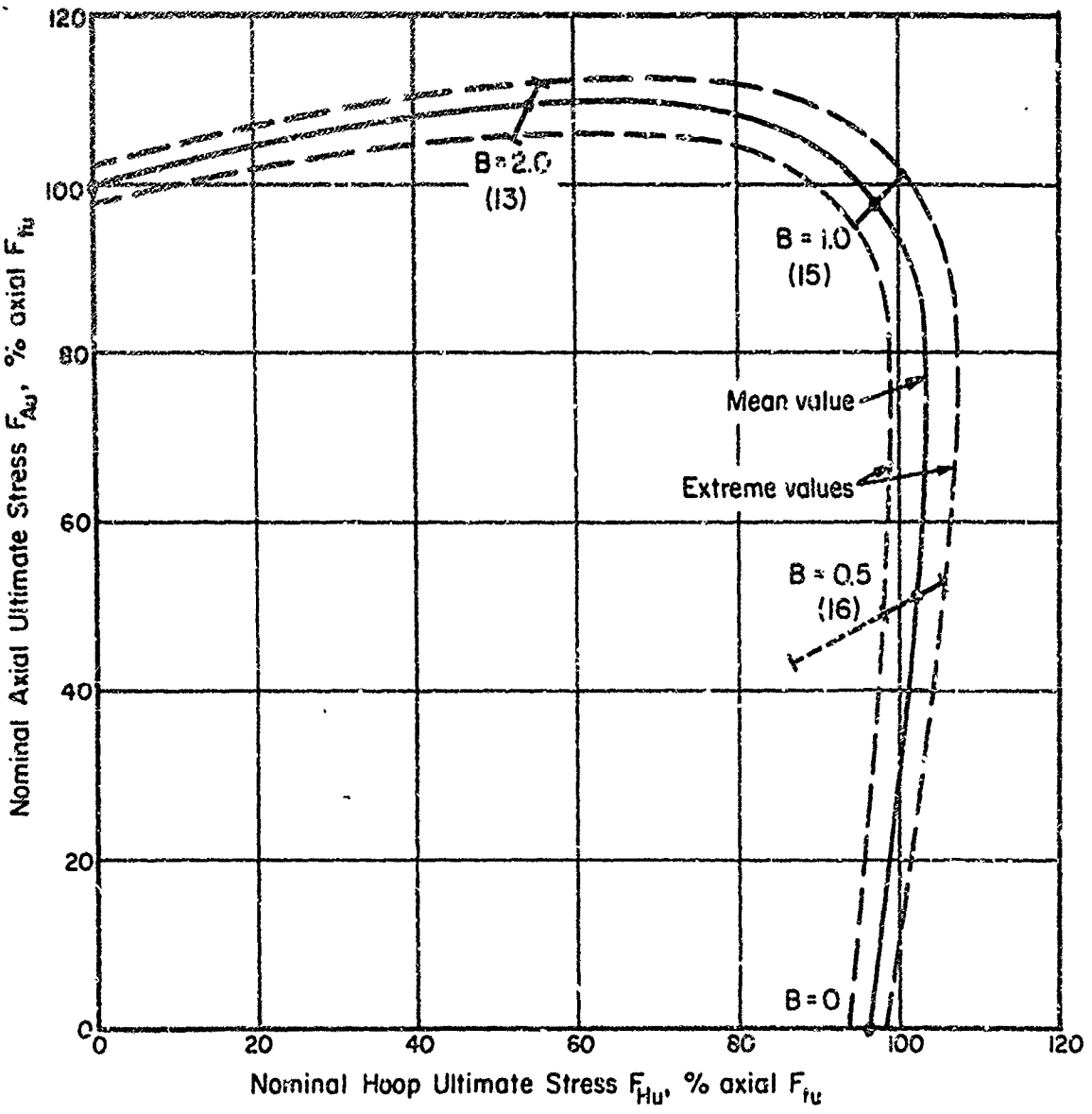

FIGURE 37 BIAXIAL ULTIMATE-STRESS ENVELOPE AT ROOM TEMPERATURE FOR AISI 4340 STEEL. NUMBERS IN PARENTHESES ARE NUMBERS OF DATA POINTS USED FOR EACH BIAXIAL-STRESS RATIO B
Data from Figures 34, 35, & 36

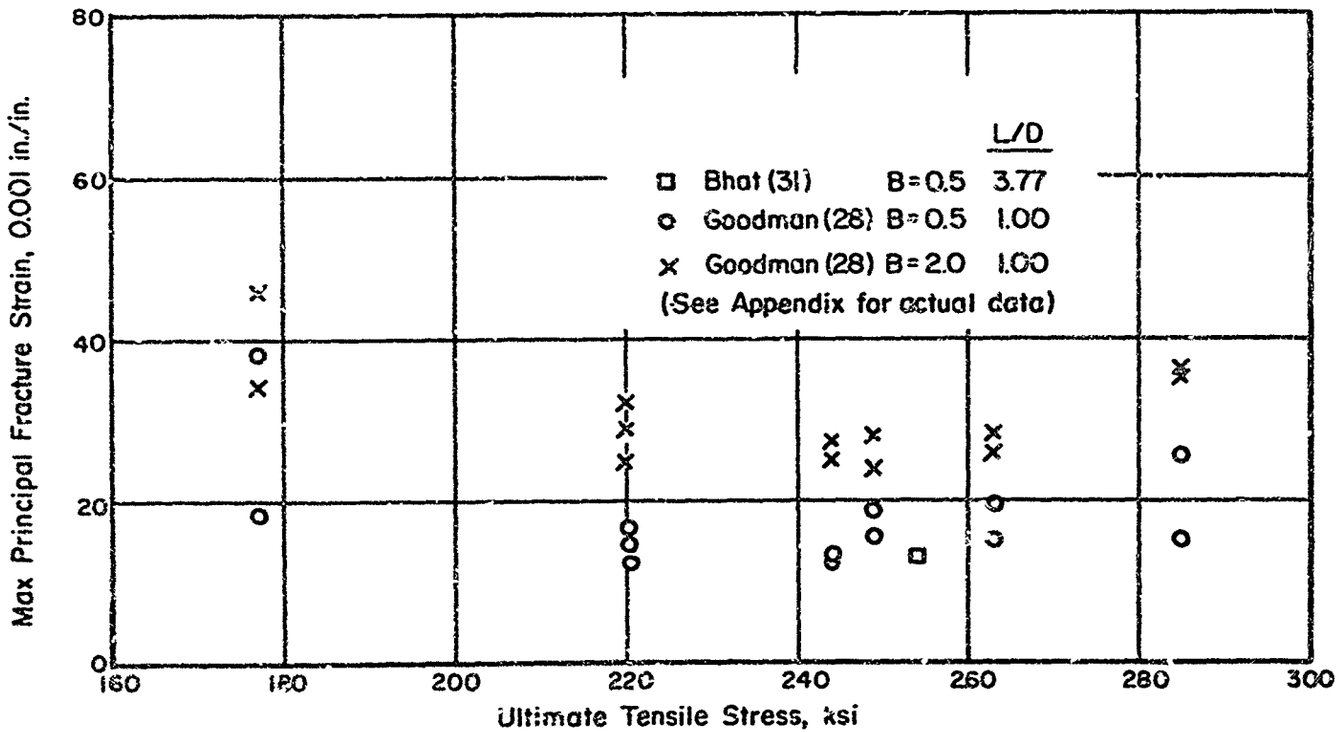

FIGURE 38. EFFECT OF ULTIMATE TENSILE STRESS ON MAX PRINCIPAL FRACTURE STRAIN AT BIAXIAL-STRESS RATIOS OF 0.5 AND 2.0 AND ROOM TEMPERATURE FOR AISI 4340 STEEL. CYLINDRICAL SHELLS WITH LENGTH/DIAM RATIOS AND DATA SOURCES INDICATED IN LEGEND

Note: In every instance for B = 0.5 the maximum load occurred at fracture; in approximately one-half of the tests at B = 2 maximum load occurred at slightly smaller strain than the fracture strain

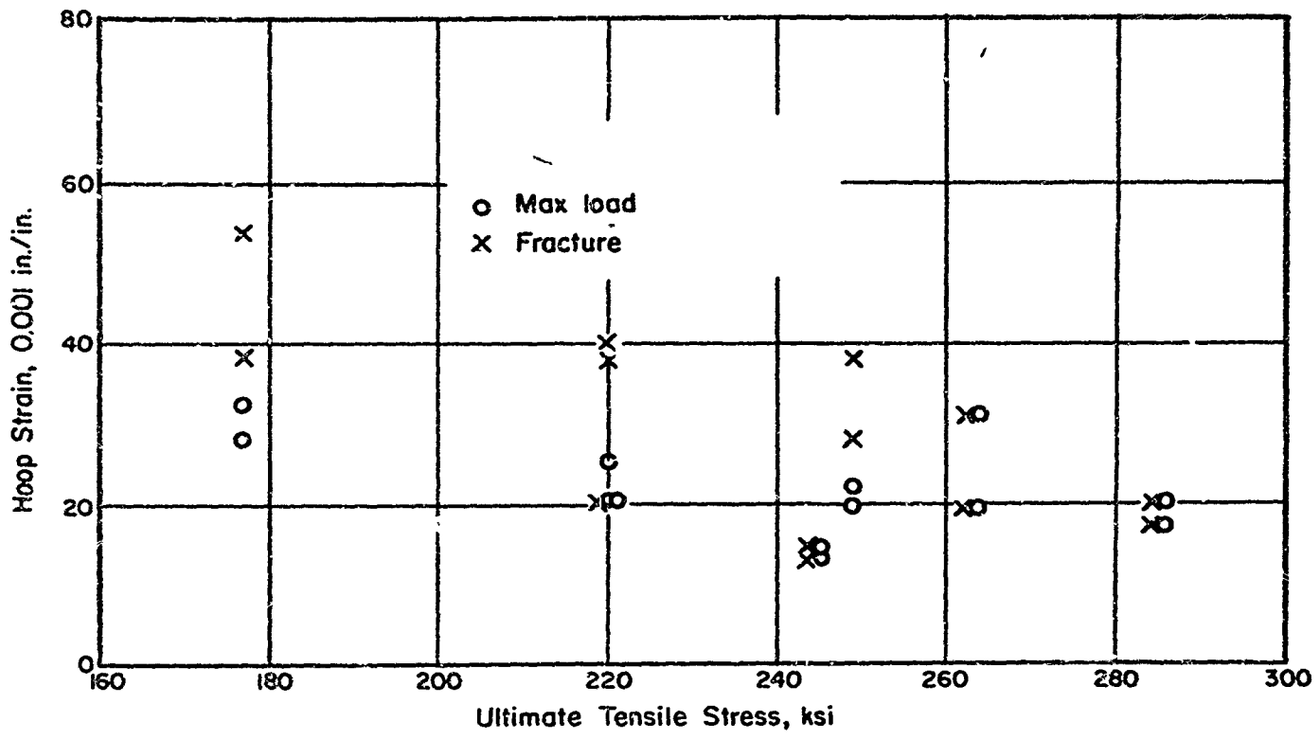

FIGURE 39. EFFECT OF ULTIMATE TENSILE STRESS ON HOOP STRAIN AT MAX LOAD AND AT FRACTURE FOR AISI 4340 STEEL AT A BIAXIAL-STRESS RATIO OF 1.0 AND ROOM TEMPERATURE. CYLINDRICAL SHELLS WITH LENGTH/DIAM RATIO OF 1

Data Source: Goodman (28)

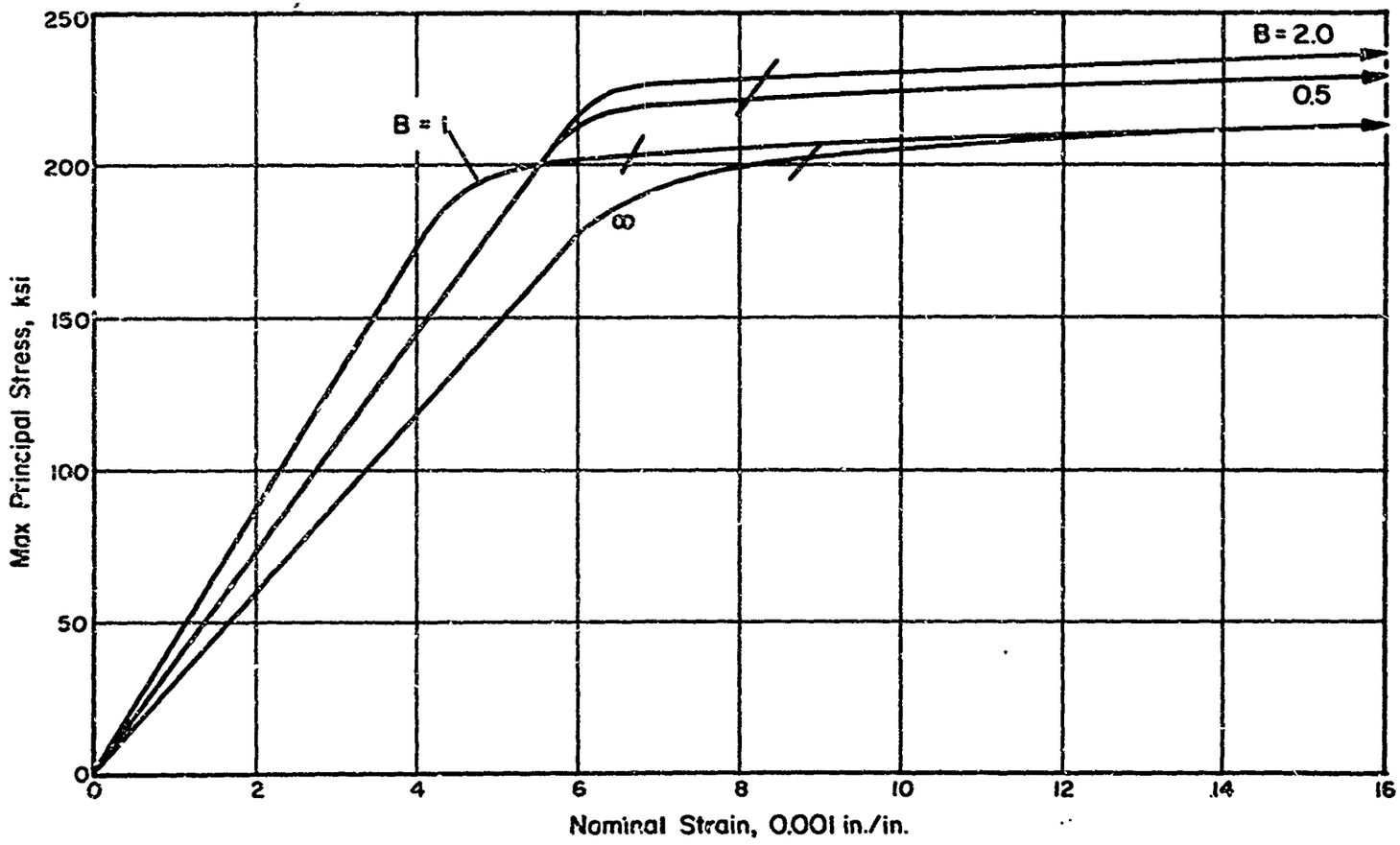

FIGURE 40. TYPICAL BIAXIAL STRESS-STRAIN CURVES AT ROOM TEMPERATURE FOR D6AC STEEL. CYLINDRICAL SHELL MACHINED FROM BAR STOCK
Data Source: Goodman (28)

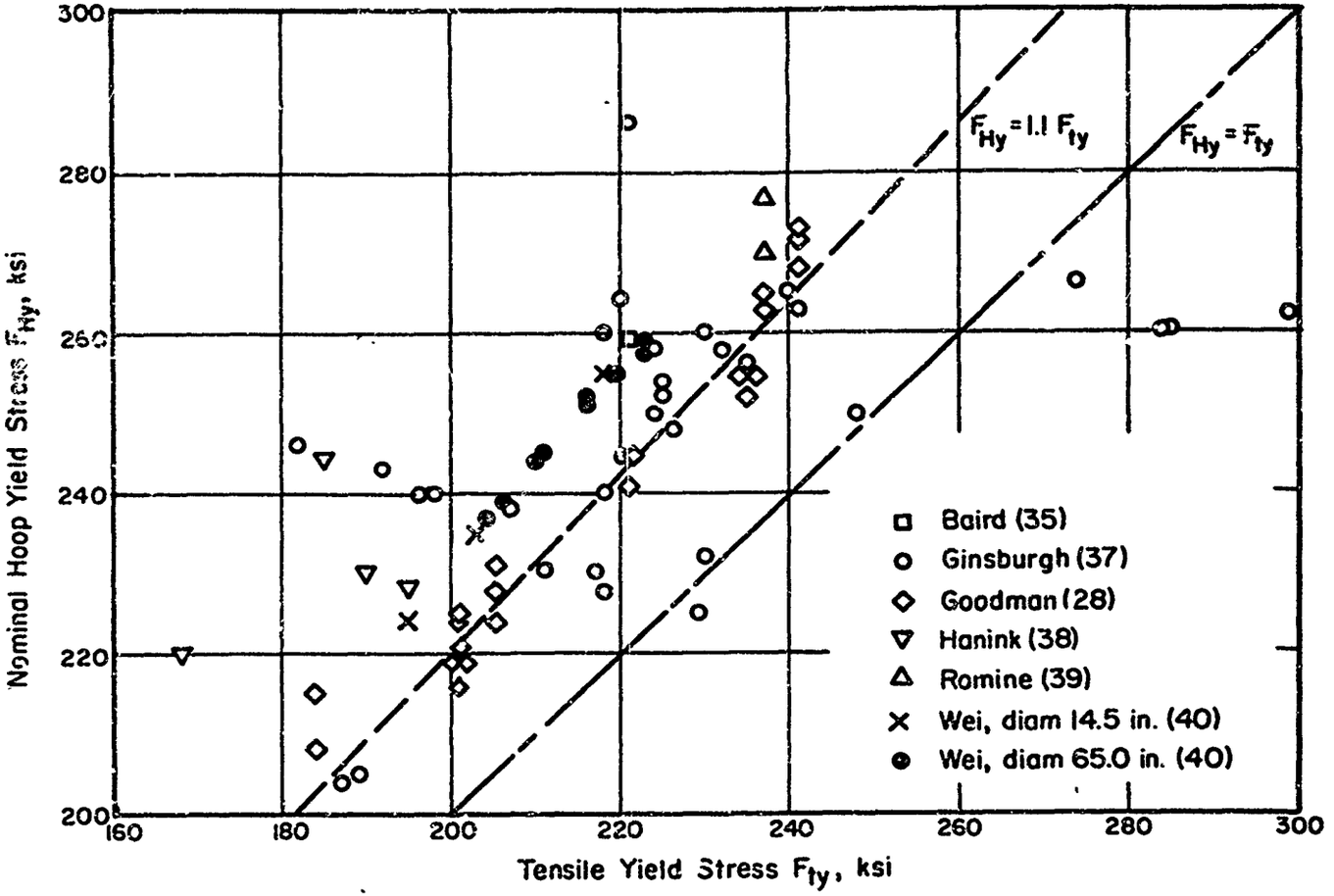

FIGURE 41. EFFECT OF TENSILE YIELD STRESS ON NOMINAL HOOP YIELD STRESS AT A BIAXIAL-STRESS RATIO OF 0.5 AND ROOM TEMPERATURE FOR D6AC STEEL. CYLINDRICAL SHELLS
Data Sources: Shown in legend

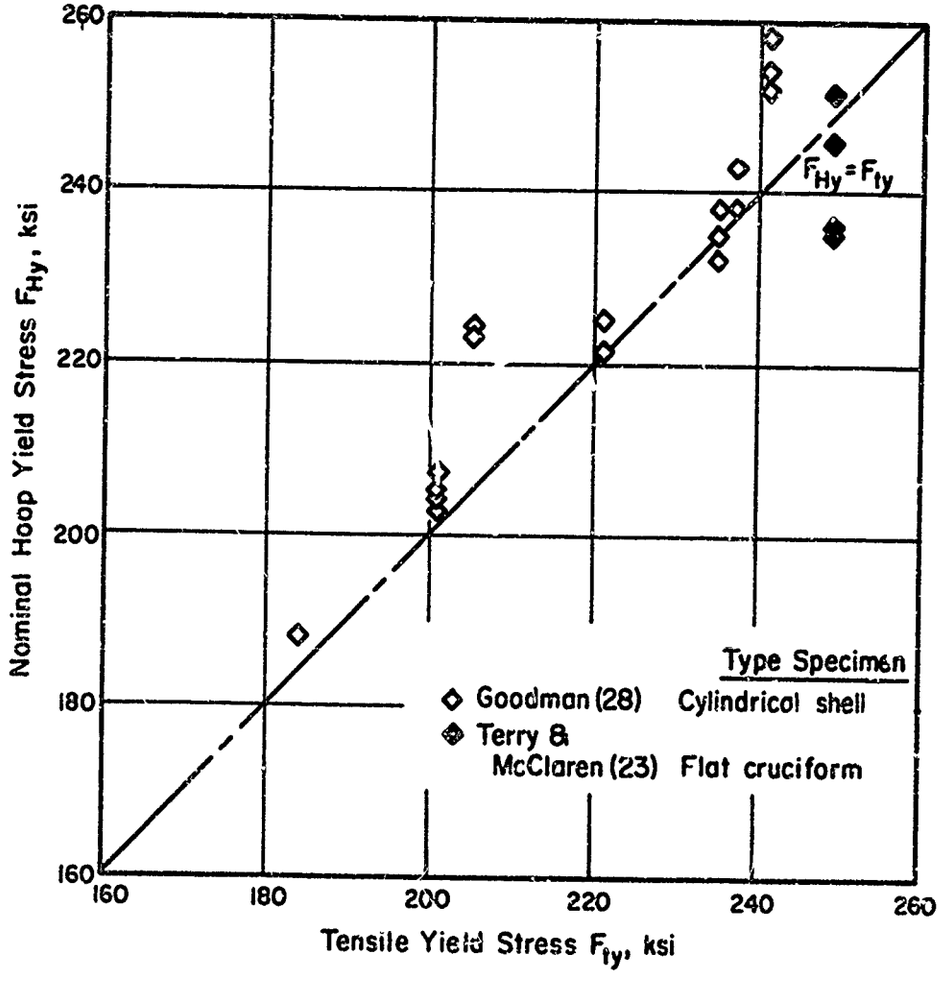

FIGURE 42. EFFECT OF TENSILE YIELD STRESS ON NOMINAL HOOP YIELD STRESS AT A BIAXIAL-STRESS RATIO OF 1.0 AND ROOM TEMPERATURE FOR D6AC STEEL
Data Sources: Shown in legend

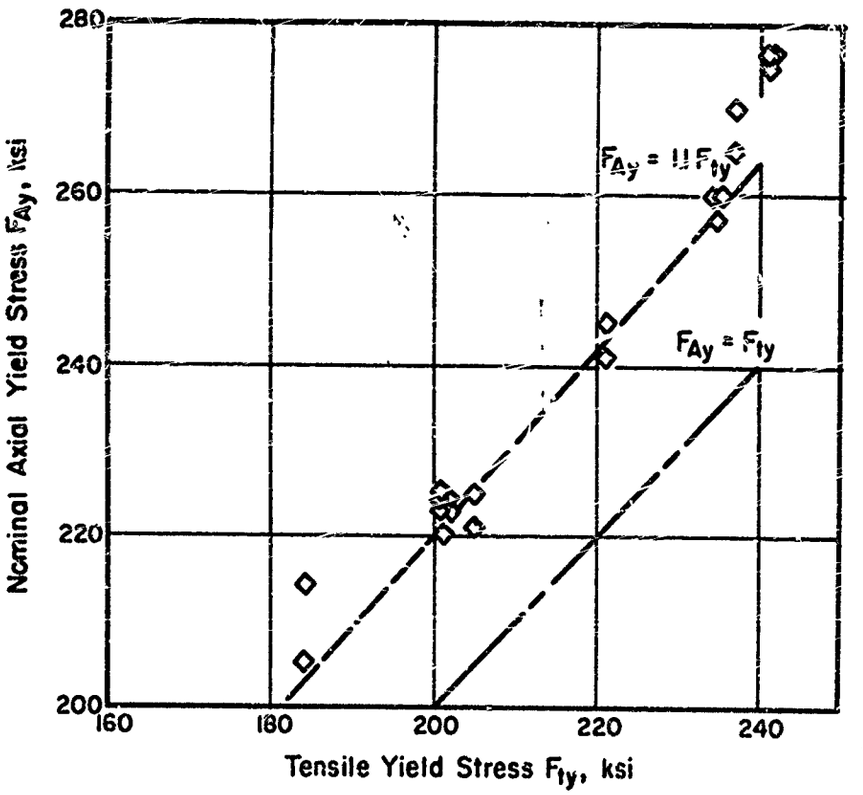

FIGURE 43. EFFECT OF TENSILE YIELD STRESS ON NOMINAL AXIAL YIELD STRESS AT A BIAXIAL-STRESS RATIO OF 2.0 AND ROOM TEMPERATURE FOR D6AC STEEL. CYLINDRICAL SHELLS
Data Source: Goodman (28)

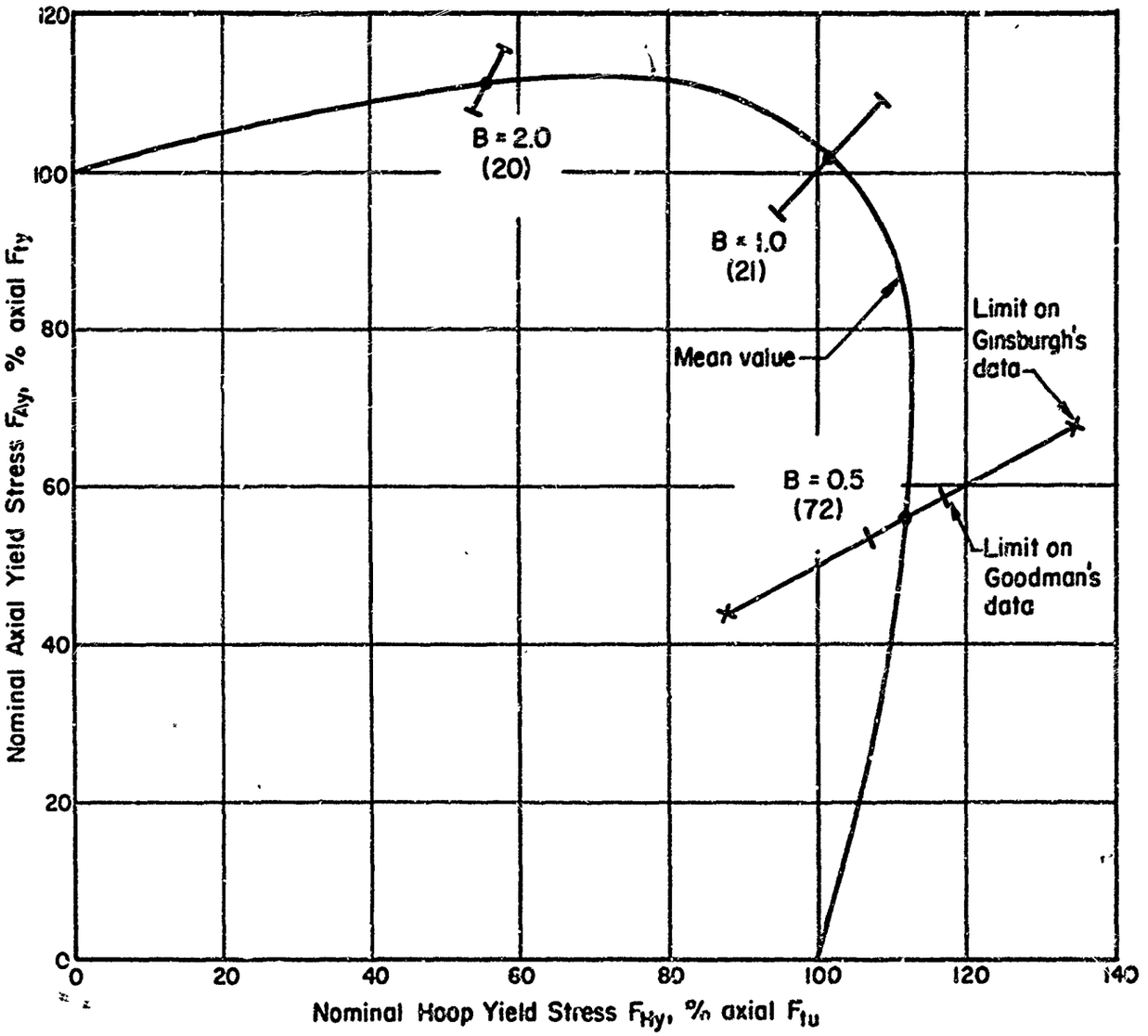

FIGURE 44. BIAXIAL YIELD-STRESS ENVELOPE AT ROOM TEMPERATURE FOR D6AC STEEL. NUMBERS IN PARENTHESES ARE THE NUMBERS OF DATA POINTS USED FOR EACH BIAXIAL-STRESS RATIO B.
Data from Figures 41, 42, & 43

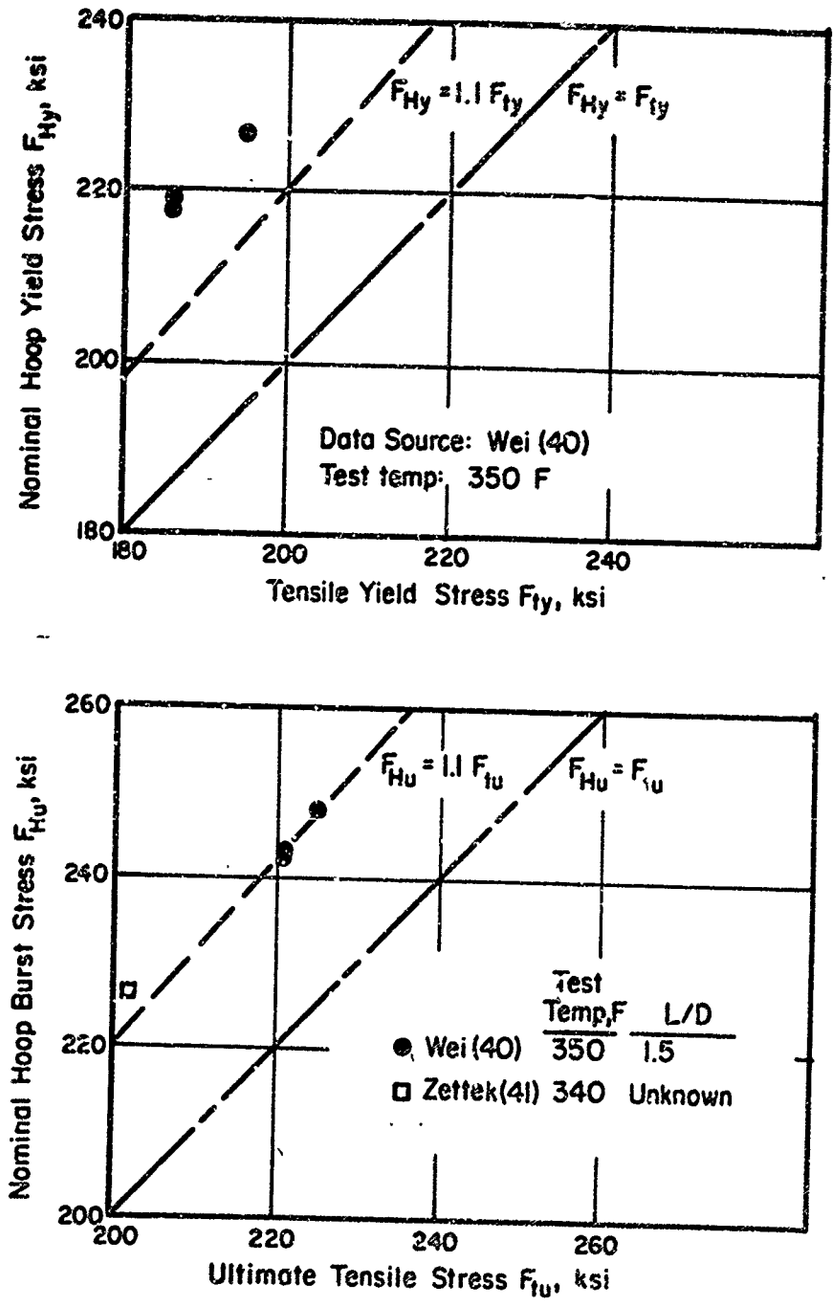

FIGURE 45. EFFECT OF TENSILE YIELD STRESS ON NOMINAL HOOP YIELD STRESS AND OF ULTIMATE TENSILE STRESS ON NOMINAL HOOP BURST STRESS AT A BIAXIAL-STRESS RATIO OF 0.5 AND MODERATELY ELEVATED TEMPERATURES FOR D6AC STEEL. CYLINDRICAL SHELLS
Data Sources: Shown in legend

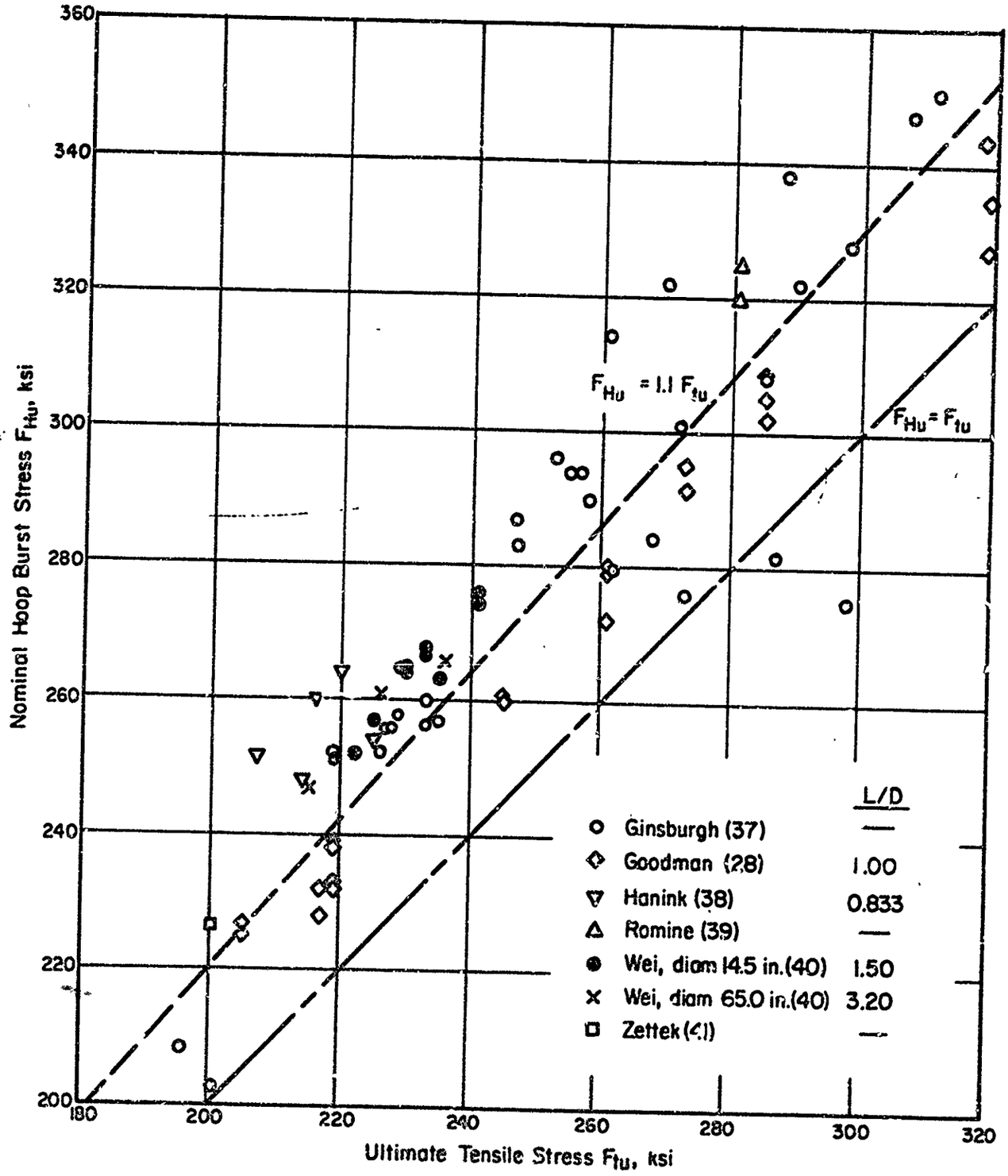

FIGURE 46. EFFECT OF ULTIMATE TENSILE STRESS ON NOMINAL HOOP BURST STRESS AT A BIAXIAL-STRESS RATIO OF 0.5 AND ROOM TEMPERATURE FOR D6AC STEEL. CYLINDRICAL SHELLS WITH LENGTH/DIAM RATIOS INDICATED IN LEGEND

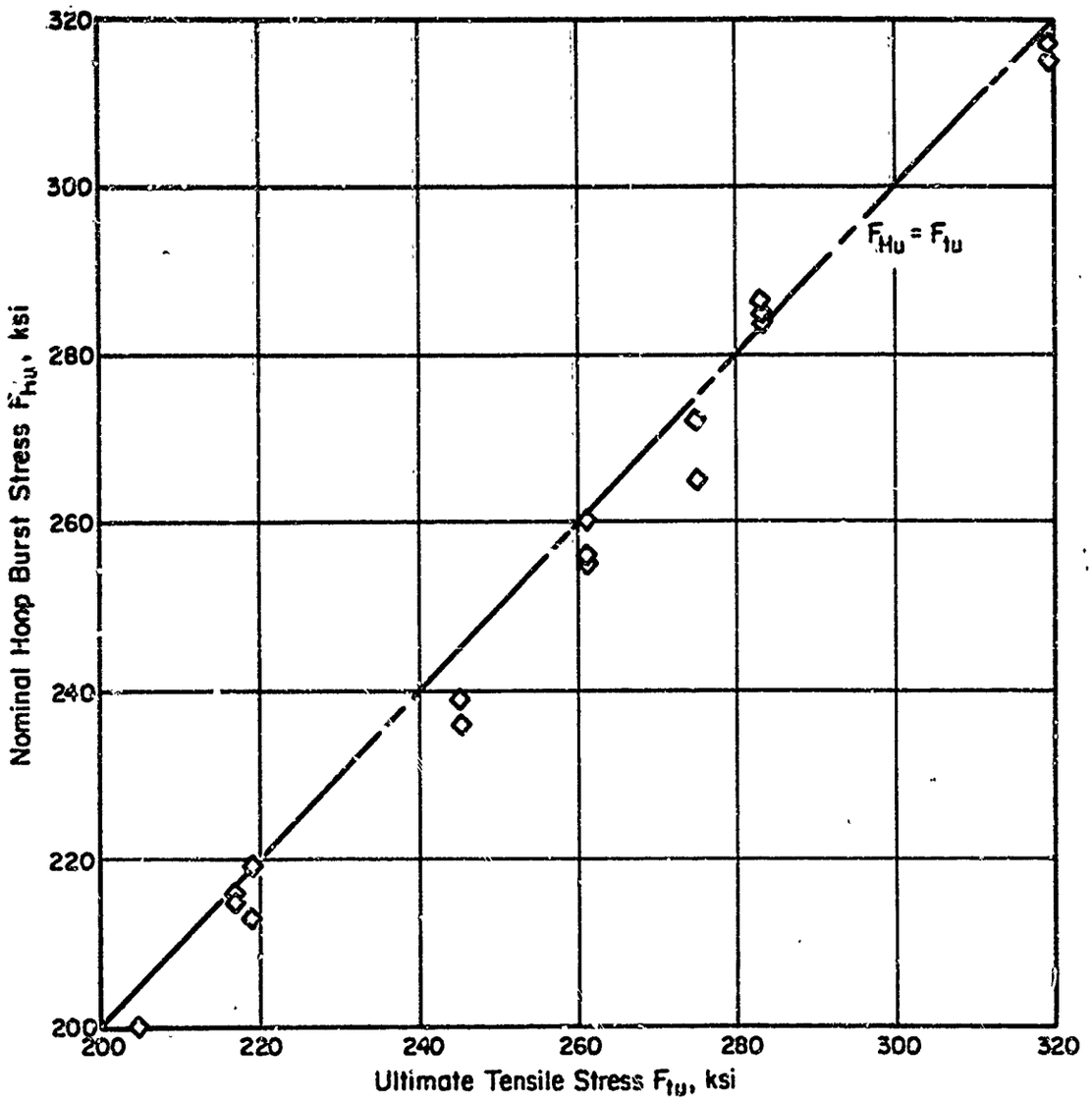

FIGURE 47. EFFECT OF ULTIMATE TENSILE STRESS ON NOMINAL HOOP BURST STRESS AT A BIAXIAL-STRESS RATIO OF 1.0 AND ROOM TEMPERATURE FOR D6AC STEEL CYLINDRICAL SHELLS WITH LENGTH/DIAM RATIO OF 1.0

Data Source: Goodman (28)

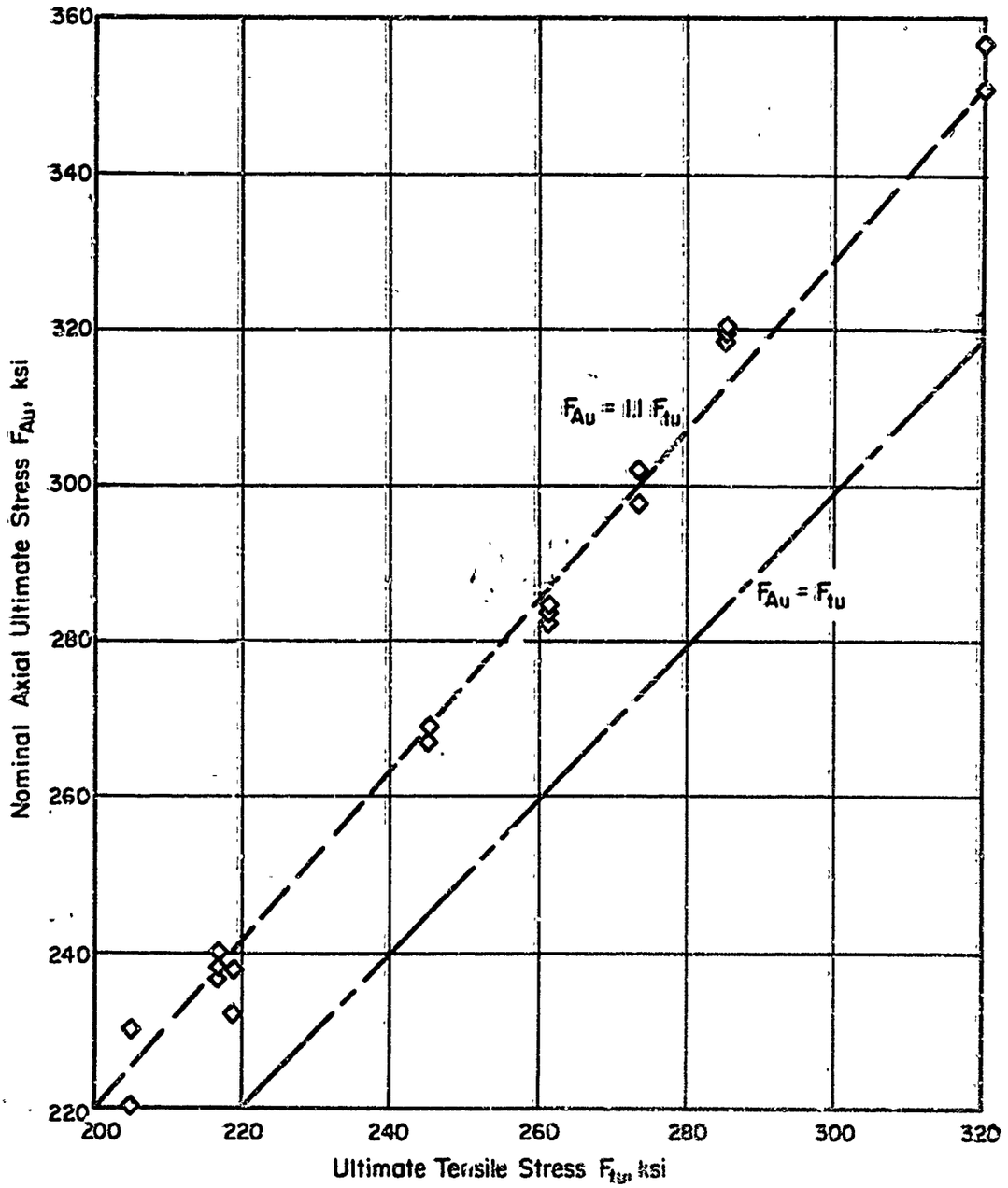

FIGURE 48. EFFECT OF ULTIMATE TENSILE STRESS ON NOMINAL AXIAL ULTIMATE STRESS AT A BIAXIAL-STRESS RATIO OF 2.0 AND ROOM TEMPERATURE FOR D6AC STEEL. CYLINDRICAL SHELLS WITH LENGTH/DIAM RATIO OF 1.0
Data Source: Goodman (28)

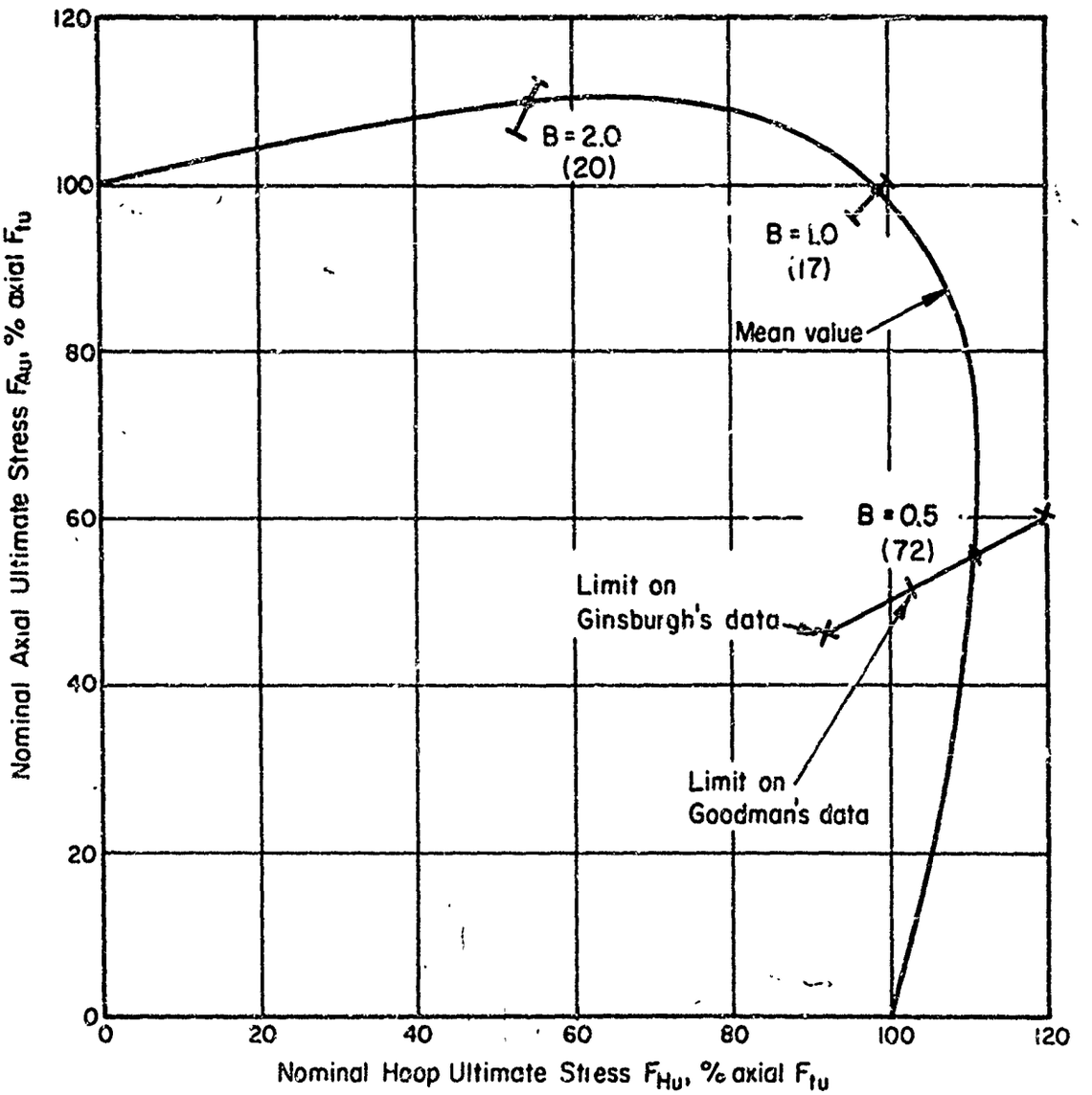

FIGURE 49. BIAXIAL ULTIMATE-STRESS ENVELOPE AT ROOM TEMPERATURE FOR D6AC STEEL. NUMBERS IN PARENTHESES ARE THE NUMBERS OF DATA POINTS USED FOR EACH BIAXIAL-STRESS RATIO B.
Data from Figures 45, 46, & 47

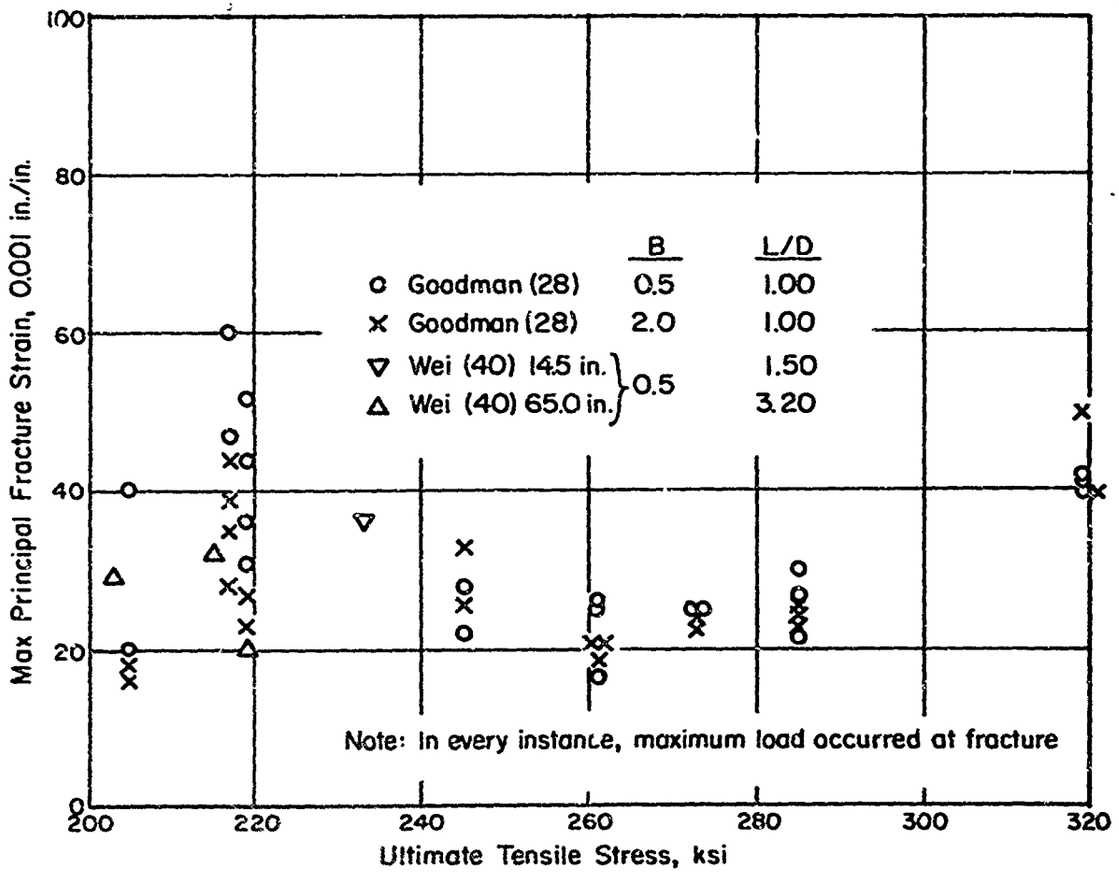

FIGURE 50. EFFECT OF ULTIMATE TENSILE STRESS ON MAX PRINCIPAL FRACTURE STRAIN AT BIAXIAL-STRESS RATIOS OF 0.5 AND 2.0 AND ROOM TEMPERATURE FOR D6AC STEEL. CYLINDRICAL SHELLS WITH LENGTH/DIAM RATIOS AND DATA SOURCES INDICATED IN LEGEND

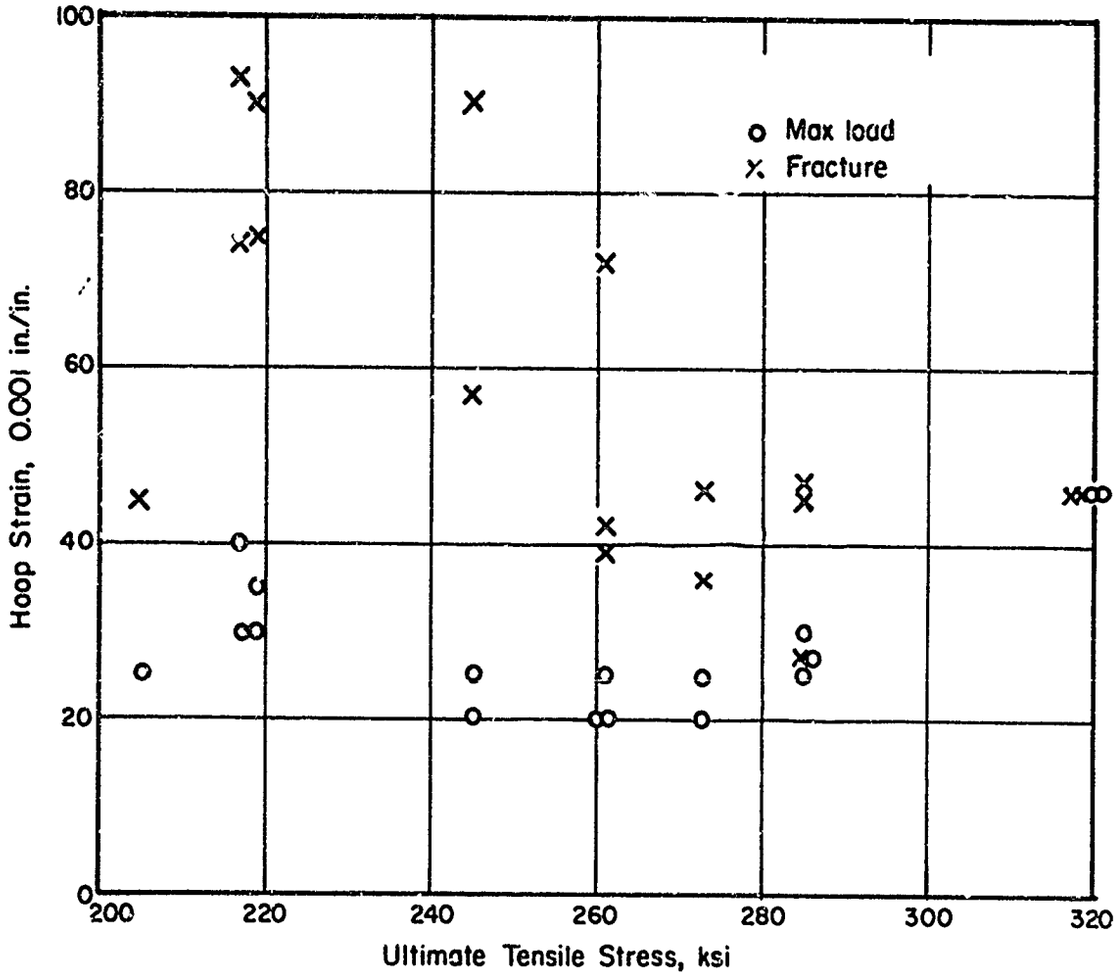

FIGURE 51. EFFECT OF ULTIMATE TENSILE STRESS ON HOOP STRAIN AT MAX LOAD AND AT FRACTURE FOR D6AC STEEL AT A BIAXIAL-STRESS RATIO OF 1.0 AND ROOM TEMPERATURE. CYLINDRICAL SHELLS WITH LENGTH/DIAM RATIO OF 1.0.
Data Source: Goodman (28)

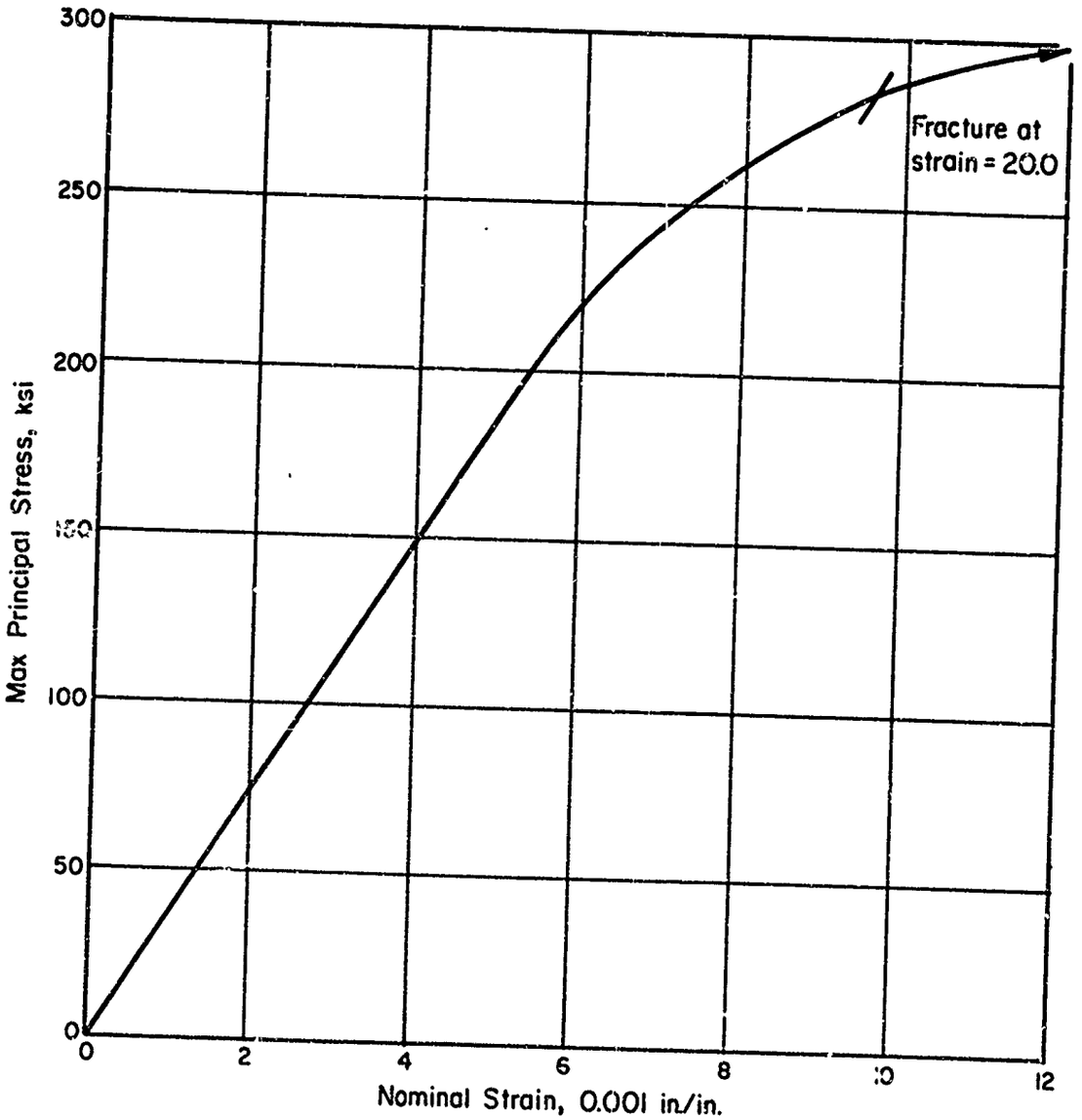

FIGURE 52. TYPICAL BIAXIAL STRESS-STRAIN CURVE AT ROOM TEMPERATURE FOR 300M STEEL AT A BIAXIAL-STRESS RATIO OF 0.5. CYLINDRICAL SHELL WITH LENGTH/DIAM RATIO OF 3.77.
Data Source: Bhat (31)

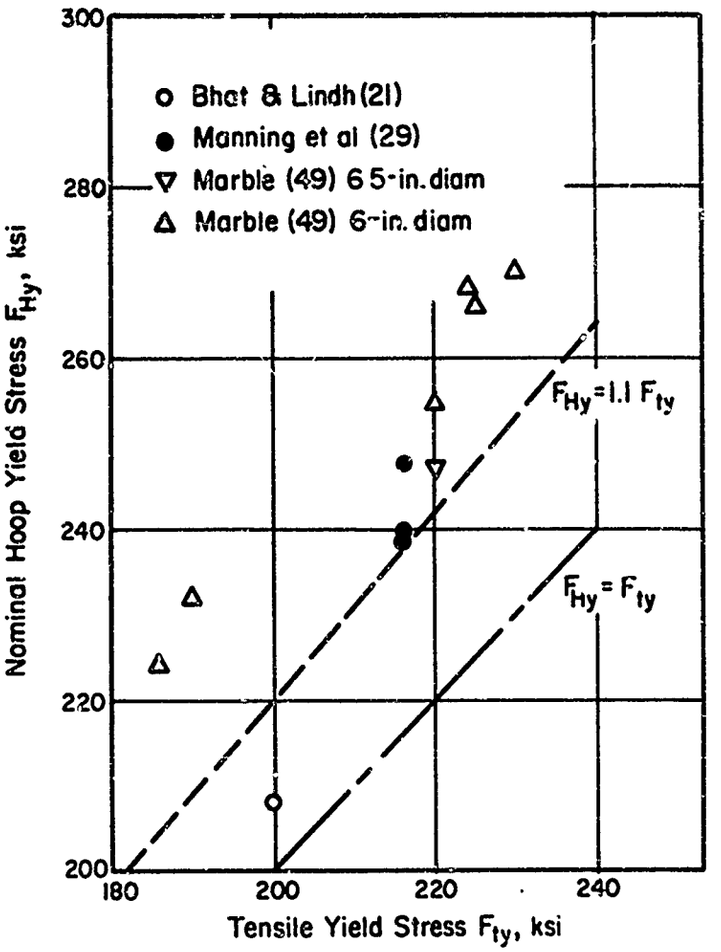

FIGURE 53. EFFECT OF TENSILE YIELD STRESS ON NOMINAL HOOP YIELD STRESS AT A BIAXIAL-STRESS RATIO OF 0.5 AND ROOM TEMPERATURE FOR 300M STEEL. CYLINDRICAL SHELLS
Data Sources: Shown in legend

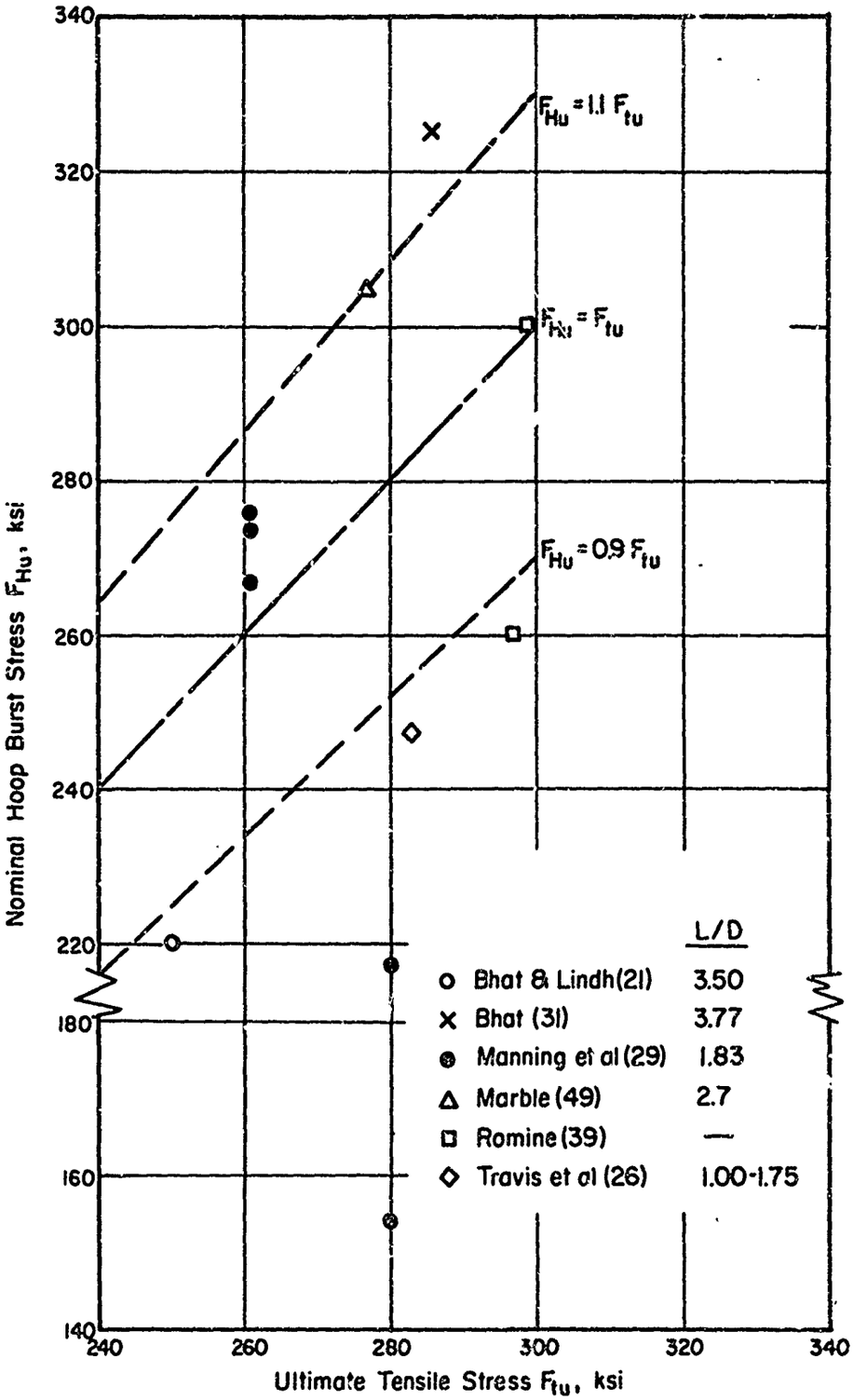

FIGURE 54. EFFECT OF ULTIMATE TENSILE STRESS ON NOMINAL HOOP BURST STRESS AT A BIAXIAL-STRESS RATIO OF 0.5 AND ROOM TEMPERATURE FOR 300M STEEL. CYLINDRICAL SHELLS WITH LENGTH/DIAM RATIOS AND DATA SOURCES INDICATED IN LEGEND

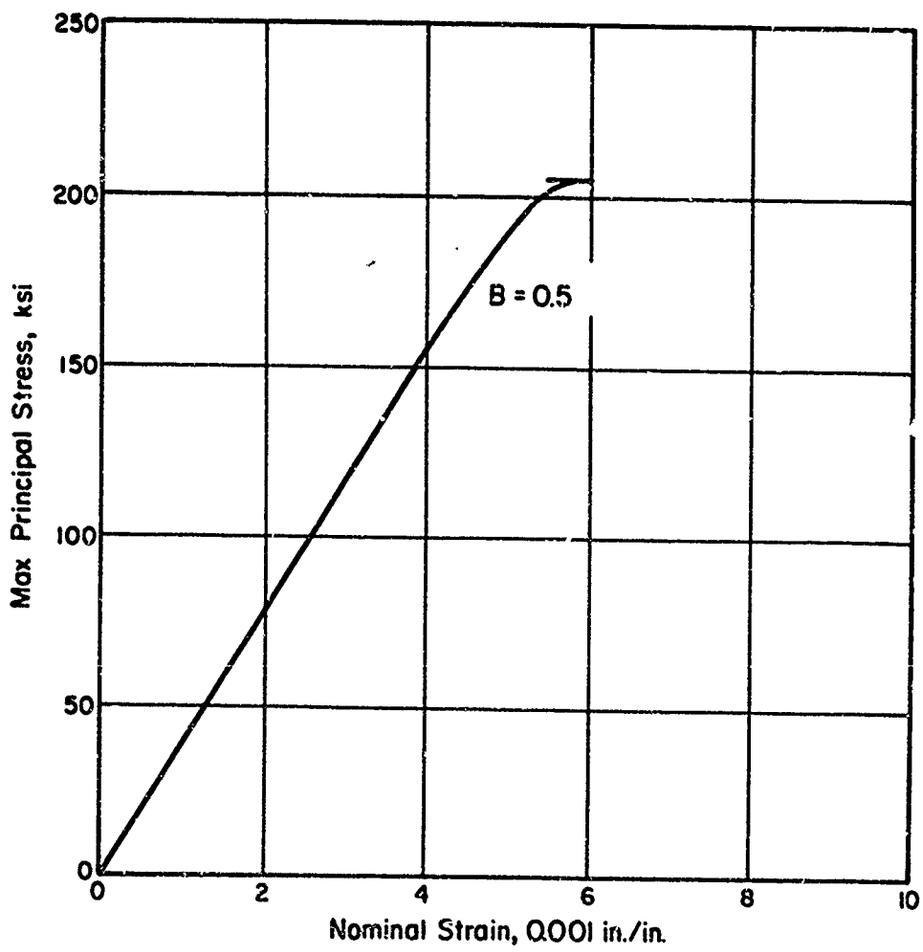

FIGURE 55. TYPICAL BIAXIAL STRESS-STRAIN CURVE AT ROOM TEMPERATURE FOR X-200 STEEL. CYLINDRICAL SHELL WITH LENGTH/DIAM RATIO OF 3.89
Data Source: Bhat (31)

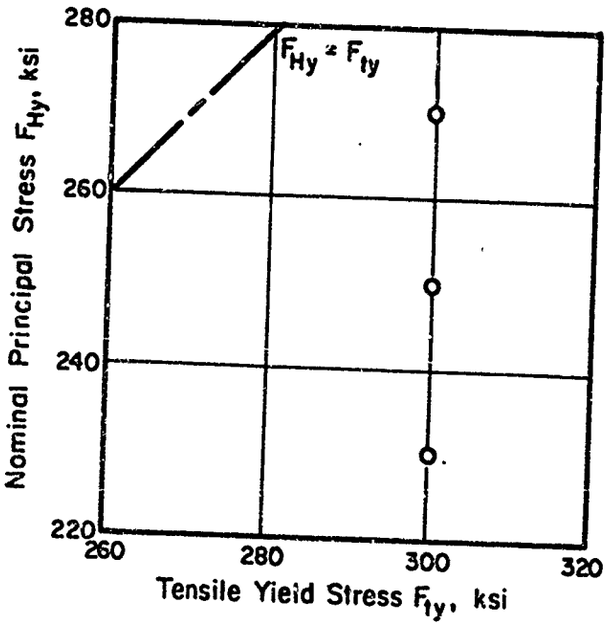

FIGURE 56. EFFECT OF TENSILE YIELD STRESS ON NOMINAL PRINCIPAL STRESS AT A BIAXIAL-STRESS RATIO OF 1.0 AND ROOM TEMPERATURE FOR X-200 STEEL. FLAT CRUCIFORM SPECIMENS WERE USED
Data Sources: Terry, McClaren (23)

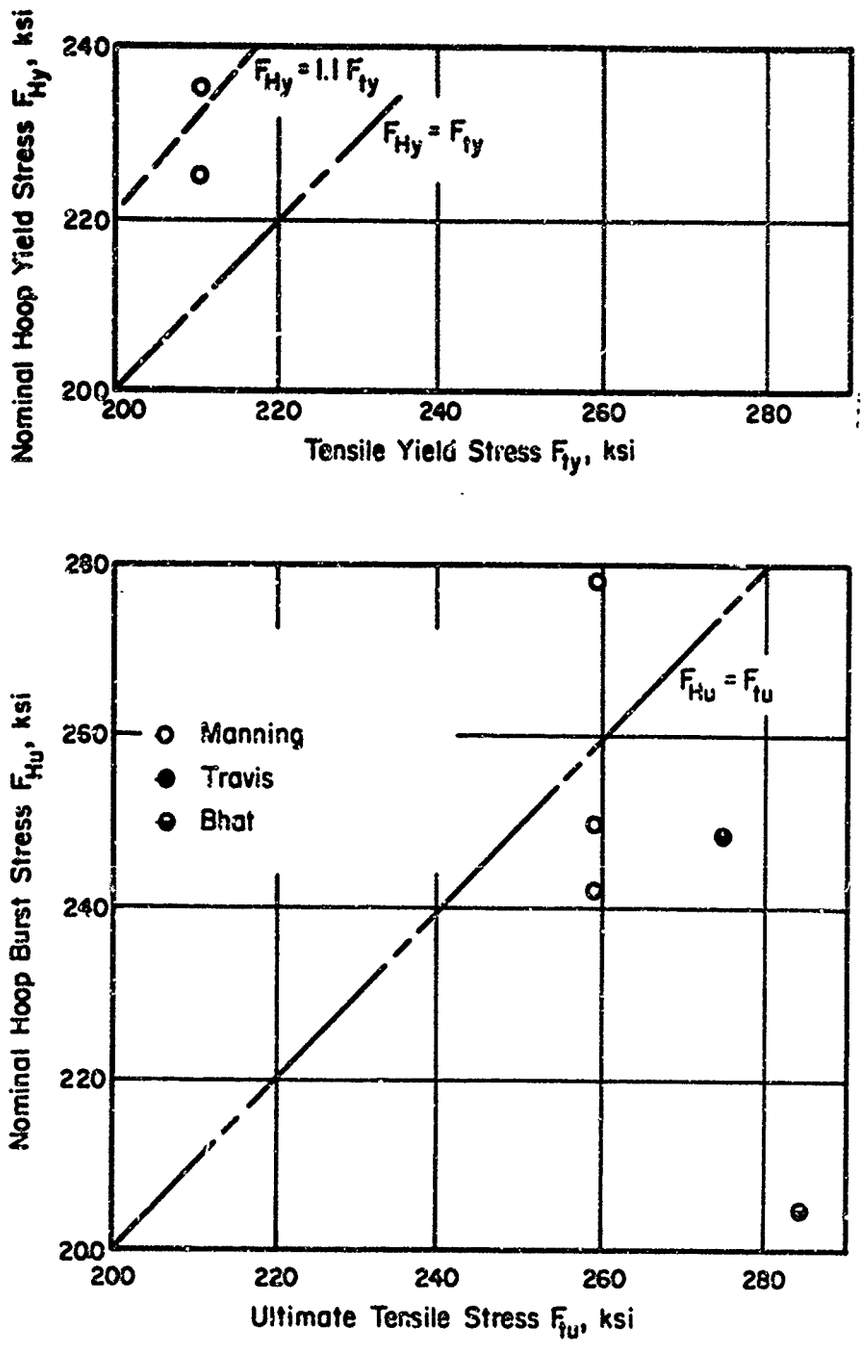

FIGURE 57. EFFECT OF TENSILE YIELD STRESS ON NOMINAL HOOP YIELD STRESS AND OF ULTIMATE TENSILE STRESS ON NOMINAL HOOP BURST STRESS AT A BIAXIAL-STRESS RATIO OF 0.5 AND ROOM TEMPERATURE FOR X-200 STEEL. CYLINDRICAL SHELLS WITH LENGTH/DIAM RATIO OF 1.83(MANNING) 1.0-1.75(TRAVIS)
Data Sources: Manning, Murphy, Nichols, Caine (29)
Travis, Ardito, Adams (26)
Bhat (31)

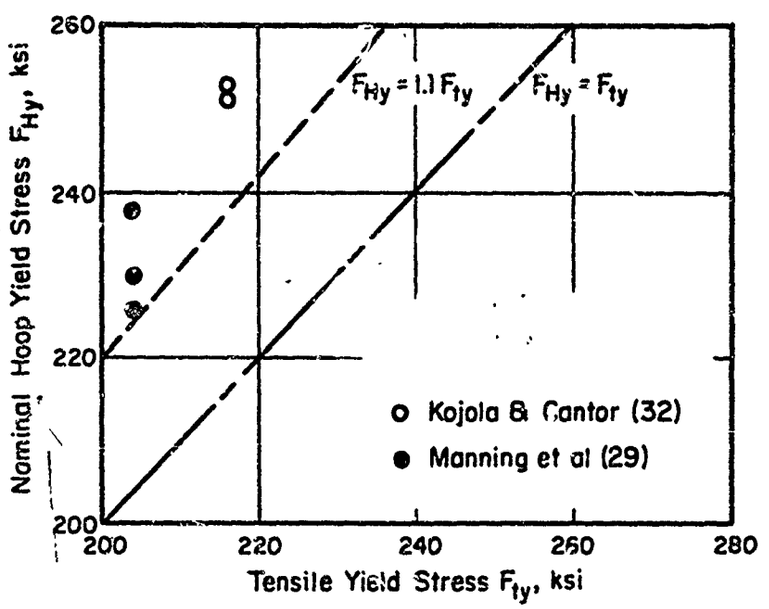

FIGURE 58. EFFECT OF TENSILE YIELD STRESS ON NOMINAL HOOP YIELD STRESS AT A BIAXIAL-STRESS RATIO OF 0.5 AND ROOM TEMPERATURE FOR MBMC-1 STEEL. CYLINDRICAL SHELLS
Data Sources: Shown in legend

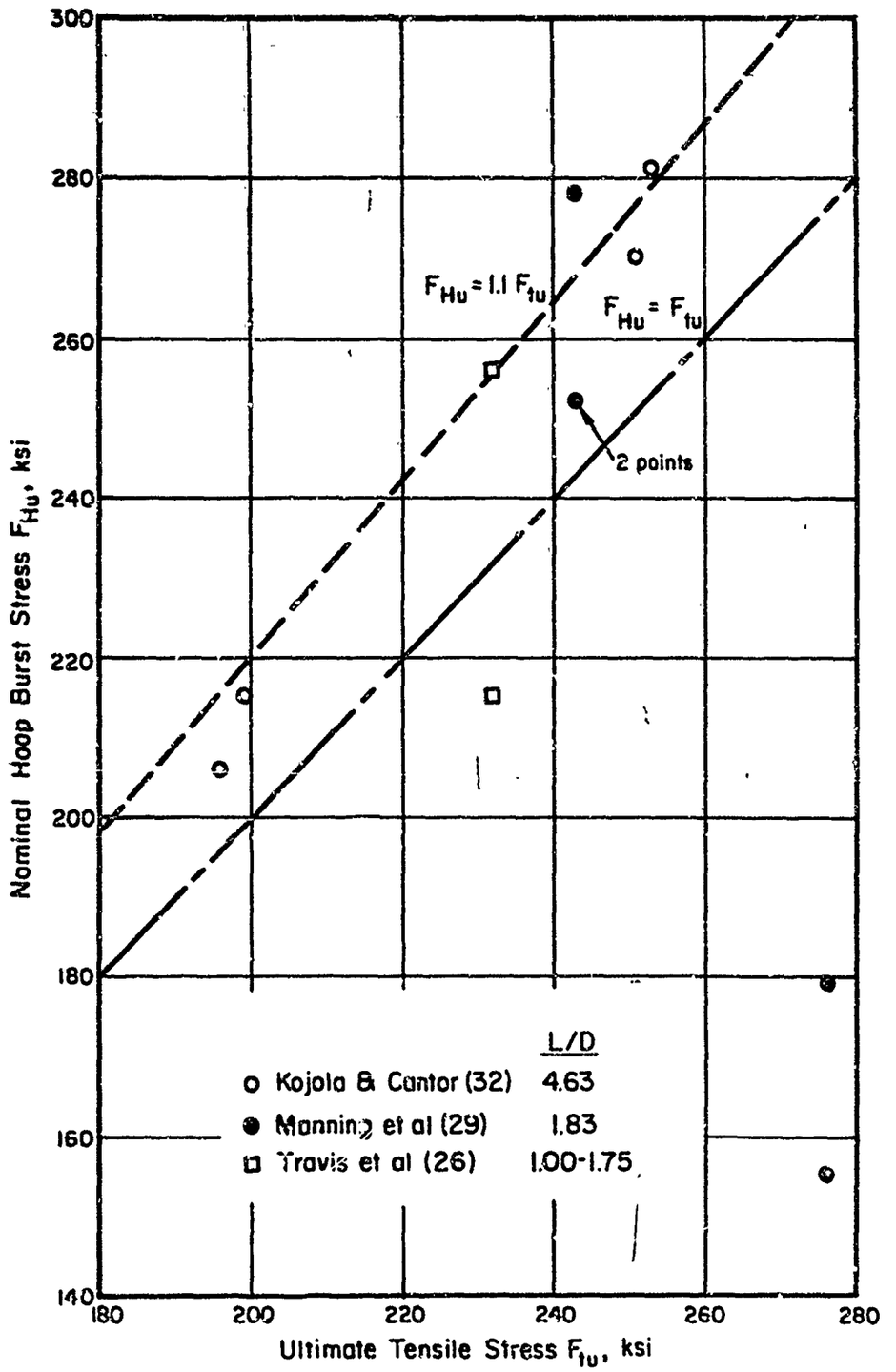

FIGURE 59. EFFECT OF ULTIMATE TENSILE STRESS ON NOMINAL HOOP BURST STRESS AT A BIAXIAL-STRESS RATIO OF 0.5 AND ROOM TEMPERATURE FOR MBMC-1 STEEL. CYLINDRICAL SHELLS WITH LENGTH/DIAM RATIOS AND DATA SOURCES INDICATED IN LEGEND

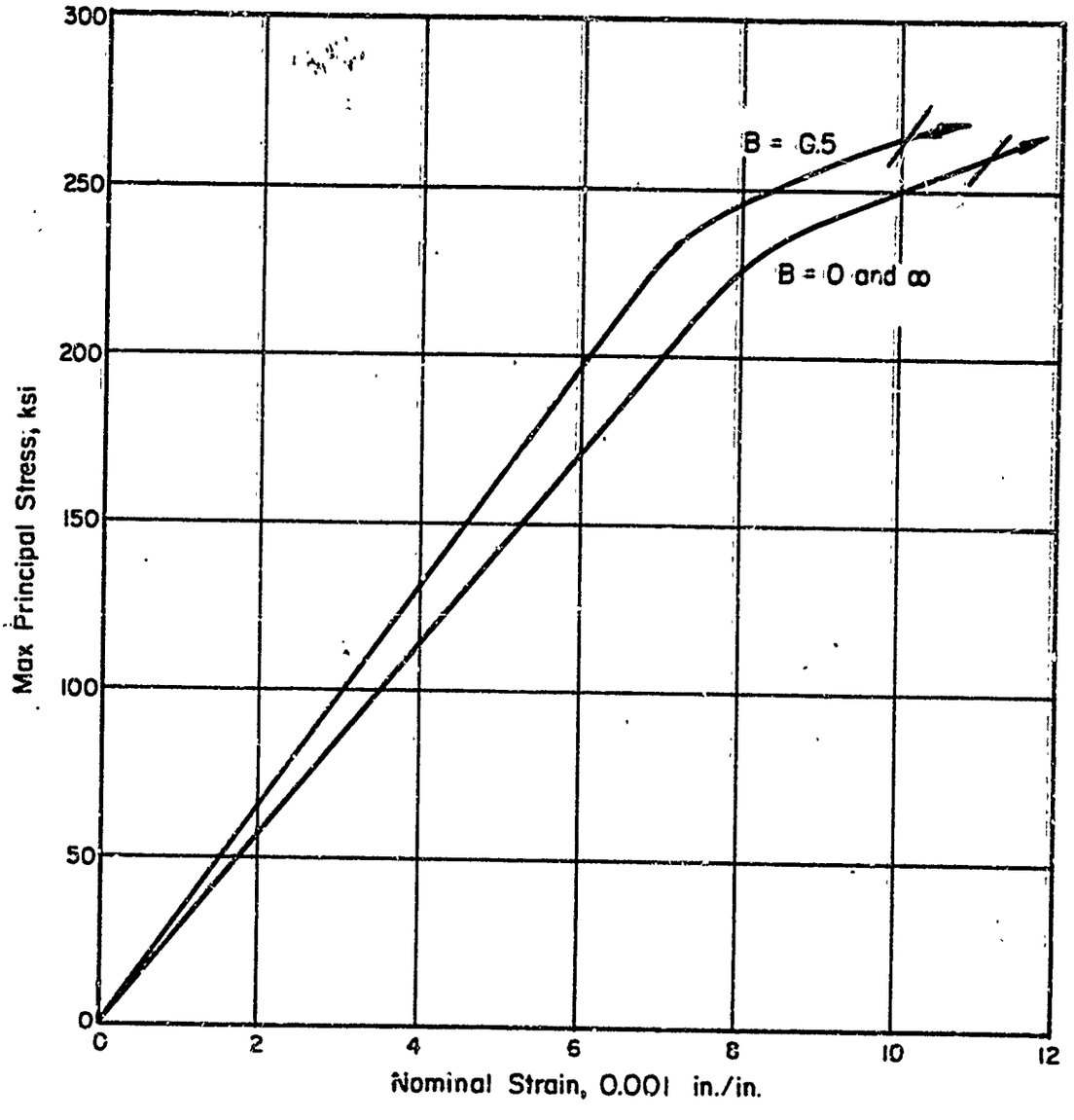

FIGURE 60. TYPICAL BIAXIAL STRESS-STRAIN CURVES AT ROOM TEMPERATURE FOR ROCOLOY 270 STEEL. CYLINDRICAL SHELL WITH LENGTH/DIAM RATIO OF 3.50
Data Source: Bhat & Lindh (21)

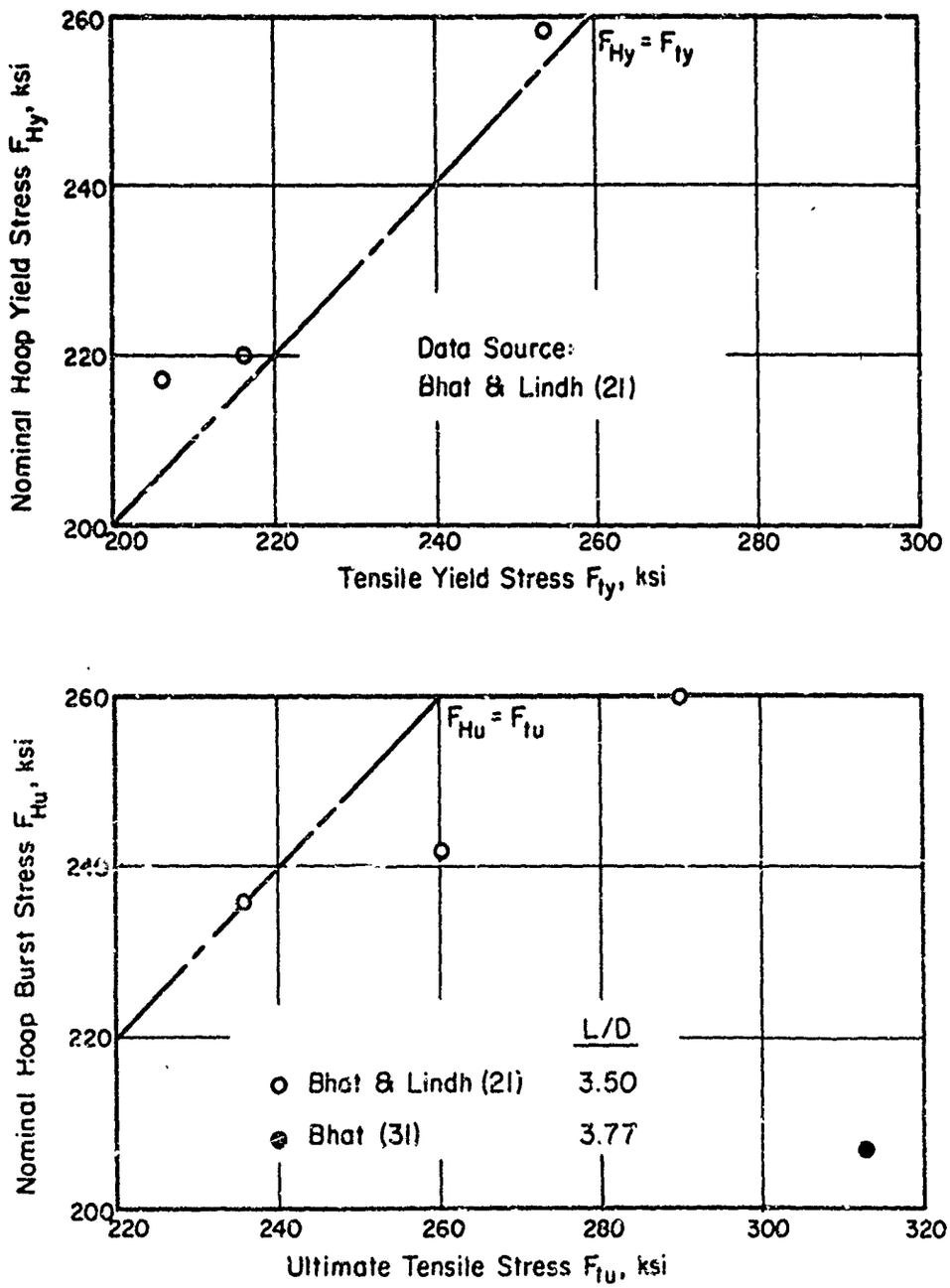

FIGURE 61. EFFECT OF TENSILE YIELD STRESS ON NOMINAL HOOP YIELD STRESS AND OF ULTIMATE TENSILE STRESS ON NOMINAL HOOP BURST STRESS AT A BIAXIAL STRESS RATIO OF 0.5 AND ROOM TEMPERATURE FOR ROCOLOY 270 STEEL. CYLINDRICAL SHELLS WITH LENGTH/DIAM RATIOS AND DATA SOURCES INDICATED IN LEGEND

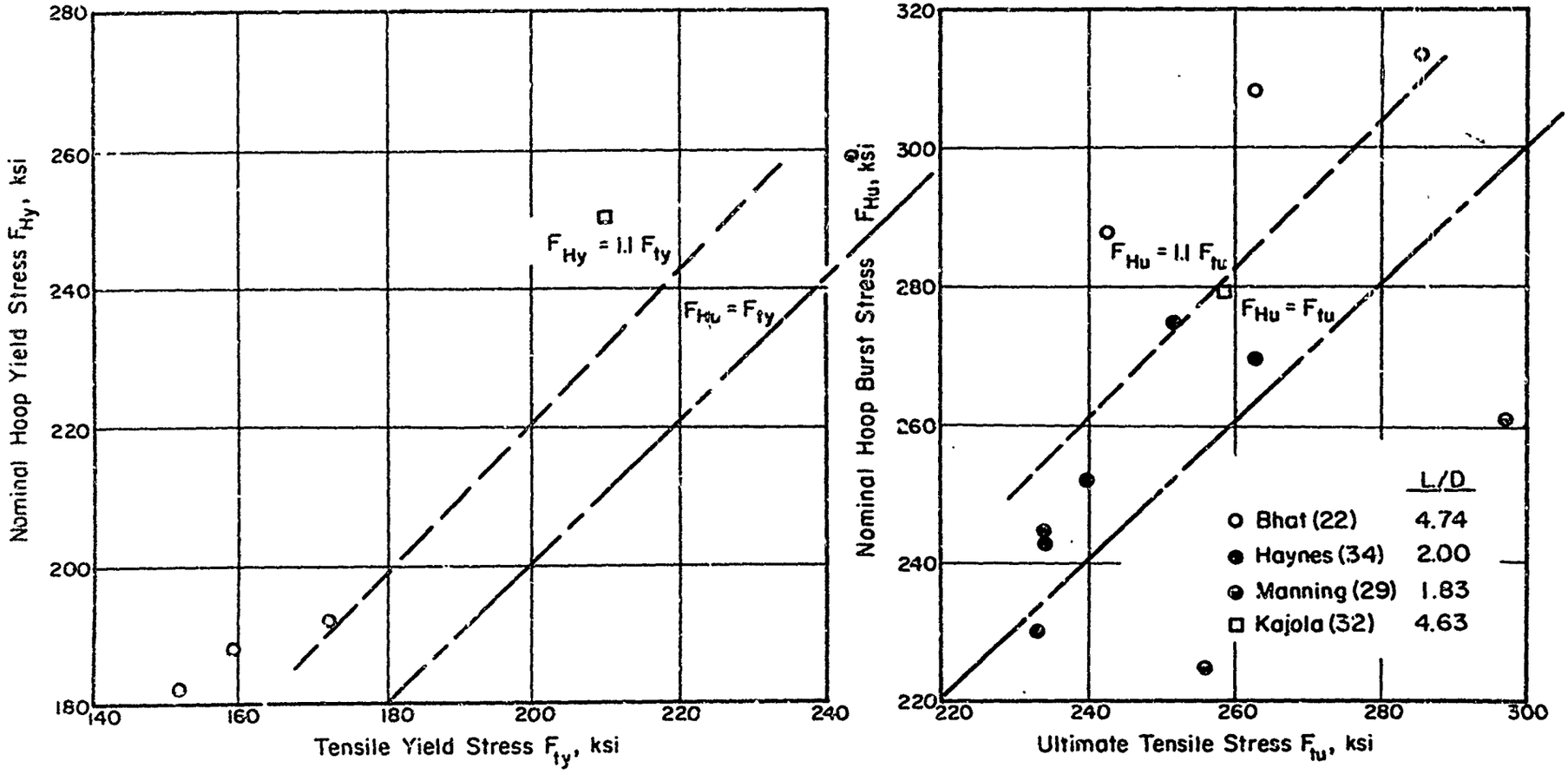

FIGURE 62. EFFECT OF TENSILE YIELD STRESS ON NOMINAL HOOP YIELD STRESS AND OF ULTIMATE TENSILE STRESS ON NOMINAL HOOP BURST STRESS AT A BIAXIAL STRESS RATIO OF 0.5 AND ROOM TEMPERATURE FOR H-11 STEEL CYLINDRICAL SHELLS
Data Sources: Bhat (22); Haynes, Valdez (34); Manning, Murphy, Nichols, Caine (29), Kajola, Cantor (32)

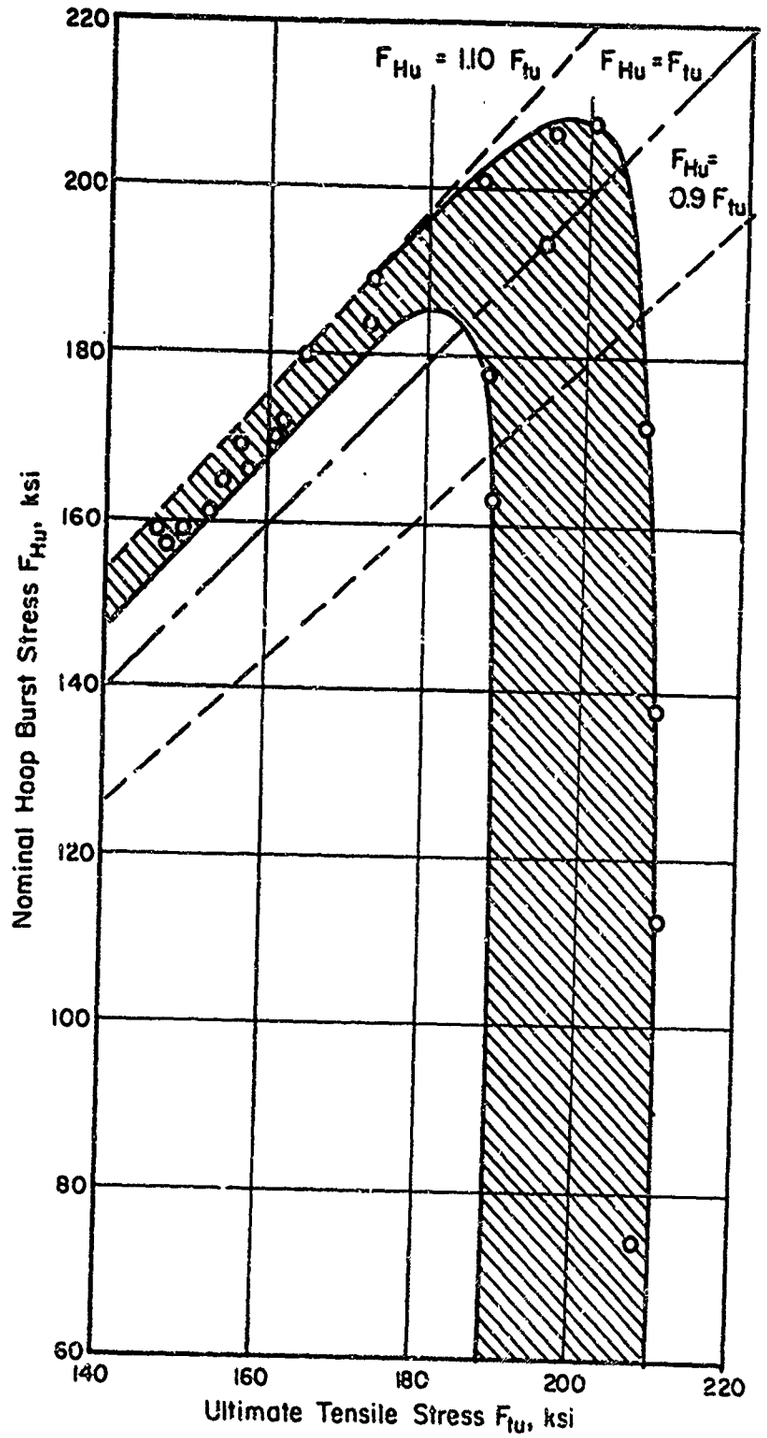

FIGURE 63. EFFECT OF ULTIMATE TENSILE STRESS ON NOMINAL HOOP BURST STRESS AT A BIAXIAL-STRESS RATIO OF 0.5 AND ROOM TEMPERATURE FOR 17-7 PH (TH 1050) STAINLESS STEEL. CYLINDRICAL SHELLS

Data Source: Kinnamon et al (33)

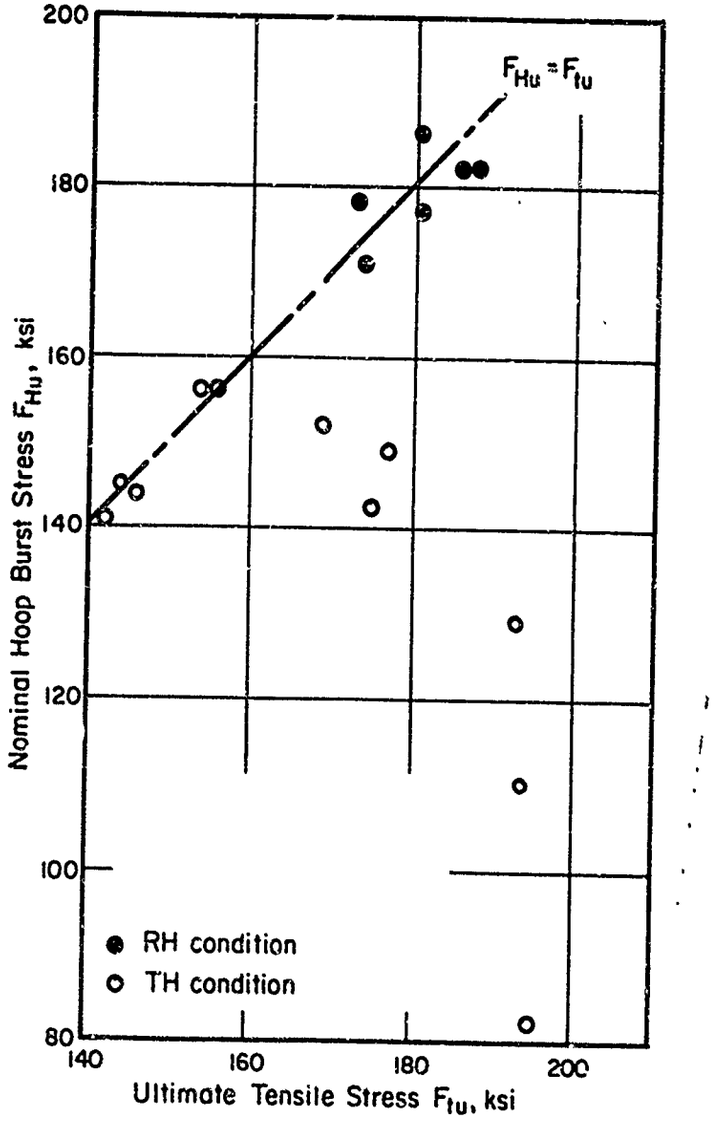

FIGURE 64. EFFECT OF ULTIMATE TENSILE STRESS ON NOMINAL HOOP BURST STRESS AT A BIAXIAL-STRESS RATIO OF 1.0 AND ROOM TEMPERATURE FOR 17-7 PH (TH & RH) SPHERICAL SHELLS

Data Source: Kinnaman et al (33)

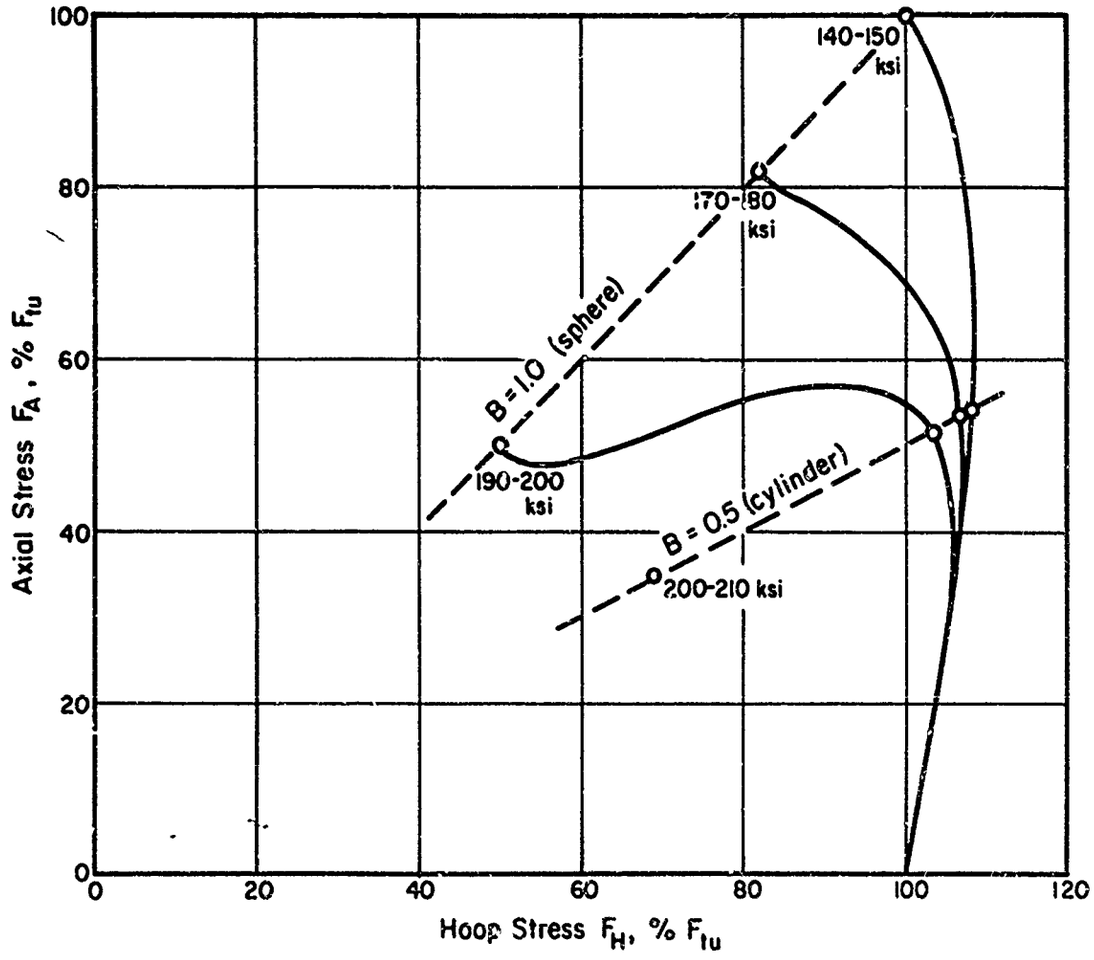

FIGURE 65. BIAXIAL ULTIMATE-STRESS ENVELOPE AT ROOM TEMPERATURE FOR 17-7 PH (TH 1050 CONDITION) STAINLESS STEEL FOR VARIOUS ULTIMATE TENSILE-STRESS RANGES
Data Source: Kinnaman et al (33)

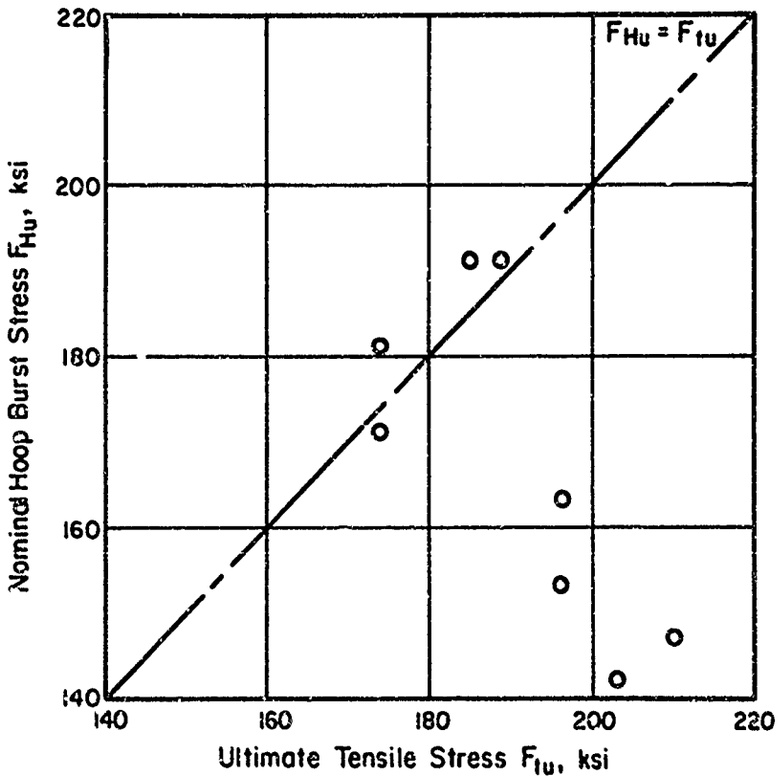

FIGURE 66. EFFECT OF ULTIMATE TENSILE STRESS ON NOMINAL HOOP BURST STRESS AT A BIAXIAL-STRESS RATIO OF 1.0 AND ROOM TEMPERATURE FOR AM-350 STAINLESS STEEL. SPHERICAL SHELLS
Data Source: Kinnaman et al (33)

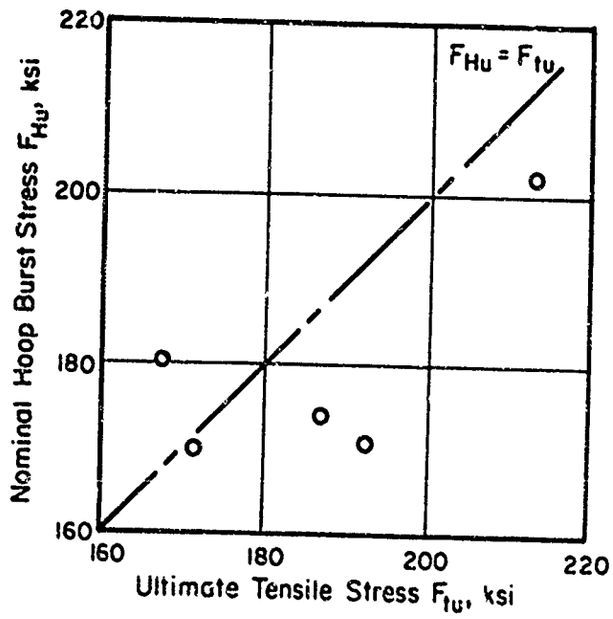

FIGURE 67. EFFECT OF ULTIMATE TENSILE STRESS ON NOMINAL HOOP BURST STRESS AT A BIAXIAL-STRESS RATIO OF 0.5 AND ROOM TEMPERATURE FOR PH 15-7 Mo STEEL. CYLINDRICAL SHELLS WITH LENGTH/DIAM RATIO OF 2.0

Data Source: Haynes, Valdez (34)

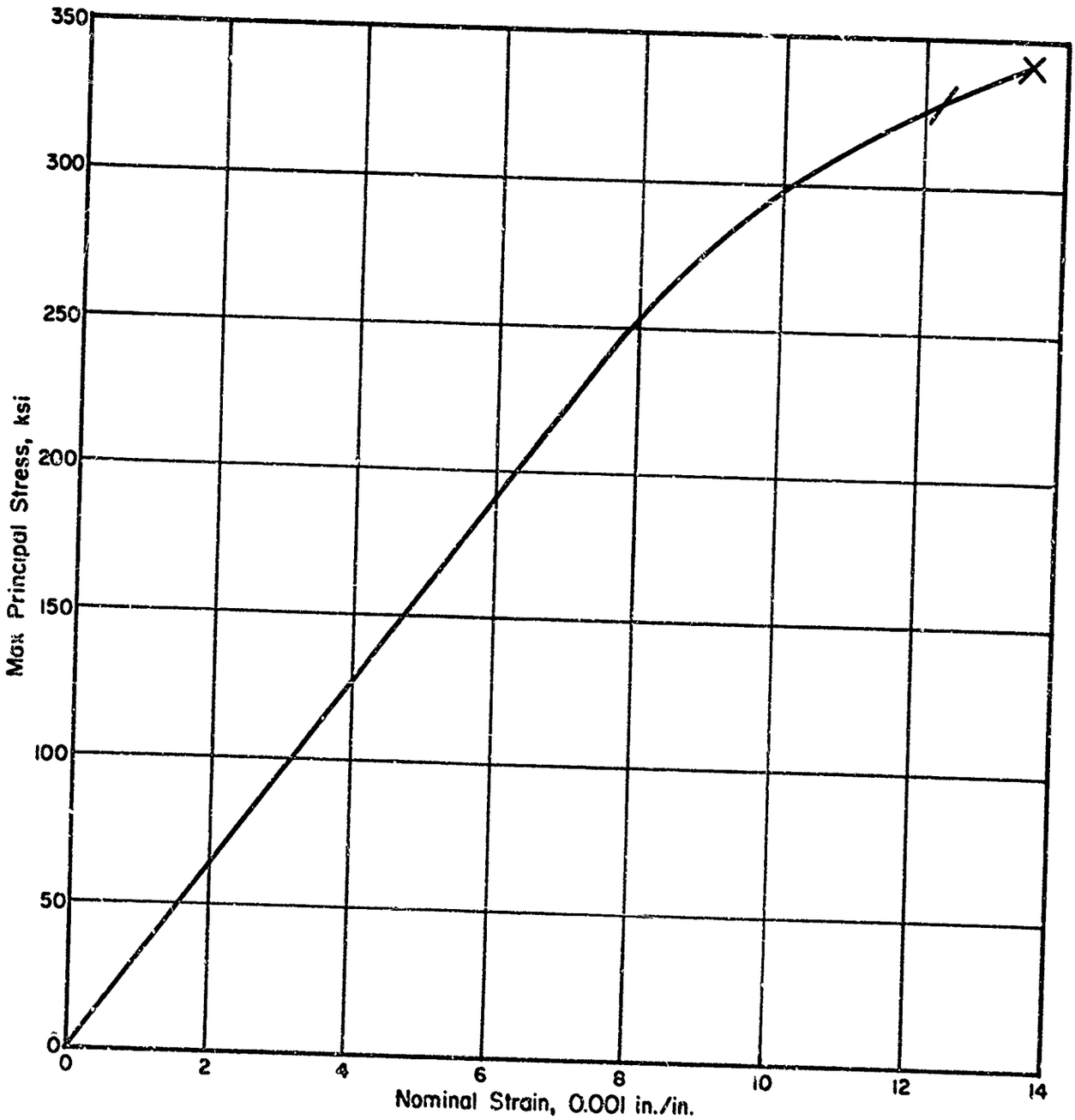

FIGURE 68. TYPICAL BIAXIAL STRESS-STRAIN CURVE AT ROOM TEMPERATURE FOR 18 Ni MARAGING STEEL AT A BIAXIAL-STRESS RATIO OF 0.5. CYLINDRICAL SHELL WITH LENGTH/DIAM RATIO OF 0.70
Data Source: Wei (40)

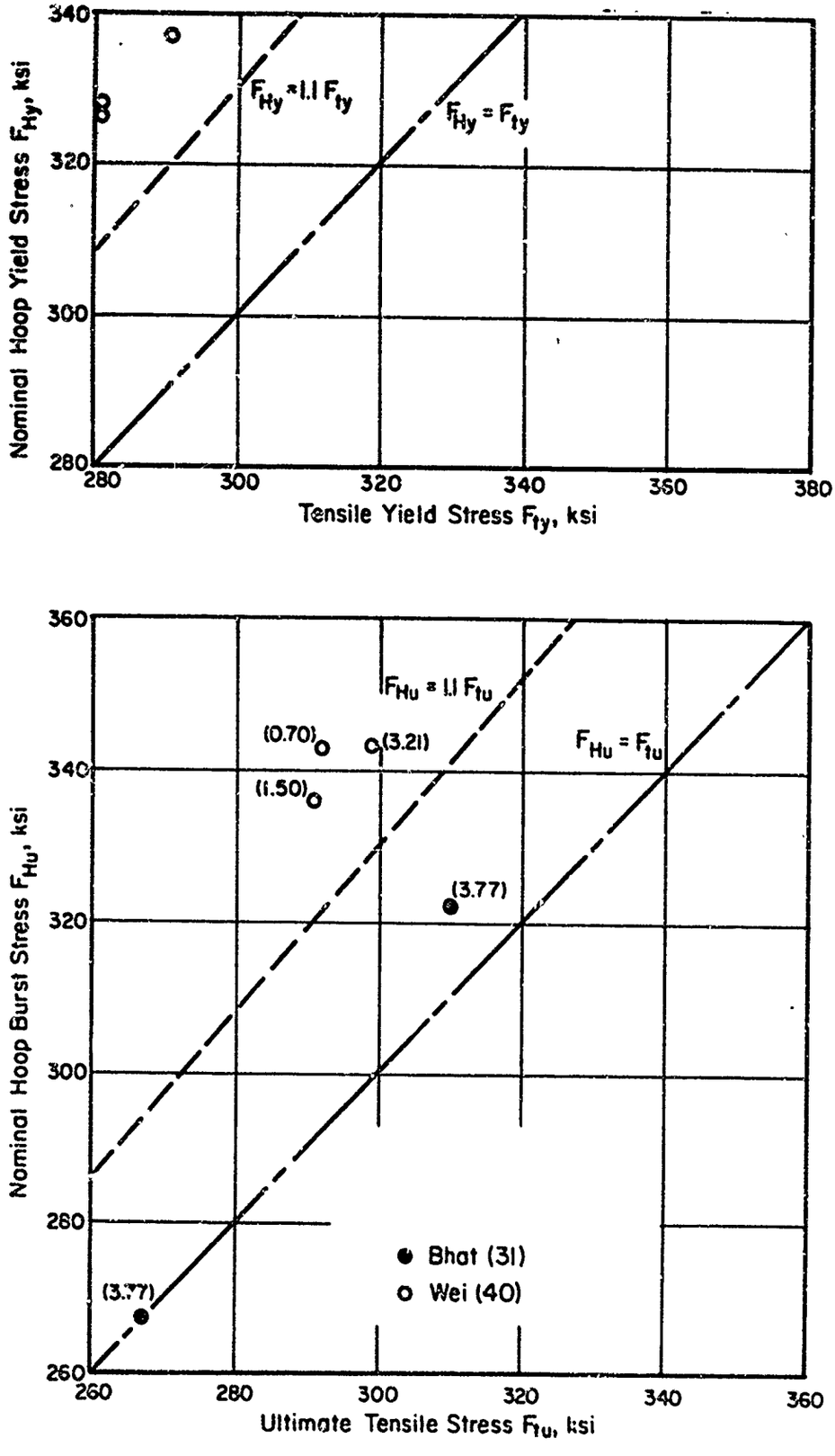

FIGURE 69. EFFECT OF TENSILE YIELD STRESS ON NOMINAL HOOP YIELD STRESS AND OF ULTIMATE TENSILE STRESS ON NOMINAL HOOP BURST STRESS AT A BIAXIAL-STRESS RATIO OF 0.5 AND ROOM TEMPERATURE FOR 18 Ni MARAGING STEEL. CYLINDRICAL SHELL WITH LENGTH/DIAM RATIOS IN PARENTHESES

Data Sources. Shown in legend

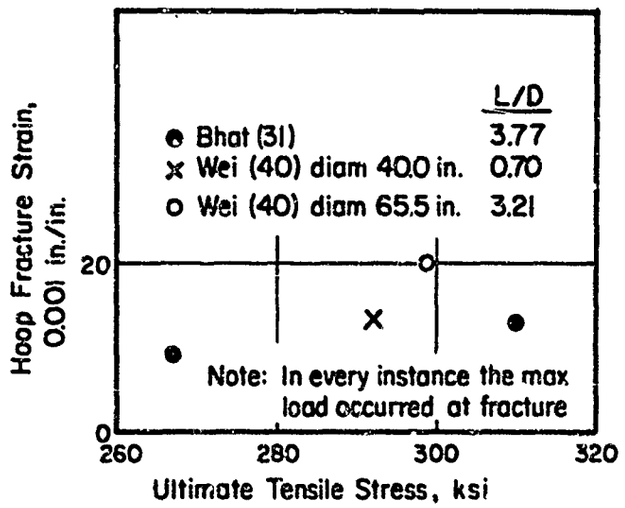

FIGURE 70. EFFECT OF ULTIMATE TENSILE STRESS ON HOOP FRACTURE STRAIN AT A BIAXIAL-STRESS RATIO OF 0.5 AND ROOM TEMPERATURE FOR 18 Ni MARAGING STEEL. CYLINDRICAL SHELLS WITH LENGTH/DIAM RATIOS AND DATA SOURCES INDICATED IN LEGEND.

Data Summary Sheet for:

25 Ni Maraging Steel

1. Typical Biaxial Stress-Strain Curves

   Not available

2. Biaxial Yield Stress:

   vs TYS BYS = 280,000 psi, TYS = 245,000 psi

   at B = 0.5 and UTS = 259,000 psi

   Envelope: Not available

3. Biaxial Ultimate Stress:

   vs UTS BUS = 314,000 psi, UTS = 259,000 psi

   at B = 0.5

   Envelope: Not available

4. Strain at Biaxial Ultimate Stress

   vs UTS Not available

   Envelope Not available

5. Remarks:

   Reference: Kitchin (43)

FIGURE 71. BIAXIAL-PROPERTY DATA SUMMARY SHEET FOR 25 Ni MARAGING STEEL

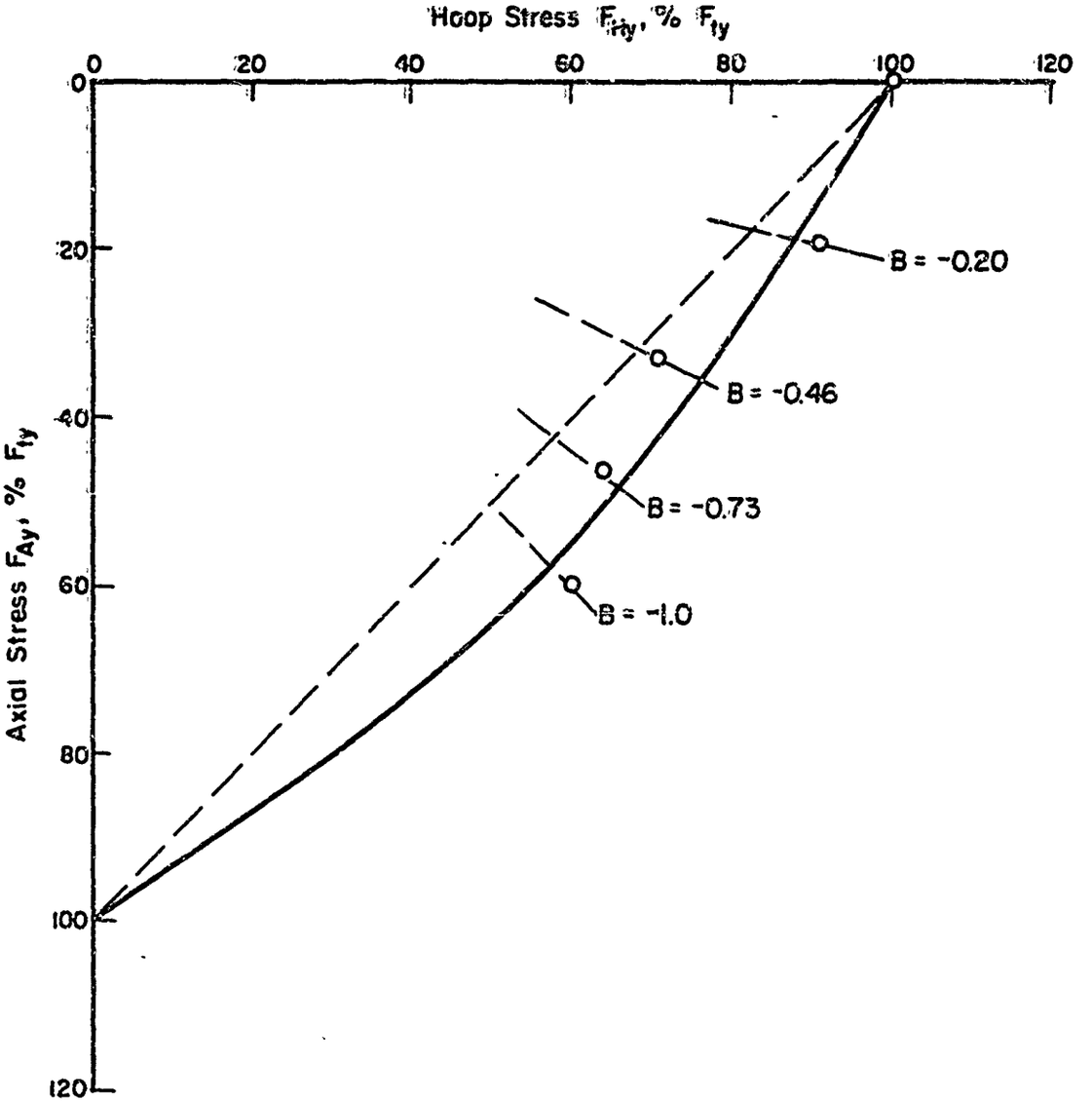

FIGURE 72. BIAXIAL YIELD-STRESS ENVELOPE AT ROOM TEMPERATURE FOR 2014-T4 ALUMINUM ALLOY. CYLINDRICAL SPECIMEN
Data Source: Marin & Wiseman (44)

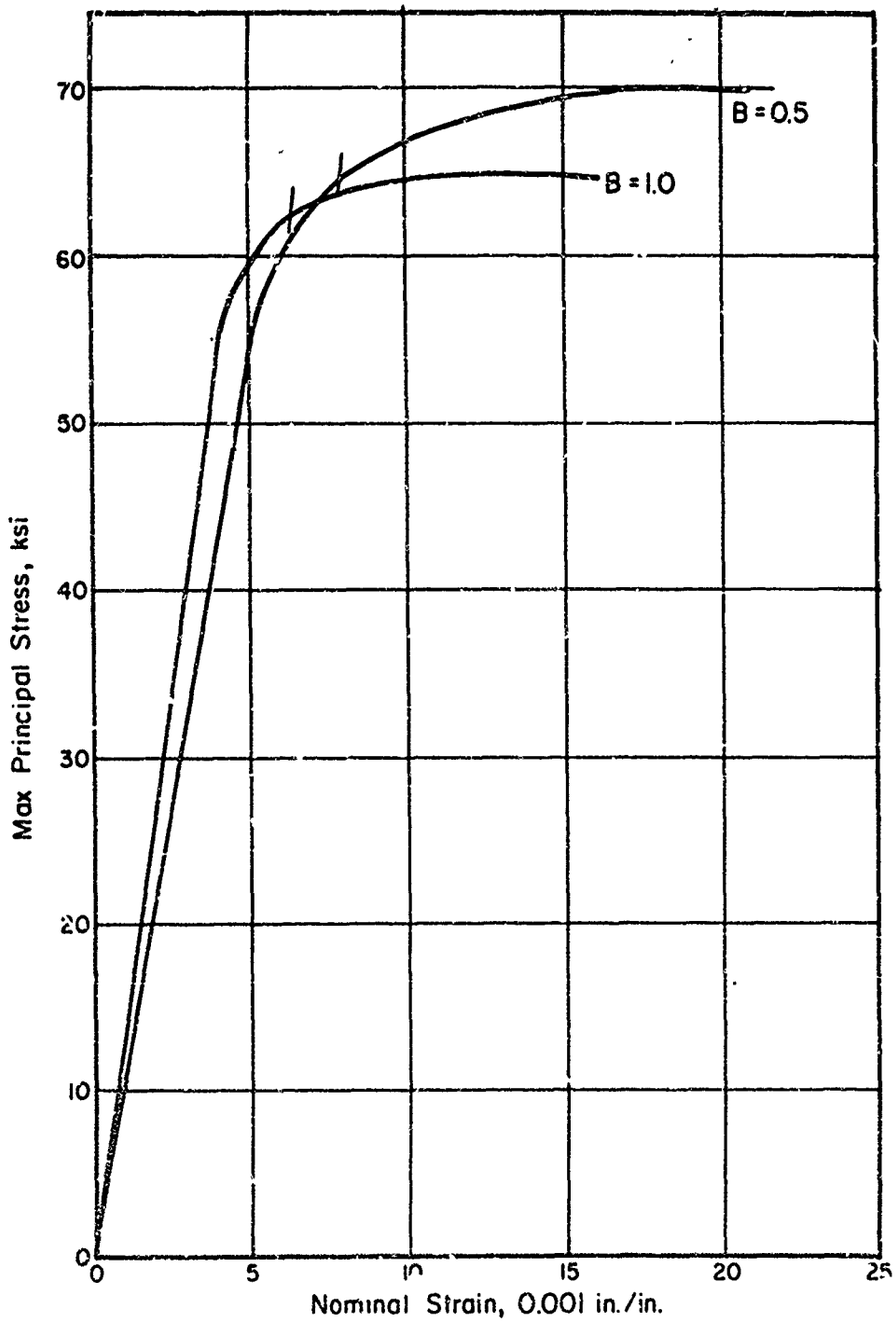

FIGURE 73. TYPICAL BIAXIAL STRESS-STRAIN CURVES AT ROOM TEMPERATURE FOR 2014-T6 ALUMINUM ALLOY. CYLINDRICAL SPECIMEN WITH LENGTH/DIAM RATIO OF 7.0
Data Source: Marin & Sauer (45)

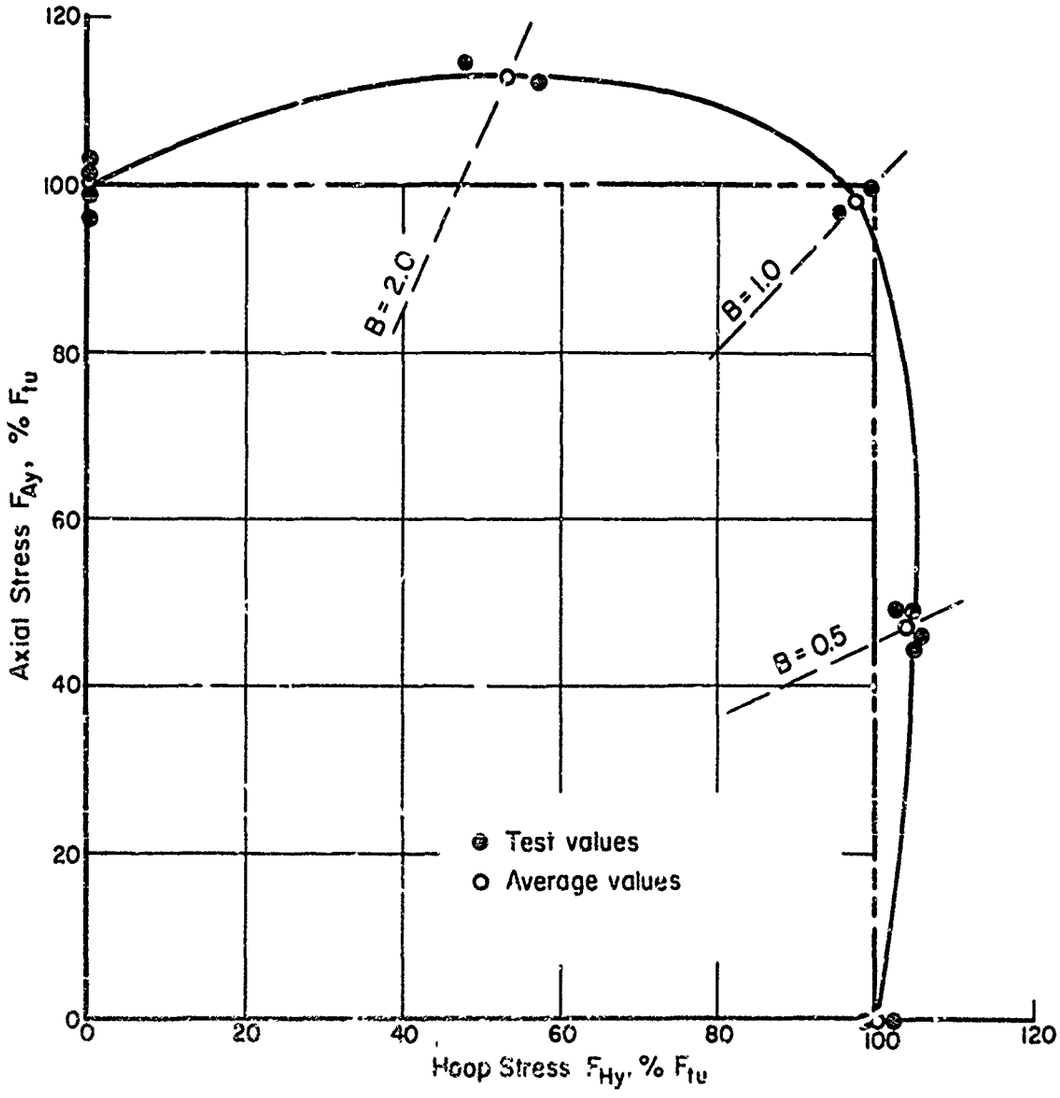

FIGURE 74. BIAXIAL YIELD-STRESS ENVELOPE AT ROOM TEMPERATURE FOR 2014-T6 ALUMINUM ALLOY
Data Source: Marin & Sauer (45)

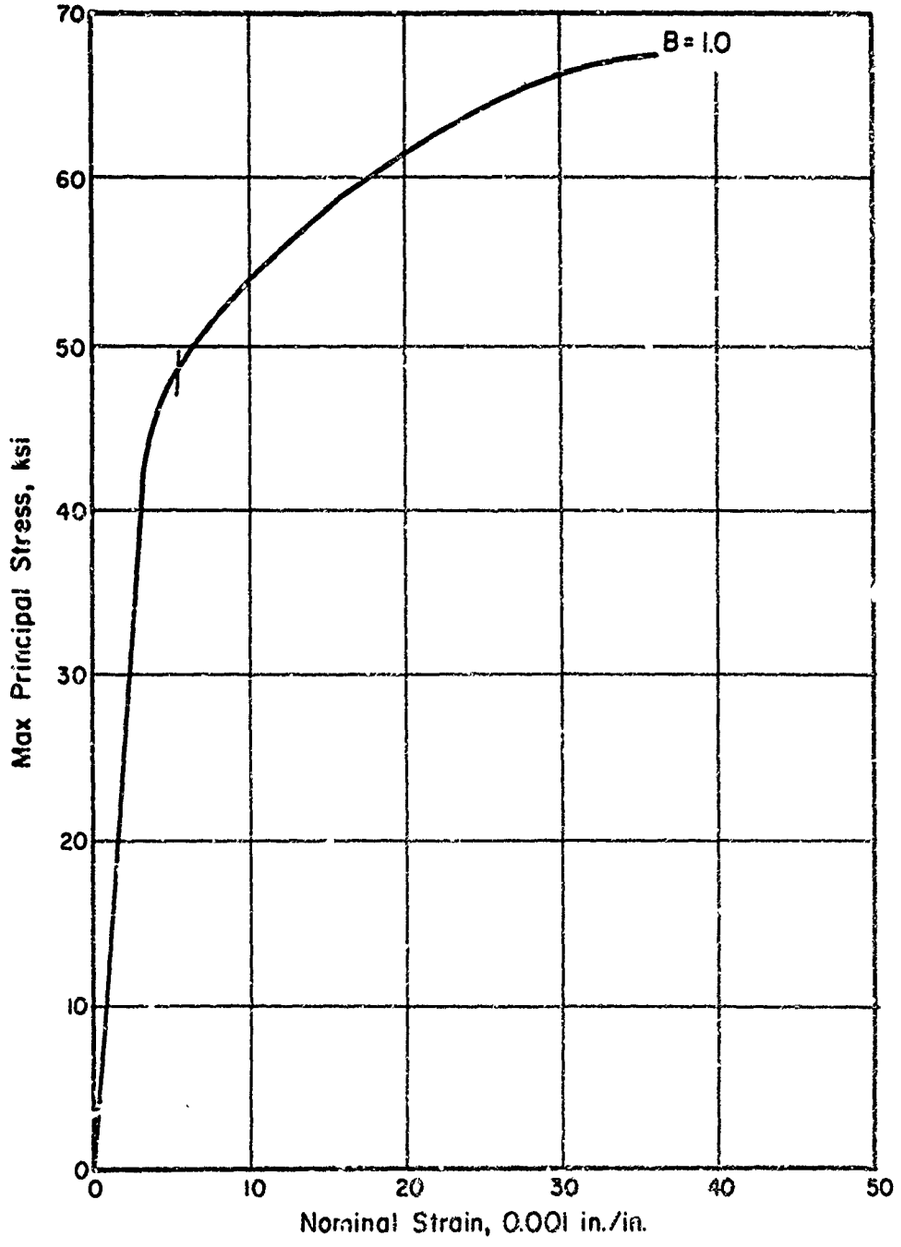

FIGURE 75. TYPICAL BIAXIAL STRESS-STRAIN CURVE AT ROOM TEMPERATURE FOR 2024-T ALUMINUM ALLOY. CYLINDRICAL SPECIMEN WITH LENGTH/DIAM RATIO OF 8.0
Data Source: Marin (9)

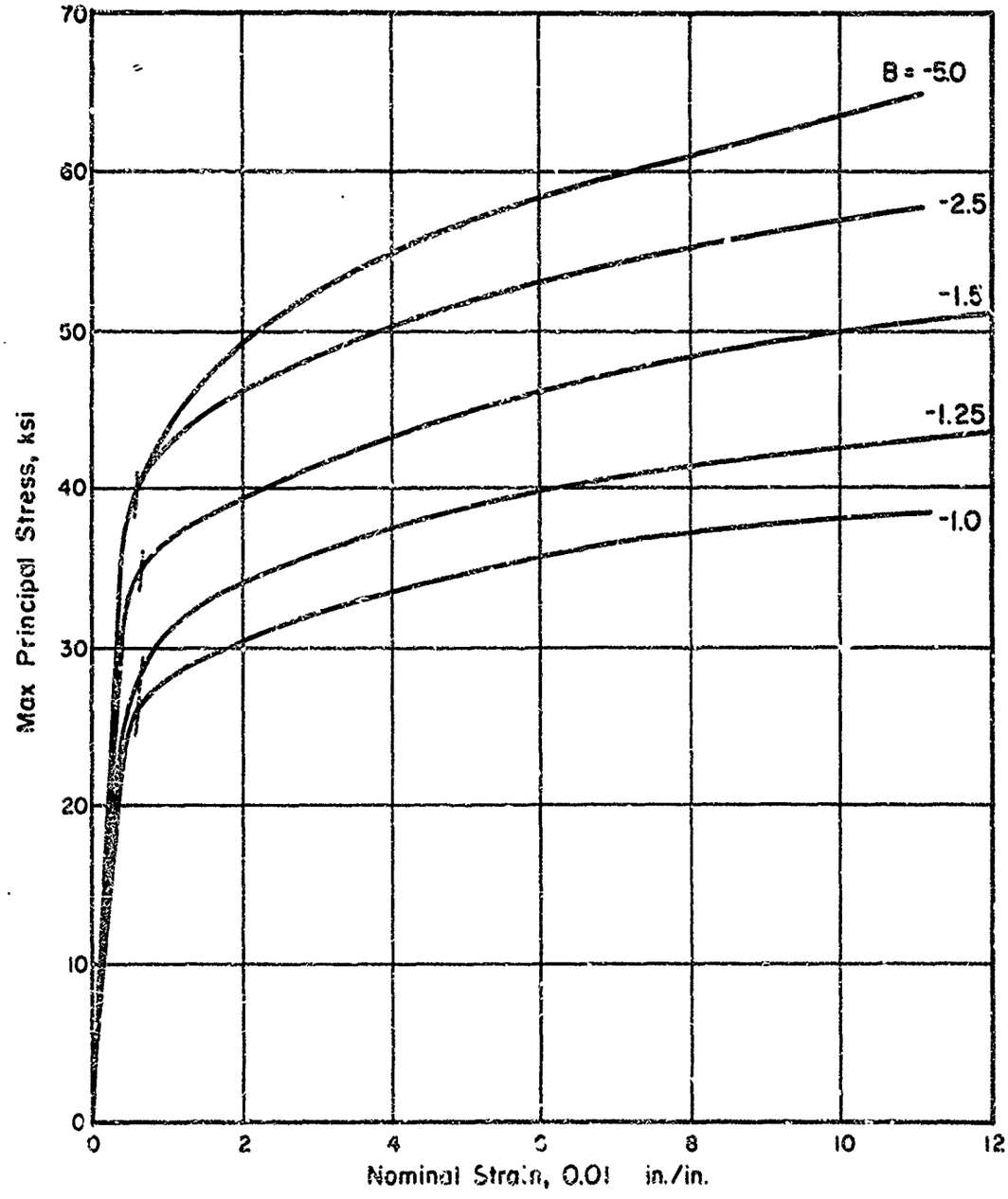

FIGURE 76. TYPICAL BIAXIAL STRESS-STRAIN CURVES AT ROOM TEMPERATURE FOR 2024-T ALUMINUM ALLOY. CYLINDRICAL SPECIMEN WITH LENGTH/DIAM RATIO OF 8.0
Data Source: Marin (12)

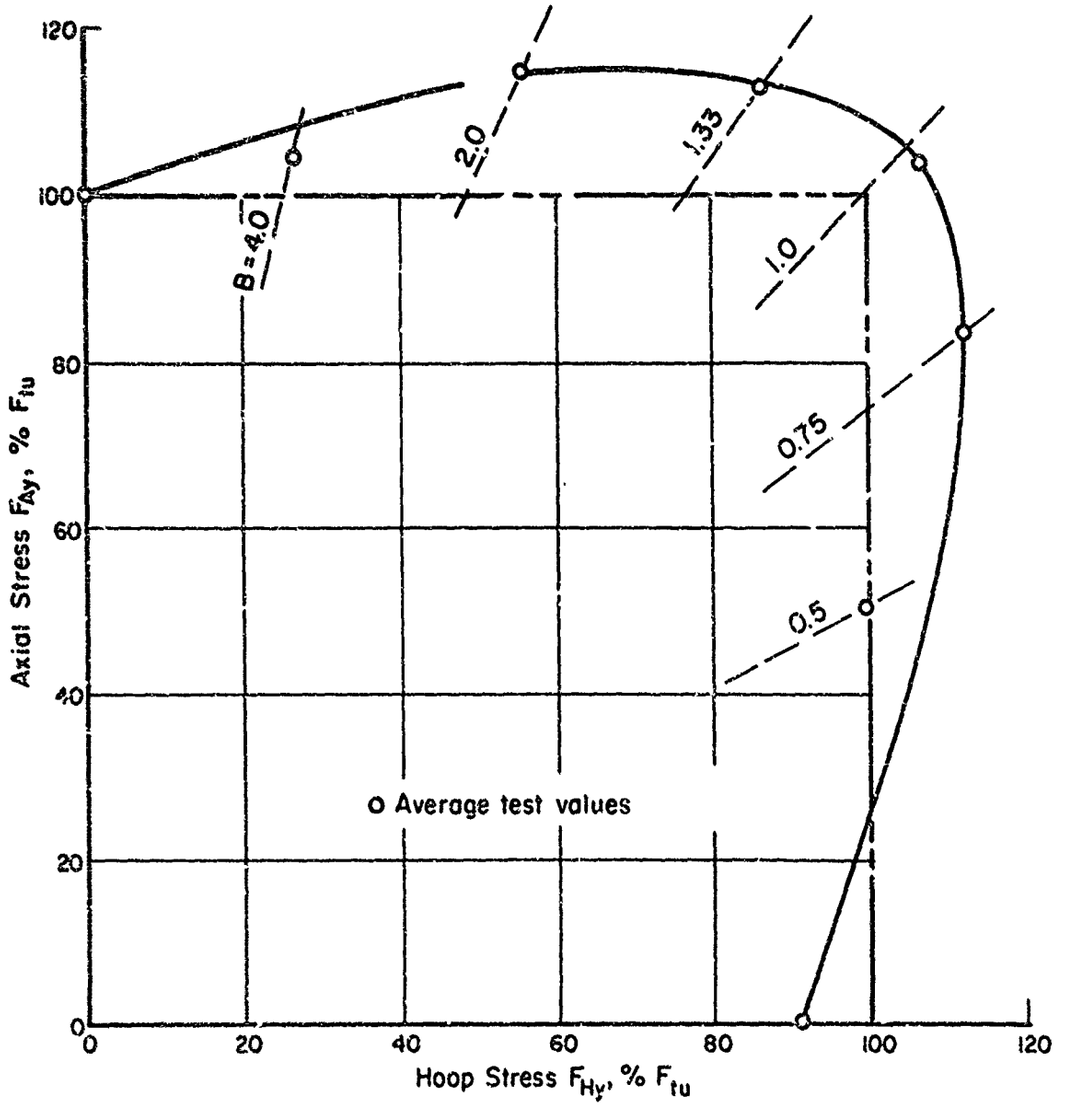

FIGURE 77. BIAXIAL YIELD-STRESS ENVELOPE AT ROOM TEMPERATURE FOR 2024-T ALUMINUM ALLOY
Data Source: Marin (9)

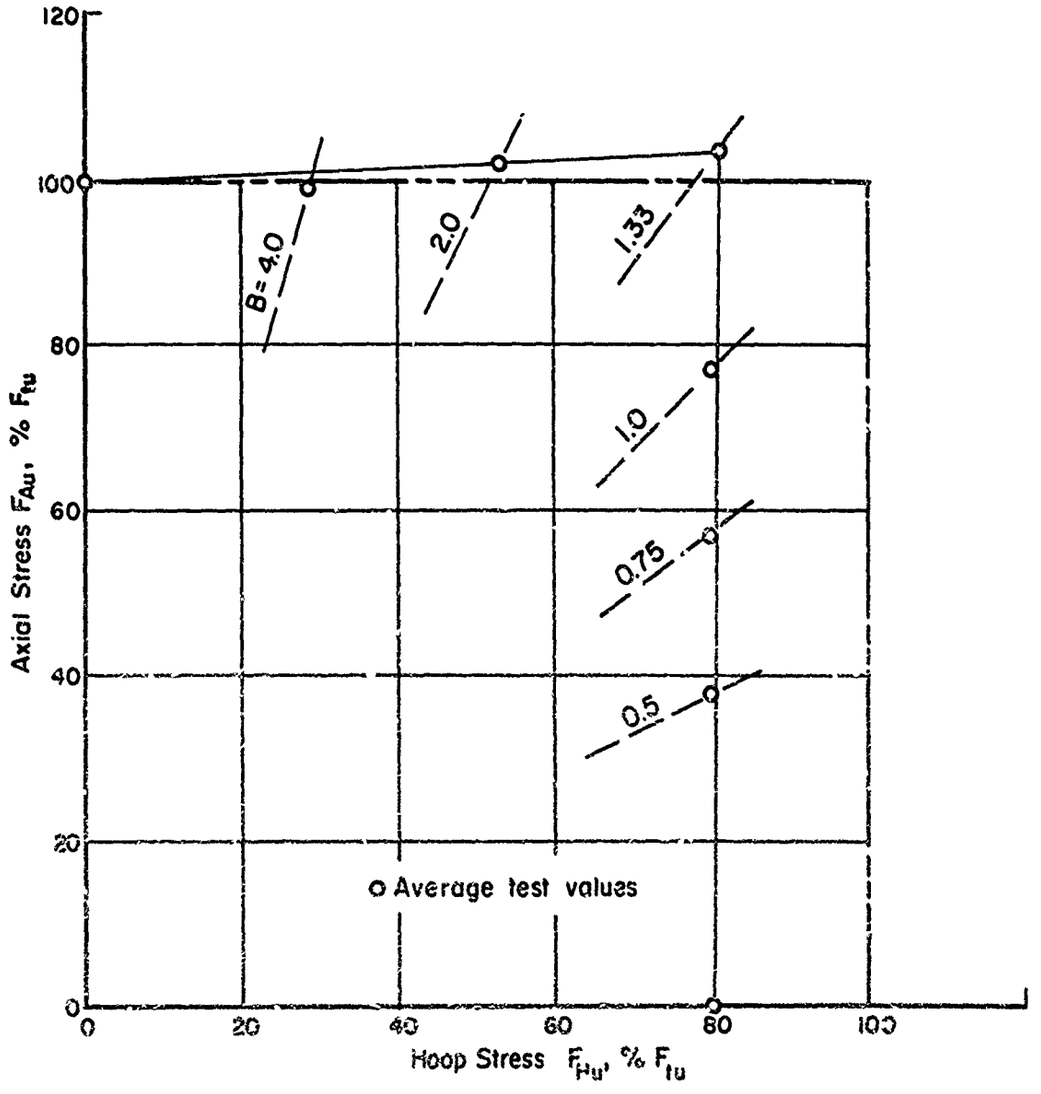

FIGURE 78. BIAXIAL ULTIMATE-STRESS ENVELOPE AT ROOM TEMPERATURE FOR 2024-T ALUMINUM ALLOY
Data Source: Marin (9)

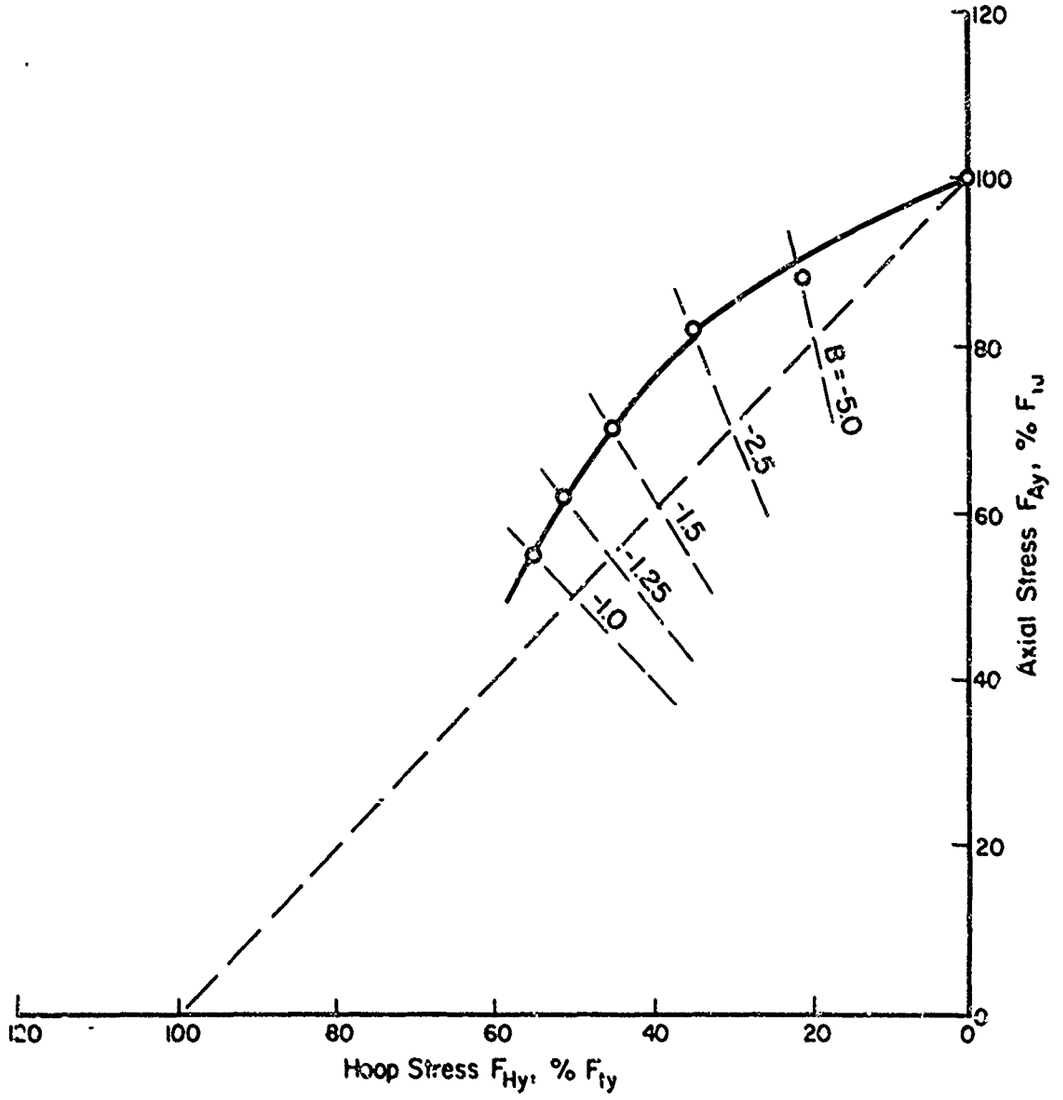

FIGURE 79. BIAXIAL YIELD-STRESS ENVELOPE AT ROOM TEMPERATURE FOR 2024-T ALUMINUM ALLOY
Data Source: Marin (12)

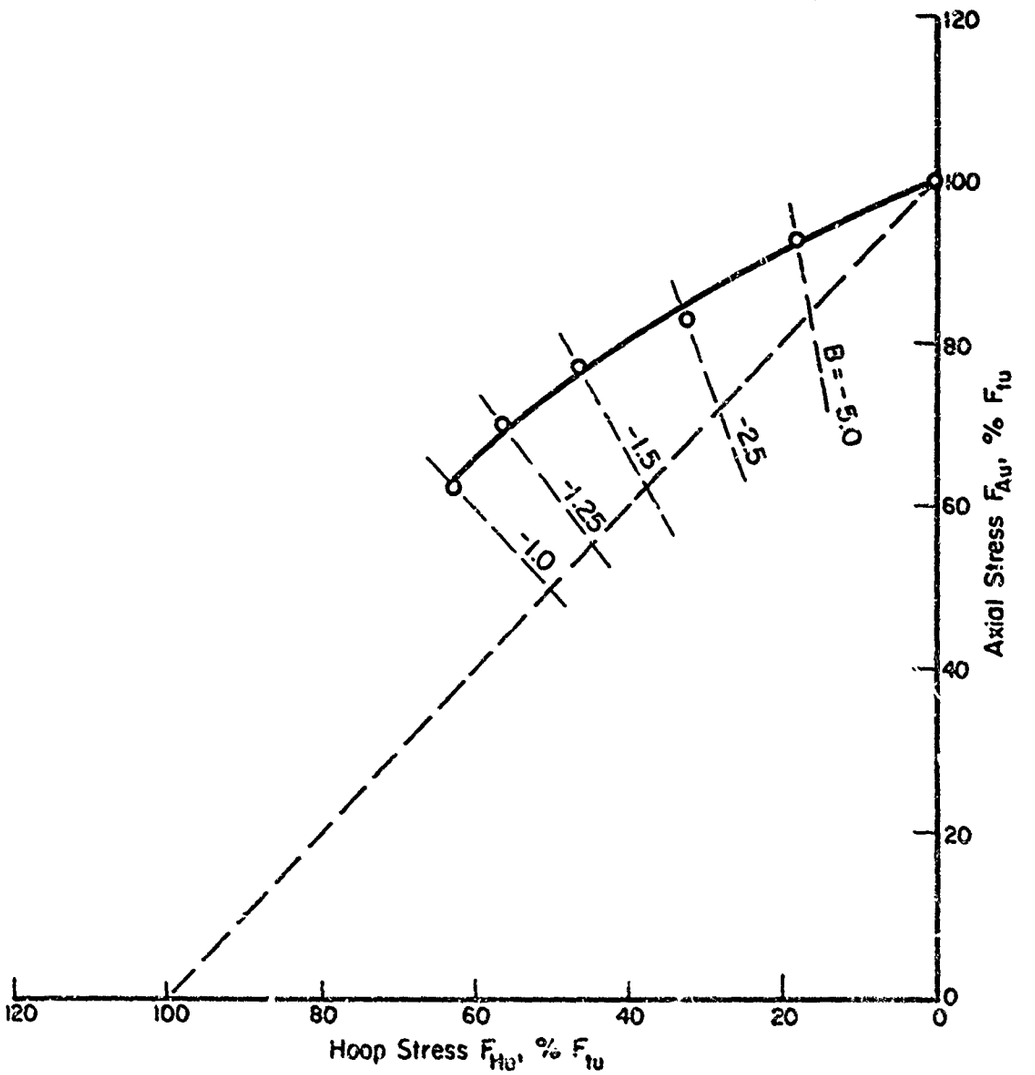

FIGURE 80. BIAXIAL ULTIMATE-STRESS ENVELOPE AT ROOM TEMPERATURE FOR 2024-T ALUMINUM ALLOY
Data Source: Marin (12)

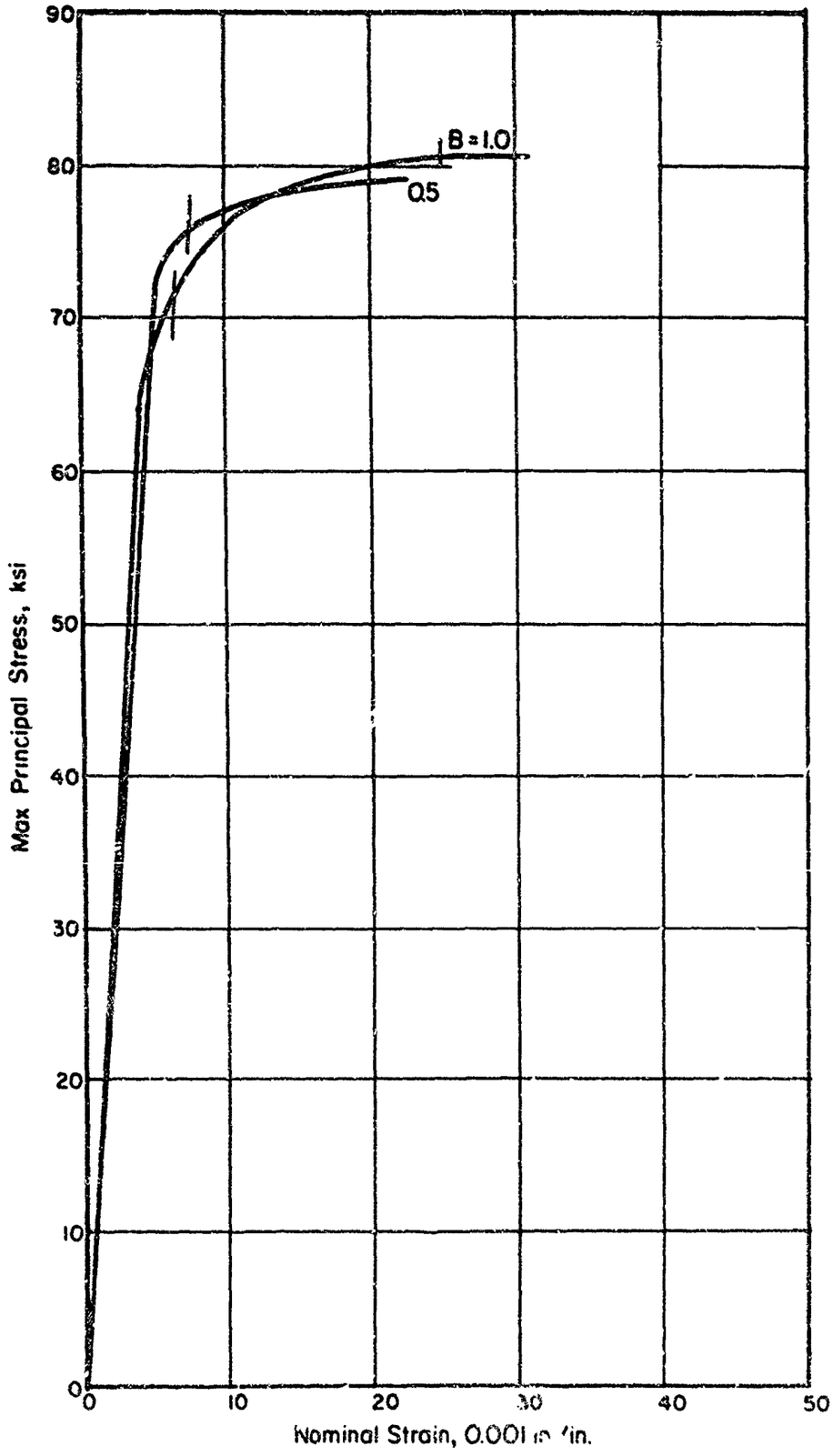

FIGURE 81. TYPICAL BIAXIAL STRESS-STRAIN CURVES AT ROOM TEMPERATURE FOR 7075-T6 ALUMINUM ALLOY. CYLINDRICAL SHELL WITH LENGTH/DIAM RATIO OF 8.0
Data Source: Marin, Ulrich, Hughes (47)

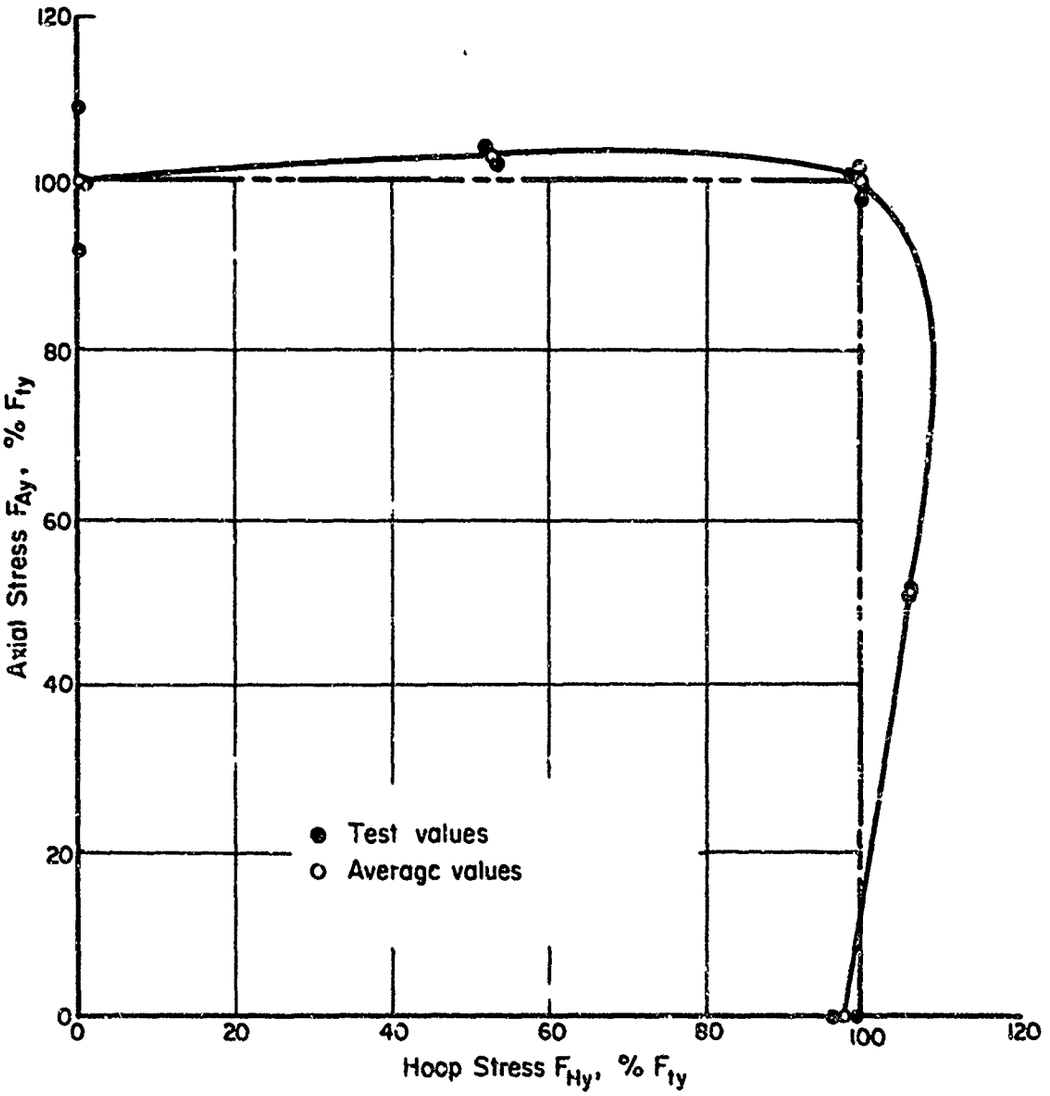

FIGURE 82. BIAXIAL YIELD-STRESS ENVELOPE AT ROOM TEMPERATURE FOR 7075-T6 ALUMINUM ALLOY
Data Source. Marin, Ulrich, Hughes (47)

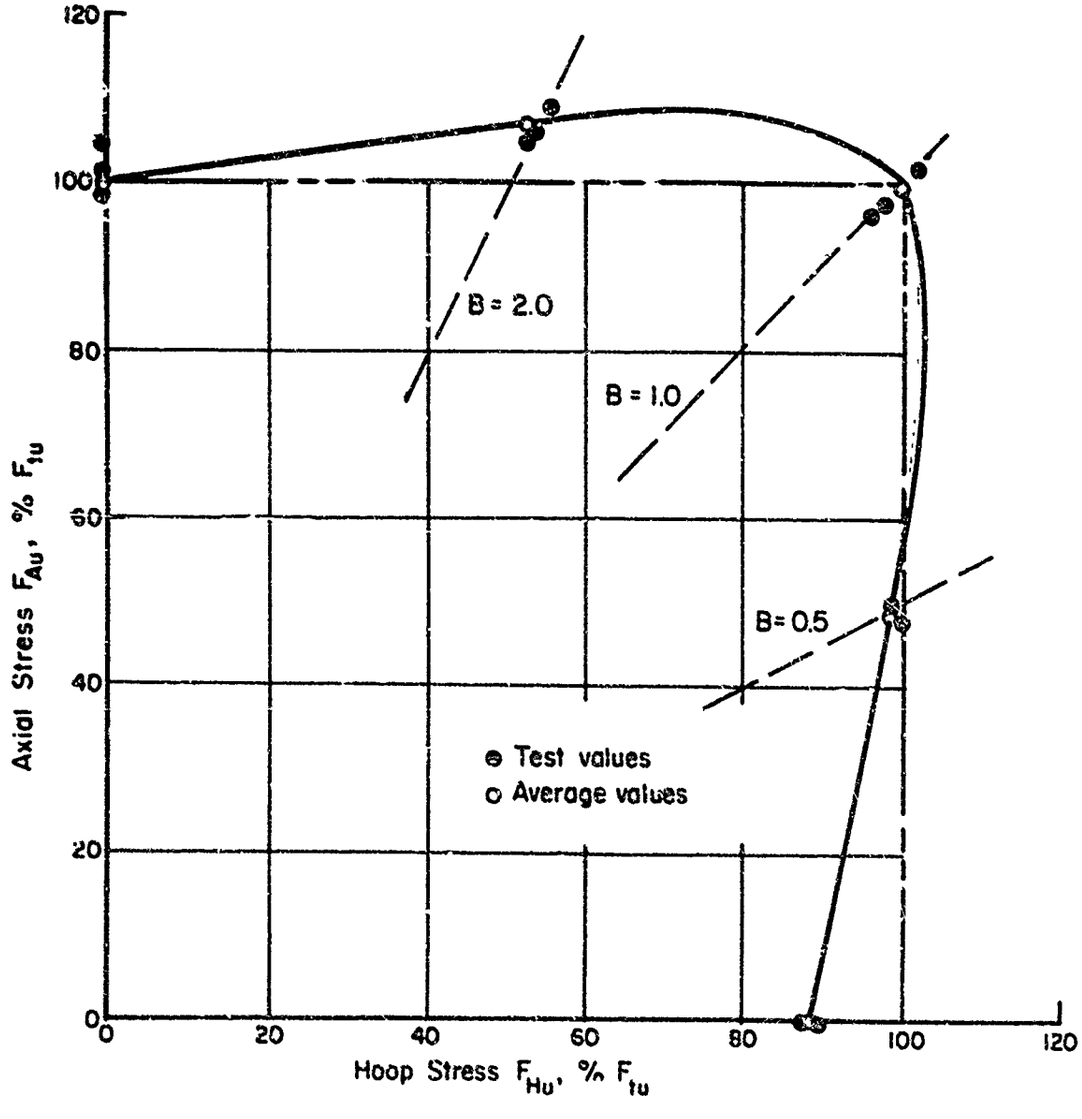

FIGURE 83. BIAXIAL ULTIMATE-STRESS ENVELOPE AT ROOM TEMP FOR 7075-T6 ALUMINUM ALLOY
Data Source: Marin, Ulrich, Hughes (47)

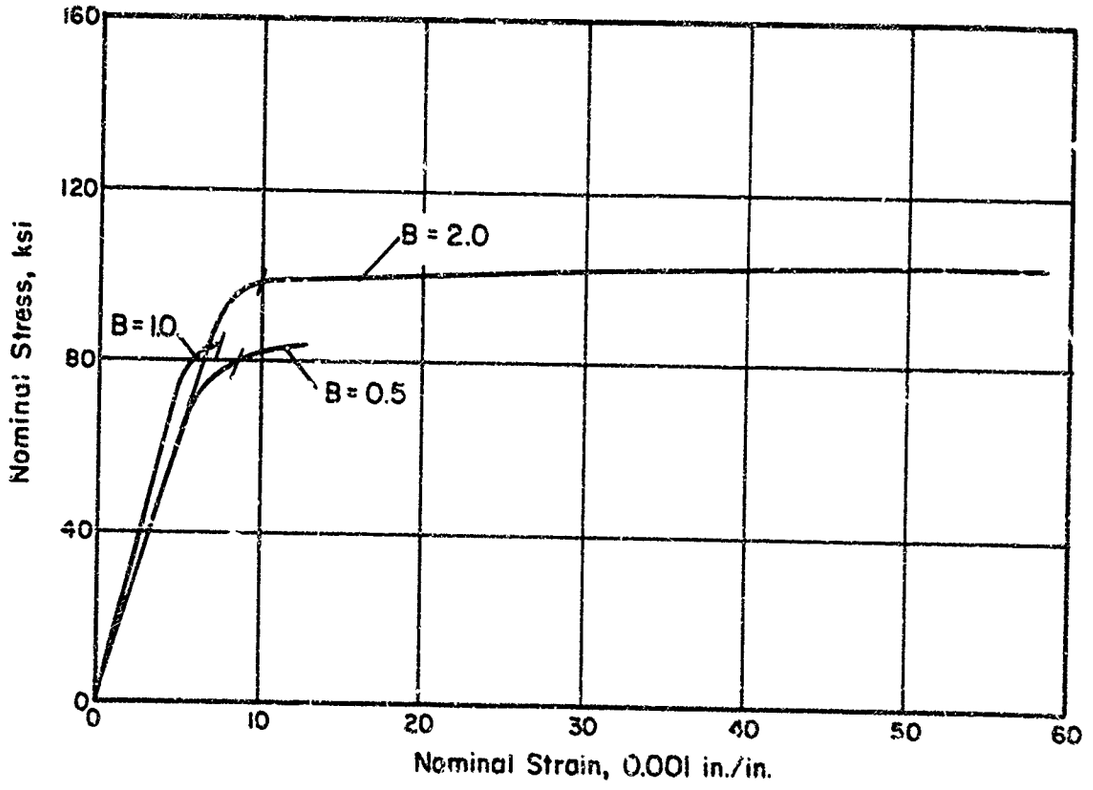

FIGURE 84. TYPICAL BIAXIAL STRESS-STRAIN CURVES AT ROOM TEMPERATURE FOR 7178 ALUMINUM
Data Source: Goodman (28)

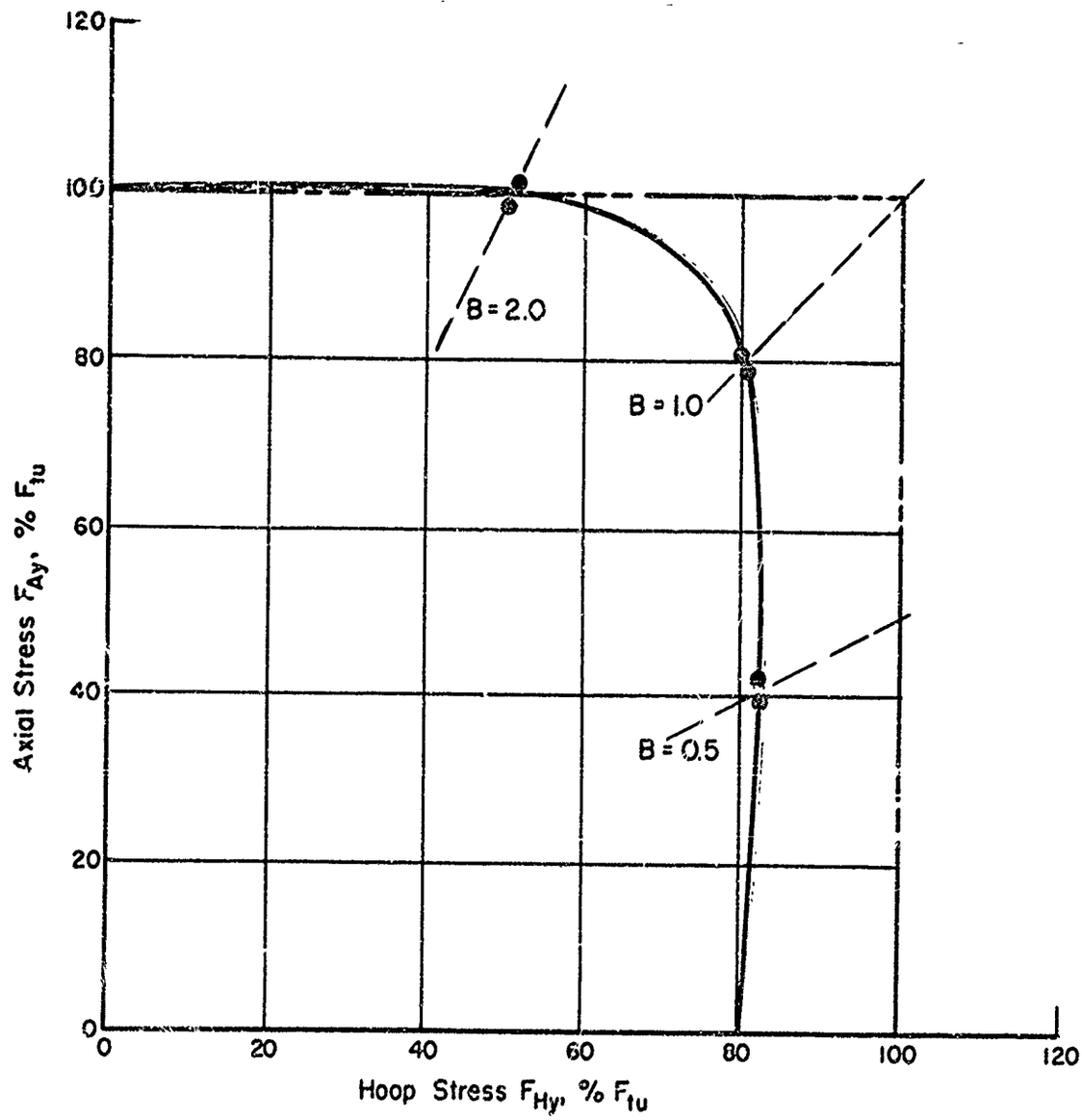

FIGURE 85. BIAXIAL YIELD-STRESS ENVELOPE AT ROOM TEMP FOR 7178-T6 ALUMINUM ALLOY
Data Source: Goodman (28)

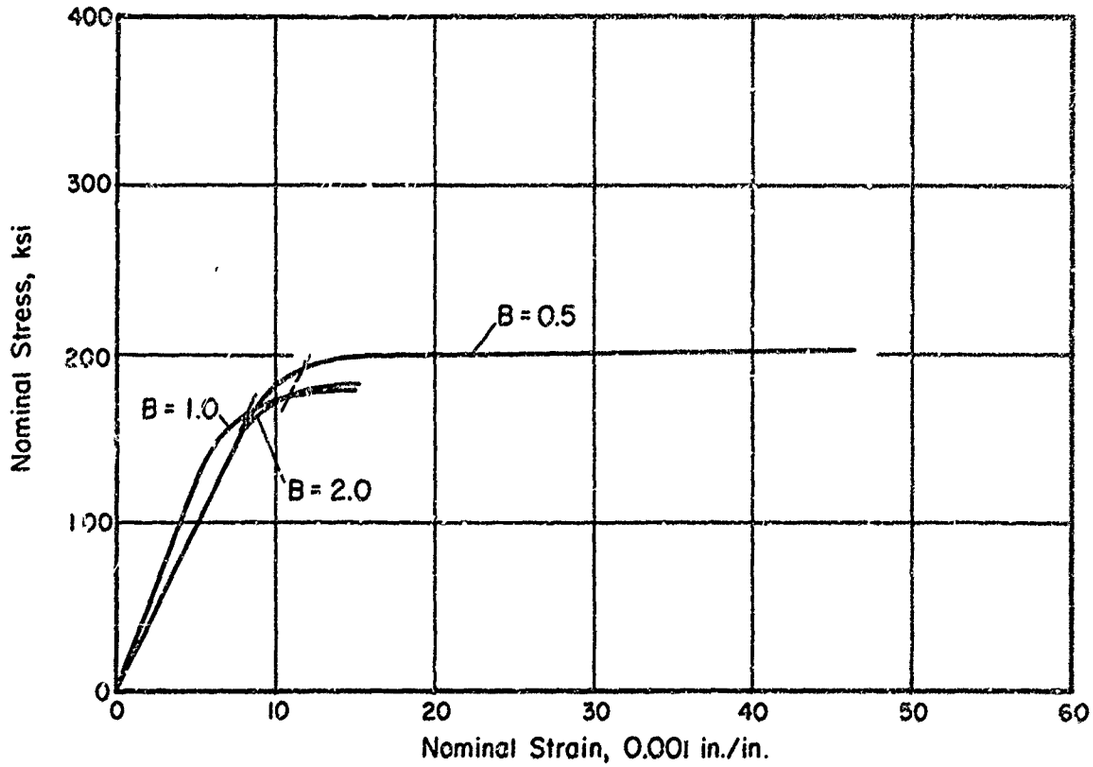

FIGURE 86. TYPICAL BIAXIAL STRESS-STRAIN CURVES AT ROOM TEMPERATURE FOR 6AI-4V TITANIUM 0.19% OXYGEN CONTENT
Data Source: Goodman (28)

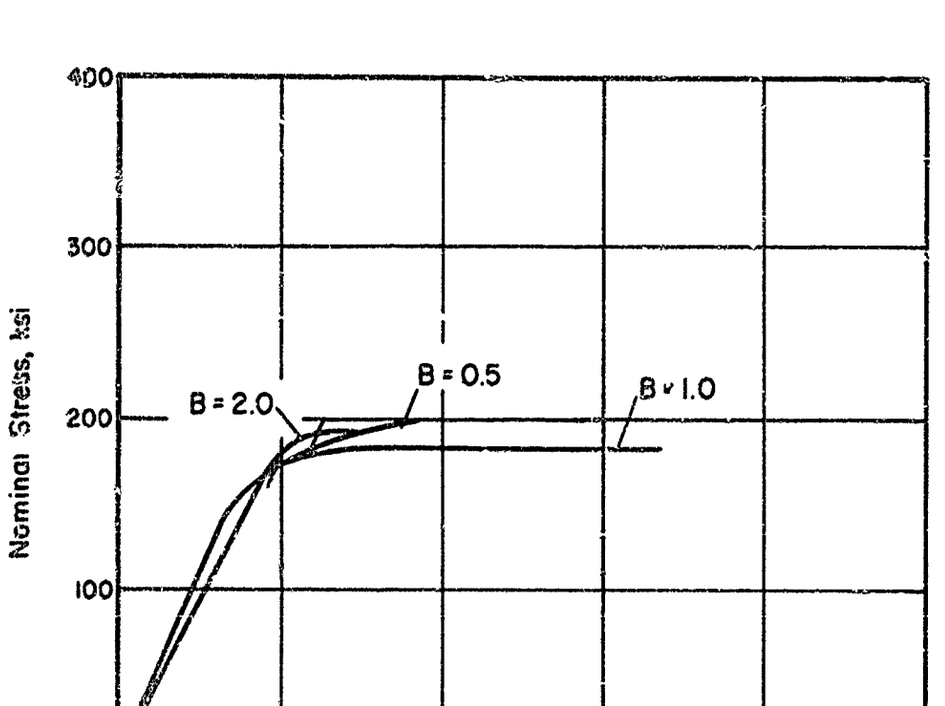

FIGURE 87. TYPICAL BIAXIAL STRESS-STRAIN CURVES AT ROOM TEMPERATURE FOR 6AI-4V TITANIUM 0.18% OXYGEN CONTENT
Data Source: Goodman (28)

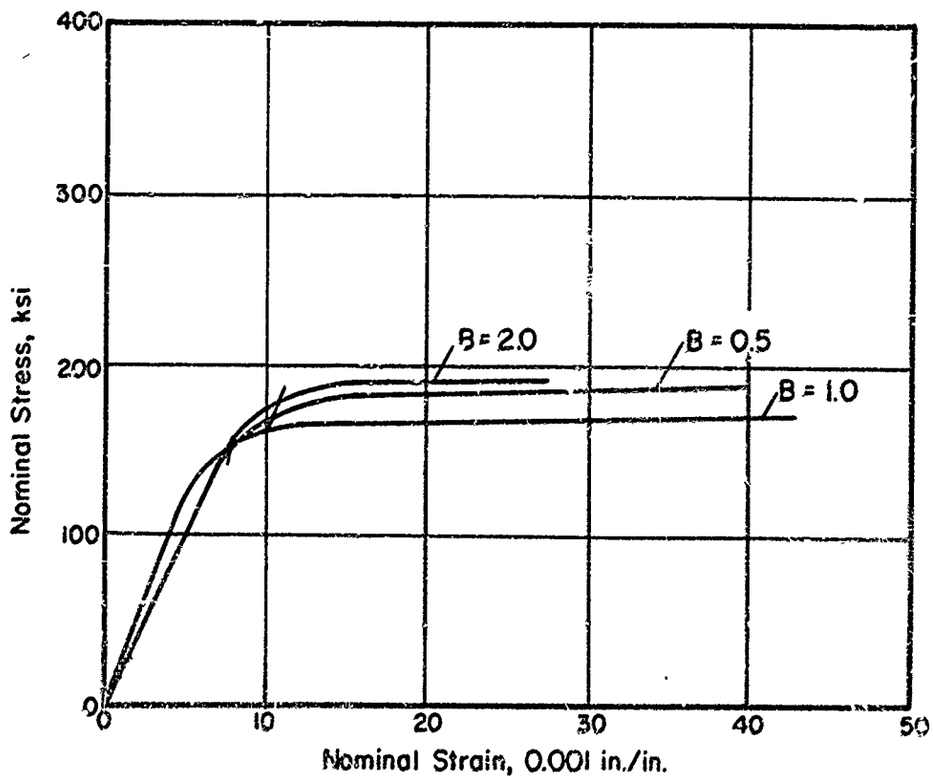

FIGURE 88. TYPICAL BIAXIAL STRESS-STRAIN CURVES AT ROOM TEMPERATURE FOR 6AI-4V TITANIUM 0.07 % OXYGEN CONTENT
Data Source: Goodmar. (28)

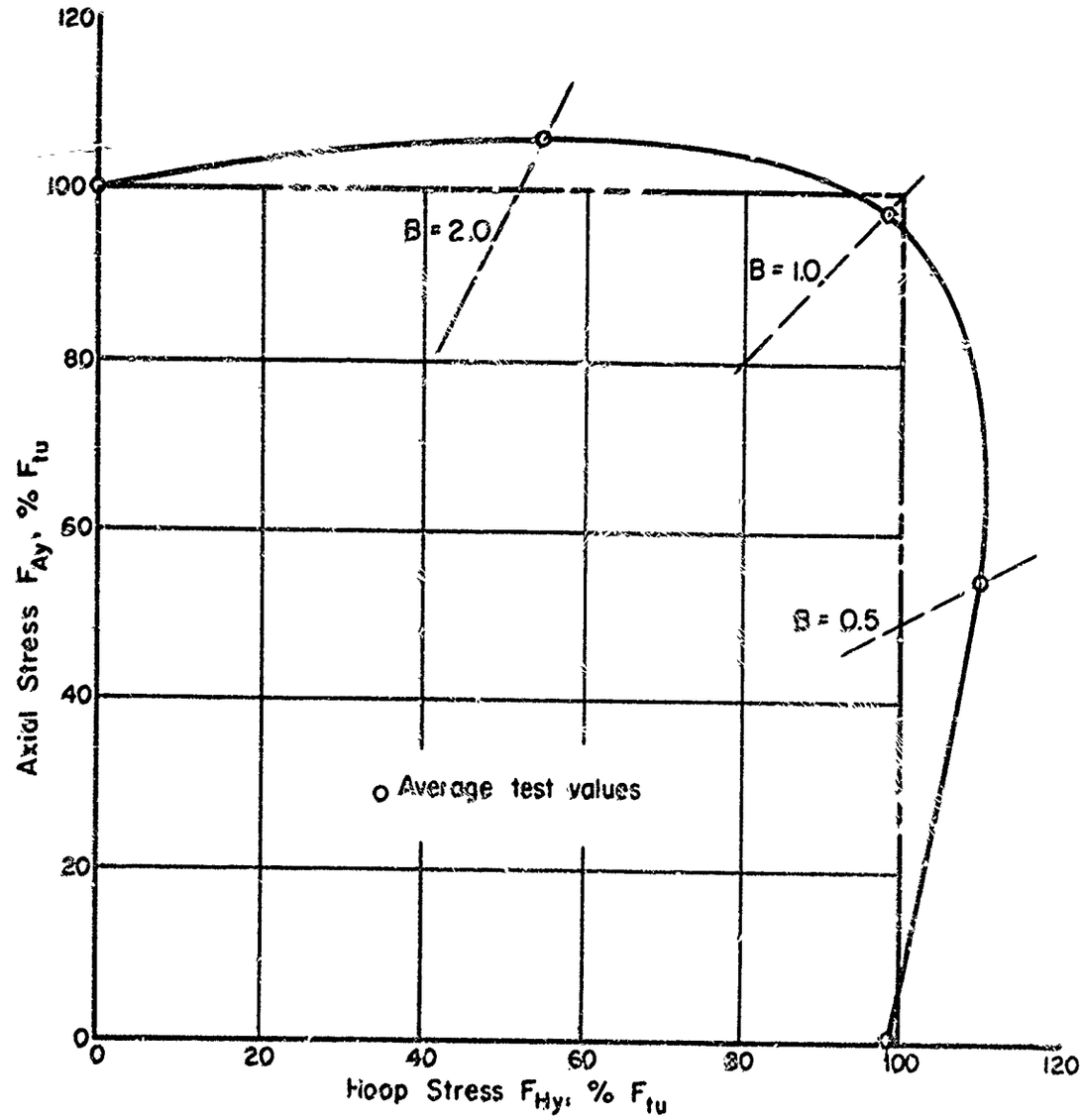

FIGURE 89. BIAXIAL YIELD-STRESS ENVELOPE AT ROOM TEMP FOR 6Al-4V TITANIUM ALLOY
Data Source: Goodman (28)

VI

DISCUSSION OF BIAXIAL-STRESS PROPERTIES AND SOME FACTORS WHICH AFFECT THEM

General

In this section, various factors affecting the biaxial-stress properties are discussed primarily from the standpoint of design application. Many of the trends described are based directly upon the biaxial-stress property data presented in Section 5; others are illustrated by direct comparisons with data from various other sources and are further supported by results of plastic-tensile-instability theory presented in Appendix III.

Effects of Type of Specimen

The main types of test specimens are described in Section III as follows:

(1) Cylindrical shell, subject to internal pressure alone or internal pressure plus externally applied axial load

(2) Spherical shell subject to internal pressure

(3) Flat-diaphragm specimen (bulge test)

(4) Formed-cup specimen

(5) Direct in-plane loading specimen (such as the cruciform specimen)

(6) Face-grooved tension specimen.

Although very few direct comparisons are possible due to the paucity of experimental data, reference to Figures 90 through 93 does indicate that in general the type of test specimen has a smaller effect on the elastic range and yield stress than the inherent scatter in the material properties as measured. In Figure 90 the stress-strain curves are compared for cylindrical, flat-diaphragm (bulge), and in-plane (cruciform) specimens of 2014-T6 aluminum alloy. In Figure 91 cylindrical versus cruciform specimens of D6AC steel are compared at $B = 1.0$, while Figure 92 covers the same comparison for H-11 at $B = 0.5$. Figure 93 compares cylindrical versus flat-diaphragm bulge specimens of 2024-T aluminum alloy. Compared with the cylinder specimens, there does seem to be a lower yield stress associated with the flat-diaphragm bulge-test specimen and a higher one for the cruciform specimen (Figures 92 and 93). However, Figure 91 suggests that this latter statement may not be valid in general.

Thus, in summary, in the elastic range the specimen type is not important. However, in some cases in the early portion of the plastic range, the specimen type may influence the results.

The effect of type of specimen on biaxial ultimate stress and biaxial ductility (strain measured either at ultimate stress or at fracture) appears to have a much larger effect. For example, compare the difference in ultimate stress and in ductility, both

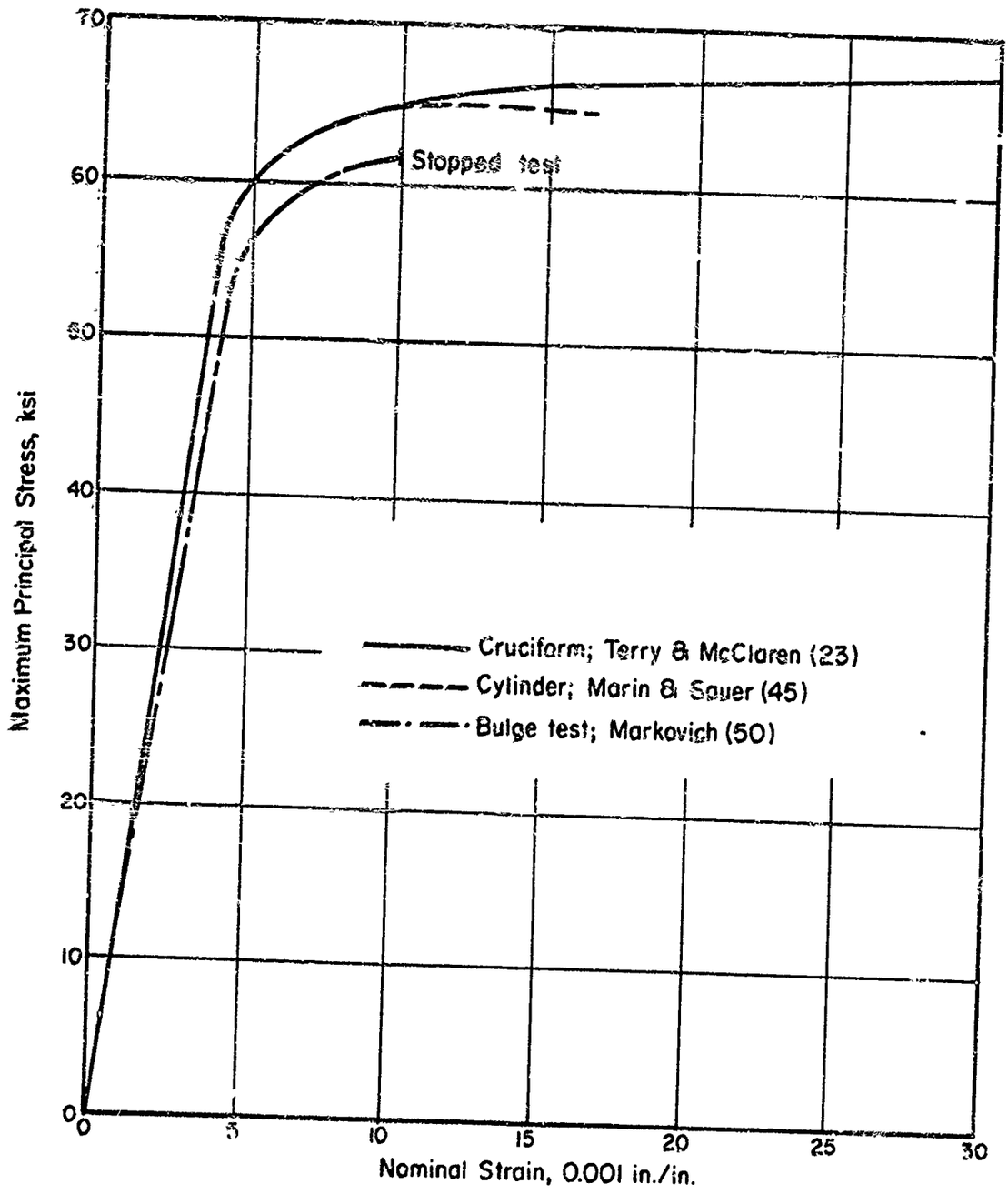

FIGURE 90. COMPARISON OF SUBSCALE PRESSURE VESSEL, FLAT (BULGE TEST) SPECIMEN, AND CRUCIFORM SPECIMEN DATA FOR 2014-T6 ALUMINUM, BIAXIAL RATIO B = 1

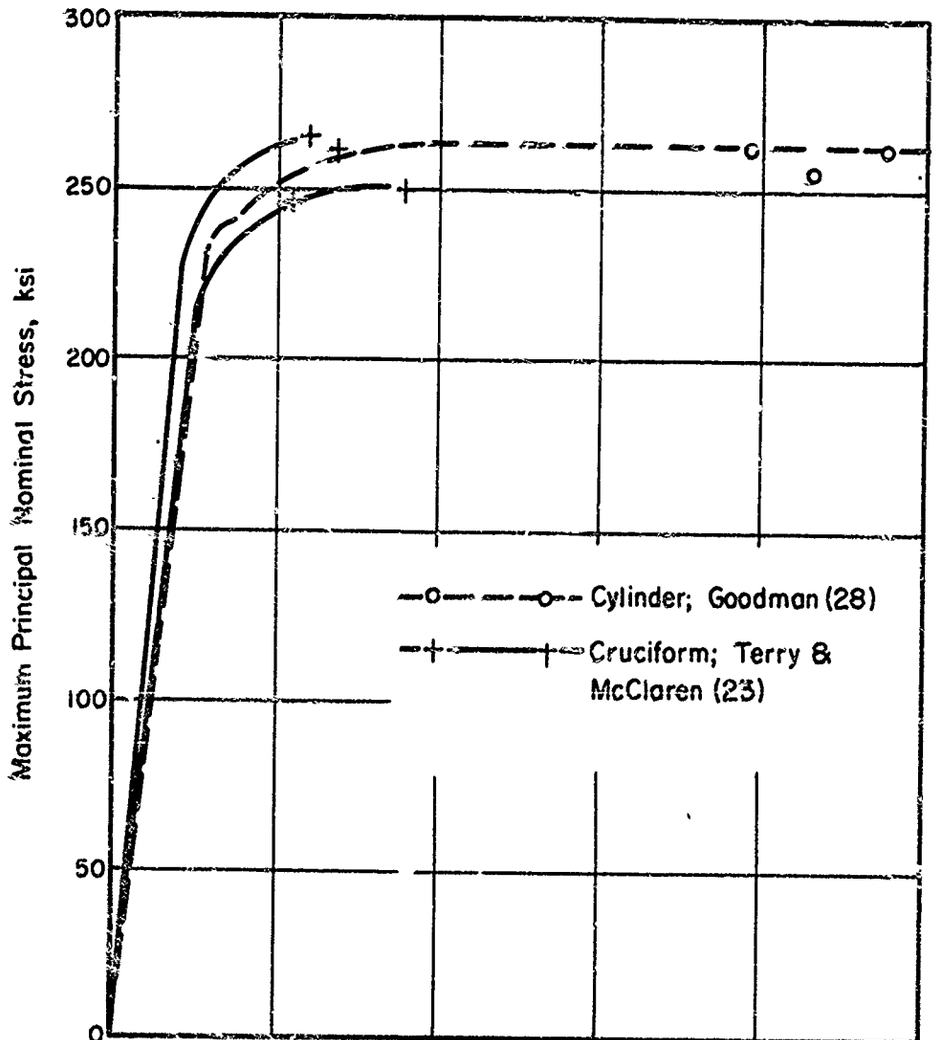

FIGURE 91. COMPARISON OF SUBSCALE PRESSURE VESSEL AND CRUCIFORM SPECIMEN DATA FOR D6AC STEEL, BIAXIAL RATIO B = 1.0

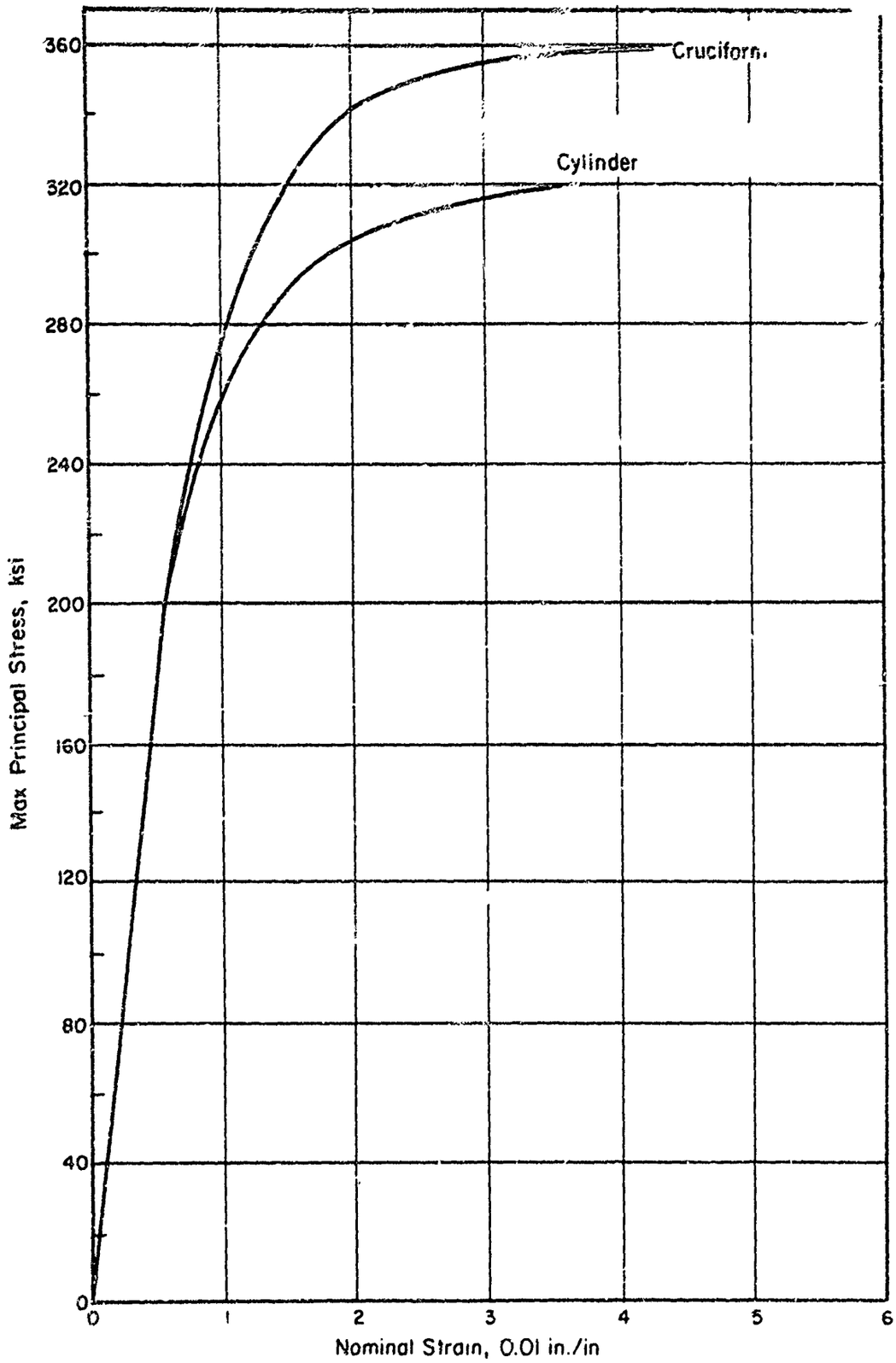

FIGURE 92 COMPARISON OF CYLINDER AND CRUCIFORM DATA FOR H-11, BIAXIAL RATIO B= 0.5. TERRY & McCLAREN (23)

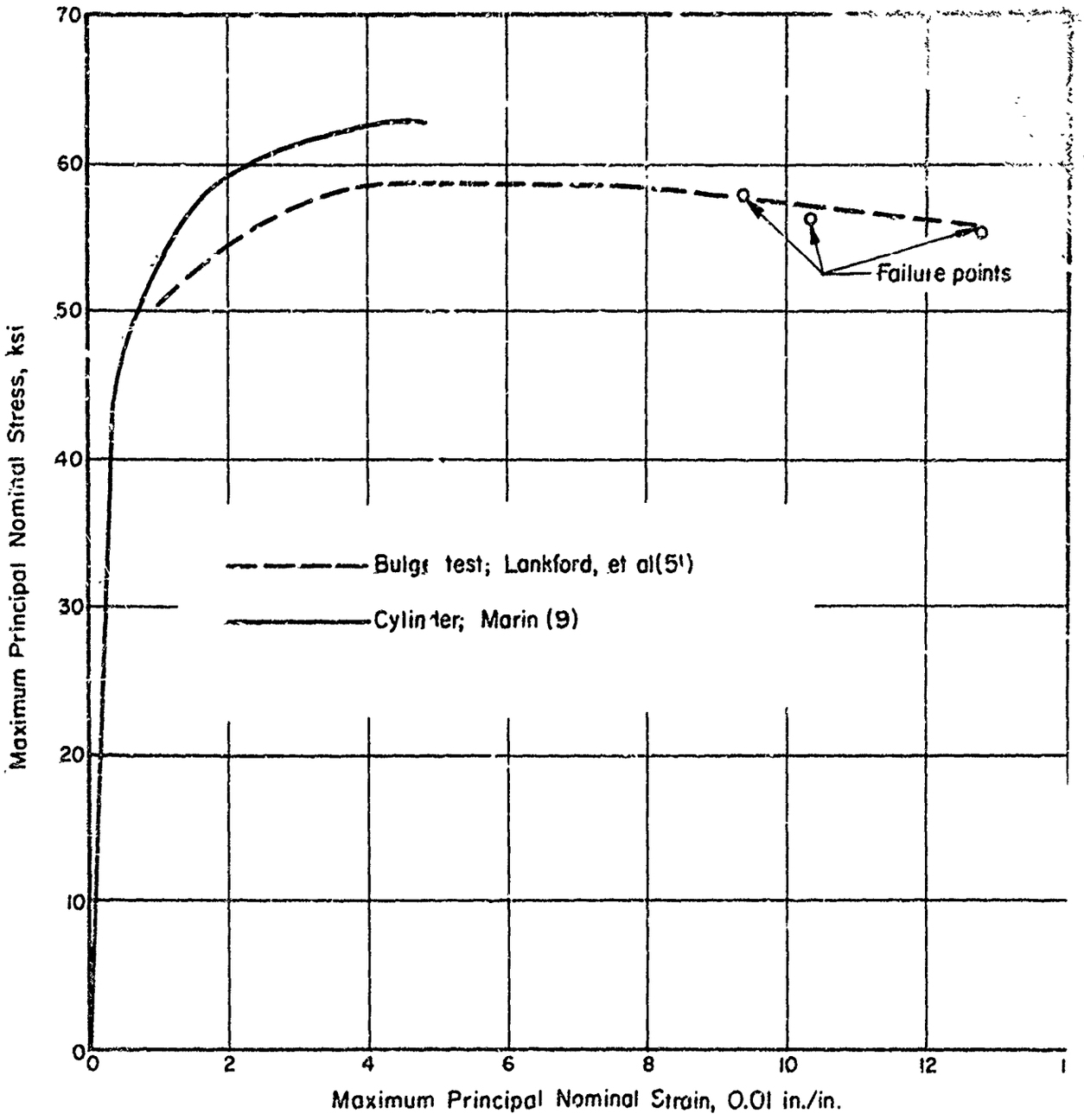

FIGURE 93. COMPARISON OF SUBSCALE PRESSURE VESSEL AND FLAT (BULGE TEST) SPECIMEN DATA FOR 2024-T ALUMINUM, BIAXIAL RATIO = 1.0

strain at ultimate and at fracture, for 2024-T in Figure 93. This indicates that the flat-diaphragm test is more severe in regard to ultimate stress and less severe in regard to ductility than the cylindrical shell. In contrast, the formed-cup specimen, as used by Bhat[22] for example, appears to give ultimate-stress values which are considerably higher than those given by cylindrical-shell specimens. This is surprising for several reasons: first, the formed cup superficially appears to be very similar to the bulge-test specimen, especially at failure. Second, the "biaxial kickup" or strength increase associated with a biaxial-stress ratio of 1/2 (or 2) would be expected to give the cylindrical shell subject to internal pressure a considerable margin over the formed cup (which, like the flat-diaphragm bulge-test specimen, has a biaxial-stress ratio of 1).

There do not appear to be any experimental data available to verify the relationship between the biaxial ultimate stress obtained from a pressurized spherical shell and that obtained from a cylindrical shell at the same biaxial ratio of unity (achieved in the cylinder by a combination of internal pressure and externally applied axial load). Fortunately, however, plastic-tensile-instability theory predicts that the ultimate stress should be identical for these two cases (see Cases 1 and 3 in Appendix III). Thus, at least for the case of fairly ductile materials, it should make little difference whether the data for B = 1 are obtained from a spherical or a cylindrical shell specimen.

As previously mentioned, the face-grooved tension specimen, although simple in concept and inexpensive to make, unfortunately does not correlate satisfactorily with cylindrical-pressure-vessel burst data and thus should not be used for pressure-vessel design purposes.

In summary, the effect of specimen type is usually small in the elastic range and early stages of yielding (say up to and including the yield stress). The effect of specimen type on ultimate-stress and ductility data appears to be quite strong. The following types of specimens are recommended for the applications indicated:

Application	Type Specimen Recommended
Pressure vessels, rocket-motor cases, liquid-propellant tankage, pressurized cabins	Cylindrical shell with internal pressure plus axial load as required to achieve biaxial-stress ratio
Flat skin panels loaded in-plane	Cruciform specimen
Material-formability studies	Formed-cup or flat-diaphragm bulge specimens

Effect of Heat Treatment

For the steels, various heat treatments are selected in order to increase the ultimate tensile strength of the material. This increase is usually determined by measurements made on uniaxial tensile specimens. The effects on biaxial properties are shown on the numerous figures presented in Section V of this report. These figures show the nominal hoop burst and yield stress versus the uniaxial tensile ultimate and yield stresses respectively.

As an example, Figures 16, 18, 19, 21, and 23 show these curves and data points for 4130, 4135, 4137, 4140, and MX-2 steels. There appears to be some scatter in the

data points as can be expected, but the points generally follow the lines $F_{Hu} = 1.1\ F_{tu}$ and $F_{Hy} = 1.1\ F_{ty}$. Thus, as the ultimate tensile strength and yield strength are increased, the hoop burst and yield strengths are increased by a factor of 1.1. This example is not necessarily applicable to all of the steels, however, as shown in the subsequent figures in Section V. For instance, in 4340 steel as shown on Figures 31 through 39, the increase factor is between 1.0 and 1.1.

The stainless steel, 17-7 PH, shows a peculiar behavior regarding the effect of heat treatment. Figures 63 and 64 show that for the TH heat treatment, all of the data points fall below the $F_{Hu} = 1.1\ F_{tu}$ line. That is, as the ultimate tensile stress increases from say 150 ksi to nearly 190 ksi, the nominal hoop burst stress increases from about 160 ksi to about 198 ksi. But after the ultimate tensile strength is increased to above 200-ksi level, the hoop burst stress drops off drastically. This dramatic change is shown most clearly on Figure 63. With regard to the RH heat treatment, it is not certain whether the same condition occurs at strength levels equivalent to the usual draw temperature used for the RH condition. This level will be in the range 210 ksi to 240 ksi.

Effects of Biaxial-Stress Ratio

The biaxial-stress ratio B affects the following biaxial-strength properties:

(1) The slope of the elastic portion of the biaxial stress-strain curve, i.e., it affects the biaxial modulus discussed in "Elastic Deformation Under Biaxial Stresses"

(2) The biaxial yield stress

(3) The biaxial ultimate stress

(4) The total strain reached at the biaxial ultimate stress.

In the paragraphs to follow, these various effects are discussed from both a plasticity-theory point of view and in the light of the actual test data reported.

The effect of the biaxial-stress ratio on the biaxial modulus E_B is easily predicted by Equation (12) in "Elastic Deformation Under Biaxial Stresses", repeated here for convenience:

$$E_B = E/(1 - \mu B) \quad .$$

From this expression, it is readily seen that the effect of B is not a strong one, since Poisson's ratio μ is approximately 0.3 for most alloys of structural importance. Also it is apparent that E_B is a maximum for a biaxial-stress ratio of unity when it is recalled that B as used in Equation (12) is defined as the ratio of the smallest in-plane principal stress to the other in-plane principal stress (i.e., $B \leq 1$). There is good agreement between theory and experiment for the effect of B on E_B.

Numerous theories of multiaxial strength have been proposed over the years to predict the effect of multiaxial-stress conditions on the yield stress of materials, especially metals and alloys. Some of these are mentioned and depicted in Appendix II. However, by far the most popular theory for yield stress of "ductile" alloys is the

octahedral-shear-stress theory, proposed by von Mises. Applied to the case of biaxial-stress loading, this theory predicts an elliptical-shaped biaxial-stress envelope as shown by Curve 3 in Figure 96 in Appendix II. Using the equation for this ellipse, it can be shown that the octahedral-shear-stress theory predicts that the largest yield stress occurs at biaxial-stress ratios of 0.5 and 2.0, where the predicted value is 15.5 percent greater than the uniaxial tension yield stress.

For all of the alloys reported in Section V, the highest yield-stress values do occur either at B values of 0.5 or 2.0. In many cases the yield-stress values at B values of 0.5 and 2.0 are equal; however, in some cases there is a slight difference between them. This slight difference indicates a small amount of anisotropy, either inherent in the material or more likely due to the nature of the material processing. For example, Figures 17, 25, 30, 40, and 60 show the effect of biaxial-stress ratio on yield stress for various steels. In all of the alloys represented by these figures, the highest yield-stress values were associated with a B ratio of 2.0. In every instance, the hoop-stress direction was perpendicular to the rolling direction with the possible exception of the 4340 alloy. The 4340 specimens were machined from hot-rolled bar stock and all of the other specimens under discussion here were made from either machined forgings or by deep drawing. These latter two processing methods may produce more grain orientation than hot rolling, but generally it is not considered to be great enough to influence the data of the type presented in this report.

Further comparison of the yield stress at biaxial-stress ratios of 2.0 or 0.5 with the uniaxial tension yield stress for the steels indicates that the biaxial gain or increase in yield stress compared to the uniaxial value is less than the 15.5 percent increase predicted by the octahedral-shear-stress theory. For the steels covered, it appears to range from approximately 8 to 12 percent. This slight reduction in actual biaxial gain compared to the theoretically predicted value can be accommodated quite easily by the generalized-conic biaxial-strength theory discussed in Appendix II, at the expense of more terms in the equations and consequently more data reduction effort. However, this latter theory can be adjusted to give excellent biaxial yield-stress predictions for steels, compared with the slightly unconservative values predicted by the octahedral-shear-stress theory. As explained in Appendix II, the difference is due to the inclusion of the "linear terms" in Equation (26); these terms are associated with the slight effect of the "hydrostatic" or mean-principal-stress effect on yielding.

Among the metals other than steels, the general picture for the effect of biaxial-stress ratio on biaxial yield stress of titanium alloy (6Al-4V, in particular) is similar to that of steel, although there does seem to be a greater difference between the yield-stress values for B = 0.5 and B = 2.0. This may be partially explained by material anisotropy.

The picture is not nearly so clear-cut in the case of aluminum alloys. There appear to be large deviations between yield stress values for B = 0.5 and 2.0 as illustrated on Figure 84. These greater deviations between values predicted by the octahedral-shear-stress theory and those actually measured can be explained, at least partially, on the basis of the greater strain hardening (increase in stress with strain during plastic deformation) in the metals other than steel, as follows: The octahedral-shear-stress theory as originally proposed by von Mises is intended to predict the beginning of plastic deformation, however, the standard offset value used as the MIL-HDBK-5 criterion of yield stress is 0.002 in./in. Thus, in undergoing the first 0.002 in./in. of plastic strain most of the steels exhibit very little increase (if any) in stress, while the other alloys show a significant strain-hardening effect in the initial yield region.

So far the discussion has been limited to positive values of the ratio B, i.e., to stress fields in which both of the in-plane principal stresses have the same sign. Very little data are available on the effect of negative biaxial-stress ratios on yield stress for materials of aerospace structural importance. However, the general trend predicted by either the octahedral-shear-stress theory or the maximum-shear-stress theory appears to be verified. This trend is that for pure shear (B = -1.0) the yield stress is lowest and as the ratio B moves either above or below this value of -1.0, the yield stress increases. This trend is exemplified by Figure 76, for example.

In regard to biaxial-yield-stress data, mention should be made of a relatively recent development in metallurgical process apparently most promising for materials with hexagonal close-packed crystalline structure, such as titanium. In this process, by orienting slip systems, the crystallographic texture is changed in such a way that the yield stress in the thickness direction is increased and thus the in-plane yield stress (under certain biaxial stress conditions) is increased appreciably. The concept seems to have been originated by Backofen and his associates.[52] It has the effect of modifying the biaxial-yield-stress envelope so that there is an appreciable increase in the convex bulge in the envelope in a certain range of positive biaxial-stress ratios. For instance, if a material is originally governed by the octahedral-shear-stress theory, its biaxial-yield-stress envelope is governed by the following equation, with the symbols as defined in Appendix II:

$$x^2 + y^2 - xy = 1 \quad ,$$

However, if this same material is texture hardened, it may have an envelope expressed by

$$x^2 + y^2 - Axy = 1 \quad ,$$

where the coefficient A may range as high as 1.7 from experimental data[53]. This corresponds to an increase in biaxial yield stress (at B = 1.0) of 82 percent based on the assumptions in the reference. No pressure vessels were used to determine the data. The texture-hardening process has not yet been used in production applications. However, with the considerable promise it holds and the intensive research presently being carried out on it, the texture-hardening process probably will go into use in production items requiring high biaxial yield stresses.

The effect of biaxial-stress ratio on the biaxial ultimate stress is a much more complicated subject than the effect on yield. One reason for this is the anisotropy induced by large plastic deformations; in other words, a material which is initially isotropic can have its stress-strain curve under loading in a certain direction raised as a result of extensive plastic deformation in that direction. Furthermore, the mechanism of failure depends upon the biaxial-stress ratio. Thus, for example, the ultimate-stress-failure phenomenon under conditions involving a maximum principal stress which is tension is often the plastic-tensile-instability phenomenon which is quite different from the phenomenon of failure under conditions of pure shear (B = -1.0). It is beyond the scope of this report to give an extensive discussion of plastic-tensile-instability theory as applied to the ultimate stress of biaxially stressed materials such as pressure vessels, rocket-motor cases, pressurized cabins, etc. Such a discussion, with particular reference to rocket-motor-case applications, is given by Bert and Hyler[54], and more recently the theory has been extended to arbitrary pressurized shells of revolution, including ellipsoids, paraboloids, torsipheroids, etc., by Bert[55].

Since the theory of ultimate-stress failure under biaxial-stress conditions seems to be adequately developed only for the tension-tension quadrant of the biaxial envelope (i.e., positive values of B), agreement between theory and experiment can be discussed for that quadrant only. For the materials tested by Goodman there was excellent agreement between plastic-tensile-instability theory and test data.[28] For other cases, there has been a lack of sufficient data for positive verification; however, the trend has definitely been verified.

One interesting thing about biaxial ultimate stresses for pressure vessels subject to various biaxial-stress ratios is the slight "apparent anisotropy" due to the differences in mechanical behavior of different B ratios. For example, the predicted (and measured) ultimate stress of a pressure vessel of isotropic material at a ratio B of 2.0 is slightly lower than that for a B value of 0.5. The difference is due to the greater contribution of hoop stress in the first instance compared with the second.

The effect of texture hardening on the biaxial ultimate stress has not been adequately explored to date; however, there is some theoretical indication that this process may actually decrease the ultimate stress at the same biaxial-stress ratio for which it produces a significant increase in yield stress.

Effect of Cylindrical-Shell Specimen Geometrical Parameters

For pressure-vessel type applications, in "Effects of Type of Specimen", the cylindrical-shell-type specimen was recommended. In this section, the effects of the geometrical parameters of the cylinder are discussed. The basic geometrical characteristics are defined as follows:

(1) Cylinder nominal diameter D
(2) Wall thickness t
(3) Length of cylindrical portion L
(4) End-closure configuration.

For convenience, by application of dimensional analysis, the following geometrical parameters are found to be more convenient than those listed above:

(1) Wall thickness t
(2) Diameter/thickness ratio D/t
(3) Length/diameter ratio L/D
(4) End-closure configuration.

The effect of wall thickness is an effect on the basic material properties such as the uniaxial-tension properties F_{ty} and F_{tu}. This is the reason that different uniaxial strength properties are listed in MIL-HDBK-5 for a variety of thickness or "size effect" should be expected to carry over into the biaxial properties. Unfortunately, however, insufficient biaxial-stress property data have been gathered for materials of different thickness to provide quantitative details on this point.

Other than the inherent relationship among stress, internal pressure, and D/t, and the effect of thickness described in the preceding paragraphs, there is no known cause for any appreciable effect of D/t, provided that the D/t value is within the range considered to be the thin-walled range, say D/t greater than 20. Again, however, no experimental data are available to substantiate this hypothesis.

The effect of length/diameter ratio is one effect which has been observed experimentally[37, 38] and has been predicted analytically using plastic tensile-instability theory[56-60]. In contrast to a long cylinder which expands uniformly along its length up to the point of localized tensile instability (ductile thinning of the wall), a short cylinder bulges considerably near the center prior to initiation of tensile instability. This difference is due to the girdle-like restraint afforded by the end closure in the short cylinder. Thus, the short cylinder tends to approach the shape of a sphere, which inherently has a higher burst pressure than a cylinder. Thus, the shorter is the cylindrical portion (i.e., the smaller the L/D ratio), the higher is the ultimate stress.

Closely related to the L/D ratio effect is the effect of the end-closure configuration. Since the so-called girdle effect described in the preceding paragraph is primarily due to radial restraint, it is logical to expect that the more rigid is the end closure, the greater the girdle effect and thus the higher the ultimate stress. This was borne out by analytical work carried out by Costantino, Salmon, and Weil, who found that a hemispherical end closure results in a lower ultimate stress than a rigid flat end closure.[61]

VII

CONCLUDING REMARKS

This report contains a comprehensive summary of existing data on biaxial-stress properties of metallic alloys of aerospace structural importance. The data are presented graphically in a number of ways. When available, biaxial stress-strain curves are shown. Also when sufficient testing of a given material was done, biaxial yield-stress and ultimate-stress envelopes are presented in the form agreed upon for presentation in MIL-HDBK-5. More often, however, individual investigators or groups of investigators have evaluated materials of interest at only one or two biaxial-stress ratios but over the useful strength range of the material. In these cases, the biaxial-stress envelopes could not be constructed. Instead, the graphical displays show the biaxial-strength property plotted as a function of the corresponding uniaxial-strength property.

Examination of the large compilation of test results shows that considerable variation exists in the types of specimens employed and in the quantity of useful measurements made during testing. Since test type and specimen configuration affect quite significantly the usefulness of the results, and since the instrumentation and consequent measurements determine the quantity and quality of data, it appears that future programs should focus attention on these details.

Although it would be commendable to expect or hope that standardized biaxial-stress test procedures could be established, it may not be feasible to do so, since many tests are conducted on prototype hardware. However, from the standpoint of establishing design allowables for a document such as MIL-HDBK-5, specimen design and test procedures should be such that properties should reflect the material behavior rather than that of the test specimen. To this end it appears that the cylindrical-shell test specimen may be a useful and versatile one, since with this specimen a range of biaxial-stress conditions (of structural significance) can be evaluated readily by combined internal pressure and external load (tension and compression).

With such a test, some standardization of specimen design can be done in regard to L/D, t/D and end-cap configuration to minimize end-restraint interactions. Also, specimen manufacture, either machining or forming with welding of longitudinal and circumferential seams, can be specified so that processing and flaws from processing (particularly weld flaws) do not influence behavior. Since many materials are strain-rate sensitive, a standardized rate of loading, or alternatively, strain rate should be specified. Finally, such testing should include instrumentation with which complete stress-strain curves can be determined, particularly in the region beyond the yield stress up to ultimate stress.

APPENDIX I

DISCUSSION OF VARIOUS PROPOSED BIAXIAL YIELD-STRESS CRITERIA

The purpose here is to discuss the reasoning behind the development of several yield-stress criteria which have been proposed for isotropic or nearly isotropic metals under biaxial loading. All of these are comparable to the well-known 0.2 percent offset yield-strength criterion for uniaxial loading. It is desirable that a standard biaxial yield-stress criterion be selected so that there is unanimity in analyzing and presenting data as well as in design use.

The three yield criteria discussed here are:

- Uniform plastic-strain criterion
- Equivalent plastic-strain criterion
- Equivalent plastic-work criterion.

Perhaps the most simple biaxial-yield criterion is the uniform plastic-strain criterion (described in "Biaxial Yield-Stress Criterion"). The reasoning in this case is that if 0.2 percent permanent strain is acceptable for uniaxial loading, it should also be acceptable under biaxial loading conditions. Although this criterion has been used by several aerospace companies, theoretical objections have been raised to its use because it is independent of the biaxial-stress ratio. Nevertheless, this was the yield criteria adopted for use in MIL-HDBK-5.

For a wide variety of structural metals, it has been found experimentally that under multiaxial loading the initiation of yielding occurs when a certain "effective stress" reaches a value equal to the uniaxial yield stress in tension. For many structural metals, it is agreed that this effective stress is the stress value associated with the von Mises yield criterion, which is the same as the octahedral-shear-stress theory, the distortion-energy theory[2], or improperly, the deformation-energy theory[3]. The general expression for the von Mises effective stress $\bar{f}$ is

$$\bar{f} = \left(\frac{1}{\sqrt{2}}\right)\sqrt{\left(f_1-f_2\right)^2 + \left(f_2-f_3\right)^2 + \left(f_3-f_1\right)^2} \quad , \tag{22}$$

where f_1, f_2, and f_3 are the three principal stresses. For the biaxial-loading case, which is the primary interest here, Equation (22) reduces to

$$\bar{f} = \sqrt{f_1^2 - f_1 f_2 + f_2^2} \quad . \tag{23}$$

2. Strictly speaking, the distortion-energy theory coincides with the von Mises criterion only for isotropic materials.
3. It is improper to use the term deformation-energy theory, since it does not distinguish between the total deformation energy and the distortion (shear) energy.

For practical engineering purposes, the interest is in the stress corresponding to some plastic (offset) strain, such as 0.002 in./in., rather than the stress at which yielding begins. Since the effective stress concept was well established, it was a logical step, first made by Dorn and Thomsen[62], to define an effective plastic strain $\bar{e}_p$ by an equation analogous to the von Mises criterion, namely[4],

$$\bar{e}_p = \left(\frac{\sqrt{2}}{3}\right)\sqrt{\left(e_{p1}-e_{p2}\right)^2 + \left(e_{p2}-e_{p3}\right)^2 + \left(e_{p3}-e_{p1}\right)^2} \quad , \tag{24}$$

where e_{p1}, e_{p2}, e_{p3} are the three principal plastic strains. In the general biaxial-loading case, none of the principal plastic strains are zero, since the biaxial stresses can produce plastic deformation in the thickness direction. Although the constant appearing in front of the square root in Equation (24) is different than the one in Equation (22), both expressions result in effective values ($\bar{f}$, $\bar{e}_p$) for the uniaxial case which are equal to the actual values (f_o, e_{po}).

Marin, Ulrich, and Hughes, following a suggestion by L. W. Hu, equated expressions for the effective plastic strains for the uniaxial and general biaxial cases, respectively.[65] The result was the following expression for the relationship between the plastic strain in the maximum-principal-stress direction on a biaxially stressed specimen and its equivalent uniaxial plastic strain e_{po}:

$$\frac{e_{p1}}{e_{po}} = (1-0.5B)\Big/\sqrt{1-B+B^2} \quad . \tag{25}$$

This relationship is depicted graphically in Figure 94 as a function of the biaxial ratio B.

In determination of an offset yield strain equivalent to the uniaxial yield criterion e_{po} = 0.002 in./in., it is only necessary to enter Figure 94 with the appropriate B (or 1/B) ratio, move vertically to an intersection with the curve and horizontally to the e_{p1}/e_{po} ordinate. This ordinate value when multiplied by e_{po} gives the equivalent offset strain. Except for the difference in offset strain, the procedure for determining the yield strength is the same as for the uniform plastic-strain criterion.

The equivalent plastic-strain criterion is based partially on a particular theory of plasticity (the octahedral-shear-stress theory) and partially on actual test results for the material concerned. This is because the amount of offset strain used is based on the theory in conjunction with the biaxial ratio concerned, while the actual yield-stress values are taken from test results for the material, biaxial-stress ratio, and offset[5].

4. Further discussion of the concepts of effective stress and effective plastic strain may be found in Reference (53). Also, it is noted that Equation (24) is based on the assumption that the plastic Poisson's ratio is 1/2. This assumption has been verified for the plastic portion of the strain in most metals by numerous investigators (64).

5. A more consistent procedure would be to determine the biaxial stresses for the equivalent plastic-strain values prescribed by Dorn and Thomsen's definition of effective plastic strain, next to use these stress values to determine the coefficients of the general conic curve, then to use these coefficients to define a new prescription for equivalent plastic strains, and finally to determine the stresses corresponding to these new plastic-strain values. This procedure could be repeated as many times as possible to obtain any desired accuracy. However, for the sake of standardization, it may be desirable to have the same offset for the same biaxial ratio regardless of the material. Since, in general, different materials would have different effective-stress coefficients, it is better to use the Dorn-Thomsen definition of effective plastic strain.

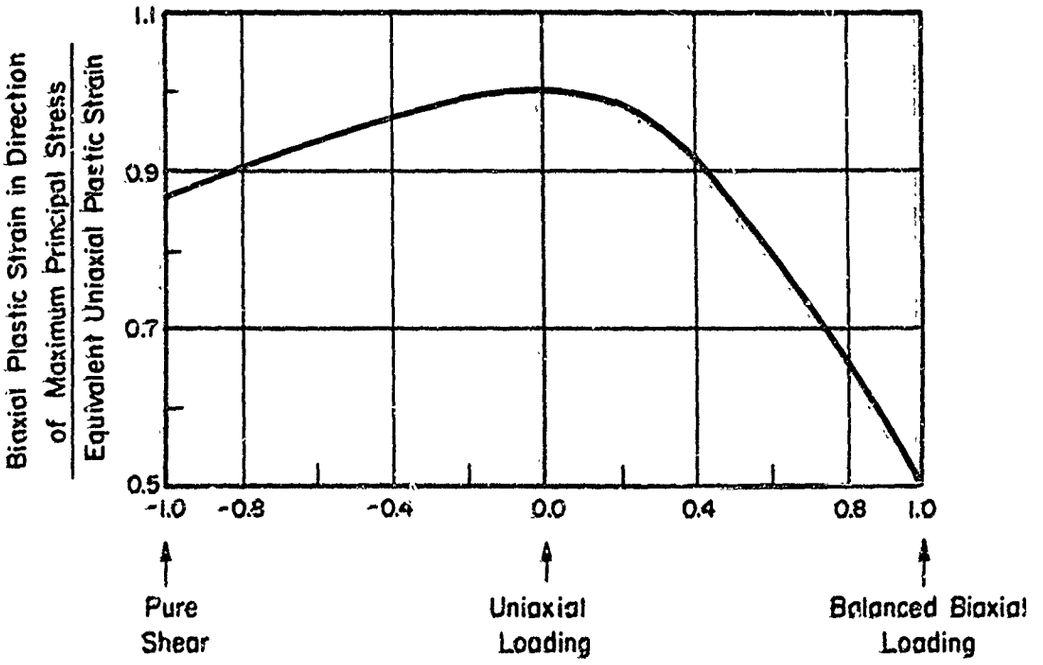

FIGURE 94. RATIO OF BIAXIAL PLASTIC STRAIN IN DIRECTION OF MAXIMUM PRINCIPAL STRESS TO EQUIVALENT UNIAXIAL PLASTIC STRAIN FOR VARIOUS BIAXIAL RATIOS

To overcome the disadvantage suffered by the two previously described criteria, Dr. L. H. Lee of the University of Notre Dame has proposed the equivalent plastic-work criterion. This criterion is based on the work of Dr. D. C. Drucker[66]. Basically, the concept here is simply to equate the plastic work done (strain energy) under biaxial loading to the plastic work done in straining uniaxially to a plastic strain of 0.002 in./in.

The unit plastic work done (measured in in-lb/cu in. of material) is equal to the total area beneath the stress-strain curve minus the elastic work, as shown schematically in Figure 95. Thus, in order to accurately determine plastic work from experimental data, it is necessary to planimeter an area from the stress-strain diagram.

Under biaxial loading, work is done in each of the biaxial principal directions. Thus, for each biaxial test, it is necessary to determine the area of the stress-strain curve for each of the two biaxial principal directions and then add these areas. This means that experimental strain measurements in the second principal direction, which usually have not been reported in the literature, are required in order to utilize this criterion.

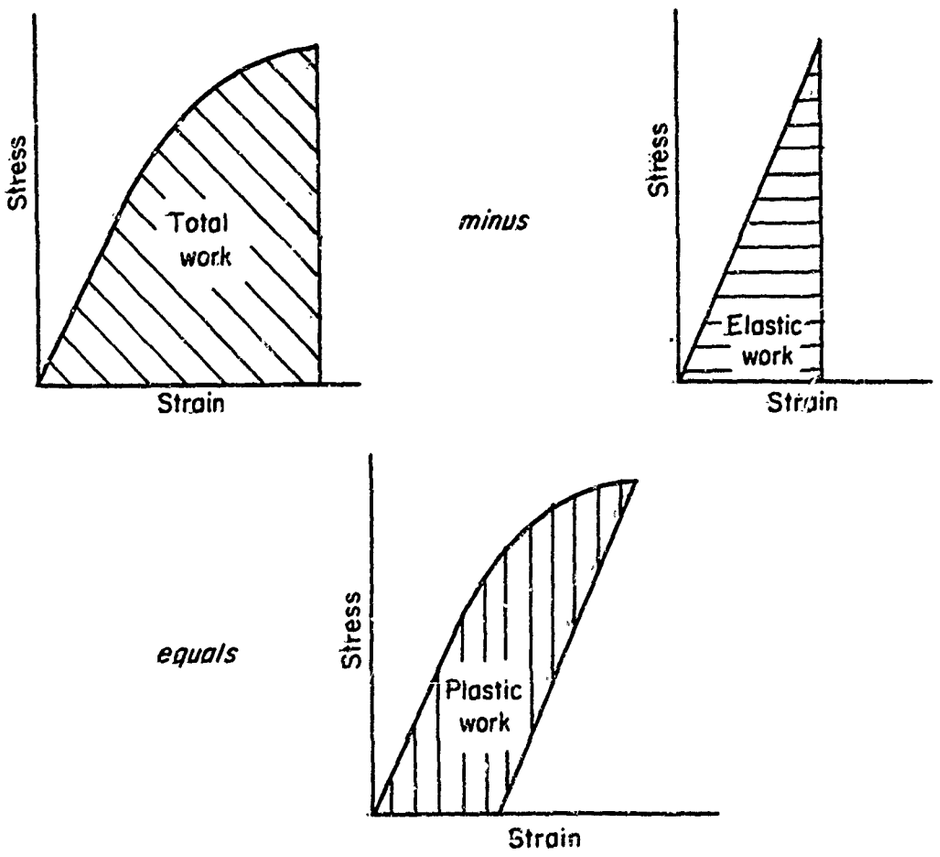

FIGURE 95. DIAGRAMS OF ELASTIC AND PLASTIC DEFORMATION

APPENDIX II

DISCUSSION OF THE GENERALIZED CONIC THEORY OF BIAXIAL STRENGTH

Many different theories of multiaxial strength have been proposed for isotropic materials. Five of these have been discussed in detail by Marin[67] and can be represented, for the tension-tension quadrant of the biaxial-strength envelope, by the following nondimensional equations, where x denotes f_H/f_{ty} (and F_{Hy}/F_{ty}) and y is f_A/f_{ty} (and F_{Ay}/F_{ty}), where f_{ty} is the uniaxial tensile yield strength.[6]

(1) Maximum-normal-stress theory, proposed by Rankine, best suited for so-called brittle materials:

$$(x-1)\,(y-1) = 0 \quad .$$

(2) Maximum-shear-stress theory, proposed by Coulomb, best suited for some ductile materials:

$$(x-1)\,(y-1) = 0 \quad .$$

(3) The octahedral-shear-stress theory, proposed by von Mises, best suited for many ductile materials:

$$x^2 + y^2 - xy = 1 \quad .$$

(4) Maximum-strain theory, proposed by Saint-Venant, not in current use:

$$(x-\mu y-1)\,(y-\mu x-1) = 0 \quad .$$

(5) Maximum total-strain-energy theory, in very limited use:

$$x^2 + y^2 - \mu\, xy = 1 \quad .$$

The nondimensional biaxial-yield-strength envelopes representing these five theories for tension-tension loading are given in Figure 96. However, there is often uncertainty in determining which of the theoretical envelopes corresponds best to actual test results for a given material under loadings corresponding to a range of biaxial-stress-ratio values. Many times it is quite difficult to determine whether test data fall closer to the maximum-shear-stress theory or to the octahedral-shear-stress theory. Sometimes it appears that the data points form a smooth curve which differs from all of the theoretical envelopes. Also, for reasons of economy, it is customary to conduct biaxial tests for only a limited number of biaxial-stress ratios (usually five: 0, 1/2, 1, 2, and ∞). This sometimes presents difficulty in fitting a smooth envelope curve to the data points. In order to overcome all of these difficulties, it is suggested here that a general conic curve, which is the most general second-degree algebraic curve, be used to reduce the data. This can be written as follows:

$$ax^2 + by^2 + cxy + dx + ey = 1 \quad , \tag{26}$$

6. As in MIL-HDBK-5, the symbol f denotes an actual or calculated stress, whereas the symbol F indicates a minimum or allowable strength.

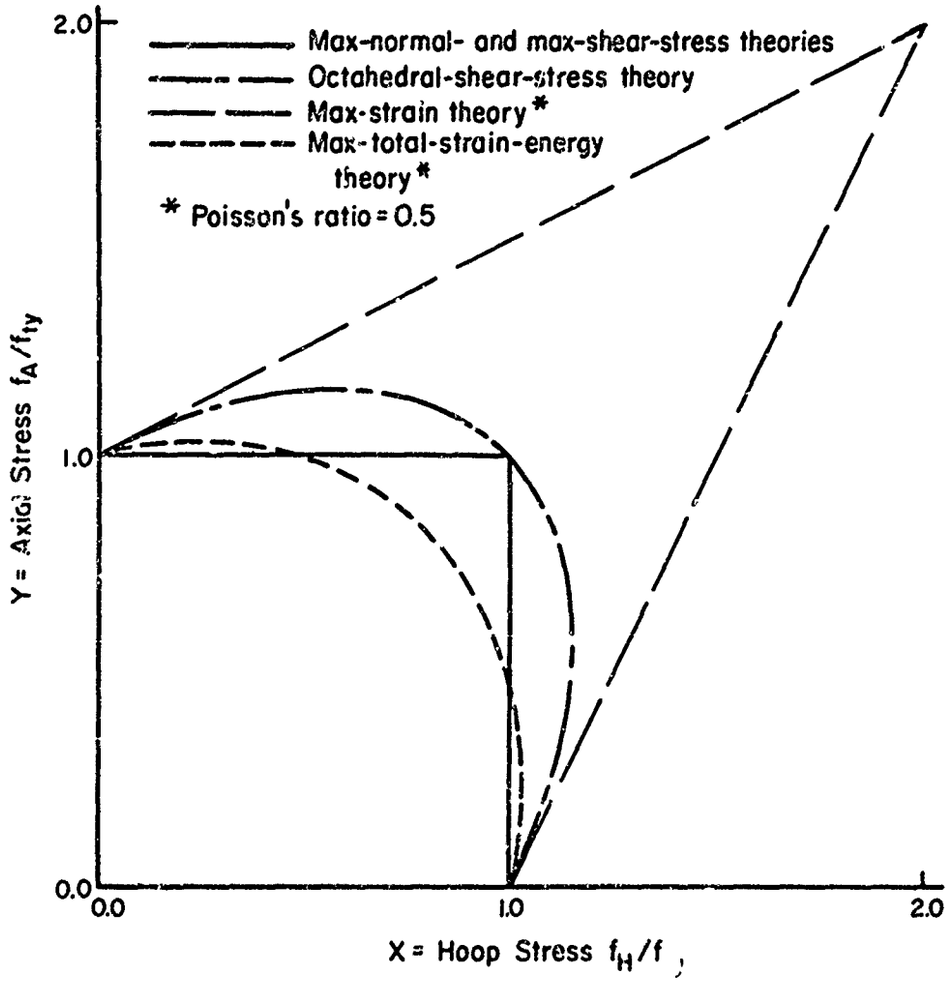

FIGURE 96. SOME COMBINED-STRESS THEORIES

where the coefficients a through e can be determined from test results for five different biaxial ratios. For an isotropic material, Equation (26) has a = b and d = e. Once the coefficients have been determined, Equation (26) can be used to compute points on the envelope curve corresponding to any intermediate biaxial ratio.

It is noted that each of the strength theories mentioned above can be represented by Equation (26) provided the coefficients are selected properly, as shown in Table IV.

TABLE IV. SPECIAL CASES OF THE GENERAL CONIC BIAXIAL-STRENGTH ENVELOPE

Strength Theory	Coefficients for Equation (26)				
	a	b	c	d	e
Maximum-normal-stress theory	0	0	-1	1	1
Maximum-shear-stress theory	0	0	-1	1	1
Octahedral-shear-stress theory	1	1	-1	0	0
Maximum-strain theory	μ	μ	$-(1+\mu^2)$	$1-\mu$	$1-\mu$
Maximum-total-strain-energy theory	1	1	$-\mu$	0	0
Hill's anisotropic plasticity equation	a*	b*	c*	0	0

*Arbitrary value.

For those who desire a more fundamental basis for the conic equation, reference is made to an equation given by Hill for triaxial stress in an anisotropic material.[68] First, the third normal stress and the two out-of-plane shear stresses in Hill's equation are set equal to zero since here we are dealing only with the biaxial case. Next, it is noted that when the biaxial normal-stress values used are principal-stress values, the in-plane shearing stress is zero. Furthermore, normal stresses appeared only as differences in Hill's equation (thus, d = e = 0 in Table IV), because he assumed that the superposition of a hydrostatic stress does not influence yielding. However, more recent experimental evidence obtained by Hu suggested that hydrostatic stress can affect yielding significantly.[69] Thus, the final result is the general conic equation suggested above.

APPENDIX III

ANALYSIS OF ULTIMATE STRESS OF DUCTILE MATERIALS UNDER BALANCED BIAXIAL LOADING FOR THREE SPECIMEN CONFIGURATIONS, USING PLASTIC-TENSILE-INSTABILITY THEORY

Provided that there are no severe local discontinuities such as notches, cracks, metallurgical flaws, so that flaw failure (brittle fracture) does not occur, the ultimate stress of a structure is determined by a particular kind of instability phenomenon known as plastic instability[7]. This instability phenomenon is not to be confused with buckling, which is a compressive instability phenomenon. In fact, plastic instability occurs only under tension loadings. The most simple example of plastic instability is the so-called necking phenomenon which occurs in a uniaxial tensile specimen as the ultimate tensile stress is reached.

By definition, the ultimate tensile stress is the maximum load reached in a tensile test divided by the original cross-sectional area. Now as a tensile specimen is stretched well into the plastic range, its cross-sectional area becomes smaller and smaller due to the Poisson contraction effect. At the same time, the material usually undergoes a certain amount of strain hardening; that is, as the specimen is stretched, it can accommodate higher and higher stresses. However, depending upon the exact shape of the stress-strain curve for the particular specimen, eventually a point is reached at which the relative area decreases at a rate exactly equal to the relative rate of strain hardening. At this point, which is the plastic instability point corresponding to the ultimate tensile stress, a local neck begins to develop somewhere along the length of the specimen. Further extension is concentrated at the necked region and the load decreases.

As is well known to materials engineers, the ultimate tensile stress is a basic material property for a given material, material condition, temperature, specimen size, and rate of loading. However, in the general case of biaxial loading, the ultimate stress is highly dependent upon geometrical configuration, as illustrated by the three examples treated subsequently.

To vividly illustrate the effect of geometrical configuration on biaxial ultimate stress, theoretical calculations will be carried out for three configurations with the same biaxiality:

(1) A thin-walled sphere with internal pressure

(2) A square plate loaded uniformly in all directions

(3) A thin-walled closed-end cylinder with internal pressure and sufficient external tensile load to give a balanced biaxial-tension-stress field.

7. It would be better nomenclature to use the term "tensile instability", since it can occur in highly elastic materials such as rubber, as well as in the plastic range in the case of structural metals.

Case 1. Thin-Walled Sphere

The true stress (in the wall of the sphere) which is the same in all directions is easily computed by

$$\sigma = pD/4t \quad , \tag{27}$$

where p is the internal pressure, D is the instantaneous diameter, and t is the instantaneous wall thickness.

Now the volume V of material in the shell (not the space volume enclosed by the shell) is

$$V = \pi D^2 t \quad . \tag{28}$$

If it is assumed that the material volume does not change during plastic deformation, Equations (27) and (28) can be combined so as to eliminate D, with the following result:

$$p = C_1 \sigma t^{3/2} \quad , \tag{29}$$

where C_1 is a constant equal to $4\sqrt{\pi/V}$.

The ultimate stress in a spherical vessel is the engineering stress corresponding to the maximum pressure. The condition at which the maximum pressure is reached is found by setting the total differential dp of Equation (29) equal to zero.

Thus

$$3/2\, t_m^{1/2}\, \sigma_m\, dt_m + t_m^{3/2}\, d\sigma_m = 0$$

or

$$dt_m/t_m = -2/3\, d\sigma_m/\sigma_m \quad , \tag{30}$$

where the subscript m denotes the maximum-pressure point.

Now the quantity dt/t represents the change in wall thickness as a ratio to the instantaneous wall thickness. This is the negative of the differential of the true strain (sometimes called the logarithmic strain) ϵ^* in the thickness direction. Thus, Equation (30) reduces to

$$\sigma_m = (2/3) d\sigma_m/d\epsilon^*_m \quad . \tag{31}$$

Since $d\sigma_m/d\epsilon^*_m$ is merely the slope of the true stress-true strain curve, the simple graphical construction shown as a solid straight line in Figure 97 can be used to obtain the value of the true ultimate stress σ_m.

Case 2. Biaxially-Loaded Square Plate

The total load P acting on each edge of a square plate of edge length L and thickness t is simply

$$P = Lt\sigma \quad ,$$

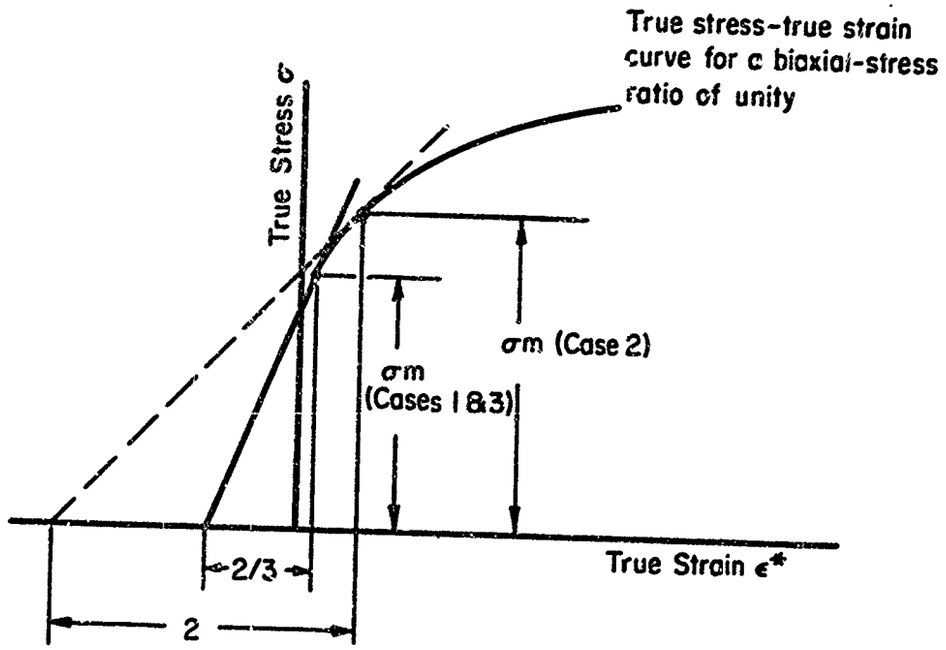

FIGURE 97. TRUE STRESS-TRUE STRAIN CURVE

and the material volume of the plate is merely

$$V = L^2 t \quad .$$

Thus

$$P = C_2 q t^{1/2} \quad . \tag{32}$$

Differentiating Equation (32) to obtain the maximum load point and substituting the definition for the true strain in the thickness direction in similar fashion as in the previous example, it is found that

$$\sigma_m = 2 d\sigma_m / d\epsilon_m^* \quad , \tag{33}$$

which is represented graphically by the dotted-line construction in Figure 97.

Case 3. Thin-Walled Tube With Axial Tension

Recently Felgar has demonstrated that the governing relationship for Case 3 is the same as that given above for Case 1.[70]

* * * * * *

From these three cases, it is evident that ultimate stress (or plastic instability) is not necessarily a constant value, but will depend rather directly upon the geometry of the part, the type of loading and the biaxial-stress ratio. For this reason, when reporting biaxial ultimate stress values in a handbook such as MIL-HDBK-5, it is necessary to identify the type of specimen from which the data were obtained.

In the above discussion use was made of true stress-true strain relations. However, material design criteria usually are expressed in terms of engineering stresses, which are based on the original cross-sectional area. Thus, it is necessary to convert from true-stress values to engineering-stress values. The following equation can be used for this conversion:

$$f_m = \frac{\sigma_m}{e^{2\mu_m^* \epsilon_m^*}} \quad , \tag{34}$$

where here e denotes the base of the natural logarithmic system (approximately 2.72), ϵ_m^* is the true strain corresponding to σ_m, and $\bar{\mu}_m^*$ is the effective Poisson's ratio (defined here in terms of true strains, rather than the usual definition in terms of engineering strains). Application of these results to Figure 97 shows that the ultimate stress for Case 2 can be appreciably higher than that for Cases 1 and 3 for materials with a large amount of strain hardening.

REFERENCES

(1) Bert, C. W., "Biaxial Properties of Metals for Aerospace Applications", AIAA Paper No. 2893-63, presented at the Launch and Space Vehicle Shell Structures Conference (April, 1963).

(2) "Special Task Group on Biaxial Properties: Proposal on Biaxial Properties of Metals", Attachment 60-10(25)a to the Minutes of the 25th Meeting, Military Handbook 5 Working Group (1963).

(3) Dove, R. C. and Adams, P. H., Experimental Stress Analysis and Motion Measurement, C. E. Merrill Books, Inc., Columbus, Ohio (1964), p 251.

(4) Hearman, R. F. S., An Introduction to Applied Anisotropic Elasticity, Oxford University Press, New York (1961).

(5) Timoshenko, S. and Goodier, J. N., Theory of Elasticity, 2d ed., McGraw-Hill Book Company, Inc., New York (1951), p 7.

(6) Lubahn, J. D. and Felgar, R. P., Plasticity and Creep of Metals, John Wiley and Sons, Inc., New York (1961).

(7) Lode, W., "Tests on the Effect of the Intermediate Principal Stress on the Yield Strength" (in German), Zeitschrift Physik, 36, 913 (1926).

(8) Osgood, W. R., "Combined-Stress Tests on 24S-T Aluminum-Alloy Tubes", Journal of Applied Mechanics, 14, Trans. ASME, 69, A147-A153 (1947).

(9) Marin, J., "A Biaxial Stress Machine for Determination of Plastic Stress-Strain Relations", Proc. SESA, 7, (1), 71-82 (1949).

(10) Fitzgibbon, D. P., "Experimental Method for Testing Materials in Biaxial Stress Fields", Space Technology Laboratories, Inc., Report No. STL/TR-60-0000-09028 (EM 10-6) (February 25, 1960).

(11) Taylor, G. I. and Quinney, H., "The Plastic Distortion of Metals", Philosophical Trans. of the Royal Soc. (London), Series A, 230, 323-362 (1931).

(12) Marin, J., "Stress-Strain Relations in the Plastic Range for Biaxial Stresses", Journal of the Franklin Institute, 248, 231-249 (1949).

(13) Pugh, H. L. D., Mair, W. M., and Rapier, A. C., "An Apparatus for Combined-Stress Testing in the Plastic Range", Experimental Mechanics, 4 (10), 281-288 (October, 1964).

(14) Marin, J., Dutton, V. L., and Faupel, J. H., "Tests of Spherical Shells in the Plastic Range", Welding Journal, 27, 593s-607s (1948).

(15) Lankford, W. T., Low, J. R., and Gensamer, M., "The Plastic Flow of Aluminum Alloy Sheet Under Combined Loads", Trans. AIME, Inst. of Metals Div., 171, 574-604 (1947).

(16) Parson, E., Marin, J., and Hu, L. W., "Mechanical Properties of a Magnesium Alloy Under Biaxial Tension at Low Temperatures", Proc. ASTM, 55, 810-823 (1955).

(17) Markovich, R., "Biaxial Mechanical Properties of High-Strength Weldable Aluminum Alloys", Advances in Cryogenic Engineering, 7, 459-465 (1961).

(18) Smith, B. W., "Evendale Bulge Testing Facility for Biaxial Stress Application", General Electric Company, Flight Propulsion Division, Report No. DF 59FPD522 (July 20, 1959).

(19) Freymeyer, R. D., "Evaluation of the Notch Sensitivity and Strength Under Biaxial Stress for Ultra High Strength Steels", Aerojet-General Corporation, Contract No. NOrd 17017, Report No. M-1724, Parts I and II (1959).

(20) Wilson, W. M. and Marin, J., "Tests of Thin Hemispherical Shells Subjected to Internal Hydrostatic Pressure", University of Illinois, Engineering Experiment Station Bulletin No. 295 (May, 1937), and Welding Journal, 22, 214s-220s (1943).

(21) Bhat, G. K. and Lindh, D. V., "Evaluation of Ultra-High-Strength Steels for Thin-Walled Pressure Vessels and Rocket Motor Cases", ASME Paper No. 62-MET-16 (April, 1962).

(22) Bhat, G. K., "4137 Co - a New Steel for Rocket Motor Cases", Metal Progress, 77 (6), 75-79 (June, 1960).

(23) Terry, E. L. and McClaren, S. W., "Biaxial Stress and Strain Data on High Strength Alloys for Design of Pressurized Components", Chance Vought Corp., ASD-TDR-62-401 (May, 1962).

(24) "Crack Propagation Prediction and Crack-Stopper Techniques for Stiffened and Unstiffened Flat Sheet in a Supersonic Transport Environment", Douglas Aircraft Company, Inc., Aircraft Division, ASD-TDR-63-773 (September, 1963).

(25) Corrigan, D. A., Travis, R. E., Ardito, V. P., and Adams, C. M., Jr., "Biaxial Strength of Welds in Heat-Treated Sheet Steel", Welding Journal, 41, 123s-128s (1962).

(26) Travis, R. E., Ardito, V. P., and Adams, C. M., Jr., "Comparison of Processes for Welding Ultra-High Strength Sheet Steels", Welding Journal, 42, 9s-17s (1963).

(27) "Proposal on Biaxial Properties of Metals", Attachment 60-10(24) to the Minutes of the 24th Meeting, Military Handbook 5 Working Group, (1962).

(28) Goodman, J. W., "Final Report on Pressure Vessel Design Criteria", Space Technology Laboratories, Inc., STL/TR-60-0000-19427, (AFBMD/TR 61-9, December 31, 1960).

(29) Manning, R. D., Murphy, W. J., Nichols, H. J., and Caine, K. E., "Simulated Service Tests of Steels for Solid-Propellant Missile Motor Cases", Materials Research and Standards, 2, 392-395, 469-475 (1962).

(30) Morrison, J. D. and Kattus, J. R., as reported by Campbell, J. E., "Steels for Large Solid-Propellant Rocket-Motor Cases", DMIC Report 178 (November 20, 1962).

(31) Bhat, G. K., "A Study of the Behavior of Small Pressure Vessels Under Biaxial Stress Conditions and in the Presence of Surface Cracks", Mellon Institute Contract No. NOnr-3764(00)(X), Final Report (June 25, 1963).

(32) Kojola, K. L. and Cantor, B. R., "Correlation of Laboratory Toughness Tests With Burst Tests of Deep-Drawn Pressure Vessels", U. S. Naval Weapons Plant, NAVORD Report 6965 (December 20, 1960).

(33) Kinnaman, E. B., Jacobsen, R. E., and Tiffany, C. F., "An Approach to the Practical Design of Reliable, Light Weight, High Strength Pressure Vessels", IAS Paper No. 59-109 (1959).

(34) Haynes, C. W. and Valdez, P. J., "Rocket Motor Case Material Evaluation by Pressure Vessel Testing", Aerospace Engineering, 19 (12), 30-36 (December, 1960).

(35) Baird, B. L., "Studies of Design Criteria for Welded Structures Subjected to a Biaxial Stress Field", Bruce L. Baird, Inc., ASD-TDR-62-1109 (January, 1963).

(36) Harrington, N. M., "Plastic Instability of Pressure Vessels", Douglas Aircraft Company, Inc., Missile and Space Systems Division, Report No. SM-38785 (August 29, 1960).

(37) Ginsburgh, A. S., "Pressure Vessel and Mechanical Test Evaluation of Ladish D-6ac Steel", Aerojet-General Corporation, AFBMD TN 60-3 (November, 1960).

(38) Hanink, D. K., as reported by Sachs, G., Schapiro, L., and Hoffman, O., "Strength of Ductile Metal Motor Cases", American Rocket Society Paper No. 2419-62 (April, 1962).

(39) Romine, H. E., "Fracture Toughness of H-11, 300M, and D6C Steels Used in Experimental Solid-Propellant Rocket Motor Casings at the 240,000 psi Yield Strength Level and Comparison With Hydrostatic Burst Test Results", U. S. Naval Weapons Laboratory Report No. 1825 (August 24, 1962).

(40) Wei, B. C. F., "Destructive Testings of Full Size Rocket Motor Cases and Their Application to Lightweight Design", AIAA Paper No. 64-445 (1964).

(41) Zettek, J. J., "An Investigation of the Structural Characteristics of Subscale Minuteman Chambers of Ladish D6AC Steel", Aerojet-General Corp., Report No. 0162-01TN-11 (March 1, 1962).

(42) Tidwell, C. A., "Full Scale Pershing Motor Case Burst Tests (Titanium and Steels)", abstract only, pp VI 73. Proc. of the 7th Sagamore Ordnance Materials Research Conference (1960).

(43) Kitchin, A. L., as reported by Campbell, J. E., "Steels for Large Solid-Propellant Rocket Motor Cases", DMIC Report 178 (November 20, 1962).

(44) Marin, J. and Wiseman, H. A. B., "Plastic Stress-Strain Relations for Combined Tension and Compression", NACA TN 2737 (July, 1952).

(45) Marin, J. and Sauer, J. A., "Plastic Stress-Strain Relations Under Radial and Non-Radial Combined Stress Loading", Journal of the Franklin Institute, 256, 119-128 (1953).

(46) Clarke, J. W. and Woodburn, W. A., discussion of "The Significance of the Tensile Test to Pressure Vessel Design", Welding Journal, 36 (1), 54s-55s (January, 1957).

(47) Marin, J., Ulrich, B. H., and Hughes, W. P., "Plastic Stress-Strain Relations for 75S-T6 Aluminum Alloy Subjected to Biaxial Tensile Stresses", NACA TN 2425 (August, 1951).

(48) Thomson, E. G., Dorn, J. E., "The Effect of Combined Stresses on the Ductility and Rupture Strength of Magnesium-Alloy Extrusions", Journal of Aeronautical Sciences, 11, 125-136 (1944).

(49) Marble, J. D., "Rocket Casing Behavior Predicted by Laboratory Tests", abstract only, Proc. of the 7th Sagamore Ordnance Materials Research Conference, pp VI 89-VI 90 (1960).

(50) Markovich, R., "Biaxial Mechanical Properties of High-Strength Weldable Aluminum Alloys", Advances in Cryogenic Engineering, 7, 459-465 (1961).

(51) Lankford, W. T., Low, J. R., and Gensamer, M., "The Plastic Flow of Aluminum Alloy Sheet Under Combined Loads", Trans. AIME, Institute of Metals Division, 171, 574-604 (1947).

(52) Backofen, W. A., Hosford, W. F., and Burke, J. J., "Texture Hardening", Trans. Am. Soc. for Metals, 55, 264-267 (1962).

(53) Hatch, A. J., "Texture Strengthening of Titanium Alloys", Trans. Metallurgical Soc. of AIME, 233, 44-50 (1965).

(54) Bert, C. W., Hyler, W. S., "Structures and Materials for Solid-Propellant Rocket-Motor Cases", Chapter in Advances in Space Science and Technology, 8, edited by F. I. Ordway III, Academic Press, New York (1966), 65-194.

(55) Bert, C. W., "Plastic Tensile Instability in Pressurized Shells of Revolution", Journal of Applied Mechanics, 32, Trans. ASME, 87E, 449-451 (1965).

(56) Weil, N. A., "Tensile Instability of Thin-Walled Cylinders of Finite Length", Internaticnal Journal of Mechanical Sciences, 5, 487-506 (1963).

(57) Fraser, A. F. and Jablonski, H., "Plastic Instability of Finite Cylinders", Aerojet-General Corporation (Sacramento, California), Report No. TD-13 (1961).

(58) Salmon, M. A., "Plastic Instability of Cylindrical Shells With Rigid End Closures", Journal of Applied Mechanics, 30, Trans. ASME, 85E, 401-409 (1963).

(59) Mann-Nachbar, P., Hoffman, O., and Jahsman, W. E., "Plastic Instability of Cylindrical Pressure Vessels of Finite Length", AIAA Journal, 1, 1607-1613 (1963).

(60) Weil, N. A., Salmon, M. A., and Constantino, C. J., "Approximate Burst Strength of Thin-Walled Cylinders With Hemispherical Caps", AIAA Journal, 1, 2088-2092 (1963).

(61) Constantino, C. J., Salmon, M. A., and Weil, N. A., "Effect of End Conditions on the Burst Strength of Finite Cylinders", American Soc. of Mech. Engrs. Paper No. 63-WA-180 (1963).

(62) Dorn, J. and Thomsen, E. G., "The Ductility of Metals Under Conditions of Stress and Strain", Trans. Am. Soc. Metals, 39, 741-772 (1947).

(63) Lubahn, J. D. and Felgar, R. P., Plasticity and Creep of Metals, John Wiley and Sons, Inc., New York (1961) 285-202.

(64) Lubahn, J. D. and Felgar, R. P., Plasticity and Creep of Metals, John Wiley and Sons, Inc., New York (1961) 299-304.

(65) Marin, J., Ulrich, B. H., and Hughes, W. P., "Plastic Stress-Strain Relations for 75S-T6 Aluminum Alloy Subjected to Biaxial Tensile Stresses", NACA TN 2425 (August, 1951).

(66) Drucker, D. C., "The Significance of the Criterion for Additional Plastic Deformation of Metals", Journal of Colloid Science, 4, 299-311 (1949).

(67) Marin, J., Engineering Materials, Prentice-Hall, Inc., Englewood Cliffs, New Jersey (1952), pp 127-137. Also Marin, J., Mechanical Behavior of Engineering Materials, Prentice-Hall, Inc., Englewood Cliffs, New Jersey (1962), pp 112-130.

(68) Hill, R., The Mathematical Theory of Plasticity, Oxford University Press, London (1950), p 318.

(69) Hu, L. W. and Pae, K. D., "The Inclusion of Hydrostatic Stress Component in Yield Condition and Application", pp 78-100 in "Effects of Triaxial Stresses on Mechanical Properties of Metals Under High Pressure". The Pennsylvania State University, Department of Engineering Mechanics, Contract No. AF 49(638)-676, Final Report AFOSR 1716 (September, 1961).

(70) Felgar, R. P., "Plastic Analysis of the Instability of Pressure Vessels Subjected to Internal Pressure and Axial Load", ASME Paper No. 61-WA-144.

Unclassified

Security Classification

DOCUMENT CONTROL DATA - R&D

(Security classification of title, body of abstract and indexing annotation must be entered when the overall report is classified)

1. ORIGINATING ACTIVITY (Corporate author) Battelle Memorial Institute 505 King Avenue Columbus, Ohio	2a. REPORT SECURITY CLASSIFICATION Unclassified 2b. GROUP N/A

3. REPORT TITLE MECHANICAL PROPERTIES OF AEROSPACE STRUCTURAL ALLOYS UNDER BIAXIAL-STRESS CONDITIONS

4. DESCRIPTIVE NOTES (Type of report and inclusive dates)
January 1965 to January 1966

5. AUTHOR(S) (Last name, first name, initial)
Bert, Dr. Charles W., Mills, Earl J., and Hyler, Walter S.

6. REPORT DATE	7a. TOTAL NO. OF PAGES	7b. NO. OF REFS
August 1966	143	70

8a. CONTRACT OR GRANT NO.	9a. ORIGINATOR'S REPORT NUMBER(S)
AF 33(657)-10076 b. PROJECT NO. 7381, Task No. 738103 c. d.	9b. OTHER REPORT NO(S) (Any other numbers that may be assigned this report) AFML-TR-66-229

10. AVAILABILITY/LIMITATION NOTICES This document is subject to special export controls, and each transmittal to foreign governments or foreign nationals may be made only with prior approval of Air Force Materials Application Division (MAAM), Wright-Patterson Air Force Base, Ohio 45433.

11. SUPPLEMENTARY NOTES	12. SPONSORING MILITARY ACTIVITY
	Air Force Materials Laboratory Research and Technology Division Air Force Systems Command Wright-Patterson Air Force Base Ohio 45433

13. ABSTRACT

This report is concerned with the mechanical properties of metals under biaxial-stress conditions. First, there is presented a discussion of the fundamentals of biaxial-stress systems; this is followed by descriptions and critical evaluations of various types of biaxial-stress tests, the associated test specimens, biaxial-stress property criteria, and data presentation for Military-Handbook-5. The major portion of the report is devoted to the graphical presentation of biaxial-stress property data from various published and unpublished sources.

DD FORM 1 JAN 64 1473

Unclassified

Security Classification